The solubility, speciation, and transport of the high field strength elements (HFSE) niobium, tantalum, and uranium

by Alexander Timofeev

April 2018

A thesis submitted to McGill University in partial fulfillment of the requirements for the degree of Doctor of Philosophy

---

Department of Earth and Planetary Sciences

McGill University

Montreal, QC, Canada

Abstract

The high field strength elements (HFSE) are considered to be immobile in many geochemical environments, within which hydrothermal fluids at elevated temperature play a key role in their transport. Of the metals considered in this thesis, niobium is often used as a reference element, against which the mobility of other elements is compared, tantalum, the geochemical "twin" of niobium, is assumed to be equally difficult to transport, and uranium, known to be highly mobile in oxidizing environments, is deemed to be immobile in reducing systems. Through the use of field-based and experimental studies, this thesis evaluates the actual mobility of these metals and, through qualitative and quantitative means, determines their solubility and speciation.

The behaviour of niobium and tantalum in a hydrothermally altered setting was first described in the Nechalacho rare metal deposit, situated in the Northwest Territories of Canada. Whole rock geochemical data, petrography, and electron microprobe analyses were used to separate the magmatic and hydrothermal components of the behavior of these metals in a deposit that underwent pervasive hydrothermal alteration. Niobium and tantalum were found to be hosted in zircon, columbite-(Fe), fergusonite-(Y), uranopyrochlore and samarskite-(Y) and a genetic model incorporating the magmatic crystallization of these minerals followed by a hydrothermal overprint was proposed to explain their occurrence. Local remobilization of the two metals was observed, but was limited to a sub-meter scale.

Further work was carried out experimentally, in order to determine the solubility and speciation of niobium in solutions containing the ligand most likely to form complexes with this metal, fluoride, at 150, 200, and 250 °C. These experiments, carried out in titanium autoclaves, identified the presence of the species $Nb(OH)_4^+$ at low HF concentration and $NbF_2(OH)_3^\circ$ at high

HF concentration. The presence of the latter hydroxyl-fluoride species increases the solubility of niobium in acidic fluoride-rich solutions, by orders of magnitude. Destabilization of this complex is most easily accomplished through a reduction in the HF concentration of the fluid, for example, by fluid-rock interaction involving carbonate rich formations.

Similar autoclave experiments were carried out with tantalum at 100-250 °C. At low HF concentration $Ta(OH)_5^0$ predominates, whereas at high HF concentration TaF_5, at $\leq$150 °C, and, more commonly, $TaF_3(OH)_3^-$, result in rapid increases in tantalum solubility. However, in the same fluid, tantalum is almost invariably less soluble than niobium. Geochemical modeling of hydrothermal alteration involving acidic brines demonstrated that Nb/Ta ratios may decrease in hydrothermally altered crystals and that removing HF from the fluid, or increasing its pH, result in niobium and tantalum mineral deposition. These experimental data, together with the above observations from the Nechalacho deposit, demonstrate that hydrothermal mobilization of niobium and tantalum is indeed possible, particularly in fluoride-rich acidic systems.

Whereas niobium and tantalum are found predominantly in the 5+ valence state, redox conditions play a major role in the geochemical behavior of uranium. The solubility and speciation of uranium was evaluated at oxidizing and reducing conditions, at 200-350 °C, using autoclave experiments containing redox buffers employed to control oxygen fugacity. The experimental data revealed that the species $UO_2Cl_2^\circ$ dominates at oxidizing conditions and UCl_4° at reducing conditions. Both species increase rapidly in abundance with increasing chloride activity, but UCl_4° does so more rapidly than $UO_2Cl_2^\circ$. Geochemical modelling of an iron-oxide copper gold (IOCG) system, demonstrated that the formation of uranium ore deposits could arise from an influx of reducing fluids, and the long-held belief that uranium is immobile under reducing conditions is unwarranted.

Résumé

Les éléments à champ électrostatique élevé (HFSE, high field strength elements) sont considérés comme étant immobiles dans de nombreux environnements géochimiques, dans lesquels les fluides hydrothermaux de température élevée jouent un rôle important dans leur transport. Parmi les métaux considérés dans cette thèse, le niobium est souvent utilisé comme élément de référence, par rapport auquel la mobilité des autres éléments est comparée; le tantale, le « jumeau » géochimique du niobium, est également considéré comme étant difficile à transporter; et l'uranium, connu pour être particulièrement mobile dans les environnements oxydants, est considéré comme étant immobile dans les systèmes réduits. À l'aide d'observations de terrain et d'études expérimentales, cette thèse évalue la mobilité réelle de ces métaux et, en utilisant des moyens qualitatifs et quantitatifs, détermine leur solubilité et leur spéciation.

Le comportement du niobium et du tantale dans un environnement hydrothermal a été décrit pour la première fois dans le gisement de métaux rares de Nechalacho, situé dans les Territoires du Nord-Ouest du Canada. L'analyse géochimique des roches, la pétrographie et les analyses à la microsonde électronique ont été utilisées pour distinguer les comportements magmatiques et hydrothermaux de ces métaux dans un gisement ayant subi une altération hydrothermale pervasive. Le niobium et le tantale sont portés notamment par le zircon, la colombite-(Fe), la fergusonite-(Y), l'uranopyrochlore et la samarskite-(Y). Un modèle génétique impliquant la cristallisation magmatique de ces minéraux, suivie d'un épisode hydrothermal, a été proposé pour expliquer leur présence. La remobilisation locale de ces deux métaux a été observée, mais est limitée à une échelle inférieure au mètre.

D'autres travaux ont été effectués de façon expérimentale afin de déterminer la solubilité et la spéciation du niobium dans des solutions contenant du fluor, le ligand le plus susceptible de former des complexes avec ce métal, à 150, 200 et 250 °C. Ces expériences, réalisées dans des autoclaves en titane, ont permis d'identifier la présence de l'espèce $Nb(OH)_4^+$ à faible concentration en HF, et de $NbF_2(OH)_3^\circ$ à forte concentration en HF. La présence de cette dernière espèce d'hydroxyl-fluorure augmente de plusieurs ordres de grandeur la solubilité du niobium dans les solutions acides et riches en fluorure. La déstabilisation de ce complexe est le plus facilement obtenue par une réduction de la concentration de HF dans le fluide, par exemple par interaction avec des formations riches en carbonate.

Des expériences similaires ont été réalisées en autoclave pour le tantale, à des températures de 100-250°C. À faible concentration en HF, $Ta(OH)_5^0$ prédomine, alors qu'à une forte concentration en HF, TaF_5 prédomine à des températures moindres que 150 °C, tandis que de façon plus générale, c’est l’espèce $TaF_3(OH)_3^-$ qui domine. Ces deux dernières espèces entraînent une augmentation rapide de la solubilité du tantale. Cependant, dans le même fluide, le tantale est presque toujours moins soluble que le niobium. La modélisation géochimique de l'altération hydrothermale impliquant des saumures acides a démontré que les rapports Nb/Ta peuvent diminuer dans les cristaux altérés hydrothermalement et que l'élimination du HF du fluide ou l'augmentation du pH, entraînent la déposition du niobium et du tantale. Ces données expérimentales ainsi que les observations propres au gisement de Nechalacho démontrent que la mobilisation hydrothermale du niobium et du tantale est en effet possible, en particulier dans les systèmes acides riches en fluorure.

Alors que le niobium et le tantale se trouvent principalement dans l'état de valence 5+, les conditions redox jouent un rôle majeur dans le comportement géochimique de l'uranium. La solubilité et la spéciation de l'uranium ont été évaluées dans des conditions oxydantes et réductrices, entre 200-350 °C, en utilisant des expériences d'autoclave contenant des tampons redox utilisés pour contrôler la fugacité de l'oxygène. Les données expérimentales ont révélé que l'espèce $UO_2Cl_2^\circ$ domine dans les conditions oxydantes et l'UCl_4° dans les conditions réductrices. Les deux espèces augmentent rapidement en abondance avec une activité de chlorure croissante, mais l'UCl_4° le fait plus rapidement que l'$UO_2Cl_2^\circ$. La modélisation géochimique d'un système d'oxyde de fer-cuivre-or (IOCG) a démontré que la formation de gisements d'uranium pouvait provenir de la circulation de fluides réducteurs, et la croyance de longue date que l'uranium est immobile dans des conditions réductrices est en fait injustifiée.

i

Acknowledgements

First and foremost I would like to thank Willy for giving me the opportunity to do research prior to my completing my first year of geology and whose support since has never waned. Without his enthusiasm, insight, stories, and perpetual optimism I would not have pursued nor persevered in my graduate studies. He made this thesis "wild".

Artas Migdisov provided a great deal of support throughout the process of designing and redesigning of numerous experiments and his patience and positive attitude made the setbacks that were eventually overcome a great deal less challenging. I am indebted to him for showing me the ways of an experimentalist.

Lang Shi was instrumental in acquiring data on the electron microprobe and providing assistance regardless of the time of day. André Poirier greatly facilitated the ease with which ICP-MS analyses that were done at UQAM.

The financial support of multiple institutions including NSERC (CGS M, CGS D, and CGS-MSFSS Scholarships), FQRNT (Master's B1 Scholarship), SEG (SEGF Fellowship, Student Research Grant), in addition to the internally awarded Reinhardt C Fellowship and the Seaborg Institute Summer Research Fellowship from the Los Alamos National Laboratory made this research possible and I am sincerely grateful to each of these organizations.

I would also like to thank the staff of Avalon Rare Metals including Bill Mercer, Don Bubar, Martin Heiligmann, and Chris Pedersen for the exceptional access and support provided to me during the collection of samples over multiple field seasons in the Northwest Territories. Each field season's camp crew was a pleasure to work with and made the time fly by.

I am also grateful to every member of the EES-14 team at the Los Alamos National Laboratory, including Bob, Doug, Hakim, Florie, and Hongwu, as well as George Perkins at the ICP-MS, for making my stay at LANL an easy and successful one.

In addition, I am very grateful to David Martineau and Nicolas Gaillard for translating the thesis abstract.

The Earth & Planetary Sciences Department at McGill is unique because of its people and camaraderie. I am grateful to everyone who made it as exciting, educational, and fun as it was, from the ever changing members of the Willy group to the faculty themselves. The support of Anne, Kristy, and Angela was also invaluable and the behind the scenes work of Jim Clark kept my research and that of the Willy group afloat. The craving for cookies I have now acquired will be difficult to overcome.

Last, but certainly not least, a big Спасибо to my parents without whom I would never have been in the position of starting this thesis, much less finishing it.

ii

Table of Contents

iii

List of Figures

---

iv

List of Tables

V

List of Appendices

vi

Preface and Contributions of Authors

This thesis contains four manuscripts, which have been published in peer-reviewed journal. The first manuscript examining the Nechalacho deposit was published in Economic Geology, the second and third manuscripts on niobium and tantalum solubility and speciation, respectively, were published in Geochimica et Cosmochimica Acta and the last manuscript dealing with uranium mobility was published in Nature Communications.

The first manuscript, presented in Chapter 2 was conceived by A.E. Williams-Jones and Alexander Timofeev and the results of this research are presented as a journal manuscript written in accordance with regulations put forth by the Faculty of Graduate Studies and Research, McGill University, which is coauthored by Timofeev and Williams-Jones. Preparation of the manuscript was done by Timofeev with editing by Williams-Jones. The samples used in Chapter 2 were obtained in the summer of 2012 with the assistance of Martin Heiligmann, Chris Pedersen, and Bill Mercer of Avalon Rare Metals. Sample preparation, petrographic examination, and electron microprobe analyses for the manuscript were performed by Timofeev.

The experimental research of Chapter 3 was conducted by Alexander Timofeev in collaboration with Artas A. Migdisov and A.E. Williams-Jones. The experiments were prepared, carried out and refined iteratively in their setup by Timofeev with guidance from Migdisov in the laboratory facilities of McGill University. Analyses of experimental solutions were undertaken by Timofeev in the ICP-MS laboratory of UQAM in Montreal, Canada with the assistance of André Poirier. Michel Preda performed XRD analyses of experimental oxide powders at the

GEOTOP XRD laboratory at UQAM. Subsequent thermodynamic analysis of the experimental data was conducted by Timofeev, under the supervision of Migdisov. The prepared manuscript was written by Timofeev with editing by Migdisov and Williams-Jones. Contributions of those involved in the preparation of the manuscript in Chapter 4 are the same as for Chapter 3.

The study in Chapter 5 was conceived by Artas A. Migdisov and carried out at the radiogeochemistry laboratories of the EES-14 team at the Los Alamos National Laboratory (LANL). Doug Wares and Robert Roback familiarized Alexander Timofeev with the LANL facilities. Timofeev conducted all experiments except for those containing the UO_2 solid at reducing conditions. These were done by Migdisov. The ICP-MS analyses of experimental solutions were done at the EES-14 wet chemistry laboratory with the assistance of George Perkins. The manuscript was prepared by Timofeev, edited by Migdisov and A.E. Williams-Jones, with Roback and Andrew Nelson providing useful comments for the final draft of the manuscript.

Chapter 1

Introduction

1.1 High field strength element (HFSE) geochemistry

The term "high field strength element" (HFSE) refers to elements with small radii, high charges and a corresponding high electric field, or field strength (charge to radius ratio), from which the term is derived. Elements with a *Z/r*, or charge to radius ratio, greater than 2.0, are considered to be high field strength elements. These include the rare earth elements (REE), Ti, V, Zr, Hf, U, Th, Nb, and Ta (Salters 1998). However, in most cases, the HFSE are considered to be distinct from the REE and only the elements Nb, Ta, Zr, Hf, V and Ti are grouped together (e.g., Salters and Shimizu 1988). Moreover, the cut-off *Z/r* value of 2.0 is arbitrary and has no particular geochemical significance.

The high field strength of the HFSE results in their geochemical behavior differing from that of the other elements. Their high charge and field strength preclude their substitution in most rock-forming minerals and, during crystal fractionation, they are progressively enriched in the residual liquid, provided that crystallization of accessory phases such as rutile, which is capable of incorporating the HFSE, is suppressed. The HFSE are also considered to be highly immobile during hydrothermal fluid-rock interaction. Zirconium, niobium, and tantalum are often used as reference elements, against which the concentrations of other elements can be normalized, in order to evaluate mass gains or losses during hydrothermal alteration (MacLean and Barrett 1993). The most common use of the HFSE, in the geochemical literature, is as a differentiator between mid-ocean-ridge basalt (MORB) and basalts formed in island arcs, with the HFSE being depleted in the latter as compared to the former. This depletion is commonly attributed to the retention of the HFSE in the subducting slab due to the presence of a phase such as rutile, or the crystallisation of this phase during the ascent of a magma (Brenan et al. 1994, Kelemen et al. 1990).

Most, if not all, of the HFSE are of economic interest and are concentrated in a variety of deposit types. These deposit types are formed as a direct, or, in some cases, indirect consequence of the mobilization of the metals by high temperature hydrothermal fluids. In the sections that follow, I discuss ore deposits hosting the HFSE and, in particular, niobium, tantalum, and uranium. I then focus on the ways in which the knowledge, or lack thereof, of the solubility and speciation of these elements, in hydrothermal fluids, has contributed to our understanding of these ore deposits and other HFSE-bearing environments.

1.2 Ore deposits enriched in HFSE

As a consequence of their incompatibility in most rock-forming minerals, the HFSE are concentrated in the residual liquid of a crystallizing magma and are enriched in melts produced from small degrees of partial melting. Examples of rocks formed by such processes are alkaline igneous complexes and their associated peralkaline igneous rocks, as well as carbonatites and NYF (Nb-Y-F) and LCT (Li-Cs-Ta) pegmatites. Uranium is associated with these settings, but due to its elevated solubility in oxidized fluids is found in a range of deposit types beyond those just listed, which are discussed further below.

Peralkaline rocks form from the extensive differentiation of melts with low degrees of polymerization. The crystallization of accessory phases capable of removing HFSE from the melt is suppressed until the last stages of crystal fractionation (Linnen and Keppler 1997, Schmitt et al. 2012). Ore bodies associated with peralkaline magmatism are therefore often encountered at the top of mantle-derived magma chambers, in pegmatites, or as small-volume dikes and sills (Hadj-Kaddour et al. 1998, Möller and Williams-Jones 2016, Vasyukova et al. 2016). An intimate association between areas enriched in the HFSE and pervasive hydrothermal alteration is often observed. This alteration, stemming from an exsolved fluid, can remobilize the HFSE, with the LREE in some deposits potentially remobilized on a scale of 100s of meters and the HREE at a smaller scale (Vasyukova et al. 2016).

The spatial association of carbonatites with alkaline or peralkaline igneous rocks is common. The origin of carbonatites is hotly debated, but, as with peralkaline magmas, carbonatites are thought to originate from small degrees of partial melting of an HFSE enriched mantle. The contributions of magma immiscibility and fractional crystallization to carbonatite formation are the source of contention as carbonatites show distinct mantle isotopic signatures and their low viscosity enable them to rise rapidly through the crust (Jones et al. 2013). Carbonatites are not consistent in their HFSE enrichment or depletion, and can exhibit orders of magnitude variations in the concentrations of these elements (Chakhmouradian 2006). However, many carbonatites do contain economic concentrations of HFSE and, as discussed further below, are currently the principal source for the world's niobium. Potassic and sodic metasomatic fluids from carbonatite magmas produce fenitization haloes in the intruded country rocks (Williams-Jones and Palmer 2002).

Two classes of pegmatite, the NYF and LCT pegmatites, are thought to form through extensive igneous differentiation of granitic parent bodies. The NYF and LCT classes are derived from A-type granites and S-type granites, respectively (Černý and Ercit 2005). With the exception of these distinct HFSE associations, the geology of the two classes can be quite similar. The presence of fluxing elements such as B, P, F, and H_2O, in the source that produces the granitic melts, is essential to the formation of these pegmatites, as it is the incorporation of the fluxing elements into the melt that lowers liquidus temperatures, increases the solubility of otherwise compatible elements and allows the HFSE to accumulate to economic concentrations

(Černý et al. 2012, London and Morgan 2012). Whereas NYF pegmatites have not been historically exploited for their niobium content, LCT pegmatites in Brazil, Ethiopia, Mozambique, and other countries are the principal sources of world tantalum production. However, tantalum is not a publicly traded commodity and its primary production is considerably lower than that of niobium (Linnen et al. 2012). The role of fluids in the formation of these pegmatites is still a topic of debate, but they may play an important role in transporting niobium and tantalum in some pegmatites (Thomas et al. 2011, London and Morgan 2012). However, increases in the Ta/(Ta+Nb) and Mn/(Mn+Fe) ratios of columbite group minerals (CGM), with progressive crystal fractionation, in NYF pegmatites, are well established. Differences in the solubility of the Nb and Ta end members of the CGM in the magma and the concentration of Mn in the residual melt, through the crystallization of Fe-rich phases or high fluorine abundances in the melt, are considered to be responsible for this trend (Linnen and Keppler, 1997; Linnen, 1998; Bartels et al., 2010; Wise et al., 2012)

1.2.1 Niobium- and tantalum-bearing ore deposits

The bulk (~90%) of the world's niobium is mined at the Araxá, and Catalão I and II carbonatite complexes in Brazil, with the Araxá complex being by far the largest of the three. Despite their prominence, data on the geology of the Araxá deposit is limited, and the Catalão I and II deposits have only recently been studied. The primary niobium host in these deposits is known to be pyrochlore and weathering likely concentrated the mineralization with an extensive (up to 230 meter thick) laterite developed in the central part of the Barreiro carbonatitic complex of Araxá (Nasraoui and Waerenborgh 2001). A low temperature fluid may have modified the mineralization in the Catalão I deposit, but the mineralization is of magmatic origin (Cordeiro et al. 2011). The remaining ~10% of the world niobium is produced from the Niobec underground mine in Quebec, Canada, which is situated in the Saint-Honoré carbonatite complex (Thivierge et al. 1983, Polyak 2018). Pyrochlore is the main ore mineral and columbite-(Fe) locally replaced it, with fenitization observed in the host Grenvillian diorite and gneiss (Tremblay et al. 2015).

The sources of global tantalum production have varied with time, with the closing and reopening of mines following changes in the production and consumption of tantalum, which can vary widely, due to the small overall size of the tantalum market (less than 2000 tonnes of metal). However, current and past producers of tantalum are situated primarily in LCT pegmatites, or their associated placer deposits, and to a lesser degree in REE-enriched peraluminous granites (Mackay and Simandl 2014). Apart from the ~40 % of the world tantalum production stemming from mining, a further 30 % originates from recycling, 20 % from tin slag refining and 10 % from secondary mine concentrates, as of 2012 (Tantalum-Niobium International Study Center 2018). The introduction of Coltan, or "conflict" columbite-tantalite concentrate, from politically unstable areas of Western and Central Africa, in 1999, greatly destablized the tantalum market and resulted in the eventual closure of the main tantalum producers up until that time, including the Greenbushes (a partial closure, Li production is ongoing as of the writing of this thesis) and Wodgina mines, in Australia, and the Tanco mine, in Canada (Mackay and Simandl 2014).

The Greenbushes mine in Western Australia is situated in a zoned, more than three kilometer long, pegmatite, of Archean age, which has considerable resources of both tantalum and lithium. Metasomatism occured during the initial and final stages of a suggested three stage mineralizing process. In the initial stage, country rocks were metasomatized, whereas in the final stage remobilization of mineralization occured concurrently with deformation and metamorphism (Partington et al. 1995). The Wodgina district further to the north, in the North Pilbara Craton of Western Australia, contains the Wodgina and Mount Cassiterite pegmatite groups, which contain some of the most tantalum-enriched pegmatites among the more than 120 pegmatite deposits of the Pilbara pegmatite field. Tantalum mineralization at the Wodgina deposit is composed of primary tantalite-(Mn) with minor columbite-(Mn) and wodginite, whereas the dominant primary ore mineral at Mount Cassiterite is wodginite (Sweetapple and Collins 2002, Mackay and Simandl 2014). Tantalum mineralization in secondary albite and lepidolite units may indicate tantalum remobilization (Sweetapple and Collins 2002). Another deposit of past significance is the Archean Tanco pegmatite in Manitoba, Canada, which is among the world's largest at ~2 kilometers long, 1 kilometer wide, and up to 100 meters thick (Stilling et al. 2006). Key tantalum minerals in the deposit include columbite group minerals (CGM), microlite, wodginite group minerals and ferrotapiolite. The progressive changes in CGM mineral chemistry with increasing crystal fractionation, discussed above, are observed at Tanco, but secondary Ta-enriched overgrowths on crystals of primary phases suggest a later process affecting the tantalum mineralogy (Van Lichtervelde et al. 2007). The origin of this alteration is attributed to a late melt by Van Lichtervelde et al. (2007). However, Van Lichtervelde et al. (2008) concluded that fine-grained Li and Ta poor micas in the central zone of the deposit crystallized from an aqueous fluid. Despite these micas being Ta poor, relative to neighbouring coarser-grained muscovite, the presence of ~50 ppm Ta in these micas led these authors to suggest that ppm levels of tantalum may have been transported by the aqueous fluid. In addition to these three deposits of note, other pegmatites of economic significance are the Volta Grande and Morrua pegmatites in Brazil and Mozambique, respectively (Mackay and Simandl 2014).

In order to examine the behavior of niobium and tantalum in an environment having experienced considerable hydrothermal alteration a suitable location had to be chosen. Evidence of a considerable enrichment in these two metals sufficient to be expressed by the presence of niobium-tantalum minerals, along with extensive hydrothermal alteration, was necessary. The Nechalacho deposit in the Northwest Territories, Canada, which is a rare earth element (REE), niobium, and tantalum-bearing nepheline syentite-hosted ore deposit, was chosen as it meets both of these criteria.

1.2.1.1 The Nechalacho Layered Suite

The Nechalacho rare metal deposit is situated in the Blachford Lake Intrusive Complex (BLC), which comprises a series of alkaline to peralkaline plutons within the Slave Province of the Canadian Shield. This complex was intruded along the east arm of Great Slave Lake, into Archean mica-schists of the Yellowknife Supergroup at ~ 2.1 Ga, and is one of a number of plume-related alkaline igneous complexes that were emplaced during the final break-up of the Sclavia supercraton (Bleeker and Hall, 2007; Buchan et al. 2010). An age of 2176.0 ± 2.7 has been determined for the Nechalacho Layered Suite, based on U-Pb dating of magmatic zircon (Möller and Williams-Jones, 2016b). An identical age for the surrounding Grace Lake Granite of 2176.2 ± 1.3 Ma, as determined by Sinclair et al. (1994), indicates that the Nechalacho Layered Suite is coeval with the BLC, and its youngest member (Möller and Williams-Jones 2016a).

Following a spike in rare element prices in the early 2010s, arising from concerns regarding possible reductions in REE supplies from China, the world's dominant (>90 %) producer of the REE, the deposit was investigated by Sheard et al. (2012), Möller and Williams-

Jones (2016a), (2016b), and Möller and Williams-Jones (2017). As a result, a more detailed picture of the suite, and the deposit within it, has emerged.

The Nechalacho Layered Suite (NLS) is postulated to have formed through the extraction of an OIB-like melt from a crustal magma chamber containing a mantle-derived mafic melt that underwent crystal fractionation. Neodymium, oxygen, and hydrogen isotope data point to a mantle source for the NLS and the surrounding Grace Lake Granite and Thor Lake Syenite of the BLC, with little to no crustal contamination (Möller and Williams-Jones 2016b). The NLS formed as a dome-shaped body, approximately 1.5 kilometers in diameter, from an evolved melt at temperatures from ~800 to < 500 °C, and crystallized upwards, predominantly as a nepheline syenite, with variable proportions of nepheline, sodalite, aegirine, annite, K-feldspar, and albite. Eudialyte crystallization was initially suppressed, but the magma eventually saturated in kentbrooksite (a eudialyte group mineral) at the top of the magma chamber, which formed the cumulates and layers of the Nechalacho deposit. Other magmatic REE-Nb minerals include fluornatropyrochlore, bastnäsite-(Ce) and fluorbritholite-(Ce) (Möller and Williams-Jones 2016a). The Nechalacho deposit hosts rare earth, niobium, and tantalum mineralization in two main sub-horizontal zones, the Basal Zone and Upper Zone. The heavy rare earth elements (HREE) are more enriched within the Basal Zone than the Upper Zone, making up ≈ 21.5% and 10.1% of the total rare earth abundance, respectively (www.avalonraremetals.com, 2013).

Hydrothermal alteration is particularly intense in and above the Basal Zone, but to a lesser degree, is also found below it. Albitization resulting in the almost complete replacement of the host rock by up to centimeter sized albite is common within the uppermost 50 meters of the deposit (Sheard et al., 2012). Eudialyte is, with the exception of select samples, absent in the deposit and was replaced entirely by zircon and a variety of REE and Nb-bearing minerals. The aegirine nepheline syenite, which hosts the mineralization, was altered to variable proportions of biotite, quartz, magnetite, ankerite, and fluorite, with fresh aegirine and nepheline largely restricted to units below the Basal Zone. Large-scale removal of sodium, and the addition of magnesium accompanied the alteration (Möller and Williams-Jones 2017). In addition, Möller and Williams-Jones (2017) inferred, on the basis of mineral equilibria, that the fluids responsible for the alteration were at 300 °C, mildly reducing, and had a pH from 3.7 to 5.7, with neutralization of their acidity possibly occurring due to fluid-rock interaction. Late stage silicification, illitization, and carbonatization have been noted but, with the exception of carbonatization, did not result in redistribution of HREE (Sheard et al., 2012).

Hydrothermal monazite U-Pb age dates ranging from 1835 to 1871 Ma led Möller and Williams-Jones (2016b) and Möller and Williams-Jones (2017) to conclude that regional hydrothermal fluids during this time period, possibly associated with the nearby Compton Intrusive Suite, were responsible for monazite formation and possibly much of the hydrothermal alteration in the upper portions of the deposit. However, given the available textural evidence, it is unlikely that this conclusion is correct. Whereas hydrothermal alteration in the Basal Zone and its overlying units is pervasive, hydrothermal alteration in the layered nepheline syenites below the Basal Zone, as well as in the surrounding Grace Lake Granite and Thor Lake Syenite, is of much lower intensity. In fact, it is not uncommon to observe a rapid transition, with depth, from a Basal Zone containing pervasively altered eudialyte pseudomorphs to a unit with abundant fresh green aegirine, less than 10 meters below it. It is therefore difficult to reconcile such an observation with the presence of solely a regional fluid, which would not be restricted to the upper reaches of the deposit. In addition, the ease with which monazite ages can be reset has been well documented (e.g. Poitrasson et al. 1996).

1.2.2 Uranium bearing ore deposits

According to the widely used OECD/IAEA classification scheme there are 15 classes of uranium deposits (OECD/NEA-IAEA 2010). Of these, the two most important deposit types for the world's production of uranium, as of 2018, are unconformity-related deposits and sandstone-hosted deposits. Among all the deposit types, unconformity related deposits contain the highest grades and reserves of uranium. Unconformity-related deposits have been the subject of numerous studies, a short summary of which is provided in section 1.2.2.1. Nevertheless, sandstone-hosted deposits are noteworthy, as Kazakhstan has become the world's largest producer of uranium and it is from the Moinkum deposit complex and its sandstone-hosted roll-front systems that this production stems (Kyser 2014).

Sandstone-hosted uranium deposits are formed in medium- to coarse-grained sandstone interbedded with impermeable shale and mustone units. The uranium is mobilized in oxidizing fluids and precipitates as uraninite and coffinite upon contact with reducing agents in the sandstone, which can include carbonaceous material, sulfides, hydrocarbons, and mafic volcanics. The deposits typically contain <0.5 % U, of which the Moinkum deposit is no exception (0.06 % U), and the uranium is often leached using in-situ recovery methods with sulfuric acid. Despite being found on almost every continent and in host rocks ranging in age from the Carboniferous to the Tertiary, sandstone-hosted uranium deposits are often quite similar and the two main sandstone-hosted deposit types are tabular and roll-front deposits (Kyser, 2014).

In addition, some iron-oxide copper gold (IOCG) deposits, which are discussed further below, contain considerable reserves of uranium. However, uranium ore grades in these deposits are low (<0.1 % U) and were these deposits not polymetallic they would be uneconomic. The importance of this deposit class to uranium production is due largely to the discovery of the Olympic Dam U-Cu-Au-Ag deposit, which is the largest (~2,200,000 tonnes U) uranium deposit in the world, but is an outlier among IOCG deposits and derives most of its value from the production of copper, rather than uranium (Kyser, 2014).

1.2.2.1 Unconformity-related uranium deposits

Unconformity-related uranium deposits occur proximal to an unconformity between Archean to Paleoproterozoic metasedimentary basement rocks and the Paleo- to Mesoproterozoic sandstones that overlie this basement. The deposits are typically associated with faults in the basement gneiss and their formation is thought to involve the circulation, and infiltration into faults, of basinal brines at 200-250 °C. Deposits enriched solely in uranium tend to be found more than 50 meters below the unconformity, whereas polymetallic deposits are commonly associated with the sandstones. Two main basins host the majority of known unconformity-related deposits; the Athabasca Basin in Canada and the Kombolgie Basin in Australia (Kyser, 2014).

The generally accepted genetic model of formation for unconformity type deposits involves the circulation of highly saline brines in the sandstone, which break down and transport uranium from detrital minerals such zircon, monazite, and fluor-apatite, of which only zircon now remains (Fayek and Kyser 1997). Upon contact of the basinal brine with reduced basement lithologies, such as a graphite-bearing pelitic gneiss (Hoeve and Sibbald 1978), or its mixing with a rising, reduced basement fluid (Fayek and Kyser 1997), uranium is precipitated as disseminated uraninite grains (Kyser, 2014). Alternatives to, and unresolved issues of, this model, are discussed further in section 1.3.2.1.

1.2.2.2 Iron-oxide copper gold (IOCG) deposits

Deposits fall within the iron-oxide copper gold (IOCG) category on the basis of their magnetite- and hematite-rich nature, along with elevated concentrations of Cu, Au, REE, P, U, Ag, and Co. Not only is their genetic origin debated, but so are the characteristics of the deposits that fall within this group, which in some respects are grouped together more based on their exclusion from other deposit types than as a consequence of a shared mineralogy or genetic origin (Barton 2014).

Hydrothermal fluids of magmatic and meteoric origin, at temperatures ranging from >500 to 200 °C, are considered to have been responsible for the formation of many IOCG deposits, which are can be both magnetite- and hematite-rich. Magnetite-rich ore bodies are thought to form at higher temperature than hematite-rich deposits, with hematite overprints of magnetite being not uncommon (e.g. Bastrakov et al. 2007). However, melt immiscibility may lead to the formation of Fe-rich melts and magnetite rich deposits, such as the El Laco iron oxide deposit in Chile, with a later hydrothermal overprint (Tornos et al. 2017). The largest IOCG deposit, Olympic Dam, formed from the mixing of hot magmatic or deeply circulating meteoric fluids with cooler, oxidized meteoric water at temperatures ≤ 250 °C. The unusual endowment of Olympic Dam in a variety of metals including U may have been a result of this lower temperature of formation, whereby, much as in unconformity related deposits, oxidized meteoric water could have transported Cu, U, and Au to the deposit (Haynes et al. 1995).

Certain IOCG deposits contain elevated concentrations of uranium. For example, uranium mineralization containing up to 1 wt. % U in brecciated albitites is associated with the IOCG NICO deposit, in the Great Bear magmatic zone of Canada. The uranium is inferred to have been transported in reducing fluids at a temperature ≥ 400 °C, before being precipitated due to a reduction in available ligand activity rather than redox processes (Montreuil et al. 2015). This deposit is not alone in having been formed at high temperature, with the Lightning Creek Cu-Au prospect in the U-bearing Cloncurry deposit inferred to have formed at a temperature ≥ 500 °C from a vapor and hypersaline (33-55 wt. % NaCl equiv) brine, which created halos of disseminated magnetite adjacent to magnetite veins (Perring et al. 2000). These reduced, high temperature, and high salinity conditions are considered for their uranium transporting potential in Chapter 5.

1.3 HFSE transport in high temperature aqueous fluids

Of the three elements considered this thesis, only the mobility of oxidized uranium has received significant attention and widespread acceptance. As mentioned in Section 1.1, niobium and tantalum are commonly used as immobile elements against which the abundance of other elements can be compared. Nevertheless, the possibility of transporting uranium as U^{4+}, or even niobium and tantalum as fluoride complexes, has, in limited cases, been proposed (Mercadier et al. 2013, Montreuil et al. 2015, Sheard et al. 2012). Fluoride is the most likely ligand to form complexes with niobium and tantalum on the basis of Pearson's rules, which states that ligands will complex with metals of a similar charge to radius ratio (Pearson, 1963). Niobium, tantalum, and fluorine all have elevated charge to radius ratios. Owing to its abundance in natural systems and moderate charge to radius ratio, chlorine may also play a role in HFSE complexation (Pearson 1963).

Studies designed to determine the solubility and speciation of these three elements, detailed below, have focused on either ligand-free systems, often at temperatures <100 °C, or on systems where parameters such as the oxygen fugacity are poorly constrained or the thermodynamic properties of the solid phase are not known (e.g. Parks and Pohl 1988, Zaraisky et al. 2010). As a result, there are considerable gaps in knowledge with respect to the aqueous behaviour of niobium, tantalum, and uranium.

1.3.1 Niobium and tantalum transport

Previous experimental investigations of the mobility of niobium have been limited to studies of niobium hydroxide complexes in fluoride-free solutions at ambient temperatures (Peiffert et al. 2010, Shock et al. 1997), a qualitative study of the solubility of columbite-tantalite in fluoride bearing solutions at varying redox conditions, temperature (300 to 550 °C), and pressure (50 to 100 MPa) (Zaraisky et al. 2010), a kinetic study examining the dissolution of niobium and tantalum from columbite and tantalite, at a temperature less than 100 °C (Majima et al. 1988), and a hydrometallurgical study investigating the extraction of niobium and tantalum from low grade ores (Wang et al. 2009). A recent synthesis paper by Lukyanova et al. (2017) compares the results from Chapter 2 of this thesis with the higher temperature niobium solubility results of Korzhinskaya and Kotova (2012), Kotova (2012), and Kotova (2014), as well as the lower temperature measurements made by Peiffert et al. (2010). The obscure nature of the journals within which these high temperature data were published made it impossible to include these data for comparison in this thesis, despite this data being a direct high temperature extension to the results presented in Chapter 2.

Of these, the most relevant papers to the experiments presented in this thesis are those of Peiffert et al. (2010) and Zaraisky et al. (2010). The study of Peiffert et al. (2010) concluded that in fluoride-free solutions, at temperatures ≤ 70 °C, niobium hydroxide complexes are responsible for the solubility of niobium and, by extension, the pH of the solution plays a key role in determining the solubility of niobium at these temperatures. These authors considered pH values from ~1 to 9, and the effect of increasing ionic strength, with the latter found to play only a minor role in determining the solubility of Nb_2O_5 (solid). Niobium hydroxide speciation was found to change progressively from the species $Nb(OH)_4^+$ to $Nb(OH)_7^{2-}$ with increasing pH and a solubility minima was reached at a pH of ~4. By contrast, increasingly alkaline ($pH > 7$) conditions were associated with the highest concentrations of dissolved niobium. As the experiments were conducted at temperatures from 10 to 70 °C, Peiffert et al. (2010) provided extrapolations of equilibrium constants (logK) values for each niobium hydroxide species to higher temperatures. The relatively large uncertainties of their data are propagated in the extrapolations. Nevertheless, these extrapolations suggest that three out of the four niobium hydroxide species become more soluble at elevated temperature. Despite the potential to do so, Peiffert et al. (2010) did not compare the results of their study with the data of Shock et al. (1997). This omission is discussed further in Chapter 3.

The study of Zaraisky et al. (2010) addressed the solubility of columbite-(Mn) in solutions containing fluoride- (HF, NaF, KF, and LiF), carbonate- ($NaHCO_3$, Na_2CO_3) and chloride-bearing (HCl) ligands at elevated temperatures (300 to 550 °C) and pressures (50 to 100 Mpa). The concentrations of niobium and tantalum in equilibrium with columbite-(Mn) were found to be greatest in solutions containing HF and were an order of magnitude lower in the presence of HCl. The use of a complex solid, columbite-(Mn), in a poorly constrained system that included various oxygen fugacity buffers, prevents thermodynamic data or equilibrium constants from being derived from these experiments. The qualitative nature of the data, which show that increasing amounts of niobium and tantalum are soluble in progressively more fluoride-rich aqueous solutions, provides a good starting point for future studies addressing niobium-fluoride solubility and speciation. Whereas the study of Peiffert et al. (2010) suggested that the capability of a ligand-free aqueous fluid to transport niobium and tantalum will be quite poor unless it is alkaline, the results of Zaraisky et al. (2010) demonstrate that niobium and tantalum may be mobile in hydrothermal fluids akin to those observed in the Nechalacho deposit. However, the absence of any further data to that presented in these two papers prevents any precise predictions regarding the behavior of niobium and tantalum in hydrothermal environments.

1.3.2 Uranium transport

The solubility and speciation of uranium has been characterized at a variety of conditions. Thermodynamic data at 25 °C for a variety of uranium hydroxide, chloride, fluoride, phosphate, and sulfate species was summarized by Langmuir (1978), and was either measured directly by previous authors or estimated from the thermodynamic data of other species. To obtain thermodynamic data of these species at temperatures up to 200 °C, Lemire and Tremaine (1980) used an entropy extrapolation to derive Gibbs free energies and equilibrium constants for their formation. However, limited high temperature data along with the numerous assumptions by Lemire and Tremaine (1980) made the accuracy of these extrapolations highly uncertain. Recent work at 25-70 °C by Tian and Rao (2009) on U(VI)-F complexes and at 25 °C by Sanding and Bruno (1992) on U(VI)-PO_4 complexes may improve the quality of the data for these species. Nevertheless, stability constants for uranium complexes should be considered speculative above 25 °C, with the exception of those for U-OH complexes, which are relatively well characterized.

Studies of U^{4+} speciation have been restricted to investigations of U^{4+} hydrolysis. However, the oxygen fugacity in these studies was poorly constrained. Experiments at ambient temperature by Rai et al. (1990) identified the U^{4+} and UOH_3^+ species and may have been conducted at relatively constant oxygen fugacity as the authors stated that they employed either Fe powder or Eu^{2+} to maintain low oxygen fugacity. They also proposed the presence of UOH_4^0 at pH values above 4, but were uncertain as to whether U^{4+} or U^{6+} was responsible for its dissolution. Equilibrium constants for the formation of the U^{4+} and UOH_4^0 species from UO_2^{cryst} were derived at 25 °C by Casas et al. (1998), who purged solutions continuously with hydrogen and maintained "nominally reducing conditions". A similar uranium hydroxide speciation scheme at temperatures from 100 to 300 °C was proposed by Parks and Pohl (1988), who maintained reducing conditions with 50 MPa H_2.

Owing to weight percent concentrations of chloride ions in settings ranging from those of unconformity-related uranium deposits to seawater, recent attempts have been made to characterize U-Cl species in oxidizing solutions at elevated (> 100 °C) temperature, using spectroscopic methods. Raman spectra were collected by Dargent et al. (2013) in solutions containing up to 12 M LiCl and at temperatures up to 350 °C. Five U-Cl species, from UO_2Cl^- to $UO_2Cl_5^{3+}$, were fitted to the data and increasing temperature was correlated to the stability of U-Cl species containing increasing numbers of chloride ions (e.g. $UO_2Cl_5^{3+}$). By contrast, Migdisov et al. (2018) conducted in-situ spectroscopic measurements of uranium-bearing solutions with up to 1.5 molal NaCl, at temperatures of 25-250 °C, and did not detect the presence of $UO_2Cl_4^{2-}$ or $UO_2Cl_5^{3-}$ in their experiments. The data of Migdisov et al. (2018) suggest the predominance of $UO_2Cl_2^0$ at temperatures above 150 °C, with the only other recognized U-Cl species being UO_2Cl^+, although the authors noted that $UO_2Cl_3^-$ may be present at higher chloride acitivity, but was not in sufficient abundance in their experiments to be recognized. The discrepancy between the results of these two studies is attributed by Migdisov et al. (2018) to the use of an activity model by Dargent et al. (2013) that may be inaccurate for highly concentrated LiCl solutions.

The only study that has investigated U-Cl speciation through direct solubility experiments is that of Richard et al. (2012). They conducted experiments at 155 °C with solid $UO_3(H_2O)_n$ in solutions of variable pH (2.9 to 8) and chloride concentration (1 to 12 molal). Concentrations of dissolved uranium in the solution reached ppm levels at acidic, $pH < 4$, conditions. The authors noted the similarity of the uranium concentrations of their acidic experiments to those measured directly in fluid inclusions from unconformity related deposits in the Athabasca basin. However, the U-Cl species responsible for this solubility of uranium were not identified and no thermodynamic data were derived. In addition, the experiments were conducted over a period of four to six months, with the pH of each experiment, following quenching, readjusted every two weeks. This cycle of quenching and reheating could cause an overestimation of uranium solubility.

1.3.2.1 Uranium mobilization in unconformity related deposits

The circulation of oxidized basinal brines is considered to be necessary for the formation of unconformity related uranium deposits, as discussed in section 1.2.2.1. In their summary of this class of deposits Kyser (2014) proposed two end-member models for their formation. In one, the sandstone-bearing basin is the source of both the fluids and uranium responsible for forming the deposits. In the other, oxidized basinal brines inflitrate the basement, which functions as the source of uranium for the mineralization. However, whereas Kyser (2014) present these end-member models on an equal footing, the literature dealing with unconformity-related deposits overwhelmingly favors the former model. Moreover, the suggestion that reducing fluids in the basement rocks could have transported some of the uranium to the site of formation of some of these ore deposits has never been considered.

Some observations made of unconformity-related deposits are difficult to reconcile in the absence of uranium transport in the basement rocks, possibly under reducing conditions. The first is that whereas detrital heavy minerals, with the exception of zircon, are absent in the Athabasca Group sandstone, formerly U-bearing monazite is common in the underlying basement rocks. In addition, detrital uranium oxides in the Athabasca Group would have been unlikely to be present owing to the oxidizing conditions and lack of organic matter in the sandstone (Jefferson et al. 2007). The second observation is that monazite in the basement rocks is commonly altered with more than 75% of its uranium remobilized (e.g. Hecht and Cuney 2000). In addition, widespread magmatic uranium oxides associated with granitic pegmatites, leucogranites, and high temperature veins have been documented in the basement rocks in the eastern part of the Athabasca Basin. Their origin is suggested to be a result of the melting of Wollaston Group metasedimentary rocks. Despite them being located far from any known unconformity-related deposits, and the rocks macroscopically not showing visible signs of alteration, uranium oxides show evidence of dissolution and alteration by percolating brines (Mercadier et al. 2013). Furthermore, dense networks of microfractures in basement lithologies away from major faults resulted in the interaction of brines with considerable volumes of the basement rock (Mercadier et al. 2010).

1.3.2.2 Nuclear reactor uranium remobilization

In the event of a catastrophic nuclear accident, such as that at the Fukushima power plant, knowledge of the mobility of uranium is crucial towards understanding the scale over which uranium could be dispersed following contact with aqueous fluids, or, as in the case of Fukushima, with seawater. A buildup of hydrogen gas causing reducing conditions is expected to limit uranium migration in such an accident. However, the extent of the reducing conditions that could be maintained in the presence of oxygenated seawater is unclear. Regardless of the oxygen fugacity of the fluid, temperatures in such an accident can exceed 1000 °C, and at these elevated temperatures the thermodynamic properties of uranium species are unknown, thereby preventing the behavior of uranium from being accurately predicted (Burns et al. 2012, Grambow and Poinssot 2012).

Moreover, whereas uranium in reactor fuel rods is not expected to come in contact with water during normal reactor operations, which in typical pressurized water reactors is at ~300 C, defects in fuel rod cladding produced during fabrication, as a result of transport and handling, after removal from the reactor, or simply due to intrinsic material flaws, could cause such contact to occur (Croucher 1980).

1.3.2.3 Nuclear waste repositories

The behaviour of uranium in aqueous fluids is of importance to the long term viability of nuclear waste repositories, as it is essential that, in the event of a repository containment failure, the dispersion of radionuclides is kept to a minimum. For example, the French CIGEO repository, in clay rock formations, is expected to have its stainless steel canisters breached by water, albeit after thousands of years (Grambow and Bretesché 2014). Among the most commonly cited ways of inhibiting radionuclide migration upon contact between water and high-level radioactive waste is the presence of reducing conditions. At the Swedish Forsmack repository, hosted in granitic bedrock, it is assumed that the ceramic uranium oxide waste matrix composed of uraninite would be stable under reducing conditions (Hedin and Olsson 2016).

However, the temperature of fluids in contact with uranium-bearing waste, were they to infiltrate the repository, is not expected to exceed 150 °C, even during the beginning of the life of the repository, at which time the waste would be expected to be hottest (e.g., Berlepsch and Haverkamp 2016). In fact, the spacing of heat-generating waste-bearing canisters in the Forsmack and CIGEO repositories is expected to limit maximum temperatures in the country rocks to 100 and 90 °C, respectively (Grambow 2016, Hedin and Olsson 2016) This low temperature, and the associated low solubility of the UCl_4^0 species identified in Chapter 5, preclude us from applying the results of this thesis directly to this setting.

1.4 Objectives

The objective of this thesis is to considerably extend the range of conditions over which the solubility, speciation, and aqueous behaviour of niobium, tantalum, and uranium can be accurately predicted. From the above summary of the geochemistry of these elements, it is clear that this objective has not yet been met. Niobium and tantalum were selected, among the HFSE, due to their common use as immobile reference elements, and because of the sparse nature of experimental data addressing their speciation. Uranium, particularly in its reduced form, was chosen due to the numerous settings, outlined above, ranging from ore deposits to nuclear reactors, to which the results of a solubility and speciation study would be directly applicable. Furthermore, reduced uranium solubility was examined so as to critically evaluate the long-held assumption that uranium must be immobile in its reduced state. Strong evidence to the contrary would be necessary to challenge this ingrained belief.

To investigate the solubility and speciation of niobium and tantalum, complementary field-based and experimental studies were conducted so as to evaluate the validity of the results of each study via comparison with the other. The site chosen for examining niobium in the field was the Nechalacho Layered Suite, which, unlike the well-studied niobium-bearing NYF (Nb-Y-F) pegmatites, has experienced significant hydrothermal alteration and was known to contain a significant proportion of its niobium mineralization in secondary minerals, with the possibility of niobium remobilization having taken place (Sheard et al. 2012). As a result, the goal of the field-based study, presented in Chapter 2, was to develop a genetic model for niobium and tantalum mineralization in the Nechalacho Layered Suite and to determine the extent and scale over which niobium and tantalum remobilization may have taken place.

Whereas qualitative evidence regarding the mobility of niobium and tantalum was obtained from the field based study, the objectives of the two subsequent experimental studies were to characterize the exact species responsible for mobilizing niobium and tantalum in an HF-bearing aqueous solution. These data allow for an evaluation of whether the experimental solubility of niobium and tantalum are of sufficient magnitude as to be responsible for the remobilization of these elements in an ore deposit setting.

The aim of the uranium experimental research, presented in Chapter 5, was to obtain experimental data through the autoclave solubility method on the U-Cl species present at oxidizing and reducing conditions in an acidic brine, at temperatures of 250-350 °C. This would allow comparison with the spectroscopic study of Migdisov et al. (2018) and the species responsible for uranium transport under reducing conditions to be identified.

1.5 Organization of thesis

This thesis is organized into six chapters. The first, introductory chapter outlines the objectives of the thesis and includes a review of the geochemical literature pertinent to the subsequent chapters. The second through fifth chapters have been written in the form of manuscripts. The second chapter was published in Economic Geology, the third and fourth chapters were published in Geochimica et Cosmochimica Acta and the last chapter was published in Nature Communications. These are followed by the sixth chapter that summarizes the major conclusions of the thesis and potential avenues of future research.

1.6 References

Avalon Rare Metals Inc. News Release No. 13-07, August 15, 2003 (http://avalonraremetals.com/_resources/news/2013/NR_13_07.pdf).

Bartels A., Holtz F. and Linnen R. L. (2010) Solubility of manganotantalite and manganocolumbite in pegmatitic melts. *Am. Mineral.* **95**, 537-544.

Barton M. D. (2014) Iron Oxide(–Cu–Au–REE–P–Ag–U–Co) Systems. In *Treatise on Geochemistry 2nd Edition*, H. Holland, K. Turekian, Ed. (Oxford: Elsevier, 2014), 515-541.

Bastrakov E. N., Skirrow R. G. and Davidson G. J. (2007) Fluid Evolution and Origins of Iron Oxide Cu-Au Prospects in the Olympic Dam District, Gawler Craton, South Australia. *Econ. Geo.* **102**, 1415-1440.

Berlepsch T. and Haverkamp B. (2016) Salt as a host rock for the geological repository for nuclear waste. *Elements* **12**, 257-262.

Bleeker W. and Hall B. (2007) The Slave Craton: geology and metallogenic evolution. Mineral Deposits of Canada: A Synthesis of Major Deposit-Types, District Metallogeny, the

Evolution of Geological Provinces, and Exploration Methods. Geological Association of Canada, Mineral Deposits Division, Special Publication **5**, 849-879.

Brenan J. M., Shaw H. F., Phinney D. L. and Ryerson F. J. (1994) Rutile-aqueous fluid partitioning of Nb, Ta, Hf, Zr, U and Th: implications for high field strength element depletions in island-arc basalts. *Earth Planet Sci. Lett.* **128**, 327-339.

Buchan K., Ernst R., Bleeker W., Davis W., Villeneuve M., van Breemen O., Hamilton M. and Söderlund U. (2010) Proterozoic magmatic events of the Slave craton, Wopmay orogen and environs. Geological Survey of Canada, Open File 5985.

Burns P. C., Ewing R. C. and Navrotsky A. (2012) Nuclear Fuel in a Reactor Accident. *Science* **335**, 1184-1188.

Casas I., De Pablo J., Giménez J., Torrero M. E., Bruno J., Cera E., Finch R. J. and Ewing R. C. (1998) The role of pe, pH, and carbonate on the solubility of UO_2 and uraninite under nominally reducing conditions. *Geochim. Cosmochim. Acta* **62**, 2223-2231.

Černý P. and Ercit T. S. (2005) The classification of granitic pegmatites revisited. *Can. Mineral.* **43**, 2005-2026.

Černý P., London D. and Novák M. (2012) Granitic pegmatites as reflections of their sources. *Elements* **8**, 289-294.

Chakhmouradian A. R. (2006) High-field-strength elements in carbonatitic rocks: Geochemistry, crystal chemistry and significance for constraining the sources of carbonatites. *Chem. Geo.* **235**, 138-160.

Cordeiro P. F., Brod J. A., Palmieri M., Oliveira C. G., Barbosa E. S. R., Santos R. V., Gaspar J. C. and Assis L. C. (2011) The Catalão I niobium deposit, central Brazil: resources, geology and pyrochlore chemistry. *Ore Geol. Rev.* **4**, 112–121.

Croucher D. W. (1980) Behavior of defective pressurized water reactor fuel rods during power ramp and power-cooling-mismatch conditions. *Nucl. Technol.* **195**, 111-123.

Dargent M., Dubessy J., Truche L., Bazarkina E. F., Nguyen-Trung C. and Robert P. (2013) Experimental study of uranyl(VI) chloride complex formation in acidic LiCl aqueous solutions under hydrothermal conditions (T = 21 °C-350 °C, Psat) using Raman spectroscopy. *Eur. J. Mineral.* **25**, 765-775.

Fayek M. and Kyser T. K. (1997) Characterization of multiple fluid-flow events and rare earth-element mobility associated with formation of unconformity-type uranium deposits in the Athabasca Basin, Saskatchewan. *Can. Mineral.* **35**, 627–658.

Grambow B. and Poinssot C. (2012) Interactions between nuclear fuel and water at the Fukushima Daiichi reactors. *Elements* **8**, 213-219.

Grambow B. and Bretesché S. (2014) Geological disposal of nuclear waste: II. From laboratory data to the safety analysis – Addressing societal concerns. *Appl. Geochem.* **49**, 247-258.

Grambow B. (2016) Geological disposal of radioactive waste in clay. *Elements* **12**, 239-245.

Hadj-Kaddour Z., Liégeois J.-P., Demaiffe D. and Caby R. (1998) The alkaline–peralkaline granitic post-collisional Tin Zebane dyke swarm (Pan-African Tuareg shield, Algeria): prevalent mantle signature and late agpaitic differentiation. *Lithos* **45**, 223-243.

Haynes D. W., Cross K. C., Bills R. T. and Reed M. H. (1995) Olympic Dam ore genesis: a fluid-mixing model. *Econ. Geo.* **90**, 281-307.

Hecht L. and Cuney M. (2000) Hydrothermal alteration of monazite in the Precambrian crystalline basement of the Athabasca Basin (Saskatchewan, Canada): implications for the formation of unconformity-related uranium deposits. *Miner. Depos.* **35**, 791-795.

Hedin A. and Olsson O. (2016) Crystalline rock as a repository for Swedish spent nuclear fuel. *Elements* **12**, 247-252.

Jefferson C. W., Thomas D. J., Gandhi S. S., Ramaekers P., Delaney G., Brisbin D., Cutts C., Quirt D., Portella P., and Olson R. A. (2007) Unconformity associated uranium deposits of the Athabasca Basin, Saskatchewan and Alberta. In Goodfellow W. D., ed., Mineral Deposits of Canada: A Synthesis of Major Deposit-Types, District Metallogeny, the Evolution of Geological Provinces, and Exploration Methods: Geological Association of Canada, Mineral Deposits Division, Special Publication No. 5, 273-305.

Jones A. P., Genge M., Carmody L. (2013) Carbonate Melts and Carbonatites. *Rev. Mineral. Geochem.* **75**, 289-322.

Kelemen P. B., Johnson K. T. M., Kinzler R. J. and Irving A. J. (1990) High-field-strength element depletions in arc basalts due to mantle–magma interaction. *Nature* **345**, 521-524.

Korzhinskaya V.S. and Kotova N.P. (2012) Experimental modeling of possibility of hydrothermal niobium transport by fluid solutions. *Vestn. Otd. Nauk Zemle Ross. Akad. Nauk* **4**, NZ9001.

Kotova N.P. (2012) Experimental study of concentration dependence of solubility of niobium oxide in fluoride solutions at T = 550°C, P = 1000 bar and low oxygen fugacity (buffer Co–CoO). *Vestn. Otd. Nauk Zemle Ross. Akad. Nauk* **4**, NZ9001.

Kotova N.P. (2014) Experimental study of Nb_2O_5 solubility in fluoride solutions at T = 550°C and P = 500 bar. *Eksp. Geokhim.* **2**, 319–321.

Kyser K. (2014) Uranium Ore Deposits. In *Treatise on Geochemistry 2nd Edition*, H. Holland, K. Turekian, Ed. (Oxford: Elsevier, 2014), 489-512.

Langmuir D. (1978) Uranium solution-mineral equilibria at low temperatures with applications to sedimentary ore deposits. *Geochim. Cosmochim. Acta* **42**, 547-569.

Lemire R. J. and Tremaine, P. R. (1980) Uranium and plutonium equilibria in aqueous solutions to 200 °C. *J. Chem. Eng. Data* **25**, 361-370.

Linnen R. L. (1998) The Solubility of Nb-Ta-Zr-Hf-W in Granitic Melts with Li and Li + F: Constraints for Mineralization in Rare Metal Granites and Pegmatites. *Econ. Geo.* **93**, 1013-1025.

Linnen R. L. and Keppler H. (1997) Columbite solubility in granitic melts: Consequences for the enrichment and fractionation of Nb and Ta in the Earth's crust. *Contributions Mineral. Petrol.* **128**, 213–227.

Linnen R. L., Van Lichtervelde M. and Černý P. (2012) Granitic pegmatites as sources of strategic elements. *Elements* **8**, 275-280.

London D. and Morgan G.B. V.I. (2012) The pegmatite puzzle. *Elements* **8**, 263-268.

Lukyanova E. V., Akinfiev N. N., Zotov A. V., Rass I. T., Kotova N. P. and Korzhinskaya V. S. (2017) Niobium in hydrothermal systems related to alkali granites: Thermodynamic description of hydroxo and hydroxofluoride complexes. *Geol. Ore Deposits* **59**, 305-314.

Mackay D. A. R. and Simandl G. J. (2014) Geology, market and supply chain of niobium and tantalum—a review. *Miner. Deposita* **49**, 1025-1047.

MacLean W. H. and Barrett T. J. (1993) Lithogeochemical techniques using immobile elements. *J. Geochem. Explor.* **48**, 109-133.

Majima H., Awakura Y., Mashima M. and Hirato T. (1988) Dissolution of columbite and tantalite in acidic fluoride media. *Metall. Trans. B* **19**, 355-363.

Mercadier J., Richard A., Boiron M.-C., Cathelineau M. and Cuney M. (2010) Migration of brines in the basement rocks of the Athabasca Basin through microfracture networks (P-Patch U deposit, Canada). *Lithos* **115**, 121-136.

Mercadier J., Annesley I. R., McKechnie C. L., Bogdan T. S. and Creighton S. (2013) Magmatic and metamorphic uraninite mineralization in the western margin of the Trans-Hudson orogen (Saskatchewan, Canada): A uranium source for unconformity-related deposits?. *Econ. Geo.* **108**, 1037-1065.

Migdisov A. A., Boukhalfa H., Timofeev A., Runde W., Roback R. and Williams-Jones A.E. (2018) A spectroscopic study of uranyl speciation in chloride-bearing solutions at temperatures up to 250 °C. *Geochim. Cosmochim. Acta* **222**, 130-145.

Möller V. and Williams-Jones A.E. (2016a) Petrogenesis of the Nechalacho Layered Suite, Canada: magmatic evolution of a REE-Nb-rich nepheline syenite intrusion. *J. Petrol.* **57**, 229–276.

Möller V. and Williams-Jones A.E. (2016b) Stable and radiogenic isotope constraints on the magmatic and hydrothermal evolution of the Nechalacho Layered Suite, northwest Canada. *Chem. Geo.* **440**, 248–274.

Möller V. and Williams-Jones A.E. (2017) Magmatic and Hydrothermal Controls on the Mineralogy of the Basal Zone, Nechalacho REE-Nb-Zr Deposit, Canada. *Econ. Geo.* **112**, 1823-1856.

Montreuil J.-F., Corriveau L. and Potter, E. G. (2015) Formation of albitite-hosted uranium within IOCG systems: the Southern Breccia, Great Bear magmatic zone, Northwest Territories, Canada. *Miner. Deposita* **50**, 293-325.

Nasraoui M. and Waerenborgh J. C. (2001) Fe Speciation in Weathered Pyrochlore-Group Minerals from the Lueshe and Araxa (Barreiro) carbonatites by ^{57}Fe Mossbauer Spectroscopy. *Can. Mineral.* **39**, 1073-1080.

OECD/NEA-IAEA (2010) Uranium 2009: Resources, Production and Demand (the Red Book). Paris: Organisation for Economic Co-operation and Development.

Parks G. A. and Pohl D. C. (1988) Hydrothermal solubility of uraninite. *Geochim. Cosmochim. Acta* **52**, 863-875.

Partington G. A. and McNaughton N. J. (1995) A Review of the Geology, Mineralization, and Geochronology of the Greenbushes Pegmatite, Western Australia. *Econ. Geo.* **90**, 616-635.

Pearson R. G. (1963) Hard and Soft Acids and Bases. *J. Am. Chem. Soc.* **85**, 3533-3539.

Perring C. S., Pollard P. J., Dong G., Nunn A. J. and Blake K. L. (2000) The Lightning Creek sill complex, Cloncurry District, northwest Queensland: a source of fluids for Fe oxide Cu–Au mineralisation and sodic–calcic alteration. *Econ. Geo.* **95**, 1067 – 1089.

Peiffert C., Nguyen-Trung C., Palmer D. A., Laval J. P. and Giffaut E. (2010) Solubility of B-Nb_2O_5 and the Hydrolysis of Niobium(V) in Aqueous Solution as a Function of Temperature and Ionic Strength. *J. Solution. Chem.* **39**, 197-218.

Poitrasson F., Chenery S. and Bland D. J. (1996) Contrasted monazite hydrothermal alteration mechanisms and their geochemical implications. *Earth Planet. Sci. Lett.* **145**, 79–96.

Polyak D. E. (2018) Niobium (Columbium). In: United States Geological Survey, Mineral Commodity Summaries 2018, 110-111.

Rai D., Felmy A. R. and Ryan J. L. (1990) Uranium(IV) hydrolysis constants and the solubility product of $UO_2{\cdot}xH_2O$(am). *Inorg. Chem.* **29**, 260-264.

Richard A., Rozsypal C., Mercadier J., Banks D. A., Cuney M., Boiron M.-C. and Cathelineau M. (2012) Giant uranium deposits formed from exceptionally uranium-rich acidic brines. *Nature Geosci.* **5**, 142-146.

Salters V. J. M. and Shimizu N. (1988) World-wide occurrence of HFSE-depleted mantle. *Geochim. Cosmochim. Acta* **52**, 2177-2182.

Salters V. J. M. (1998) Elements: High field strength. In: Geochemistry. Encyclopedia of Earth Science. Springer, Dordrecht.

Sanding A. and Bruno J. (1992) The solubility of $(UO_2)_3(PO_4)_2 \cdot 4H_2O(s)$ and the formation of U(VI) phosphate complexes: Their influence in uranium speciation in natural waters. *Geochim. Cosmochim. Acta* **56**, 4135-4145

Schmitt A. K., Trumbull R. B., Dulski P. and Emmermann R. (2002) Zr-Nb-REE Mineralization in Peralkaline Granites from the Amis Complex, Brandberg (Namibia): Evidence for Magmatic Pre-enrichment from Melt Inclusions. *Econ. Geo.* **97**, 399-413.

Sheard E.R., Williams-Jones A.E., Heiligmann M., Pederson C. and Trueman D.L. (2012) Controls on the Concentration of Zirconium, Niobium, and the Rare Earth Elements in the Thor Lake Rare Metal Deposit, Northwest Territories, Canada. *Econ. Geo.* **107**, 81-104.

Shock E. L., Sassani D. C., Willis M. and Sverjensky D. A. (1997) Inorganic species in geologic fluids: correlations among standard molal thermodynamic properties of aqueous ions and hydroxide complexes. *Geochim. Cosmochim. Acta* **61**, 907-950.

Sinclair W. D., Hunt P. A. and Birkett T.C. (1994) U-Pb zircon and monazite ages of the Grace Lake Granite, Blatchford Lake Intrusive Suite, Slave Province, Northwest Territories. *In* Radiogenic Age and Isotopic Studies: Report 8; Geological Survey of Canada, Current Research 1994-F, 15-20.

Sweetapple M. T. and Collins P. L. F. (2002) Genetic Framework for the Classification and Distribution of Archean Rare Metal Pegmatites in the North Pilbara Craton, Western Australia. *Econ. Geo.* **97**, 873-895.

Tantalum-Niobium International Study Center (2018) Tantalum (Ta) – Production of raw materials. https://tanb.org/about-tantalum/production-of-raw-materials. Accessed 21 Feb 2018.

Thivierge S., Roy D.-W., Chown E. H. and Gauthier A. (1983) Évolution du complexe alcalin de St.-Honoré (Québec) après sa mise en place. *Mineral. Depos.* **18**, 267-283.

Thomas R., Davidson P. and Beurlen H. (2011) Tantalite-(Mn) from the Borborema Pegmatite Province, northeastern Brazil: conditions of formation and melt- and fluid-inclusion constraints on experimental studies. *Mineral. Depos.* **46**, 749-759.

Tian G. and Rao L. (2009) Effect of Temperature on the Complexation of Uranium(VI) with Fluoride in Aqueous Solutions. *Inorg. Chem.* **48**, 6748-6754.

Tornos F., Velasco F. and Hanchar J. M. (2017) The Magmatic to Magmatic-Hydrothermal Evolution of the El Laco Deposit (Chile) and Its Implications for the Genesis of Magnetite-Apatite Deposits. *Econ. Geo.* **112**, 1595-1628.

Tremblay J., Bédard L. P. and Matton G. (2015) A petrographic study of Nb-bearing minerals at the Saint-Honoré niobium deposit. In: Simandl G. J. and Neetz M., (Eds.), Symposium on Strategic and Critical Materials Proceedings, November 13-14, 2015, Victoria, British Columbia. British Columbia Ministry of Energy and Mines, British Columbia Geological Survey Paper 2015-3, 75-81.

Van Lichtervelde M., Salvi S. and Béziat D. (2007) Textural features and chemical evolution in tantalum oxides: magmatic versus hydrothermal origins for Ta mineralization in the Tanco Lower Pegmatite, Manitoba, Canada. *Econ. Geol.* **102**, 257-276.

Van Lichtervelde M., Grégoire M., Linnen R. L., Béziat D. and Salvi S. (2008) Trace element geochemistry by laser ablation ICP-MS of micas associated with Ta mineralization in the Tanco pegmatite, Manitoba, Canada. *Contrib. Mineral. Petrol.* **155**, 791-806.

Vasyukova O. V., Williams-Jones A. E. and Blamey N. J. F. (2016) Fluid evolution in the Strange Lake granitic pluton, Canada: Implications for HFSE mobilisation. *Chem. Geo.* **444**, 83-100.

Wang X., Zheng S., Xu H. and Zhang Y. (2009) Leaching of niobium and tantalum from a low-grade ore using a KOH roast-water leach system. *Hydrometallurgy* **98**, 219-223.

Williams-Jones A. E. and Palmer D. A. S. (2002) The evolution of aqueous-carbonic fluids in the Amba Dongar carbonatite, India: implications for fenitisation. *Chem Geo.* **185**, 283-301.

Wise M. A., Francis C. A. and Černý P. (2012) Compositional and Structural Variations in Columbite-Group Minerals from Granitic Pegmatites of the Brunswick and Oxford Fields, Maine: Differential Trends in F-poor and F-rich Environments. *Can. Mineral.* **50**, 1515-1530.

Zaraisky G. P., Korzhinskaya V. and Kotova N. (2010) Experimental studies of Ta_2O_5 and columbite-tantalite solubility in fluoride solutions from 300 to 550°C and 50 to 100 MPa. *Miner. Petrol.* **99**, 287-300.

Preface to Chapter 2

The introduction to high field strength element (HFSE) behaviour, presented in Chapter 1, demonstrates our poor understanding of the mobility of a number of the HFSE, in hydrothermal fluids. Niobium and tantalum are considered to be especially difficult to transport. In particular, previous research has focused on the mechanisms by which niobium and tantalum can be concentrated to economic concentrations, by magmatic processes. However, it has been assumed that niobium and tantalum are immobile in hydrothermal fluids and field and experimental evidence supporting or disputing this assumption is sparse.

In the following chapter, we examine the behaviour of niobium in the world-class Nechalacho rare earth element deposit, the niobium-rich ore zones of which have undergone pervasive hydrothermal alteration. In addition, we compare the niobium mineralogy in the altered sections of the deposit with that of the syenites below the main ore body, which have experienced little to no alteration,. In doing so, we evaluate the mobilility of this metal in a setting that seemingly is highly favorable to the transport of niobium, with abundant fluorite indicating the presence of fluoride-rich fluids. Through the use of petrography, mineralogy, and electron-microprobe analyses, we develop a genetic model explaining the origin of niobium and tantalum mineralization in the Nechalacho deposit.

Chapter 2

The Origin of Niobium and Tantalum Mineralization in the Nechalacho REE deposit, NWT, Canada

ALEXANDER TIMOFEEV[1] AND A.E. WILLIAMS-JONES

Department of Earth & Planetary Sciences, McGill University, 3450 University Street, Montreal, QC, Canada, H3A 0E8

[1] alexander.timofeev@mail.mcgill.ca

Published in Economic Geology, November 2015

DOI: https://doi.org/10.2113/econgeo.110.7.1719

Abstract

The behaviour of niobium and tantalum is poorly understood in rocks that have undergone significant hydrothermal alteration, and niobium-tantalum minerals of hydrothermal origin are rarely mentioned in the literature. Consequently, the mobility of these critical metals, although widely considered to be negligible, has not been evaluated. In this paper, we present the results of a study of the genesis of niobium and tantalum mineralization in the Nechalacho rare metal deposit, Northwest Territories, Canada, which contains one of the largest known resources of these metals in rocks that have undergone intense hydrothermal alteration.

Analyses and examination of samples using the electron microprobe has led to the identification of a variety of niobium- and tantalum-bearing minerals in the Nechalacho deposit. Niobium-bearing zircon, columbite-(Fe), fergusonite-(Y), and samarskite-(Y) were identified in the ore zones of the deposit, uranopyrochlore, and columbite-(Fe) were found outside the ore zones, and magmatic fluornatropyrochlore was shown to be the sole niobium-tantalum mineral in relatively unaltered syenites below the Basal Ore Zone.

Based on the paragenetic relationships among the above minerals, variations in the composition of the columbite group minerals (CGM) as a function of location in the Nechalacho Layered Suite and the distribution of niobium, tantalum, zirconium and uranium in the bulk rocks, we have developed a model to explain the occurrence of niobium and tantalum in the Nechalacho deposit. The first step in the concentration of these elements was the crystallization of niobium- and tantalum-bearing zircon and eudialyte in the sub-horizontal Upper and Basal ore zones, respectively. This was accompanied by the crystallization of magmatic columbite-(Fe) in the Upper Ore Zone. Fergusonite-(Y) crystallized in the Basal Ore Zone and also formed due to the breakdown of eudialyte. Outside the ore zones, there was crystallization of pyrochlore and to

a lesser extent magmatic columbite-(Fe). This step led to the development of strong spatial associations among niobium, zirconium, and uranium that are evident as strong positive correlations in the bulk rock concentrations of these elements at the meter scale. During the ensuing intense and widespread hydrothermal alteration, niobium was locally remobilized. Hydrothermal columbite-(Fe) and fergusonite-(Y) formed at the cores of altered zircon grains. Wholesale replacement of magmatic columbite-(Fe) and fergusonite-(Y) by hydrothermal anhedral crystals occurred in the two ore zones. The estimated relative proportions of the sources of these minerals in the ore zones, although varying to some extent because of a dependence on the amount of niobium mobilized from zircon, is ~40:60. Outside the ore zones, columbite-(Fe) and uranopyrochlore are the present manifestations of the former pyrochlore. With the exception of magmatic fluornatropyrochlore in the fresher syenites below the Basal ore zone and a single example of magmatic columbite-(Fe) in an Upper Ore Zone sample, all niobium and tantalum minerals have a hydrothermal origin as a result of this pervasive alteration.

2.1 Introduction

Previous studies of the behaviour of columbite group minerals (CGM) have been restricted largely to NYF (Nb-Y-F) and LCT (Li-Cs-Ta) pegmatites, in which the CGM are the main hosts of niobium and tantalum (e.g., Wise et al., 2012). This research has shown that the Mn/(Mn+Fe) and Ta/(Ta+Nb) ratios of the CGM increase during progressive crystal fractionation, a behaviour that can be attributed to differences in the solubility of the Nb and Ta end members of the CGM in the magma and the concentration of Mn in the residual melt through the crystallization of Fe rich phases or high fluorine abundances in the melt (Linnen and Keppler, 1997; Linnen, 1998; Bartels et al., 2010; Wise et al., 2012). Little consideration, however, has been given to the effect of hydrothermal fluids on the composition of the CGM or the possibility that these fluids may deposit CGM directly. Indeed, it has been generally assumed that niobium and tantalum are essentially immobile in hydrothermal fluids and consequently that hydrothermal processes can be ignored when studying the genesis of Nb-Ta mineralization.

The Nechalacho deposit in the Northwest Territories of Canada, which is hosted by a layered alkaline igneous suite, contains considerable reserves of both niobium and tantalum (~ 109 million tons grading 0.36 wt. % Nb_2O_5 and 0.03 wt. % Ta_2O_5) in intensely and pervasively altered Upper and Basal ore zones. In contrast to most pegmatite deposits, a preliminary study by Sheard et al. (2012), showed that much of the Nb-Ta mineralization is hydrothermal, occurring as fergusonite-(Y) that formed as a result of alteration of zircon (their study focused mainly on the REE mineralization). They also identified significant columbite-(Fe) and concluded that it had both magmatic and hydrothermal origins.

Here, we use bulk rock geochemical data, petrographic observations and the results of electron microprobe analyses and X-ray element maps of niobium-tantalum-bearing minerals to develop a genetic model for niobium and tantalum mineralization in the Nechalacho deposit. In this model, we reconstruct the magmatic history of niobium and tantalum concentration, and show that these metals underwent considerable redistribution involving dissolution and re-precipitation of Nb-Ta minerals, including the CGM, during intense and pervasive hydrothermal alteration.

2.2 Geological Setting

2.2.1 Regional Geology

The Blachford Lake Intrusive Complex (BLC), which comprises a series of alkaline to peralkaline plutons, hosts the Nechalacho rare metal deposit at Thor Lake (Northwest Territories, Canada), within the Slave Province of the Canadian Shield (Fig. 2.1a). This complex, which is situated 100 km southeast of Yellowknife, was intruded along the east arm of Great Slave Lake, into Archean mica-schists of the Yellowknife Supergroup at ~2.1 Ga, and is one of a number of plume-related alkaline igneous complexes that were emplaced during the final break-up of the Sclavia supercraton (Bleeker and Hall, 2007; Buchan et al. 2010). The sub-circular peralkaline Grace Lake Granite and Thor Lake Syenite near the eastern edge of the complex are in sharp contact with the Nechalacho Layered Suite, which contains the Nechalacho deposit (Sheard et al., 2012). The granite and syenite, which have gradational contacts with each other, are interpreted to have been coeval (Davidson, 1982) and were intruded at 2176.2 ± 1.3 Ma based on U-Pb isotopic analyses of zircon and monazite in the granite as reported by Sinclair et al. (1994). An almost identical age of 2176 ± 2.5 has been determined for the Nechalacho Layered Suite, based on U-Pb dating of magmatic zircon (Möller and Williams-Jones, 2013).

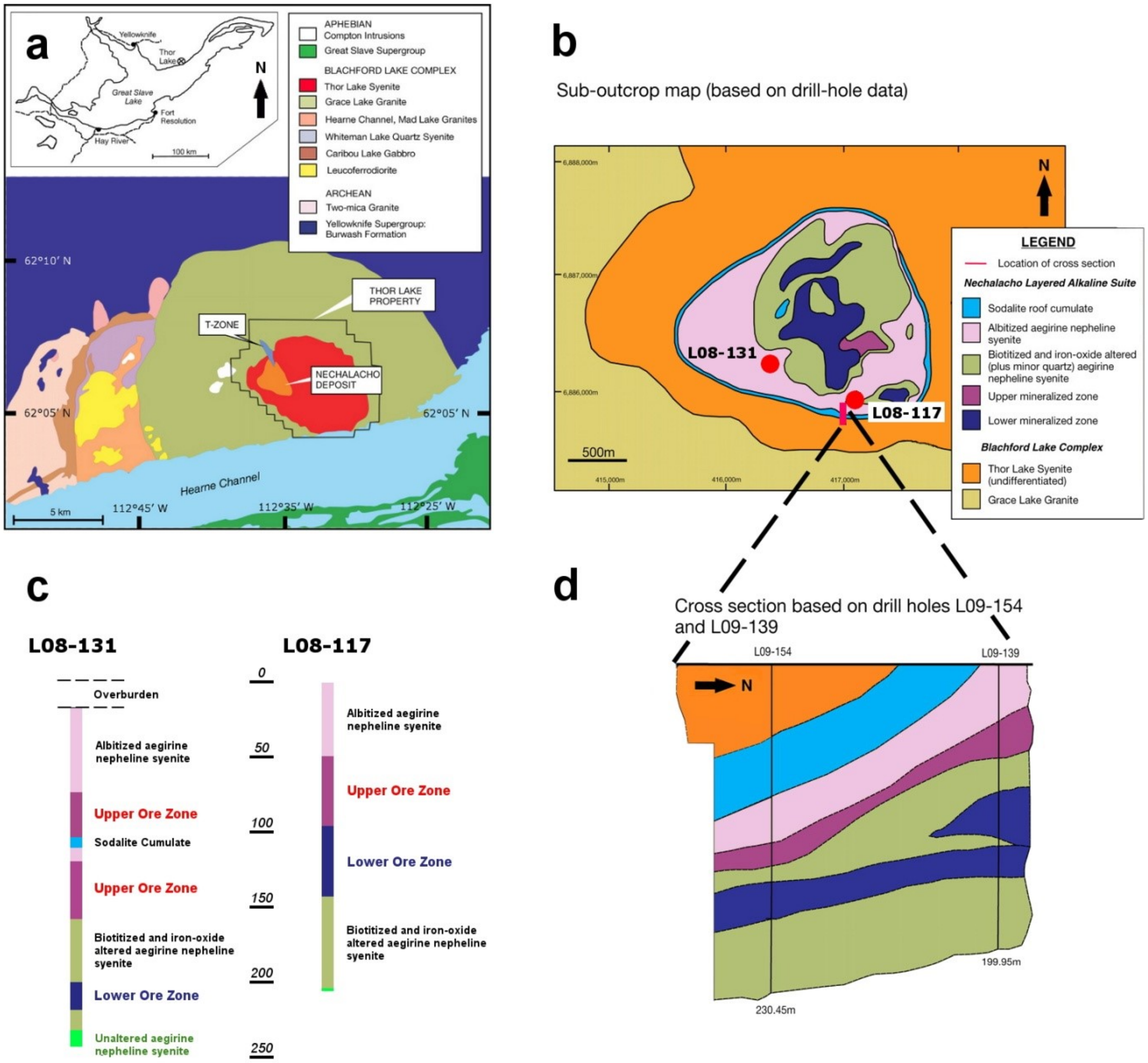

Fig. 2.1 Regional geology of the Blatchford Lake intrusive suite (a) and plan (b) and cross-sectional (c and d) views of the geology of the Nechalacho deposit (modified after Sheard et al., 2012). The plan view illustrates the inferred sub-outcrop geology of the Nechalacho layered suite. The two drill holes investigated in detail in this study are L08-117 and L08-131 (c), whereas a cross section inferred from two drill holes shows the expected sequence of lithological units within the deposit in (d). The upper and lower ore zones are the Upper Zone and Basal Zone described in the text, respectively.

2.2.2 Nechalacho Layered Suite

The Nechalacho deposit hosts the bulk of the rare earth element (REE) mineralization at Thor Lake, largely within two sub-horizontal zones. The 15 to 30 meter thick Upper Zone has an indicated resource of 47.21 million tonnes, a total rare earth oxide (TREO) concentration of 1.52 weight percent, an Nb_2O_5 concentration of 0.29 weight percent, and a Ta_2O_5 concentration of 0.02 weight percent. The 15 to 60 meter thick Basal Zone contains a measured and indicated resource of 61.90 million tonnes, a TREO concentration of 1.64 weight percent, an Nb_2O_5 concentration of 0.41 weight percent, and a Ta_2O_5 concentration of 0.04 weight percent (www.avalonraremetals.com, 2013). Heavy rare earth elements (HREE) are more enriched within the Basal Zone than the Upper Zone, making up ≈ 21.5% and 10.1% of the total rare earth abundance, respectively. The Nechalacho Layered Suite, which hosts the deposit of the same name, has little surface exposure, but based on the results of extensive diamond drilling is postulated to be a dome-shaped body approximately 1.5 kilometers in diameter, dipping shallowly beneath the Thor Lake syenite in all directions, with a thickness of > 1.1 kilometers (this corresponds to the depth of a diamond drill hole that terminated in the intrusion). Rocks of the suite comprise layers of nepheline syenite with varying proportions of K-feldspar, aegirine and locally biotite or sodalite, which underwent subsequent pervasive hydrothermal alteration that obliterated almost all igneous textures at depths shallower than 150 to 250 meters, including those of the two ore zones (Pinckston and Smith, 1995; Sheard et al., 2012). The inferred sub-outcrop geology of the deposit is shown in Figure 2.1b.

A sharp intrusive contact at the margins of the deposit marks the boundary between the Nechalacho suite and the surrounding Thor Lake Syenite or Grace Lake Granite. The granite and syenite are distinguished primarily on the basis of the presence or absence of quartz, respectively. A sequence of units, in places irregular in their order of occurrence, makes their appearance beneath this intrusive contact (Fig. 2.1d). The first unit encountered is a metasomatically altered sodalite roof cumulate. Polygonal or acicular, former magmatic sodalite crystals (up to 2 cm in diameter) were replaced entirely by fine clays (illite, and/or chlorite) that appear dark blue to green in hand specimen. The boundary between the sodalite roof cumulate and the underlying, extensively altered K-feldspar-aegirine- nepheline syenite is characteristically sharp. The latter unit, which hosts both the Basal and Upper zones, is highly variable in texture and mineralogy and has been subdivided into subunits that are pegmatitic, porphyritic, or contain zirconosilicate mineralization. One of these subunits is the 15 to 30 meter thick Upper Zone in which zircon, bastnäsite-(Ce), and other rare earth element-bearing minerals are concentrated. Mafic alteration of this zone in the form of magnetite, hematite and subordinate biotite has been sufficiently intense as to render the rock black in colour. Phenocrysts are rarely visible and zircon commonly appears disseminated to the naked eye or concentrated in laminae. Below the Upper Zone, the altered aegirine-nepheline syenite passes downward into the Basal Zone, which is typically found at depths greater than 150 meters, and locally displays a trachytic texture (foyaite). The interval between these two potential ore zones, which lacks economic mineralization, is laterally variable, ranging from a hundred meters or more in thickness in some places to being non-existent elsewhere, with the Upper Zone passing continuously into the Basal Zone. Unlike zircon in the Upper Zone, zircon in the Basal Zone occurs in well-packed pseudomorphs, and is interpreted to have formed by replacement of eudialyte; the pseudomorphs are in sufficient abundance as to constitute cumulate layers. The concentration of pseudomorphs increases gradually downwards to a sharp lower contact. Below this, a locally coarse-grained and pegmatitic, foyaitic K-feldspar-aegirine-nepheline syenite is the dominant rock-type. The hydrothermal alteration that affected the upper units decreases gradually in intensity downwards, and the foyaite passes into a sequence of much fresher layered sodic syenites. A single drill hole more than one kilometer in depth encountered a series of fine-grained aegirine ± nepheline ± sodalite syenites beneath the Basal Zone. These units experienced little metasomatic alteration and are rhythmically layered on a scale ranging from centimeters to hundreds of meters. Unaltered eudialyte was encountered in these syenites, thereby supporting the interpretation of Sheard et al. (2012) that eudialyte was one of the precursor minerals to the pseudomorphs encountered in the Basal Zone.

Rare earth elements are unequally distributed in the Nechalacho deposit. Heavy REE are concentrated in the Basal Zone, intermediate REE do not display a preference for either mineralized zone, and light REE are concentrated in the Upper Zone. Niobium and zirconium are concentrated with the REE in the two potential ore zones and both are present in slightly higher proportions in the Basal Zone. Zirconium is hosted by zircon, niobium by columbite-(Fe) and fergusonite-(Y), the HREE by fergusonite-(Y) and zircon, and the LREE by monazite-(Ce), allanite-(Ce), bastnäsite-(Ce), and parisite-(Ce) (Sheard et al., 2012). The intensity of hydrothermal alteration represented by the replacement of magmatic igneous textures and mineral assemblages is highly varied. It is particularly intense in the upper parts of the suite, but extends below the Basal Zone. Albitization, manifested by pervasive replacement of all magmatic minerals by albite, and the occurrence of numerous unfilled to partly filled vugs up to centimeters in diameter, is common within the uppermost 50 meters of the deposit, and gave rise to a rock composed almost entirely of bladed albite (cleavelandite). Partially filled vugs contain carbonate minerals, clays, fluorite, pyrite and rarely, rare earth element-bearing fluorocarbonates. The albite comprises centimeter-long crystals. Alteration in the Upper Zone was dominated by magnetite and hematite, interpreted to have largely replaced magmatic aegirine. Biotite decreases in abundance downwards towards the Basal Zone. Below this zone, hematite replaces magnetite as the dominant iron oxide mineral. Late stage silicification, illitization, and carbonatization concluded the alteration but, with the exception of carbonatization, did not result in redistribution of HREE (Sheard et al., 2012).

2.3 Methodology

A large number of drill core samples were collected from the Nechalacho Layered Suite in order to obtain representative samples of niobium and tantalum mineralization, samples with unusually high and low concentrations of these metals and samples of intensely altered and relatively unaltered rocks. As much of the niobium and tantalum mineralization is concentrated in the two potential REE ore zones, these zones were a particular focus of the sampling. Another focus was drill core intervals outside the two mineralized zones containing appreciable concentrations of niobium, in some cases accompanied by significant phosphorous, but depleted in rare earth elements.

In order to obtain a series of representative samples with no bias towards niobium and tantalum concentration, two drill holes, L08-117 and L08-131, were selected and sampled in detail. The units encountered in these drill holes are shown in Figure 2.1c. Thin sections were prepared of samples collected at intervals of ~15 meters. Drill hole L08-117 contains a zone of continuous mineralization from ~50 to ~150 meters depth with no units separating the Upper and Basal zones, the boundary between which is indicated by zircon textures and an increase in HREE concentration in the Basal Zone. Drill hole L08-131 is representative of the southern part of the deposit, in which, by contrast, there are separate Upper and Basal zones. Thin sections were prepared of ten samples collected from outside the mineralized zones.

All thin sections were examined petrographically using an optical microscope and the scanning electron microscope of the electron microprobe. The latter, a JEOL JXA-8900L instrument at McGill University, was used to analyze the compositions of all minerals of interest in wavelength-dispersive mode (WDS). The following conditions were employed: 20 kV acceleration voltage, 30 nA current, and a 5 µm beam size. Standards used for calibrating the elements analysed, as well as counting times employed during their analysis, are listed in Appendix 2.1. In addition, X-ray maps of thin section areas of interest for niobium and tantalum were prepared using a counting time of 20 ms and 40ms, respectively, and a pixel size of one micron.

2.4 Niobium-tantalum Mineralization in the REE Zones

The Upper Zone and Basal Zone differ in a number of important respects. The Basal Zone is enriched in the heavy rare earth elements and much of the REE mineralization, including zircon, is considered to have formed as pseudomorphs after precursor eudialyte (Sheard et al., 2012), whereas some of the zircon in the Upper Zone was formed magmatically. In samples of drill core from these zones, individual crystals of columbite-(Fe), fergusonite-(Y) and other niobium-tantalum minerals cannot be distinguished macroscopically and even with an optical microscope may be difficult to discern. Textural relationships among them were therefore determined using images obtained with the scanning electron microscope facility of the electron microprobe. The compositions of the various niobium-tantalum minerals, which as mentioned earlier were analyzed using the electron microprobe, are reported in Table 2.1.

Table 2.1 Average compositions and standard deviations for niobium and tantalum minerals.

	Columbite-(Fe)[1]						
	Magmatic (n = 11)	Hydrothermal (n = 100)	Fergusonite-(Y) (n = 10)	Samarskite-(Y) (n = 4)	Uranopyrochlore (n = 3)	Fluornatropyrochlore (n = 10)	Zircon (n = 68)
Y_2O_3 **wt. %**	0.52 ± 0.19	0.13 ± 0.16	20.4 ± 3.96	11.3 ± 0.90	1.44 ± 1.58	b.d.	1.20 ± 1.60
Nb_2O_5	75.3 ± 0.61	72.1 ± 2.18	46.2 ± 2.12	50.7 ± 3.07	43.5 ± 1.38	57.8 ± 1.31	1.84 ± 0.69
Ta_2O_5	0.59 ± 0.12	3.81 ± 2.61	2.54 ± 1.25	2.67 ± 0.05	0.68 ± 0.45	4.62 ± 1.05	b.d.
Na_2O	-	-	-	-	0.27 ± 0.26	8.38 ± 0.66	-
MgO	0.10 ± 0.08	0.11 ± 0.08	-	-	-	-	-
Al_2O_3	-	-	b.d.	b.d.	-	-	0.14 ± 0.12
SiO_2	-	-	b.d.	2.47 ± 1.23	2.43 ± 0.44	0.47 ± 0.33	28.8 ± 0.48
K_2O	-	-	-	-	0.09 ± 0.07	b.d.	-
CaO	0.04 ± 0.01	0.10 ± 0.13	0.34 ± 0.16	2.72 ± 0.59	4.79 ± 0.99	8.72 ± 1.18	0.14 ± 0.16
TiO_2	1.24 ± 0.35	1.72 ± 1.16	-	-	2.67 ± 0.89	2.42 ± 0.58	b.d.
MnO	11.4 ± 1.36	5.01 ± 2.75	-	-	0.14 ± 0.02	b.d.	b.d.
FeO	10.9 ± 1.73	16.1 ± 3.04	0.68 ± 0.75	5.74 ± 1.30	4.97 ± 1.72	0.16 ± 0.09	0.32 ± 0.14
ZrO_2	-	-	b.d.	0.23 ± 0.27	b.d.	2.01 ± 0.55	59.3 ± 1.86
SnO_2	0.14 ± 0.13	0.15 ± 0.13	-	-	-	-	-
HfO_2	-	-	b.d.	b.d.	-	-	1.08 ± 0.16
PbO	-	-	-	-	0.72 ± 0.14	b.d.	-
ThO_2	b.d.	b.d.	0.54 ± 0.73	1.52 ± 0.53	0.09 ± 0.06	b.d.	b.d.
UO_2	b.d.	b.d.	-	-	26.8 ± 3.18	b.d.	-
La_2O_3	-	-	b.d.	b.d.	0.24 ± 0.21	2.29 ± 0.43	b.d.
Ce_2O_3	-	-	0.88 ± 0.30	0.53 ± 0.18	1.04 ± 0.55	6.01 ± 1.11	0.23 ± 0.13
Pr_2O_3	-	-	0.36 ± 0.11	b.d.	0.15 ± 0.03	0.64 ± 0.12	b.d.
Nd_2O_3	-	-	3.85 ± 0.41	1.32 ± 0.20	0.88 ± 0.22	1.91 ± 0.46	0.97 ± 0.44
Sm_2O_3	b.d.	b.d.	2.22 ± 1.58	0.90 ± 0.18	-	-	0.66 ± 0.29
Eu_2O_3	-	-	0.46 ± 0.37	0.30 ± 0.13	-	-	b.d.
Gd_2O_3	-	-	8.84 ± 3.62	5.20 ± 0.25	-	-	0.90 ± 0.43
Dy_2O_3	-	-	5.82 ± 0.93	4.60 ± 0.31	-	-	0.33 ± 0.30
Er_2O_3	b.d.	b.d.	1.83 ± 0.85	1.12 ± 0.10	-	-	b.d.
Yb_2O_3	-	-	1.27 ± 0.73	0.83 ± 0.08	-	-	b.d.
F	b.d.	b.d.	0.60 ± 0.53	0.42 ± 0.08	b.d.	5.20 ± 0.22	0.81 ± 0.18
Total	100.2	99.4	97.0	92.8	91.0	98.5	96.8

Calculated mineral formulae: magmatic columbite-(Fe) $(Fe_{0.51}Mn_{0.54})(Nb_{1.91}Ti_{0.05})O_6$, hydrothermal columbite-(Fe) $(Fe_{0.77}Mn_{0.24})(Nb_{1.86}Ta_{0.06}Ti_{0.07})O_6$, fergusonite-(Y) $(Y_{0.52}REE_{0.40})Nb_{0.99}O_4$, samarskite-(Y) $(Y_{0.54}REE_{0.44}Fe^{2+}{}_{0.43}Ca_{0.26}Si_{0.22})(Nb_{2.06}Ta_{0.07})O_8$, uranopyrochlore (calculated on the basis of 2 B site cations) $(U_{0.55}Ca_{0.47}Fe^{2+}{}_{0.38}Si_{0.22}Ti_{0.18}REE_{0.08}Y_{0.07}Na_{0.05})(Nb_{1.80}Ti_{0.18})O_6(OH)$, fluornatropyrochlore (2 B site cations) $(Na_{1.11}Ca_{0.64}REE_{0.27})(Nb_{1.79}Ti_{0.12}Ta_{0.09}Zr_{0.07})O_6(OH,F_{1.13})$, zircon $(Zr_{0.95}REE_{0.04}Nb_{0.03})Si_{0.95}O_4$

[1] Hydrothermal columbite-(Fe) is from sample L08-131:96.0; all other analyzed minerals, with the exception of fluornatropyrochlore, are hydrothermal.

b.d.: below detection limits (three sigma above background) are as follows (wt. %): Y 0.04-0.10; Nb 0.09; Ta 0.16-0.34; F 0.14-0.21; Ca 0.03; Fe 0.03-0.10; Si 0.04; Mg 0.03; Ti 0.04; Mn 0.03; Sn 0.03-0.06; Na 0.04; Al 0.03; K 0.02; Pb 0.12; Th 0.03-0.06; U 0.05-0.10; Hf 0.26; Zr 0.08-0.10; Er 0.10-0.26; Sm 0.09-0.13; La 0.09; Ce 0.05; Pr 0.08-0.10; Nd 0.09; Eu 0.20; Dy 0.09-0.11; Gd 0.09; Yb 0.13

- : not analyzed

In the Basal Zone, niobium (and tantalum) is present as anhedral, micron-sized aggregates of fergusonite-(Y) that surround subhedral zircon grains with altered cores (Fig. 2.2a and b). Similar anhedral fergusonite-(Y) to that surrounding zircon is also observed in large pseudomorphs after eudialyte, which are described in detail by Sheard et al. (2012). In the latter, the fergusonite-(Y) is not in immediate contact with zircon. Instead, it is found in the extremely fine-grained, "gel-like" matrix of the pseudomorph. The extent to which fergusonite-(Y) and zircon are related is highly variable. In some samples of the Basal Zone, masses of fergusonite-(Y) are in immediate contact with the zircon, but do not occur within the zircon crystals (Fig. 2.2a and b). However, in other samples, many of which are highly altered, fergusonite-(Y) occurs in the cores and fractures of zircon grains (Fig. 2.3a-c).

In contrast to the Basal Zone, niobium (and tantalum) in the Upper Zone occurs as columbite-(Fe) but, as in the Basal Zone, is generally associated with zircon. Although pseudomorphs containing columbite-(Fe) do not occur in the Upper Zone, the relationship of columbite-(Fe) to zircon in this zone is quite similar to that of fergusonite-(Y) to zircon in the Basal Zone. Locally, large amounts of columbite-(Fe) surround the zircon, but are not found within it (Fig. 2.2c and d). Elsewhere, the columbite-(Fe) occurs in the cores of zircon grains (Fig. 2.3d) and along fractures radiating outward from these cores.

With the exception of a single sample, magmatic niobium and tantalum minerals, including fergusonite-(Y), were not observed in the potential ore zones. Magmatic columbite was identified in an Upper Zone sample, L08-131: 96.0, which is from a drill core interval containing high bulk concentrations of both phosphorus and iron (approximately five and two times higher, respectively, than typical values). The columbite is interpreted to be magmatic on the basis of its acicular and inclusion-free features and alteration at its margins to hydrothermal columbite,

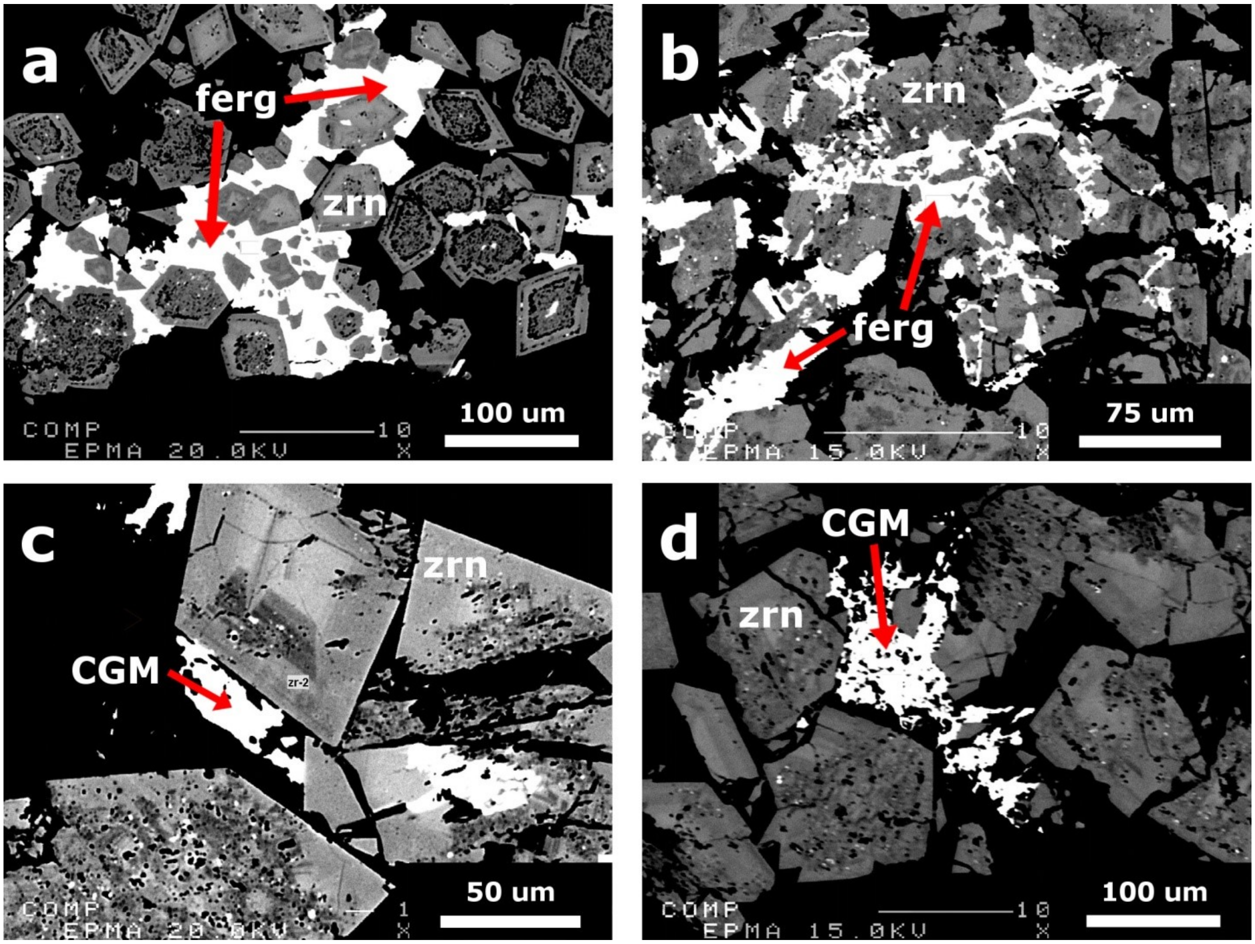

Fig. 2.2 Backscattered electron images (BSE) illustrating aggregates of hydrothermal fergusonite-(Y) in the Basal Zone (a and b) and columbite-(Fe) in the Upper Zone (c and d) surrounding altered, subhedral zircon. CGM = columbite group minerals, ferg = fergusonite-(Y), zrn = zircon.

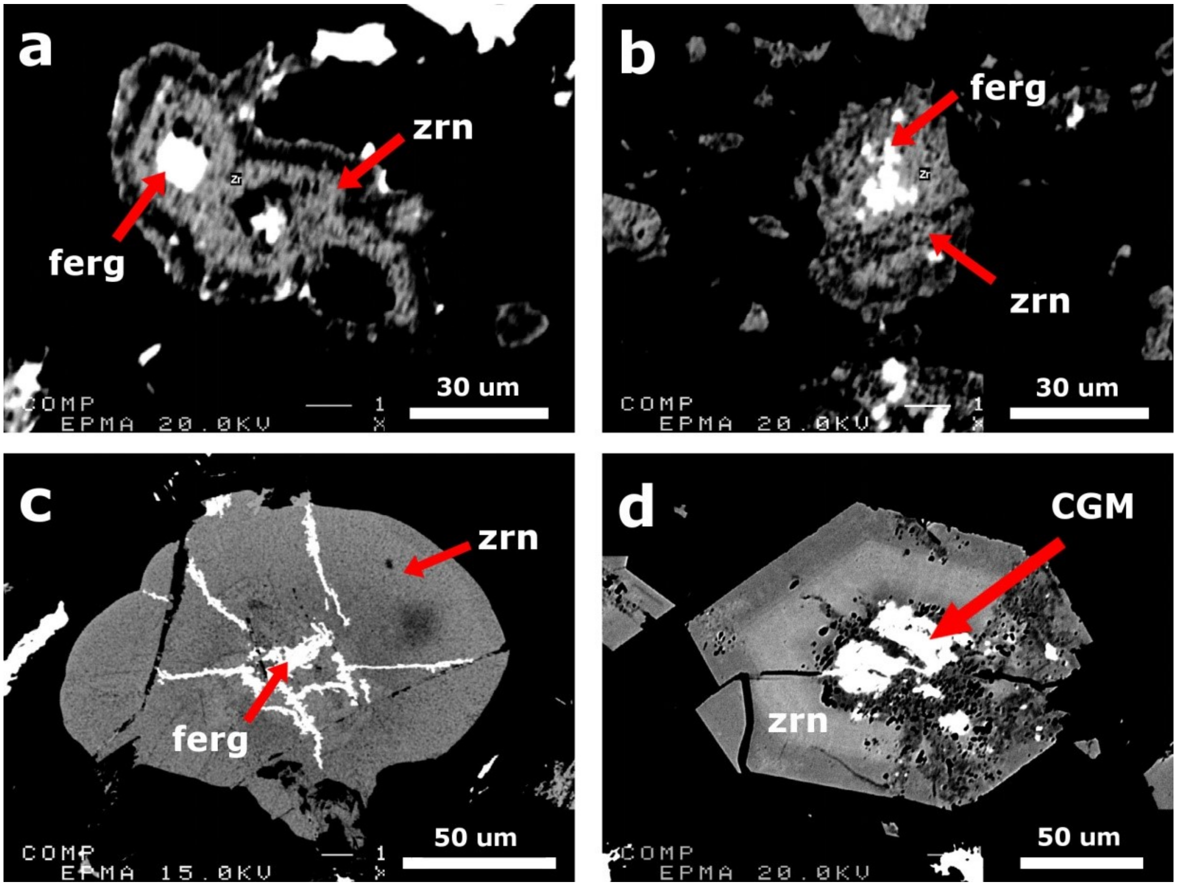

Fig. 2.3 BSE images illustrating the mode of occurrence of hydrothermal fergusonite-(Y) in the Basal Zone (a, b and c) and columbite-(Fe) in the Upper Zone (d). Fergusonite-(Y) is in the cores of zircon crystals in (a), in both the core and rim of the crystal in (b) and both within and surrounding the crystal in (c). Columbite-(Fe) is in the core of the zircon crystal in (d). Abbreviations as in Figure 2.2.

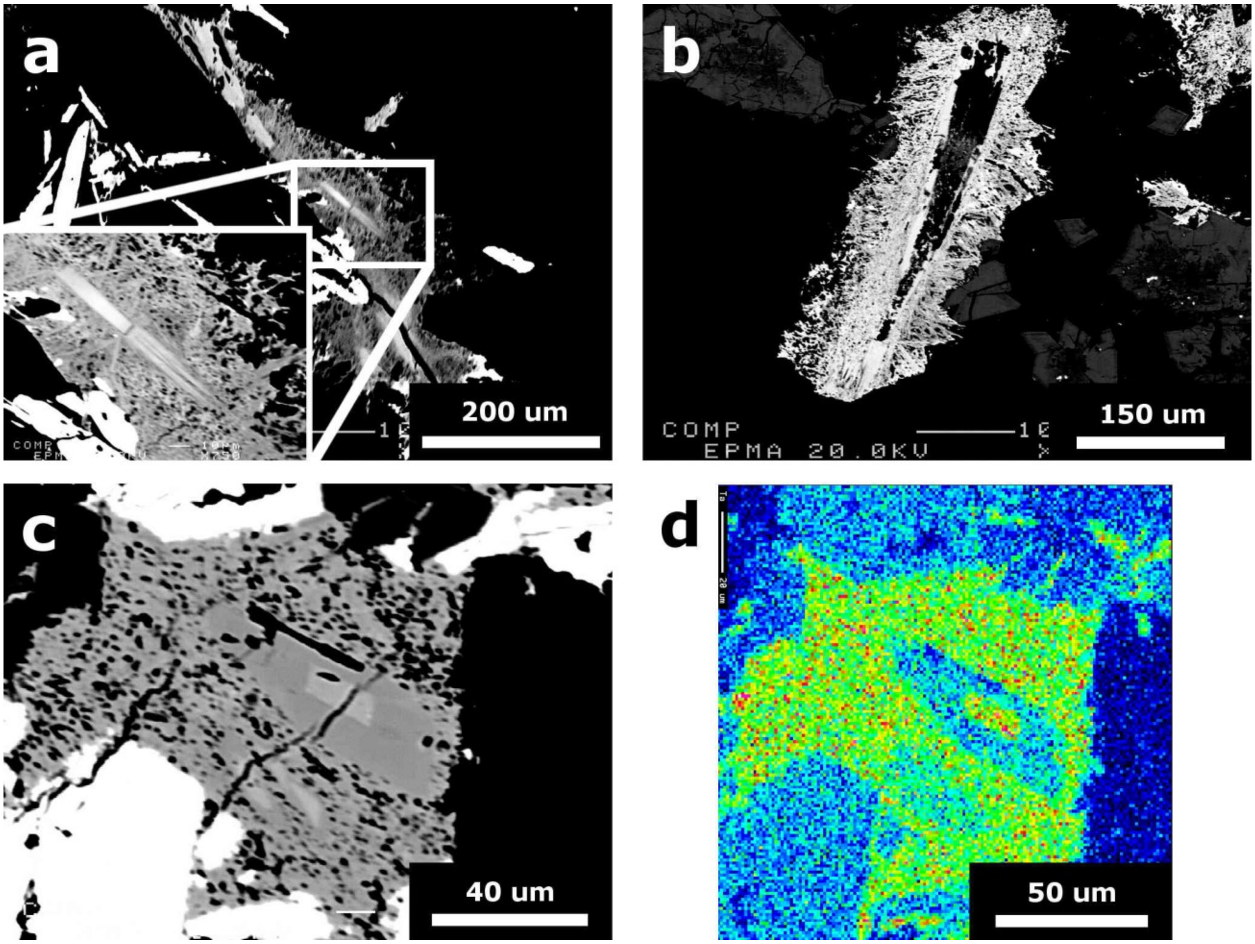

Fig. 2.4 Magmatic columbite-(Fe) in Upper Zone sample L08-131: 96.0. The acicular columbite-(Fe) ranges from being altered at its margins (a) to having almost no trace of its magmatic nature except for void space (b). Evidence of tantalum zonation in an unaltered columbite crystal is visible in a BSE image (c) and a Ta X-ray element map (d). Most of the white crystals in (a) and (c) are monazite-(Ce). CGM = columbite group minerals.

leaving behind a small remnant of the former columbite grain (Fig. 2.4a). Where alteration was more intense, only the outline of the former columbite crystal is visible (Fig. 2.4b). The magmatic nature of the columbite is particularly evident in a grain with zones of higher and lower tantalum concentration (Fig. 2.4c and d). Surrounding this and other magmatic columbite crystals are mottled areas of columbite similar in appearance to the anhedral columbite observed in most samples within the Nechalacho deposit.

2.5 Niobium-tantalum Mineralization in Altered Rocks Outside the REE Zones

Significant niobium and tantalum mineralization is rarely encountered outside the two potential REE ore zones. Important exceptions are short intervals of drill core above the Basal Zone containing abundant niobium and lacking the REE. These intervals are characterised by high bulk rock contents of uranium (Fig. 2.5a, b and c). The only niobium-tantalum minerals identified in these intervals are uranopyrochlore and columbite, which commonly occur in close spatial association with each other.

Uranopyrochlore is found as micron-sized anhedral grains and locally is enclosed by anhedral, micron-scale columbite grains (Fig. 2.6a). More frequently, however, the two minerals occur together in anhedral aggregates, in which they are evenly distributed (Fig. 2.6b-d). In a small number of cases, the aggregates appear to have shapes resembling subhedral crystals, which may indicate that they are pseudomorphs (Fig. 2.6b). Generally, however, their shapes are very irregular.

In one sample, L08-133: 33.5, from a drill core interval particularly rich in niobium, there is abundant columbite-(Fe) with almost no uranopyrochlore (Fig. 2.7a). Columbite-(Fe) in this sample forms rectangularly shaped masses, hundreds of microns in length, which are zoned with respect to tantalum parallel to their long axis (Fig. 2.7b). The zonation in many of these masses,

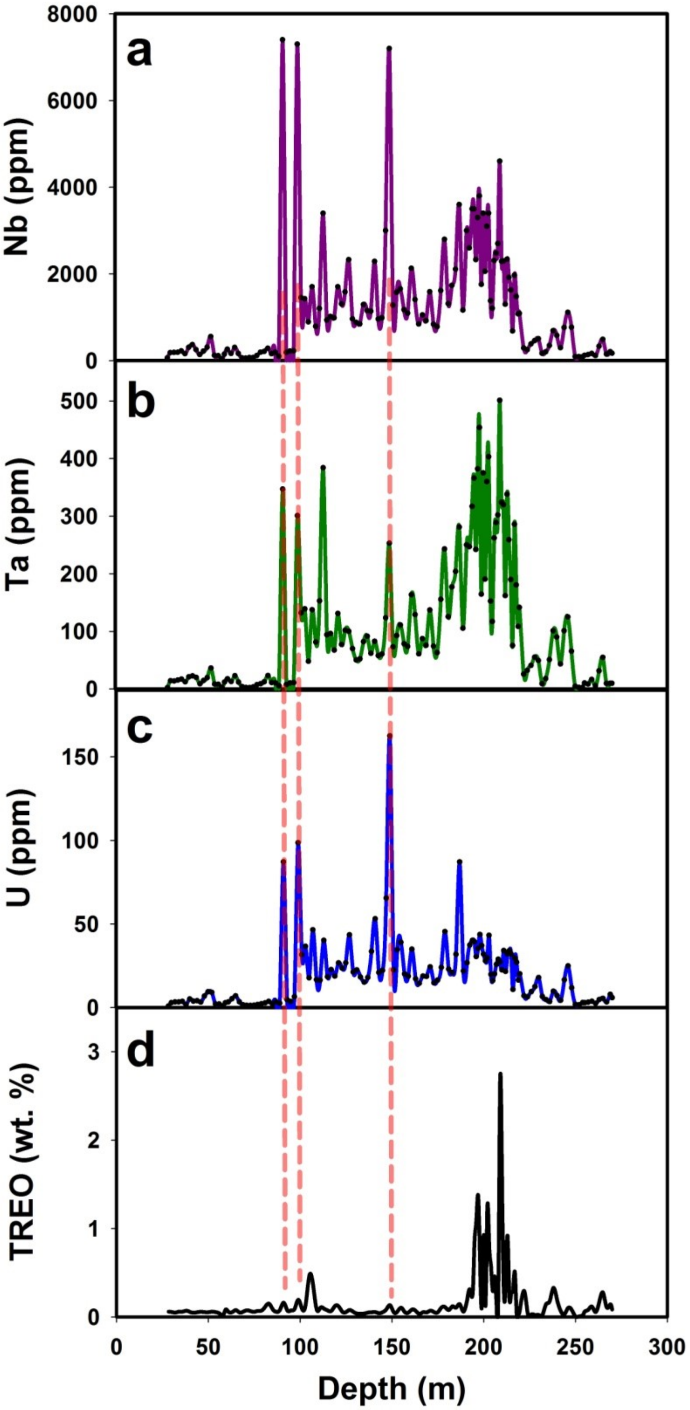

Fig. 2.5 Bulk concentrations of Nb (a), Ta (b), U (c), and TREO (d) as a function of depth in core from drill hole L11-323.

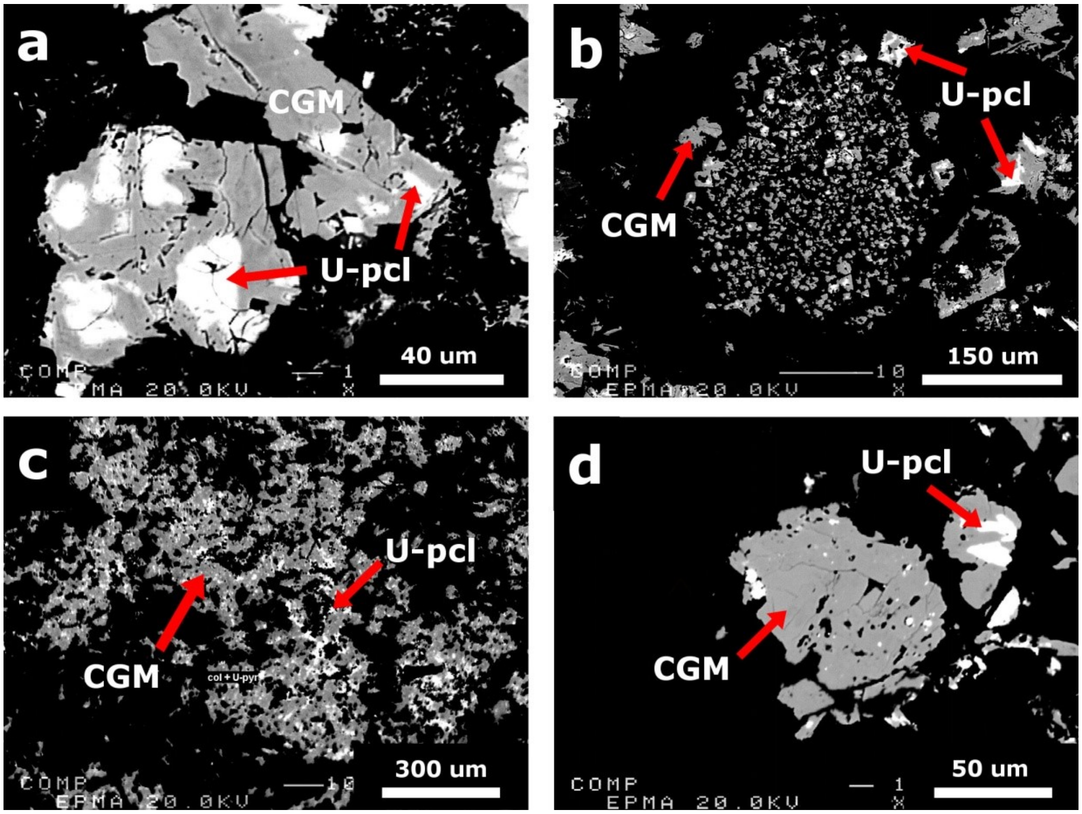

Fig. 2.6 BSE images illustrating niobium and tantalum mineralization most commonly observed outside the two ore zones; (a, c, d) aggregates of uranopyrochlore replaced by columbite-(Fe), rarely within the outline of a possible pseudomorph (b). CGM = columbite group minerals.

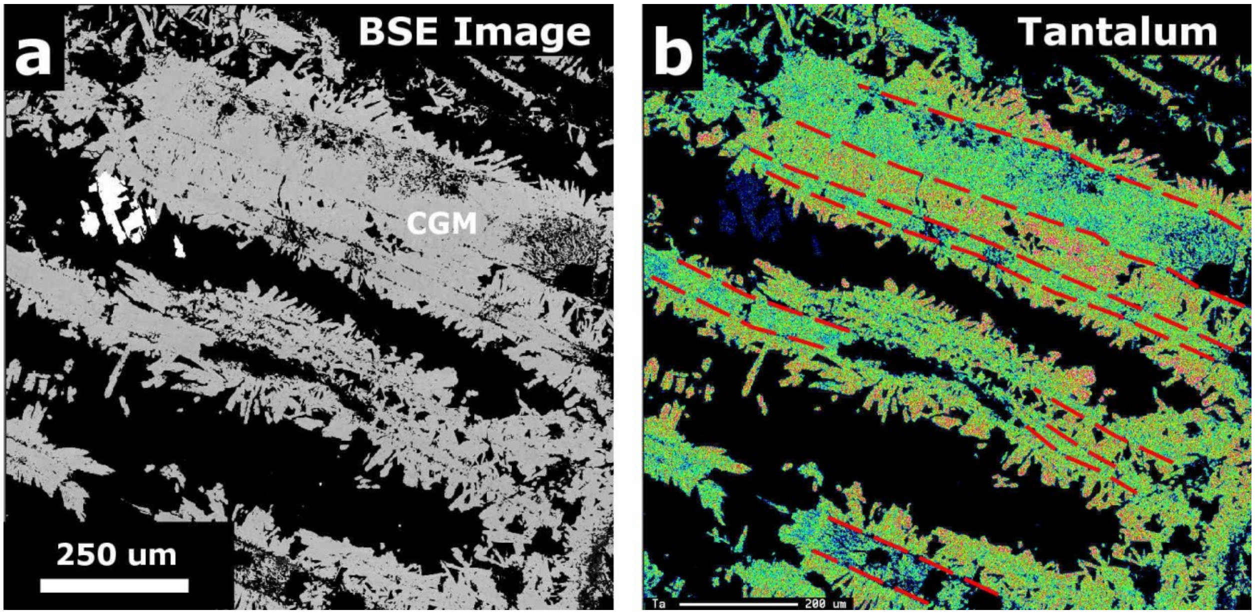

Fig. 2.7 A BSE image (a) and tantalum X-ray element map (b) showing large columbite-(Fe) aggregates zoned perpendicular to their long axis in a drill core interval containing abundant niobium, but depleted in the rare earth elements. The warm colors in (b) reflect higher Ta concentration. CGM = columbite group minerals.

which was initially sharp and continuous, as shown in Figure 2.7b, has been significantly modified making the zones diffuse, discontinuous and bent. Although the origin of this columbite is debatable and discussed further below, micron-scale columbite-(Fe) in the same sample, which forms thin rims on minerals such as quartz, can confidently be interpreted to have had a hydrothermal origin. Possible micron-scale uranopyrochlore was recognized in a single aggregate of columbite-(Fe) in this sample.

2.6 Niobium and Tantalum Mineralization in Unaltered Syenite

The unaltered syenites below the Basal Zone are depleted in niobium and tantalum relative to the units above them. Indeed, only a single sample, L09-194: 325.6, was found to contain a niobium-rich mineral in these syenites. This mineral is fluornatropyrochlore, which occurs either as concentrically zoned subhedral crystals or as highly acicular crystals (locally bent), both of which may occur within tens of microns of each other (Fig. 2.8). The fluornatropyrochlore commonly occurs as inclusions in zircon and other more common minerals such as orthoclase, suggesting that it was one of the first minerals to crystallize from the melt. In contrast to the uranopyrochlore in the altered rocks, the fluornatropyrochlore is enriched in sodium and fluorine, whereas its uranium content is below the detection limit of the electron microprobe in the crystals analysed during this study. However, a member of our group, V. Möller, has identified euhedral pyrochlore crystals with zones containing up to 3.76 wt. % UO_2 in unaltered syenite below the Basal Zone. In two samples analyzed by him, L09-194: 753.5 and L09-194: 866.2, the mean UO_2 contents of the pyrochlore crystals were 1.09 and 1.16 wt. %, respectively. Comparably zoned euhedral pyrochlore has been reported in the nepheline syenites

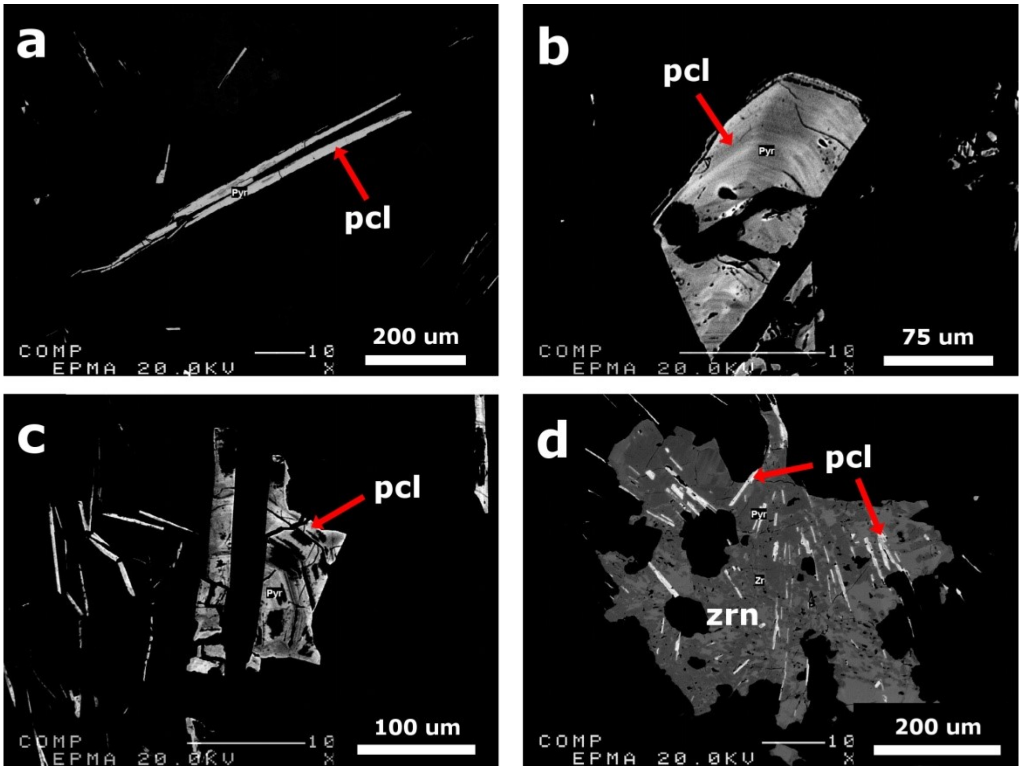

Fig. 2.8 BSE images showing textures exhibited by magmatic pyrochlore below the main intrusion. The pyrochlore is found either as individual acicular needles (a), as zoned subhedral crystals (b), (c), or as needles enclosed within zircon (d).

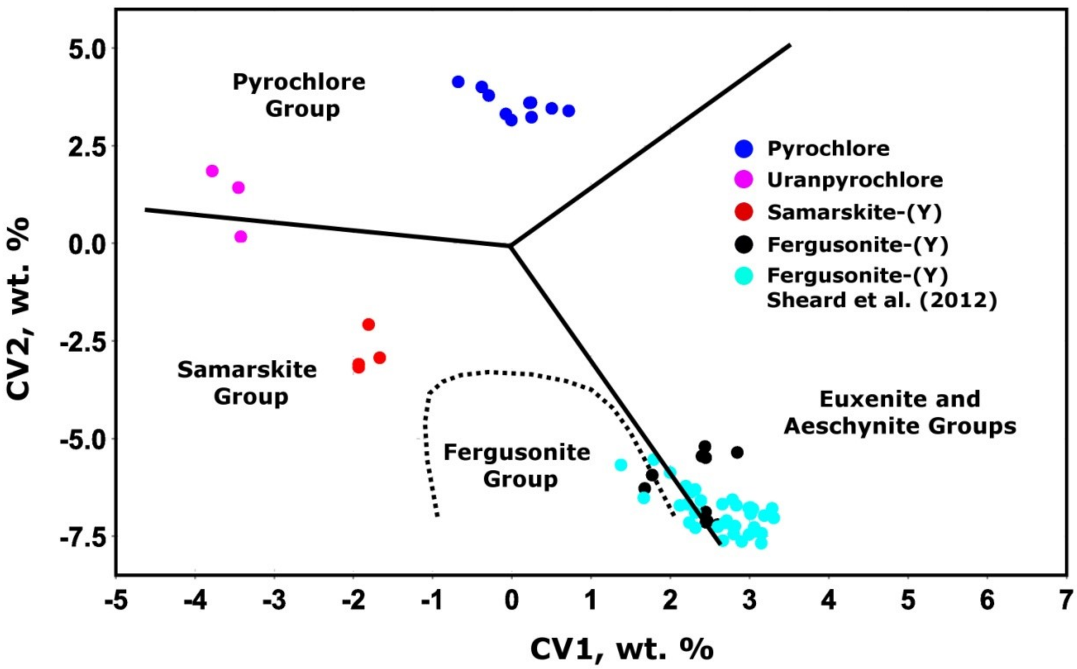

Fig. 2.9 Compositions of pyrochlore, uranopyrochlore, samarskite-(Y) and fergusonite-(Y) on the (Y,REE,U,Th)-(Nb,Ta,Ti) oxide classification diagram of Ercit (2005). See the main text for discussion of this figure.

of the Motzfeldt alkaline center in South Greenland (McCreath et al., 2013). This pyrochlore contains 1 to 5 wt. % UO_2.

2.7 The Composition and Classification of the Nb-Ta-bearing Minerals

The average compositions of the various niobium- and tantalum-bearing minerals identified in the Nechalacho Layered Suite are reported in Table 2.1. Some of these minerals could be identified with confidence on the basis of electron microprobe analyses, e.g., members of the tantalite-columbite series. The identification of the (Y,REE,U,Th)-(Nb,Ta,Ti) oxide minerals, of which there are a number in the Nechalacho Layered Suite, however, proved quite challenging. They were identified with the aid of the discrimination diagram of Ercit (2005), which distinguishes members of the pyrochlore, samarskite, fergusonite, euxenite, and aeschynite groups on the basis of two canonical variables (Fig. 2.9). As expected, compositions of crystals in the unaltered syenites below the ore zones that were initially interpreted to represent pyrochlore, based on comparisons to known compositions of pyrochlore, plot squarely in the pyrochlore field of the discrimination diagram. Similarly, the compositions of uranopyrochlore crystals in units surrounding the ore zones also plot in the pyrochlore field. By contrast, a mineral in the Basal Zone, initially interpreted to be fergusonite-(Y), plots in the samarskite-(Y) field. The compositions of most Nb-Y-bearing aggregates in the Basal Zone, however, straddle the border of the fergusonite-(Y) sub-field and the euxenite/aeschynite field, or plot in the euxenite/aeschynite field. This is also the case for fergusonite-(Y) compositions reported by Sheard et al. (2012). Either the problem of classification reflects inaccuracies in the boundaries of the discrimination diagram or there are inclusions of another phase in the fine-grained fergusonite-(Y) aggregates.

2.8 Deposit-Scale Trends in Niobium-Tantalum Mineral Chemistry and Bulk Rock Composition

Potential trends in the composition of the niobium-tantalum mineralization were evaluated from bulk rock analyses of two meter core intervals from multiple drill holes made available by Avalon Rare Metals Inc. (the samples were analyzed by Actlabs, Ancaster, Ontario, using total digestion and ICP-MS and ICP-OES methods) and the composition of CGM minerals sampled at a variety of depths. The CGM minerals are highly enriched in niobium and generally have Mn/(Mn+Fe) ratios of less than 0.5. Based on this ratio, virtually all of the columbite in the Nechalacho Layered Suite classifies as columbite-(Fe). With the exception of a single sample, L08-131: 96.0, containing visible magmatic columbite, columbite-(Fe) compositions define a linear trend of increasing Mn/(Mn+Fe) and Ta/(Ta+Nb) values (Fig. 2.10). Columbite in the exceptional sample shows no such trend. In this sample, Mn/(Mn+Fe) values range between 0.4 and 0.7 and Ta/(Ta+Nb) is very low, with most crystals yielding values between 0.001 and 0.005.

In the Upper Zone and Basal Zone, and in parts of the layered suite outside of the mineralized zones, bulk rock contents of niobium display a strong positive correlation (r' > 0.9) with those of zirconium. Outside the ore zones, including the altered units above them, and the fresher syenites below, bulk rock contents of uranium correlate strongly with those of niobium, and to a lesser extent tantalum (Fig. 2.5, Fig. 2.11). This correlation, however, does not extend into the ore zones, where niobium and tantalum concentrations are independent of uranium concentration. Finally, Mn/(Mn+Fe) ratios in the columbite increase with increasing bulk rock concentration of phosphorus (Fig. 2.12) and decreasing depth (Fig. 2.13), although within individual samples the Mn/(Mn+Fe) values of columbite crystals vary considerably.

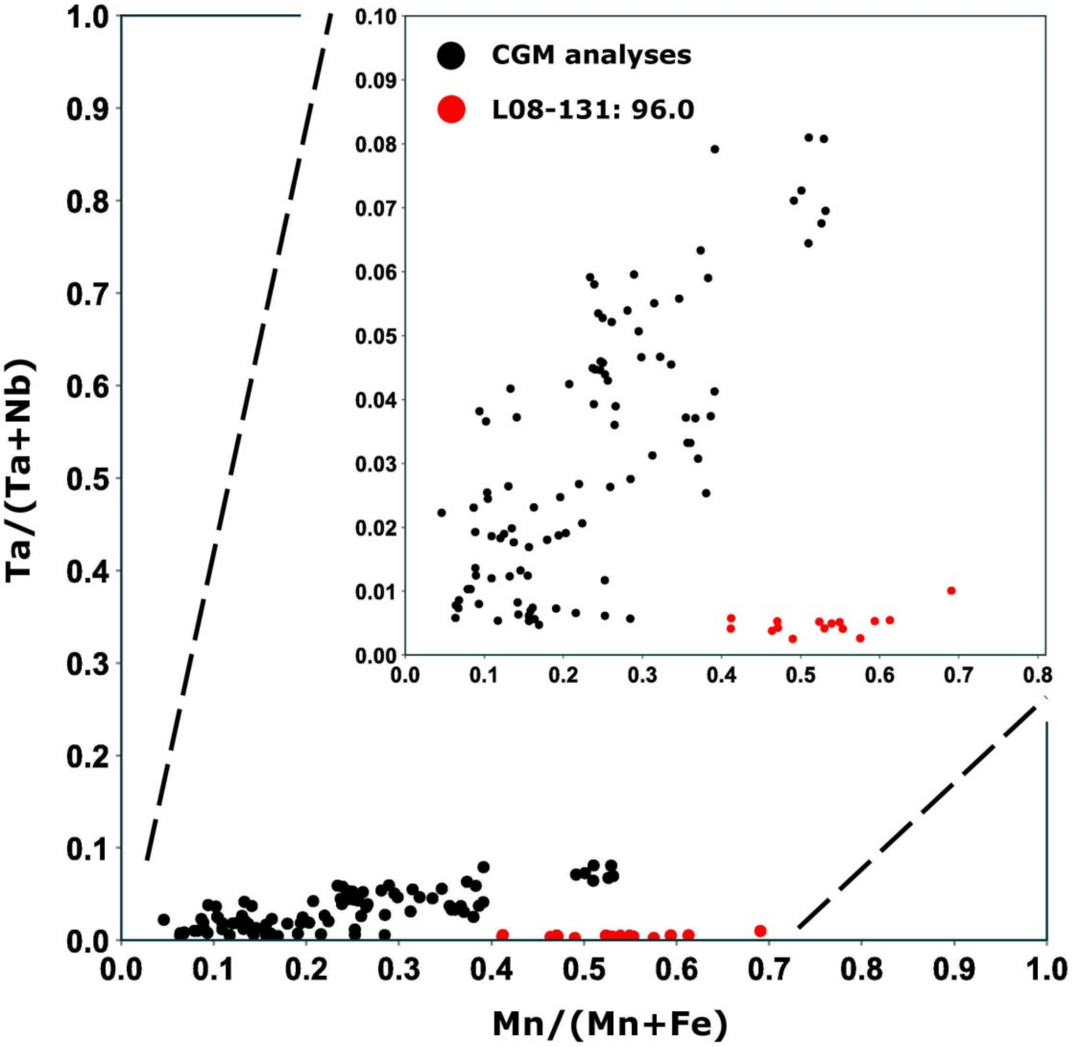

Fig. 2.10 Compositions of columbite group minerals as a function of Ta/(Ta+Nb) and Mn/(Mn+Fe). Sample L08-131:96.0, containing magmatic columbite, falls outside the trend in compositions observed for other samples.

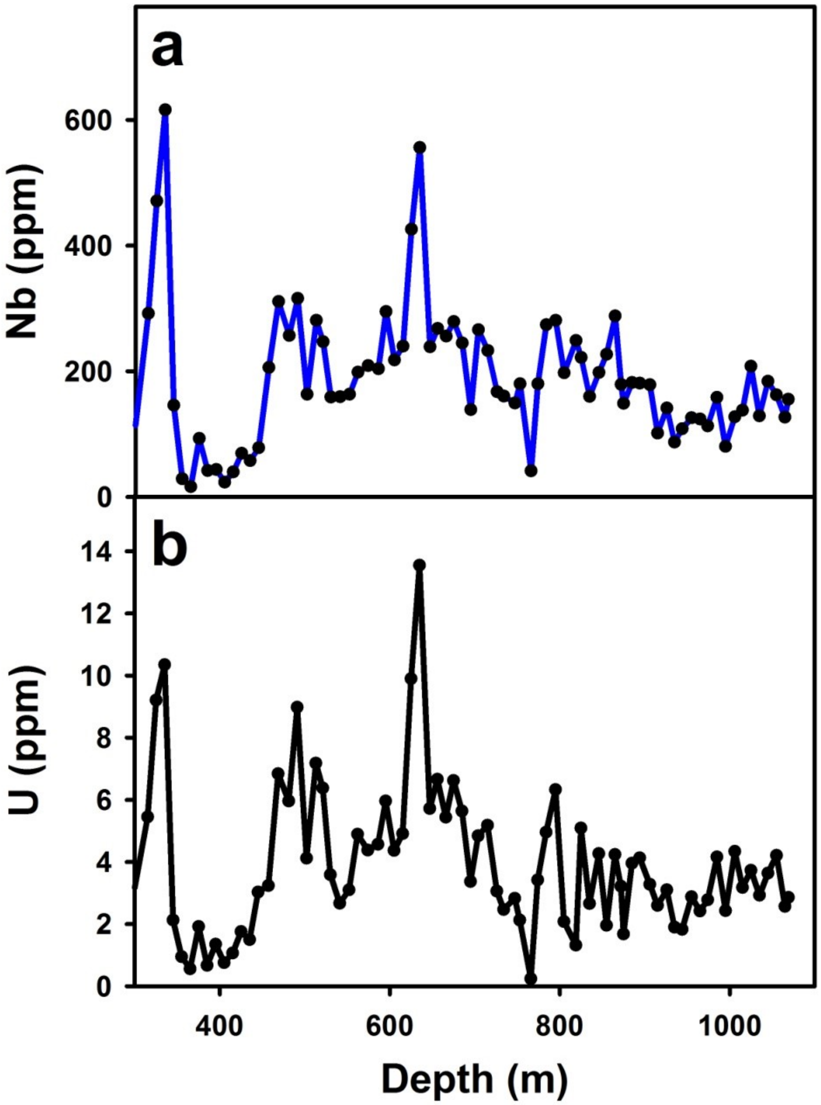

Fig. 2.11 Bulk core content of Nb (a) and U (b) as a function of depth in unaltered syenites below the Basal Zone in drill hole L09-194.

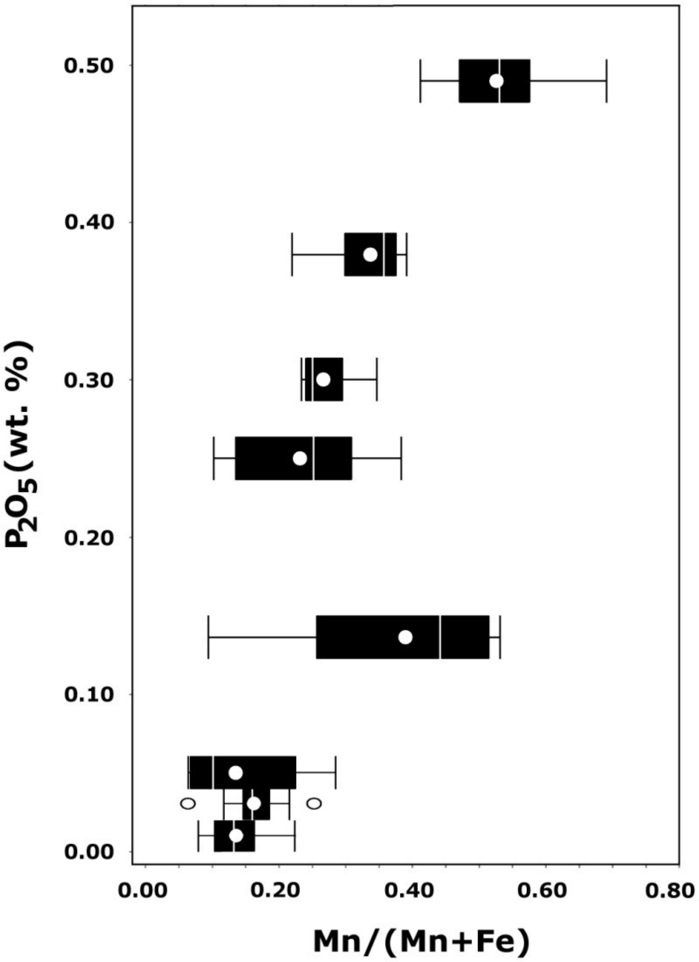

Fig. 2.12 Box and whisker plot of the Mn/(Mn+Fe) ratio in columbite-(Fe) versus bulk P_2O_5 (wt.%) abundance in drill core.

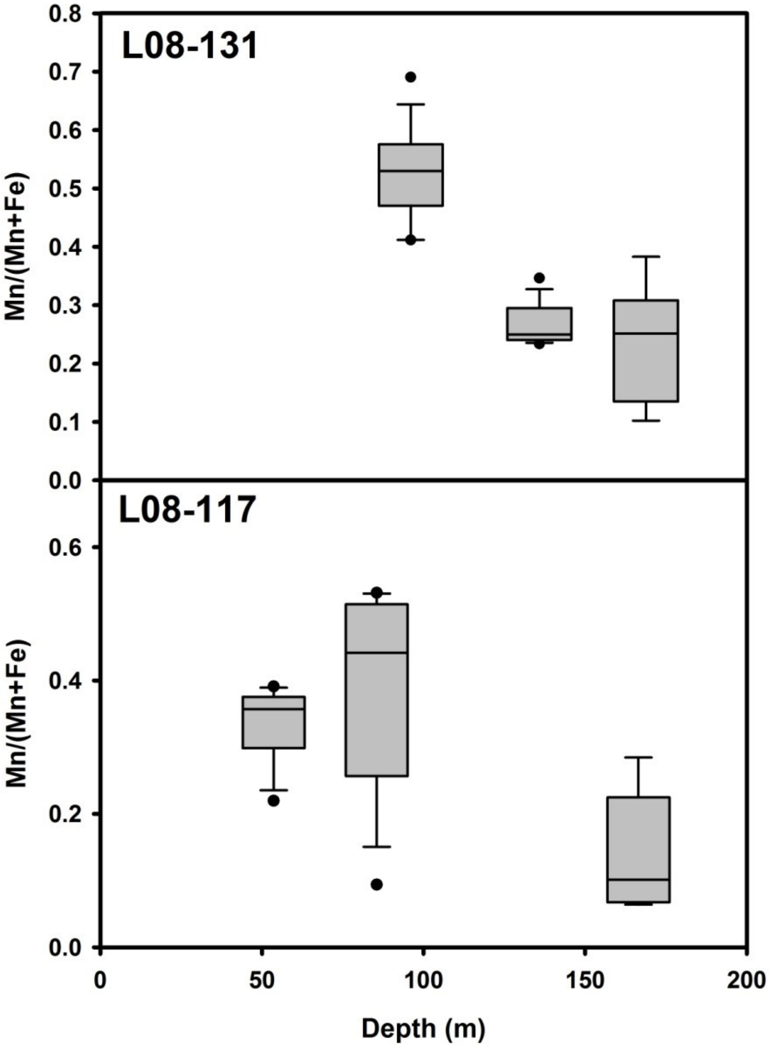

Fig. 2.13 Box and whisker plot of Mn/(Mn+Fe) ratios of columbite-(Fe) as a function of depth in drill holes L08-131 and L08-117.

2.9 Discussion

2.9.1 Introduction

From the preceding sections, it is apparent that the nature of the niobium and tantalum mineralization in the Nechalacho Layered Suite varies considerably depending on whether it occurs in the Upper Zone, the Basal Zone or fresh or altered rocks outside these two zones. In the upper, altered part of the Nechalacho Layered Suite, including the Upper Zone and Basal Zone, the niobium-tantalum minerals of all samples examined, with a single exception, are hydrothermal. This makes interpretation of the origin and evolution of the niobium-tantalum mineralization in this part of the suite difficult. However, the niobium/tantalum mineralogy in the fresh syenites below the Basal Zone, is magmatic, albeit very rarely observed, and this provides a means of potentially evaluating the genesis of the Nb-Ta mineralization of the altered rocks above them and particularly that of the Basal and Upper zones.

2.9.2 The Place of Pyrochlore in the Nechalacho Layered Suite

Fluornatropyrochlore is the only niobium-tantalum mineral to have formed in the unaltered syenites below the Basal Zone. There it occurs either as acicular needles (Fig. 2.8a) or as concentrically zoned subhedral crystals (Fig. 2.8b) and is interpreted to be magmatic. As the only magmatic niobium mineral to have been identified in unaltered syenites, fluornatropyrochlore is a strong candidate for the magmatic niobium mineral that crystallized in the altered unmineralized syenites. This candidacy is strengthened by the observation that in the fresh syenites (Fig. 2.11) and altered syenites (Fig. 2.5) outside the two potential ores zones there is a strong correlation between bulk rock niobium and uranium contents, consistent with the presence of uranopyrochlore in the altered syenites. If the correlation is a magmatic effect, this would suggest that uranium and niobium were removed from the melt at the same time by pyrochlore. However, it should be noted that, whereas the pyrochlore in the altered rocks is uranium-rich, its uranium content is relatively low, although significant, in the unaltered syenites.

The early crystallization of pyrochlore in the altered but unmineralized parts of the Nechalacho Layered Suite is supported by the observation of anhedral relicts of uranopyrochlore surrounded by equally anhedral columbite-(Fe) in altered rocks outside the two potential ore zones. The two minerals are closely associated with each other, form aggregates (Fig. 2.6a-c), and the uranium content of the columbite-(Fe) suggests a genetic relationship between them. Columbite-(Fe) surrounding uranopyrochlore contains appreciable UO_2 (locally > 2000 ppm), whereas in the Upper Zone, in which zircon is associated with columbite-(Fe), the latter contains less than 750 ppm UO_2 (Fig. 2.14a). By comparison, the uranium content of the fluornatropyrochlore in the fresh syenites ranges from below the detection limit to greater than one weight percent, depending upon the stratigraphic position of the pyrochlore. If we consider the relative abundances of uranopyrochlore and columbite-(Fe) in the altered syenites, with the former being minor relative to the latter, the average uranium contents of these two minerals closely matches the uranium content of the fluornatropyrochlore in the fresh syenites. Given this observation, together with rarely observed pseudomorphs containing columbite and uranopyrochlore that possibly replaced magmatic pyrochlore (Fig. 2.6b), we consider that pyrochlore containing less than 5 wt. % UO_2 crystallized in the altered areas of the Nechalacho suite (the maximum UO_2 content of fluronatropyrochlore in the fresh syenites is 3.76 wt. %, V. Möller pers. comm.) and experienced significant hydrothermal alteration, resulting in the formation of columbite-(Fe) and uranopyrochlore.

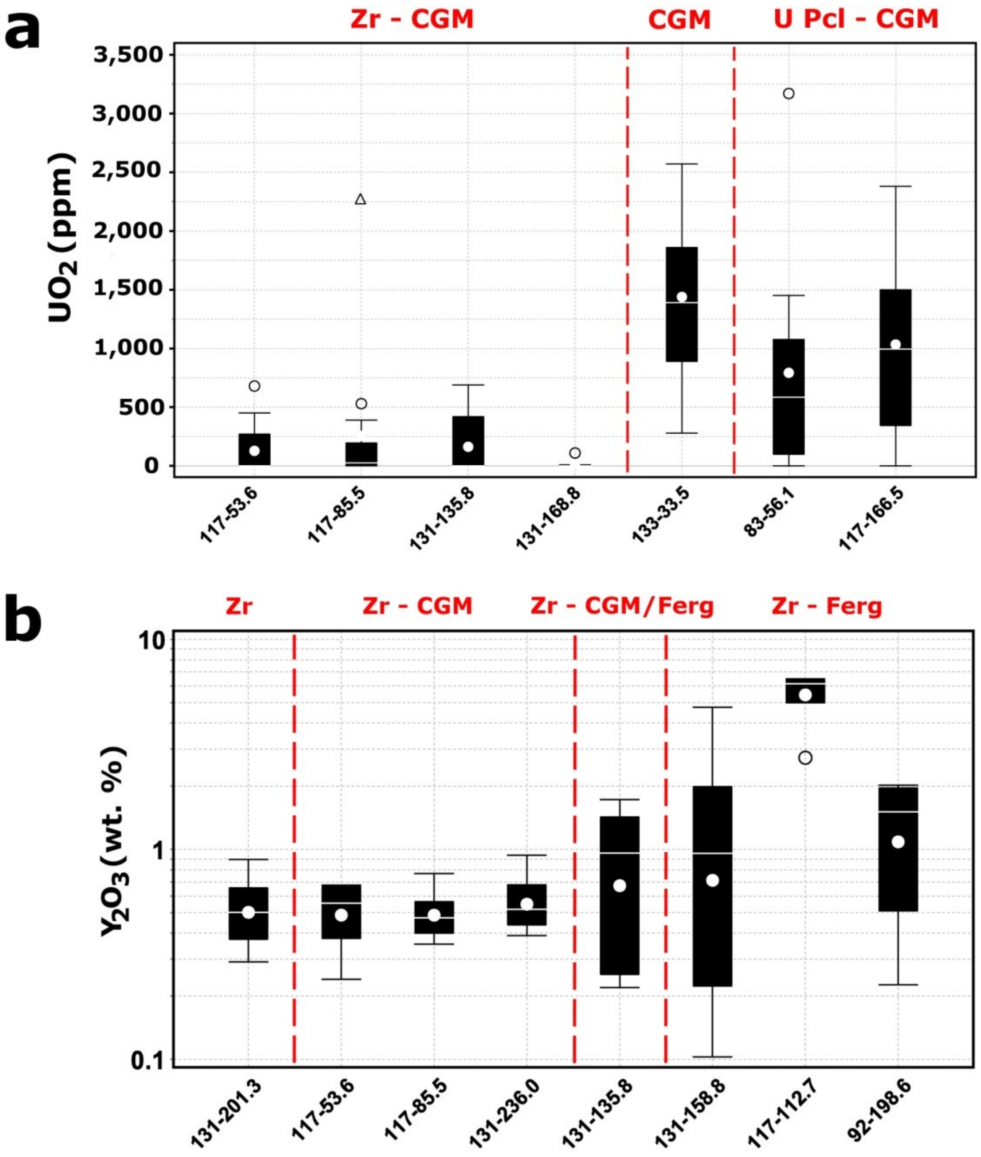

Fig. 2.14 Box and whisker plots showing a) the UO_2 content of columbite-(Fe) associated with zircon (Zr-CGM), unassociated (CGM) and associated with uranopyrochlore (U Pcl-CGM) and b) the Y_2O_3 content of zircon without a particular mineral association (Zr), associated with columbite-(Fe) (Zr-CGM), associated with columbite-(Fe) and fergusonite-(Fe) (Zr-CGM/Ferg) and associated with fergusonite-(Y) (Zr-Ferg) (b). Vertical dashed lines (red) separate the groups. CGM = columbite group minerals.

A similar alteration history to that described above has been reported for pyrochlore in the Madeira A-type granite in Brazil (Bastos Neto et al., 2009). In this granite, plumbian uranopyrochlore was altered to form uranopyrochlore, and later columbite. The increase in alteration was accompanied by an increase in the amount of UO_2 in the pyrochlore, much like that observed in the Nechalacho Layered Suite. This is consistent with the immobility of uranium during the alteration of microlite (Ta-rich pyrochlore) documented by Lumpkin and Ewing (1992). Furthermore, in this granite, alteration of the pyrochlore occurred along its cleavage planes (Bastos Neto et al., 2009), thereby providing a possible explanation for the inconsistent manner in which the uranopyrochlore is positioned in the columbite-(Fe), in the Nechalacho deposit.

There are several indications that uranium-bearing pyrochlore was a factor in the development of the columbite, even where pyrochlore is not directly observed. For example, in one thin section, taken in a core interval of high niobium content, there are millimeter-sized aggregates of columbite, many of which are elongated (Fig. 2.7a). In one rare case there are also micron-sized remnants of what might originally have been uranopyrochlore but is now columbite. Significantly, the uranium content of this columbite is similar to that of columbite surrounding uranopyrochlore, thereby implying a similar precursor (Fig. 2.14a). This, together with a sharp zonation with respect to tantalum parallel to the long axis of these columbite crystals (Fig. 2.7b), suggests the former presence of uranium-bearing pyrochlore.

The only other magmatic Nb-Ta mineral is a variety of columbite-(Fe), which was observed in a single Upper Zone sample. Significantly, in this zone and also in the Basal Zone, the bulk rock niobium content does not correlate with that of uranium. It therefore seems likely that the behaviour of niobium and tantalum was different in the two potential ore zones from that in the rest of the Nechalacho Layered Suite.

2.9.3 The Origin of Niobium Mineralization in the Upper and Basal Zones

The only niobium mineral observed in the mineralized zones that is potentially magmatic is columbite-(Fe). This mineral was found in a single sample, L08:131: 96.0, from the Upper Zone. The magmatic character of the columbite is evident from the acicular nature of the crystals, the zoning in respect to Nb and Ta and the variable alteration of this columbite-(Fe) to hydrothermal columbite-(Fe) (Fig. 2.4a and d). The latter mineral, which commonly contains numerous cavities (Fig. 2.4c), is very similar to hydrothermal columbite-(Fe) elsewhere in the Upper Zone, including that surrounding zircon (Fig. 2.2c and d), suggesting that the precursor to the hydrothermal columbite-(Fe) in the Upper Zone was, at least in part, magmatic columbite-(Fe). The lack of any observable magmatic columbite in any of the other thin sections obtained from the Nechalacho deposit, is unsurprising given the pervasive nature of the metasomatism in the altered syenites, which obliterated most traces of magmatic minerals. Indeed, this is the case for other minerals in the Nechalacho Layered Suite. For example, although eudialyte is interpreted to be the precursor to most of the pseudomorphs in the Basal Zone, magmatic eudialyte is only seen in fresh rocks deep in the intrusion, and then rarely.

Just as columbite-(Fe) is the sole niobium-rich phase in the Upper Zone, so is fergusonite-(Y) the only niobium-rich phase in the Basal Zone. It is therefore probable that analogous to magmatic columbite-(Fe) likely being one of the main precursors to hydrothermal columbite-(Fe) in the Upper Zone, magmatic fergusonite-(Y) was a precursor to hydrothermal fergusonite-(Y) in the Basal Zone. Textures supporting the interpretation that fergusonite-(Y), or its REE-depleted equivalent in the Upper Zone, columbite-(Fe), crystallized from the melt and were altered in situ to form hydrothermal aggregates are numerous. Extensive aggregates of hydrothermal anhedral fergusonite-(Y) commonly envelop zircon and individually are of a size similar to that of the zircon grains (Fig. 2.2a and b). It is difficult to envision alteration of zircon, the only other niobium-bearing mineral in the vicinity, being able to supply sufficient niobium to form these aggregates. In order to produce the amount of fergusonite-(Y) visible in the backscattered electron images (BSE) of Figures 2.2a and b, $\geq$10 wt. % Nb_2O_5 would need to have been transferred from the zircon (fergusonite-Y contains ~45 wt. % Nb_2O_5). This is unrealistic as most unaltered zircon crystals contain ~2 wt. % Nb_2O_5 and few crystals contain more than ~3 wt. % Nb_2O_5. Moreover, fergusonite-(Y) in these figures envelopes the zircon and does not emanate outwards from its cores.

The above notwithstanding, it is also evident that some fergusonite-(Y) and columbite-(Fe) formed using niobium released by the alteration of zircon as shown by the occurrence of aggregates of these minerals in the cores of zircon grains and along fractures emanating out from them (Fig. 2.3). The alteration of zircon to fergusonite-(Y) in the Basal Zone is particularly evident in sample L08-117: 123.3, which displays a complete continuum from zircon grains containing fergusonite-(Y) in their cores (Fig. 2.3a), to a grain in which the fergusonite-(Y) is more disseminated in a zircon core and had started to form beyond it (Fig. 2.3b), and finally to zircon grains in which the fergusonite-(Y) appears to have moved into the surrounding material (Fig. 2.3c). These examples illustrate the progressive outward migration of Nb (and Y) from the cores of zircon crystals. Similar examples of the preferential alteration of zircon cores to a niobium mineral are observed in the Upper Zone, but in these cases columbite-(Fe), rather than fergusonite-(Y) is the hydrothermal mineral (Fig. 2.3d).

The restriction of fergusonite-(Y) to the Basal Zone and columbite-(Fe) to the Upper Zone is consistent with the observation that the Basal Zone is considerably more enriched in the HREE than the Upper Zone. If, as proposed above, zircon was the mineral that supplied the Nb and Y or Nb needed to form fergusonite-(Y) and columbite-(Fe), respectively, then it follows that it would have been enriched in yttrium within the Basal Zone and depleted in yttrium and other HREE within the Upper Zone. This is precisely what is indicated by electron-microprobe analyses of the zircon (Fig. 2.14b). In samples below the Upper Zone, the proportion of Y_2O_3 by weight in the zircon is typically above 1 wt. % and as high as 6 wt. %. By contrast, in samples from the Upper Zone, the proportion of Y_2O_3 in the zircon is invariably less than 1 wt. %.

Although zircon in the Basal Zone commonly contains wt. % levels of Y_2O_3, it can also contain well below 1 wt. % Y_2O_3 and thus be compositionally similar to zircon in the Upper Zone. There are two reasons for this wide range. The first is that zircon in the Basal Zone has Y-rich cores, which are preferentially altered to form fergusonite-(Y) and Y-poor rims that remain relatively unaffected (Fig. 2.15a-b). The second is extensive alteration, which lowered Y_2O_3 contents. This is illustrated in Figure 2.15c-d; zircon that is relatively unaltered commonly contains more than 1 wt. % Y_2O_3, whereas parts of zircon in immediate contact with fergusonite-(Y) and columbite-(Fe) have less than 0.5 wt. % Y_2O_3.

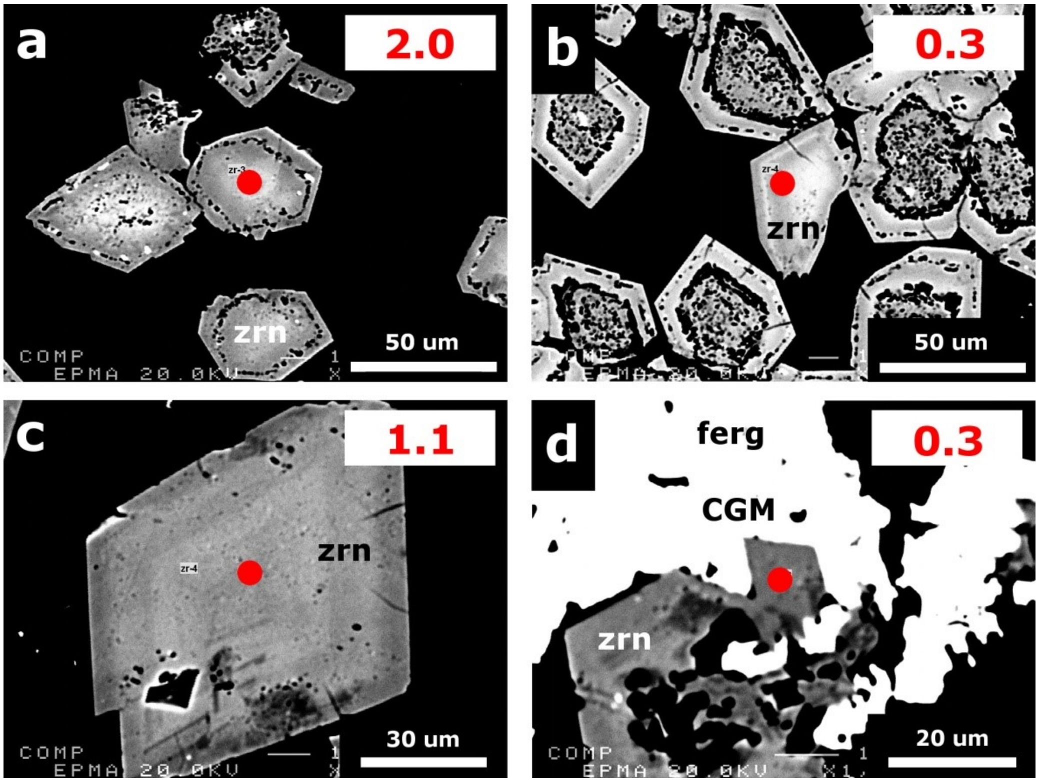

Fig. 2.15 BSE images illustrate the bright Y-rich cores (a) and dark Y-poor rims (b) of selected zircon grains from Basal Zone sample L08-131: 158.8. The Y content of zircon in crystals not surrounded by fergusonite-(Y) and columbite-(Fe) (c) is compared with crystals surrounded by these minerals (d) in Upper Zone sample L08-131: 135.8. The Y_2O_3 concentrations (wt. %) of each analyzed spot, indicated by the red circle, are shown in the upper right of each image. CGM = columbite group minerals.

2.9.4 Quantitative Evaluation of the Source of Niobium in Hydrothermal Columbite-(Fe) and Fergusonite-(Y)

In the previous section, we provided evidence that hydrothermal columbite-(Fe) and fergusonite-(Y) in the mineralized zones formed by replacing magmatic columbite-(Fe) and fergusonite-(Y), respectively, and to a lesser extent as a result of the break-down of zircon. In order to quantitatively evaluate the relative contributions of the different precursors, we carried out mass balance calculations using the bulk composition of two meter intervals of drill core and the compositions of the above minerals. From the bulk rock ZrO_2 content and the proportion of ZrO_2 in the zircon (~60 wt. %), we determined the proportion of zircon in each drill core interval. As the zircon was heavily altered and its Nb_2O_5 content ranges from 1.5 to 3.5 wt. %, we assumed that 2 wt. % Nb_2O_5 was mobilized from the zircon. This may be a conservative estimate as most of the zircon crystals analyzed were heavily altered and likely contained more niobium prior to alteration. The amounts of hydrothermal columbite-(Fe) and fergusonite-(Y) produced due to alteration of zircon were calculated using the amount of niobium mobilized from the zircon, the calculated abundance of zircon in the drill core, the Nb_2O_5 abundance of columbite (~70 wt. % Nb_2O_5) in the Upper Zone and altered syenites and the Nb_2O_5 abundance of fergusonite (~45 wt. % Nb_2O_5) in the Basal Zone. It was assumed that there was sufficient iron available in the rock for the formation of iron-rich columbite-(Fe). The amount of niobium in the hydrothermal fergusonite-(Y) or columbite-(Fe) produced from zircon was subtracted from the bulk drill core niobium abundance leaving a remainder, which was assumed to have been originally in magmatic niobium minerals. Using this remainder and the Nb_2O_5 contents of columbite-(Fe) and fergusonite-(Y), we then calculated the amounts of hydrothermal columbite-(Fe) or fergusonite-(Y) originating from the magmatic equivalents of these minerals. The results of these calculations are illustrated in Figure 16, in which the proportion of columbite-(Fe) (Upper Zone, non-ore zone) or fergusonite-(Y) (Basal Zone) resulting from the break-down of zircon is shown as a function of the wt. % Nb_2O_5 supplied by the zircon. From our assumption that 2 wt.% Nb_2O_5 was mobilized from zircon, it follows that between ~25-40 wt. % of the columbite-(Fe) in the Upper Zone and fergusonite-(Y) in the Basal Zone were derived from the breakdown of zircon. The only sample in which zircon was calculated to have been a minor source of niobium for columbite-(Fe) and fergusonite-(Y) is from a zone of intense albitization, which is largely devoid of zircon. An additional test of our calculations is provided by sample L08-131: 95-97, which as discussed earlier, contains appreciable magmatic columbite-(Fe). As expected, the calculated proportion of CGM resulting from the alteration of zircon in this sample is lower than that of any of the ore zone samples (Fig. 2.16).

2.9.5 Niobium Mobility

We have established that a large part of the niobium and tantalum mineralization at the Nechalacho deposit is hydrothermal, which allows for the possibility that niobium and tantalum were remobilized, potentially on a large scale. In thin section, however, zircon is in close spatial association with columbite-(Fe) or fergusonite-(Y), commonly on a scale of tens of microns. At the meter scale of the drill core, bulk zirconium and niobium abundances are, in general, tightly correlated, particularly in the Upper Zone and Basal Zone. In drill hole L08-117, which was sampled extensively in this study, the Pearson correlation coefficient for Zr with Nb in two meter drill core intervals is 0.94 for the entire 205 meters of the hole. If zircon, columbite-(Fe), and fergusonite-(Y) had crystallized independently of each other, their spatial distribution would vary appreciably and the correlation between Zr and Nb would be significantly poorer. Furthermore,

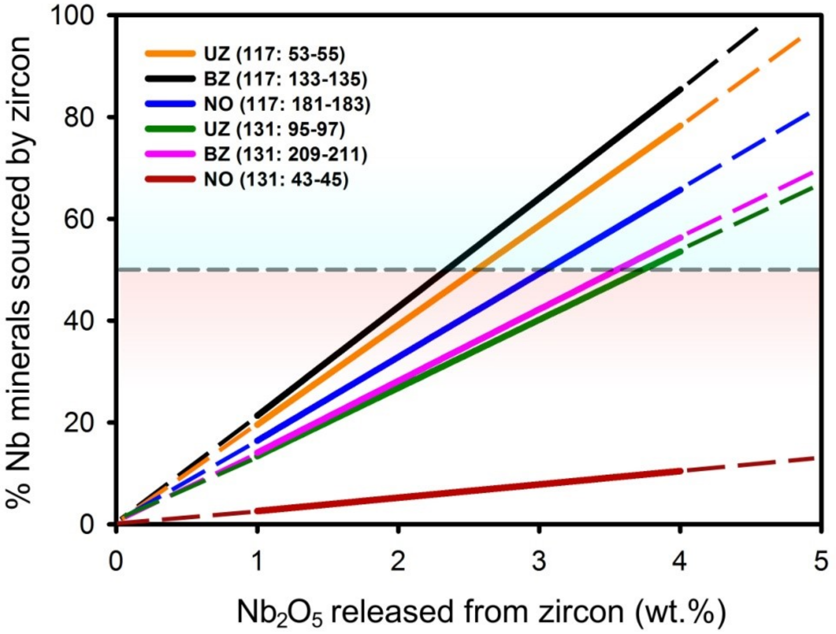

Fig. 2.16 The proportion of hydrothermal niobium-bearing minerals crystallized from niobium supplied by the alteration of zircon (% Nb minerals sourced by zircon) versus the amount of Nb_2O_5 released by the zircon. The solid lines indicate the predicted ranges in these proportions for samples of the Upper Zone (UZ), the Basal Zone (BZ) and outside the potential ore zones (NO); the numbers associated with the labels identify the drill hole and the depth of the sample. The horizontal dashed line separates a dominantly zircon-based source (high %) from a dominantly magmatic columbite-(Fe) or fergusonite-(Y) source (low %).

if metasomatism had resulted in the preferential remobilization of either Zr or Nb, the correlation would also be much poorer. It is important to note, however, that the aqueous complexation of zirconium and niobium in aqueous fluids at elevated temperature could be similar and they may have been mobilized at equivalent depths. This is supported by the observation that zirconium and niobium are transported predominantly as hydroxyl-fluoride species at elevated temperature (Migdisov et al., 2011; Timofeev et al. 2015). Significantly, the fluoride-rich mineralogy of the giant Bayan Obo Fe-REE-Nb deposit, China, suggests that high aqueous fluoride activity may have also controlled mobilization of niobium and tantalum in that system (Smith and Henderson 2000). Nevertheless, we consider it likely that the mobility of Zr and Nb was very limited in the Nechalacho deposit, because of the very strong correlation of the two elements and the very close spatial association of fergusonite-(Y) and columbite-(Fe) with zircon in the Basal Zone and Upper Zone, respectively.

2.9.6 Potential magmatic signatures in Ta/(Ta+Nb) and Mn/(Mn+Fe) trends

As mentioned in the introduction to this paper, the Ta/(Ta+Nb) and Mn/(Mn+Fe) ratios of columbite in NYF (Nb-Y-F) pegmatites can be used to monitor crystal fractionation. They increase steadily with crystal fractionation, the Mn/(Mn+Fe) ratio increasing first, presumably due to the complexation of manganese with ligands such as F or the incorporation of Fe into crystallizing phases (Wise et al., 2012). The ratio of Ta/(Ta+Nb) increases later, because of the higher solubility of the tantalum end members of columbite in the magma (Linnen and Keppler, 1997). In principle, it should be possible to use the above relationship to evaluate crystal fractionation in the Nechalacho Layered Suite. However, as a substantial proportion of the columbite-(Fe) is an alteration product of zircon and magmatic columbite-(Fe), and the latter was highly altered, these ratios are likely to have been masked and disturbed, respectively.

Preservation of the ratios would require that either Ta and Nb or Mn and Fe were not mobilized significantly during alteration and, if this were the case, it is possible that the columbite might display the magmatic signature observed in pegmatites.

A trend of steadily increasing Ta/(Ta+Nb) and Mn/(Mn+Fe) ratios is observed in the columbite-(Fe) of the Nechalacho suite. However, the range of Ta/(Ta+Nb) values in the columbite-(Fe) is limited, whereas Mn/(Mn+Fe) ratios, even in a single sample, such as L08-131:96.0, vary considerably (Fig. 2.10). In addition, no relationship could be discerned between the Ta/(Ta+Nb) ratio and the depth of sample, which would be expected, if the columbite-(Fe) had crystallized from an evolving melt. It is possible that a relationship of this type is present but was obscured by small scale cycles of fractional crystallization. Alternatively, the small differences in the values of this ratio among the samples analysed may simply have resulted from variations in the intensity of alteration, as proposed previously for the Separation Lake pegmatites, in which columbite displaying patchy replacement has a lower Ta/(Ta+Nb) ratio than unaltered columbite; Mn/(Mn+Fe) values were unaffected by this alteration (Tindle and Breaks, 2000).

In contrast to the Ta/(Ta+Nb) ratio, the Mn/(Mn+Fe) ratio is high and variable (Fig. 2.10). There is a general increase in the ratio with decreasing depth, as would be expected if crystal fractionation controlled columbite-(Fe) composition (Fig. 2.13). Moreover, the Mn/(Mn+Fe) ratio in the columbite-(Fe) correlates positively with the bulk P_2O_5 of the core (Fig. 2.12). If manganese was retained in the melt due, in part, to the presence of phosphorus, then this association may represent a magmatic signature (Bartels et al. 2010).

2.9.7 Genetic Model for Niobium and Tantalum Mineralization

Niobium and tantalum were concentrated in the two potential REE ore zones. In the Upper Zone, magmatic columbite-(Fe) was altered to form anhedral aggregates of columbite-(Fe). This was the main source of niobium for hydrothermal columbite-(Fe), although locally additional niobium was supplied by alteration of zircon. This niobium-rich and yttrium-poor zircon crystallized directly from a melt or was formed hydrothermally, and yielded niobium for the formation of columbite-(Fe) through preferential alteration of the cores of its crystals.

In part, the behaviour of niobium in the Basal Zone was similar to that in the Upper Zone. Niobium- and yttrium-rich zircon and fergusonite-(Y) formed as pseudomorphs after eudialyte. However, additional hydrothermal fergusonite-(Y) was produced by the alteration of the cores of the niobium-enriched zircon, and the alteration of magmatic fergusonite-(Y). In absolute terms, former magmatic fergusonite-(Y) and, to an unconstrained extent, pseudomorphs after eudialyte supplied the greater part of the niobium to the hydrothermal fergusonite-(Y), but the alteration of zircon played an important role, and locally supplied more niobium than the other sources.

Outside the potential ore zones, uranium-bearing pyrochlore similar to that in the fresh syenites was altered later to form uranium-enriched columbite-(Fe), leaving behind uranopyrochlore relicts. Although magmatic columbite was not observed, it is likely that alteration of this mineral was also a source for the niobium in hydrothermal columbite-(Fe). Finally, mass balance calculations suggest that niobium mobilized from the small amounts of zircon that are present in non-ore zone material was responsible for the formation of some hydrothermal columbite-(Fe).

2.10 Conclusions

The Nechalacho deposit is a significant niobium and tantalum resource as the result of the concentration of these metals by magmatic processes. Later hydrothermal alteration destroyed much of the magmatic record of niobium and tantalum enrichment through pervasive replacement of the magmatic niobium- and tantalum-bearing minerals by hydrothermal columbite-(Fe) and fergusonite-(Y). Thus relicts of this magmatic mineralogy are rare. Careful evaluation of the niobium-tantalum mineralogy and the bulk rock chemistry, however, has made it possible to reconstruct the magmatic history of niobium-tantalum enrichment. The magmatic minerals comprised columbite-(Fe) in the Upper Zone, fergusonite-(Y) in the Basal Zone, niobium-rich zircon in these two zones, and pyrochlore and columbite-(Fe) outside them. Extensive hydrothermal alteration resulted in the formation of columbite-(Fe) and fergusonite-(Y) from magmatic equivalents of these two minerals, as well as from niobium-rich zircon, and uranium-rich columbite formed from the pyrochlore. Outside the ore zones, a close association between uranium, niobium, and tantalum was observed and linked to the presence of pyrochlore, whereas within the two ore zones niobium and zirconium are strongly correlated as a result of the release of niobium from altered zircon for the formation of columbite-(Fe). This study shows that niobium and tantalum are mobile, but only at the micron scale and that despite intense hydrothermal alteration, it is possible to reconstruct the magmatic mineralogy of niobium and tantalum in igneous complexes enriched in these metals.

2.11 Acknowledgments

Avalon Rare Metals provided access to the property, essential logistical support and funding for the research, all made possible with the help of W. Mercer. The authors thank M. Heiligmann, C. Pedersen and V. Möller for their assistance in the field and the numerous discussions with them that contributed to the content of this paper. The assistance of L. Shi was important in obtaining the electron microprobe data that underpinned much of the research. Additional funding for the research was provided by a Natural Sciences and Engineering Research Council (NSERC) collaborative research and development grant to A.E. Williams-Jones and NSERC and Fonds Québécois de la Recherche sur la Nature et les Technologies (FQRNT) scholarships to A. Timofeev. Constructive reviews by M. Hoshino, F. Wall and Associate Editor Y. Watanabe, helped improve the manuscript significantly.

2.12 References

Avalon Rare Metals Inc. News Release No. 13-07, August 15, 2003 (http://avalonraremetals.com/_resources/news/2013/NR_13_07.pdf)

Bartels, A., Holtz, F. and Linnen, R.L., 2010, Solubility of manganotantalite and manganacolumbite in pegmatitic melts: American Mineralogist, v. 95, p. 537-544.

Bastos Neto, A.C., Pereira, V.P., Ronchi, L.H., De Lima, E.F., and Frantz, J.C., 2009, The World-Class Sn, Nb, Ta, F (Y, REE, Li) Deposit and the Massive Cryolite Associated with the Albite-Enriched Facies of the Madeira A-Type Granite, Pitinga Mining District, Amazonas State, Brazil: Canadian Mineralogist, v. 47, p. 1329-1357.

Bleeker, W. and Hall, B., 2007, The Slave Craton: geology and metallogenic evolution. Mineral Deposits of Canada: A Synthesis of Major Deposit-Types, District Metallogeny, the Evolution of Geological Provinces, and Exploration Methods: Geological Association of Canada, Mineral Deposits Division, Special Publication, v.5, p. 849-879.

Buchan, K., Ernst, R., Bleeker, W., Davis, W., Villeneuve, M., van Breemen, O., Hamilton, M. and Söderlund, U., 2010, Proterozoic magmatic events of the Slave craton, Wopmay orogen and environs: Geological Survey of Canada, Open File 5985.

Davidson, A., 1982, Petrochemistry of the Blachford Lake Complex Near Yellowknife, Northwest Territories, *in* Uranium in Granites (ed. Y.T. Maurice) Geological Survey of Canada Paper 81-23, p. 71-79.

Ercit, T.S., 2005, Identification and Alteration Trends of Granitic-Pegmatite-Hosted (Y,REE,U,Th)-(Nb,Ta,Ti) Oxide Minerals: A Statistical Approach: Canadian Mineralogist, v. 43, p. 1291-1303.

Linnen, R.L., 1998, The Solubility of Nb-Ta-Zr-Hf-W in Granitic Melts with Li and Li + F: Constraints for Mineralization in Rare Metal Granites and Pegmatites: ECONOMIC GEOLOGY, v. 93, p. 1013-1025.

Linnen, R.L., and Keppler, H., 1997, Columbite solubility in granitic melts: consequences for the enrichment and fractionation of Nb and Ta in the Earth`s crust: Contributions to Mineralogy and Petrology, v. 128, p. 213-227.

Lumpkin, G.R., and Ewing, R.C., 1992, Geochemical alteration of pyrochlore group minerals: Microlite subgroup: American Mineralogist, v. 77, p. 179-188.

McCreath, J.A., Finch, A.A., Herd, D.A., and Armour-Brown, A., 2013, Geochemistry of pyrochlore minerals from the Motzfeldt Center, South Greenland: The mineralogy of a syenite-hosted Ta, Nb deposit: American Mineralogist, v. 98, p. 426-438.

Migdisov, Art. A., Williams-Jones, A.E., van Hinsberg, V., and Salvi, S., 2011, An experimental study of the solubility of baddeleyite (ZrO2) in fluoride-bearing solutions at elevated temperature: Geochimica et Cosmochimica Acta, v. 75, p. 7426-7434.

Möller V., and Williams-Jones A.E., 2013, Magmatic controls on the formation of the Nechalacho rare metal deposit, Thor Lake, Northwest Territories, Canada [abs.]: Society of Economic Geologists Annual Meeting, Whistler, British Columbia, Canada, Abstracts.

Pinckston, D.R. and Smith, D.G.W., 1995, Mineralogy of the Lake Zone, Thor Lake rare-metals deposit, N.W.T., Canada: Canadian Journal of Earth Sciences, v. 32, p. 516-532.

Sheard, E.R., Williams-Jones, A.E., Heiligmann, M., Pederson, C. and Trueman, D.L., 2012, Controls on the Concentration of Zirconium, Niobium, and the Rare Earth Elements in the Thor Lake Rare Metal Deposit, Northwest Territories, Canada: ECONOMIC GEOLOGY, v. 107, p. 81-104.

Sinclair, W.D., Hunt, P.A., and Birkett, T.C., 1994, U-Pb zircon and monazite ages of the Grace Lake Granite, Blatchford Lake Intrusive Suite, Slave Province, Northwest Territories: *In* Radiogenic Age and Isotopic Studies: Report 8; Geological Survey of Canada, Current Research 1994-F, p. 15-20.

Smith, M. P., and Henderson, P., 2000, Preliminary Fluid Inclusion Constraints on Fluid Evolution in the Bayan Obo Fe-REE-Nb Deposit, Inner Mongolia, China: ECONOMIC GEOLOGY*,* v. 95, p. 1371-1388.

Timofeev, A., Migdisov, A.A., and Williams-Jones, A.E., 2015, An experimental study of the solubility and speciation of niobium in fluoride-bearing aqueous solutions at elevated temperature: Geochimica et Cosmochimica Acta, v. 158, p. 103-111.

Tindle, A.G. and Breaks, F.W., 2000, Columbite-tantalite mineral chemistry from rare-element granitic pegmatites: Separation Lake area, N.W. Ontario, Canada: Mineralogy and Petrology, v. 70, p. 165-198.

Wise, M.A., Francis, C.A., and Černý, P., 2012, Compositional and Structural Variations in Columbite-Group Minerals from Granitic Pegmatites of the Brunswick and Oxford Fields, Maine: Differential Trends in F-poor and F-rich Environments: The Canadian Mineralogist, v. 50, p. 1515-1530.

Appendix 2.1 Standards used for electron microprobe analyses (the standard used for a given element was employed for all minerals analyzed unless otherwise noted)

Standard	Elements	Counting time (sec)
CaF_2	F, Ca	20
$Vana_2$	Pb	20
TiO_2	Ti	20
Fe_2O_3_FeO	Fe	20
Diopside	Si, Ca[1]	20
Olivine	Mg	20
Spessartine	Mn	20
SnO_2	Sn	20
TaylorPyrope	Al	20
Flap	P	20
$Na_2Nb_2O_6$	Nb, Na	20
$K_2Ta_2O_6$	Ta, K	100, 20[3]
TaylorYAG	Y	20, 100[2]
UO_2	U	100, 50[3]
ThO_2	Th	20, 50[3], 100[2]
Zircon	Zr, Hf[a], Si[2]	20, 100[a]
MAC-Ce	Ce	40, 20[2]
MAC-Eu	Eu	100
MAC-La	La	50
MAC-Pr	Pr	40, 50[2]
MAC-Dy	Dy	50
MAC-Gd	Gd	50
MAC-Yb	Yb	50
MAC-Nd	Nd	40, 50[2]
MAC-Sm	Sm	50
MAC-Er	Er	60, 100[2]

[1] Columbite

[2] Zircon, fergusonite-(Y), samarskite-(Y)

[3] Pyrochlore, uranopyrochlore

Appendix 2.2: Columbite Microprobe Results

Name	#	Y2O3	F	CaO	Nb2O5	FeO	ThO2	Ta2O5	Er2O3	Sm2O3	MgO	TiO2	UO2	MnO	SnO2	P2O5	Total
133-33.5	1	0.000	-	0.089	71.79	18.34	0.000	2.414	0.017	0.000	0.136	2.640	0.123	2.820	0.203	-	98.56
	2	0.055	-	0.047	71.06	18.49	0.000	2.201	0.013	0.000	0.072	3.297	0.184	2.498	0.261	-	98.18
	3	0.075	-	0.053	73.14	17.29	0.000	2.320	0.054	0.000	0.162	2.664	0.053	4.109	0.253	-	100.17
	4	0.000	-	0.035	73.13	18.41	0.000	2.183	0.031	0.000	0.095	2.853	0.085	2.892	0.255	-	99.96
	5	0.101	-	0.062	72.64	17.63	0.009	2.215	0.090	0.000	0.104	2.883	0.048	3.807	0.280	-	99.87
	6	0.046	-	0.059	71.80	18.29	0.000	1.489	0.000	0.000	0.161	3.480	0.110	2.749	0.296	-	98.49
	7	0.060	-	0.054	72.25	17.95	0.003	1.611	0.048	0.000	0.115	3.661	0.160	3.024	0.283	-	99.21
	8	0.056	-	0.058	72.77	17.78	0.005	2.078	0.013	0.000	0.119	2.818	0.075	3.257	0.251	-	99.28
	9	0.046	-	0.065	72.80	17.39	0.000	2.224	0.062	0.000	0.120	2.367	0.104	3.758	0.189	-	99.12
	10	0.000	-	0.166	72.42	19.18	0.019	2.363	0.037	0.004	0.098	3.098	0.186	1.840	0.254	-	99.66
	11	0.054	0.000	0.097	71.50	19.18	0.006	2.807	0.027	0.039	0.053	3.095	0.172	1.795	0.213	0.014	99.05
	12	0.095	0.000	0.068	71.45	18.27	0.025	3.222	0.028	0.057	0.057	2.741	0.133	2.707	0.207	0.011	99.08
	13	0.037	0.000	0.048	70.70	18.91	0.030	3.066	0.051	0.039	0.058	3.183	0.235	2.159	0.295	0.009	98.82
	14	0.053	0.000	0.025	72.94	16.60	0.005	2.553	0.013	0.007	0.084	2.252	0.028	4.726	0.115	0.007	99.40
	15	0.166	0.000	0.076	70.90	18.77	0.000	2.953	0.041	0.000	0.014	2.899	0.227	2.165	0.305	0.011	98.53
	16	0.167	0.000	0.118	72.13	16.93	0.026	3.037	0.007	0.000	0.066	2.620	0.089	4.077	0.222	0.009	99.50
	17	0.079	0.000	0.079	73.18	19.05	0.035	2.306	0.000	0.123	0.066	2.097	0.139	2.306	0.130	0.013	99.60
	18	0.152	0.000	0.079	71.38	18.34	0.006	2.293	0.040	0.012	0.053	3.335	0.205	2.586	0.295	0.012	98.79
	19	0.162	0.000	0.146	71.08	17.52	0.021	2.796	0.042	0.096	0.038	2.709	0.175	3.361	0.204	0.019	98.37
	20	0.139	0.000	0.078	71.02	19.22	0.028	1.488	0.044	0.000	0.000	4.251	0.257	1.864	0.290	0.008	98.68
	21	0.142	0.000	0.064	72.08	19.46	0.038	1.247	0.065	0.040	0.000	3.515	0.252	1.650	0.253	0.020	98.83
	22	0.155	0.000	0.041	72.53	17.89	0.005	1.517	0.096	0.115	0.013	2.873	0.141	3.239	0.181	0.008	98.80
	23	0.076	0.000	0.023	72.76	19.50	0.000	1.669	0.000	0.016	0.005	2.963	0.128	1.874	0.236	0.024	98.56
83-56.1	24	0.000	-	0.049	74.63	18.27	0.000	0.767	0.045	0.000	0.169	1.321	0.317	3.344	0.043	-	98.96
	25	0.000	-	0.026	75.31	18.10	0.000	0.596	0.027	0.001	0.141	1.849	0.043	3.638	0.065	-	99.80
	26	0.000	-	0.052	75.34	19.36	0.012	0.678	0.009	0.000	0.164	1.721	0.046	2.537	0.073	-	100.00
	27	0.000	-	0.096	74.66	18.37	0.000	0.869	0.031	0.000	0.165	2.016	0.110	3.418	0.075	-	99.81
	28	0.000	-	0.017	75.79	18.48	0.012	0.939	0.000	0.000	0.148	1.239	0.082	3.504	0.068	-	100.27
	29	0.000	-	0.030	74.54	19.08	0.000	0.791	0.096	0.000	0.139	1.683	0.145	3.147	0.110	-	99.76
	30	0.007	0.000	0.022	76.10	16.98	0.018	0.838	0.008	0.023	0.159	1.048	0.002	4.610	0.014	0.004	99.83
	31	0.000	0.000	0.038	76.40	16.02	0.027	0.786	0.055	0.002	0.149	1.040	0.000	5.343	0.006	0.015	99.88
	32	0.048	0.000	0.016	75.52	18.12	0.007	0.710	0.034	0.015	0.098	1.232	0.101	3.495	0.055	0.015	99.46
	33	0.044	0.000	0.018	75.26	20.49	0.015	0.732	0.028	0.073	0.088	2.167	0.071	1.372	0.030	0.006	100.40
	34	0.000	0.000	0.011	76.96	18.38	0.009	0.687	0.000	0.026	0.142	0.785	0.000	3.368	0.001	0.015	100.38
	35	0.001	0.000	0.008	76.45	17.40	0.028	0.932	0.016	0.010	0.175	1.008	0.034	4.052	0.034	0.011	100.16

117-53.6	36	0.648	-	0.133	70.70	12.17	0.029	5.056	0.085	0.171	0.061	0.979	0.025	7.718	0.223	-	98.00
	37	0.059	-	0.040	72.35	13.69	0.000	4.640	0.050	0.000	0.060	0.608	0.000	7.437	0.066	-	99.00
	38	0.058	-	0.037	73.49	13.53	0.006	4.193	0.007	0.000	0.061	0.544	0.000	7.530	0.072	-	99.53
	39	0.000	-	0.045	73.33	13.82	0.015	4.733	0.000	0.000	0.069	0.398	0.000	8.594	0.063	-	101.07
	40	0.260	-	0.045	73.66	13.05	0.000	3.882	0.084	0.000	0.056	0.355	0.000	7.575	0.049	-	99.01
	41	0.499	-	0.146	69.54	13.48	0.058	5.506	0.095	0.008	0.071	1.586	0.029	6.745	0.197	-	97.97
	42	0.070	-	0.014	74.13	13.39	0.000	4.742	0.048	0.000	0.020	0.477	0.000	7.659	0.059	-	100.61
	43	0.017	-	0.032	73.03	13.56	0.000	4.170	0.037	0.000	0.053	0.729	0.000	7.433	0.131	-	99.19
	44	0.115	0.000	0.066	72.06	16.25	0.000	3.293	0.077	0.000	0.010	1.774	0.000	4.518	0.299	0.005	98.47
	45	0.116	0.000	0.165	74.65	15.68	0.040	3.353	0.000	0.000	0.011	0.939	0.000	5.417	0.180	0.010	100.56
	46	0.177	0.000	0.069	73.49	14.61	0.000	3.940	0.049	0.032	0.026	0.845	0.068	6.560	0.151	0.005	100.03
	47	0.051	0.000	0.034	73.52	15.36	0.014	3.461	0.034	0.006	0.000	0.764	0.045	6.042	0.190	0.005	99.52
	48	0.248	0.000	0.043	72.31	12.90	0.000	3.123	0.053	0.032	0.014	1.636	0.000	7.821	0.289	0.008	98.48
117-85.5	49	0.018	-	0.041	71.05	16.97	0.000	5.229	0.018	0.000	0.081	0.877	0.004	4.384	0.181	-	98.85
	50	0.042	-	0.024	69.96	13.28	0.000	7.861	0.029	0.006	0.050	0.692	0.000	7.819	0.067	-	99.83
	51	0.024	-	0.084	69.72	15.24	0.000	6.605	0.059	0.000	0.070	1.540	0.039	5.883	0.317	-	99.58
	52	0.028	-	0.027	69.53	16.02	0.001	6.353	0.015	0.000	0.073	1.439	0.009	5.586	0.274	-	99.35
	53	0.023	-	0.052	68.28	10.76	0.000	8.897	0.029	0.000	0.095	0.600	0.000	10.67	0.050	-	99.46
	54	0.139	-	0.201	67.27	9.857	0.000	9.852	0.025	0.000	0.065	0.615	0.000	10.14	0.053	-	98.22
	55	0.078	-	0.047	69.23	10.53	0.008	8.809	0.103	0.000	0.077	0.530	0.001	10.05	0.000	-	99.46
	56	0.000	-	0.030	69.30	16.12	0.000	6.506	0.009	0.000	0.037	1.281	0.009	5.140	0.242	-	98.68
	57	0.419	0.000	0.172	63.00	18.51	0.138	4.153	0.087	0.065	0.000	7.962	0.227	1.895	0.930	0.007	97.56
	58	0.269	0.000	0.082	70.06	9.392	0.000	8.700	0.032	0.029	0.000	0.537	0.053	10.52	0.000	0.000	99.68
	59	0.216	0.000	0.030	70.89	9.820	0.010	8.536	0.056	0.014	0.007	0.547	0.000	10.78	0.081	0.000	100.98
	60	0.573	0.000	0.087	69.00	12.94	0.000	9.858	0.035	0.054	0.000	0.512	0.013	8.218	0.018	0.005	101.31
	61	0.167	0.000	0.038	69.51	9.711	0.000	10.15	0.064	0.000	0.000	0.544	0.001	10.78	0.049	0.003	101.03
	62	0.146	0.000	0.045	70.53	10.22	0.000	8.075	0.000	0.018	0.027	0.463	0.000	10.50	0.009	0.006	100.05
117-166.5	63	0.031	-	0.083	74.56	16.08	0.000	1.468	0.040	0.002	0.328	1.883	0.081	5.360	0.030	-	99.95
	64	0.000	-	0.005	74.30	20.32	0.002	0.996	0.048	0.000	0.224	2.172	0.075	2.062	0.026	-	100.23
	65	0.000	-	0.018	73.37	20.94	0.000	0.901	0.000	0.000	0.165	2.767	0.021	1.492	0.029	-	99.71
	66	0.000	-	0.009	76.72	15.61	0.000	0.731	0.043	0.006	0.346	1.135	0.000	6.130	0.011	-	100.73
	67	0.000	-	0.087	72.66	19.49	0.022	1.468	0.000	0.000	0.211	2.339	0.238	2.358	0.030	-	98.90
	68	0.000	-	0.012	72.42	21.19	0.005	1.041	0.033	0.000	0.162	3.044	0.141	1.527	0.044	-	99.62
	69	0.009	-	0.166	73.01	18.56	0.000	1.008	0.082	0.016	0.198	2.628	0.153	3.037	0.023	-	98.89
	70	0.000	-	0.017	71.85	20.85	0.001	0.937	0.090	0.000	0.157	3.898	0.118	1.407	0.059	-	99.39
117-133.1	71	0.000	-	0.000	73.42	21.23	0.001	2.778	0.048	0.000	0.094	0.688	0.000	1.012	0.067	-	99.34
131-135.8	72	0.102	-	0.092	71.07	14.74	0.012	6.305	0.037	0.000	0.163	0.835	0.000	6.094	0.114	-	99.57
	73	0.079	-	0.114	70.68	13.65	0.000	6.940	0.000	0.000	0.157	0.750	0.000	7.139	0.056	-	99.56
	74	0.419	-	0.410	69.85	15.12	0.053	6.466	0.083	0.106	0.158	1.083	0.000	4.965	0.099	-	98.81
	75	0.182	-	0.289	70.68	14.23	0.037	6.844	0.030	0.016	0.155	1.027	0.000	6.453	0.096	-	100.03

	76	0.239	-	0.253	70.68	16.16	0.010	5.523	0.068	0.000	0.184	1.198	0.003	4.956	0.141	-	99.41
	77	0.189	-	0.499	69.95	14.28	0.013	7.362	0.088	0.000	0.152	1.051	0.012	5.739	0.120	-	99.45
	78	0.364	-	0.311	68.93	15.41	0.007	7.055	0.035	0.027	0.168	1.622	0.000	4.780	0.229	-	98.93
	79	0.255	-	0.927	70.65	13.91	0.012	5.740	0.000	0.054	0.141	1.266	0.000	5.848	0.170	-	98.97
	80	0.299	0.000	0.223	70.03	15.58	0.000	7.315	0.042	0.073	0.114	1.166	0.000	4.693	0.171	0.008	99.71
	81	0.344	0.000	0.111	72.86	15.26	0.000	5.435	0.069	0.000	0.107	1.098	0.069	5.187	0.138	0.007	100.68
	82	0.462	0.000	0.445	72.18	15.11	0.089	5.602	0.091	0.221	0.124	1.214	0.057	4.882	0.130	0.008	100.61
	83	0.182	0.000	0.084	72.26	15.45	0.000	5.519	0.040	0.033	0.125	0.855	0.062	5.154	0.120	0.000	99.88
	84	0.268	0.000	0.358	72.72	15.32	0.088	5.653	0.060	0.086	0.149	1.048	0.000	4.787	0.145	0.011	100.70
	85	0.377	0.000	0.388	71.41	15.27	0.000	5.717	0.070	0.008	0.110	1.373	0.042	4.948	0.178	0.006	99.90
	86	0.288	0.000	0.272	73.77	15.56	0.004	5.876	0.063	0.141	0.136	1.032	0.000	5.122	0.093	0.002	102.36
131-168.8	87	0.077	-	0.066	70.05	19.05	0.000	4.419	0.000	0.000	0.158	2.714	0.011	2.141	0.381	-	99.07
	88	0.017	-	0.014	72.79	18.34	0.000	5.263	0.009	0.000	0.180	0.441	0.000	2.779	0.075	-	99.91
	89	0.090	-	0.242	70.36	12.56	0.012	7.333	0.043	0.021	0.325	0.859	0.000	7.695	0.100	-	99.63
	90	0.000	-	0.008	72.68	18.13	0.000	4.668	0.025	0.009	0.150	0.783	0.000	2.939	0.071	-	99.47
	91	0.059	-	0.093	71.12	14.13	0.000	5.786	0.035	0.010	0.260	1.151	0.000	6.636	0.136	-	99.41
	92	0.340	-	0.258	70.78	15.61	0.032	4.808	0.074	0.000	0.219	1.645	0.000	4.827	0.339	-	98.93
	93	0.052	-	0.062	73.35	16.44	0.003	4.554	0.017	0.000	0.194	0.862	0.000	5.845	0.088	-	101.47
	94	0.235	-	0.143	71.27	15.43	0.016	4.799	0.081	0.000	0.203	1.220	0.001	5.522	0.223	-	99.14
131-236.0	95	0.000	-	0.105	70.17	18.82	0.000	2.269	0.012	0.010	0.055	1.821	0.000	4.733	0.347	-	98.34
131-96.0	96	0.681	0.013	0.178	72.11	6.418	0.270	1.220	-	-	-	1.385	0.048	14.146	-	-	97.05
	97	0.474	0.006	0.031	73.18	11.63	0.067	0.308	-	-	-	1.347	0.000	11.029	-	-	98.41
	98	0.398	0.000	0.032	72.66	11.79	0.088	0.519	-	-	-	0.825	0.045	10.384	-	-	97.25
	99	0.408	0.000	0.030	72.69	10.15	0.010	0.499	-	-	-	1.332	0.000	12.409	-	-	97.70
	100	0.517	0.000	0.032	75.87	10.03	0.051	0.652	0.108	0.019	0.000	1.126	0.002	12.07	0.026	0.019	100.53
	101	0.500	0.000	0.037	76.15	8.997	0.000	0.676	0.171	0.005	0.000	1.528	0.040	12.98	0.000	0.014	101.10
	102	0.415	0.000	0.043	75.32	10.47	0.073	0.621	0.125	0.006	0.000	1.427	0.000	12.10	0.000	0.015	100.61
	103	0.711	0.000	0.049	75.13	12.05	0.032	0.476	0.130	0.101	0.000	1.289	0.020	10.30	0.000	0.015	100.30
	104	0.349	0.000	0.020	75.82	10.72	0.072	0.529	0.076	0.000	0.000	1.413	0.035	11.94	0.006	0.007	100.99
	105	0.419	0.000	0.031	75.13	11.96	0.192	0.662	0.075	0.055	0.000	0.843	0.000	10.49	0.034	0.022	99.91
	106	1.009	0.000	0.059	75.32	8.974	0.007	0.329	0.130	0.090	0.000	1.887	0.006	12.01	0.000	0.007	99.82
	107	0.399	0.000	0.056	74.17	13.50	0.097	0.512	0.039	0.041	0.000	0.814	0.000	9.331	0.000	0.017	98.98
	108	0.453	0.000	0.036	75.00	10.89	0.084	0.653	0.108	0.044	0.000	1.087	0.000	11.82	0.000	0.016	100.18
	109	0.491	0.000	0.031	75.62	8.512	0.053	0.690	0.039	0.033	0.000	1.445	0.000	13.30	0.000	0.013	100.23
	110	0.424	0.000	0.045	74.34	13.46	0.098	0.716	0.142	0.046	0.000	0.750	0.000	9.320	0.000	0.025	99.37
183-24.9	111	0.002	0.078	0.040	72.10	20.13	0.006	1.250	-	-	-	3.000	0.138	1.791	-	-	98.63

Detection limits (wt. %): Y 0.08; Nb 0.09; Ta 0.16; F 0.14; Ca 0.03; Fe 0.03; Mg 0.03; Ti 0.04; Mn 0.03; Sn 0.03; Th 0.03; U 0.05; Er 0.10; Sm 0.09; Ce 0.05; P 0.02

Appendix 2.3: Columbite Results in Cation Units

Name	#	Y2O3	F	CaO	Nb2O5	FeO	ThO2	Ta2O5	Er2O3	Sm2O3	MgO	TiO2	UO2	MnO	SnO2	P2O5	Total
133-33.5	1	0.00	-	0.01	1.85	0.88	0.00	0.04	0.00	0.00	0.01	0.11	0.00	0.14	0.00	0.00	3.04
	2	0.00	-	0.00	1.84	0.88	0.00	0.03	0.00	0.00	0.01	0.14	0.00	0.12	0.01	0.00	3.04
	3	0.00	-	0.00	1.86	0.81	0.00	0.04	0.00	0.00	0.01	0.11	0.00	0.20	0.01	0.00	3.04
	4	0.00	-	0.00	1.86	0.87	0.00	0.03	0.00	0.00	0.01	0.12	0.00	0.14	0.01	0.00	3.03
	5	0.00	-	0.00	1.85	0.83	0.00	0.03	0.00	0.00	0.01	0.12	0.00	0.18	0.01	0.00	3.04
	6	0.00	-	0.00	1.84	0.87	0.00	0.02	0.00	0.00	0.01	0.15	0.00	0.13	0.01	0.00	3.04
	7	0.00	-	0.00	1.84	0.85	0.00	0.02	0.00	0.00	0.01	0.16	0.00	0.14	0.01	0.00	3.04
	8	0.00	-	0.00	1.86	0.84	0.00	0.03	0.00	0.00	0.01	0.12	0.00	0.16	0.01	0.00	3.03
	9	0.00	-	0.00	1.87	0.83	0.00	0.03	0.00	0.00	0.01	0.10	0.00	0.18	0.00	0.00	3.04
	10	0.00	-	0.01	1.85	0.90	0.00	0.04	0.00	0.00	0.01	0.13	0.00	0.09	0.01	0.00	3.03
	11	0.00	-	0.01	1.84	0.91	0.00	0.04	0.00	0.00	0.00	0.13	0.00	0.09	0.00	0.00	3.03
	12	0.00	-	0.00	1.84	0.87	0.00	0.05	0.00	0.00	0.00	0.12	0.00	0.13	0.00	0.00	3.03
	13	0.00	-	0.00	1.83	0.90	0.00	0.05	0.00	0.00	0.00	0.14	0.00	0.10	0.01	0.00	3.04
	14	0.00	-	0.00	1.87	0.79	0.00	0.04	0.00	0.00	0.01	0.10	0.00	0.23	0.00	0.00	3.03
	15	0.01	-	0.00	1.84	0.90	0.00	0.05	0.00	0.00	0.00	0.13	0.00	0.11	0.01	0.00	3.04
	16	0.01	-	0.01	1.85	0.80	0.00	0.05	0.00	0.00	0.01	0.11	0.00	0.20	0.01	0.00	3.03
	17	0.00	-	0.00	1.88	0.90	0.00	0.04	0.00	0.00	0.01	0.09	0.00	0.11	0.00	0.00	3.04
	18	0.00	-	0.00	1.84	0.87	0.00	0.04	0.00	0.00	0.00	0.14	0.00	0.12	0.01	0.00	3.04
	19	0.00	-	0.01	1.85	0.84	0.00	0.04	0.00	0.00	0.00	0.12	0.00	0.16	0.00	0.00	3.04
	20	0.00	-	0.00	1.82	0.91	0.00	0.02	0.00	0.00	0.00	0.18	0.00	0.09	0.01	0.00	3.04
	21	0.00	-	0.00	1.85	0.92	0.00	0.02	0.00	0.00	0.00	0.15	0.00	0.08	0.01	0.00	3.04
	22	0.00	-	0.00	1.86	0.85	0.00	0.02	0.00	0.00	0.00	0.12	0.00	0.16	0.00	0.00	3.04
	23	0.00	-	0.00	1.86	0.92	0.00	0.03	0.00	0.00	0.00	0.13	0.00	0.09	0.01	0.00	3.04
83-56.1	24	0.00	-	0.00	1.92	0.87	0.00	0.01	0.00	0.00	0.01	0.06	0.00	0.16	0.00	0.00	3.04
	25	0.00	-	0.00	1.91	0.85	0.00	0.01	0.00	0.00	0.01	0.08	0.00	0.17	0.00	0.00	3.04
	26	0.00	-	0.00	1.91	0.91	0.00	0.01	0.00	0.00	0.01	0.07	0.00	0.12	0.00	0.00	3.04
	27	0.00	-	0.01	1.90	0.86	0.00	0.01	0.00	0.00	0.01	0.09	0.00	0.16	0.00	0.00	3.05
	28	0.00	-	0.00	1.92	0.87	0.00	0.01	0.00	0.00	0.01	0.05	0.00	0.17	0.00	0.00	3.04
	29	0.00	-	0.00	1.90	0.90	0.00	0.01	0.00	0.00	0.01	0.07	0.00	0.15	0.00	0.00	3.05
	30	0.00	-	0.00	1.94	0.80	0.00	0.01	0.00	0.00	0.01	0.04	0.00	0.22	0.00	0.00	3.03
	31	0.00	-	0.00	1.94	0.75	0.00	0.01	0.00	0.00	0.01	0.04	0.00	0.25	0.00	0.00	3.02
	32	0.00	-	0.00	1.93	0.86	0.00	0.01	0.00	0.00	0.01	0.05	0.00	0.17	0.00	0.00	3.03
	33	0.00	-	0.00	1.90	0.96	0.00	0.01	0.00	0.00	0.01	0.09	0.00	0.06	0.00	0.00	3.04
	34	0.00	-	0.00	1.95	0.86	0.00	0.01	0.00	0.00	0.01	0.03	0.00	0.16	0.00	0.00	3.03
	35	0.00	-	0.00	1.94	0.82	0.00	0.01	0.00	0.00	0.01	0.04	0.00	0.19	0.00	0.00	3.02

117-53.6	36	0.02	-	0.01	1.87	0.60	0.00	0.08	0.00	0.00	0.01	0.04	0.00	0.38	0.01	0.00	3.01
	37	0.00	-	0.00	1.89	0.66	0.00	0.07	0.00	0.00	0.01	0.03	0.00	0.36	0.00	0.00	3.03
	38	0.00	-	0.00	1.90	0.65	0.00	0.07	0.00	0.00	0.01	0.02	0.00	0.37	0.00	0.00	3.02
	39	0.00	-	0.00	1.88	0.66	0.00	0.07	0.00	0.00	0.01	0.02	0.00	0.41	0.00	0.00	3.05
	40	0.01	-	0.00	1.92	0.63	0.00	0.06	0.00	0.00	0.00	0.02	0.00	0.37	0.00	0.00	3.01
	41	0.02	-	0.01	1.84	0.66	0.00	0.09	0.00	0.00	0.01	0.07	0.00	0.33	0.00	0.00	3.03
	42	0.00	-	0.00	1.90	0.64	0.00	0.07	0.00	0.00	0.00	0.02	0.00	0.37	0.00	0.00	3.01
	43	0.00	-	0.00	1.90	0.65	0.00	0.07	0.00	0.00	0.00	0.03	0.00	0.36	0.00	0.00	3.02
	44	0.00	-	0.00	1.88	0.78	0.00	0.05	0.00	0.00	0.00	0.08	0.00	0.22	0.01	0.00	3.02
	45	0.00	-	0.01	1.91	0.74	0.00	0.05	0.00	0.00	0.00	0.04	0.00	0.26	0.00	0.00	3.02
	46	0.01	-	0.00	1.89	0.70	0.00	0.06	0.00	0.00	0.00	0.04	0.00	0.32	0.00	0.00	3.02
	47	0.00	-	0.00	1.90	0.74	0.00	0.05	0.00	0.00	0.00	0.03	0.00	0.29	0.00	0.00	3.03
	48	0.01	-	0.00	1.88	0.62	0.00	0.05	0.00	0.00	0.00	0.07	0.00	0.38	0.01	0.00	3.02
117-85.5	49	0.00	-	0.00	1.86	0.82	0.00	0.08	0.00	0.00	0.01	0.04	0.00	0.22	0.00	0.00	3.04
	50	0.00	-	0.00	1.84	0.64	0.00	0.12	0.00	0.00	0.00	0.03	0.00	0.38	0.00	0.00	3.03
	51	0.00	-	0.01	1.82	0.74	0.00	0.10	0.00	0.00	0.01	0.07	0.00	0.29	0.01	0.00	3.04
	52	0.00	-	0.00	1.82	0.78	0.00	0.10	0.00	0.00	0.01	0.06	0.00	0.27	0.01	0.00	3.05
	53	0.00	-	0.00	1.81	0.53	0.00	0.14	0.00	0.00	0.01	0.03	0.00	0.53	0.00	0.00	3.05
	54	0.00	-	0.01	1.81	0.49	0.00	0.16	0.00	0.00	0.01	0.03	0.00	0.51	0.00	0.00	3.02
	55	0.00	-	0.00	1.83	0.51	0.00	0.14	0.00	0.00	0.01	0.02	0.00	0.50	0.00	0.00	3.02
	56	0.00	-	0.00	1.83	0.79	0.00	0.10	0.00	0.00	0.00	0.06	0.00	0.25	0.01	0.00	3.04
	57	0.01	-	0.01	1.63	0.89	0.00	0.06	0.00	0.00	0.00	0.34	0.00	0.09	0.02	0.00	3.07
	58	0.01	-	0.01	1.84	0.46	0.00	0.14	0.00	0.00	0.00	0.02	0.00	0.52	0.00	0.00	3.00
	59	0.01	-	0.00	1.84	0.47	0.00	0.13	0.00	0.00	0.00	0.02	0.00	0.52	0.00	0.00	3.01
	60	0.02	-	0.01	1.80	0.63	0.00	0.15	0.00	0.00	0.00	0.02	0.00	0.40	0.00	0.00	3.03
	61	0.01	-	0.00	1.82	0.47	0.00	0.16	0.00	0.00	0.00	0.02	0.00	0.53	0.00	0.00	3.01
	62	0.00	-	0.00	1.85	0.50	0.00	0.13	0.00	0.00	0.00	0.02	0.00	0.52	0.00	0.00	3.02
117-166.5	63	0.00	-	0.00	1.89	0.76	0.00	0.02	0.00	0.00	0.03	0.08	0.00	0.26	0.00	0.00	3.04
	64	0.00	-	0.00	1.88	0.95	0.00	0.02	0.00	0.00	0.02	0.09	0.00	0.10	0.00	0.00	3.06
	65	0.00	-	0.00	1.86	0.98	0.00	0.01	0.00	0.00	0.01	0.12	0.00	0.07	0.00	0.00	3.07
	66	0.00	-	0.00	1.93	0.73	0.00	0.01	0.00	0.00	0.03	0.05	0.00	0.29	0.00	0.00	3.04
	67	0.00	-	0.01	1.87	0.93	0.00	0.02	0.00	0.00	0.02	0.10	0.00	0.11	0.00	0.00	3.06
	68	0.00	-	0.00	1.84	1.00	0.00	0.02	0.00	0.00	0.01	0.13	0.00	0.07	0.00	0.00	3.08
	69	0.00	-	0.01	1.87	0.88	0.00	0.02	0.00	0.00	0.02	0.11	0.00	0.15	0.00	0.00	3.06
	70	0.00	-	0.00	1.83	0.98	0.00	0.01	0.00	0.00	0.01	0.16	0.00	0.07	0.00	0.00	3.07
117-133.1	71	0.00	-	0.00	1.90	1.02	0.00	0.04	0.00	0.00	0.01	0.03	0.00	0.05	0.00	0.00	3.05
131-135.8	72	0.00	-	0.01	1.86	0.71	0.00	0.10	0.00	0.00	0.01	0.04	0.00	0.30	0.00	0.00	3.03
	73	0.00	-	0.01	1.85	0.66	0.00	0.11	0.00	0.00	0.01	0.03	0.00	0.35	0.00	0.00	3.03
	74	0.01	-	0.03	1.84	0.74	0.00	0.10	0.00	0.00	0.01	0.05	0.00	0.24	0.00	0.00	3.03
	75	0.01	-	0.02	1.84	0.68	0.00	0.11	0.00	0.00	0.01	0.04	0.00	0.31	0.00	0.00	3.03

	76	0.01	-	0.02	1.84	0.78	0.00	0.09	0.00	0.00	0.02	0.05	0.00	0.24	0.00	0.00	3.05
	77	0.01	-	0.03	1.83	0.69	0.00	0.12	0.00	0.00	0.01	0.05	0.00	0.28	0.00	0.00	3.02
	78	0.01	-	0.02	1.81	0.75	0.00	0.11	0.00	0.00	0.01	0.07	0.00	0.24	0.01	0.00	3.03
	79	0.01	-	0.06	1.85	0.67	0.00	0.09	0.00	0.00	0.01	0.06	0.00	0.29	0.00	0.00	3.03
	80	0.01	-	0.01	1.83	0.75	0.00	0.12	0.00	0.00	0.01	0.05	0.00	0.23	0.00	0.00	3.02
	81	0.01	-	0.01	1.87	0.73	0.00	0.08	0.00	0.00	0.01	0.05	0.00	0.25	0.00	0.00	3.01
	82	0.01	-	0.03	1.86	0.72	0.00	0.09	0.00	0.00	0.01	0.05	0.00	0.24	0.00	0.00	3.02
	83	0.01	-	0.01	1.87	0.74	0.00	0.09	0.00	0.00	0.01	0.04	0.00	0.25	0.00	0.00	3.02
	84	0.01	-	0.02	1.87	0.73	0.00	0.09	0.00	0.00	0.01	0.04	0.00	0.23	0.00	0.00	3.01
	85	0.01	-	0.02	1.85	0.73	0.00	0.09	0.00	0.00	0.01	0.06	0.00	0.24	0.00	0.00	3.02
	86	0.01	-	0.02	1.87	0.73	0.00	0.09	0.00	0.00	0.01	0.04	0.00	0.24	0.00	0.00	3.01
131-168.8	87	0.00	-	0.00	1.82	0.91	0.00	0.07	0.00	0.00	0.01	0.12	0.00	0.10	0.01	0.00	3.05
	88	0.00	-	0.00	1.89	0.88	0.00	0.08	0.00	0.00	0.02	0.02	0.00	0.14	0.00	0.00	3.02
	89	0.00	-	0.01	1.84	0.61	0.00	0.12	0.00	0.00	0.03	0.04	0.00	0.38	0.00	0.00	3.03
	90	0.00	-	0.00	1.89	0.87	0.00	0.07	0.00	0.00	0.01	0.03	0.00	0.14	0.00	0.00	3.02
	91	0.00	-	0.01	1.85	0.68	0.00	0.09	0.00	0.00	0.02	0.05	0.00	0.32	0.00	0.00	3.03
	92	0.01	-	0.02	1.84	0.75	0.00	0.08	0.00	0.00	0.02	0.07	0.00	0.24	0.01	0.00	3.03
	93	0.00	-	0.00	1.87	0.77	0.00	0.07	0.00	0.00	0.02	0.04	0.00	0.28	0.00	0.00	3.05
	94	0.01	-	0.01	1.86	0.74	0.00	0.08	0.00	0.00	0.02	0.05	0.00	0.27	0.01	0.00	3.04
131-236.0	95	0.00	-	0.01	1.83	0.91	0.00	0.04	0.00	0.00	0.00	0.08	0.00	0.23	0.01	0.00	3.11
131-96.0	96	0.02	-	0.01	1.89	0.31	0.00	0.02	0.00	0.00	0.00	0.06	0.00	0.69	0.00	0.00	3.04
	97	0.01	-	0.00	1.89	0.56	0.00	0.00	0.00	0.00	0.00	0.06	0.00	0.53	0.00	0.00	3.08
	98	0.01	-	0.00	1.90	0.57	0.00	0.01	0.00	0.00	0.00	0.04	0.00	0.51	0.00	0.00	3.07
	99	0.01	-	0.00	1.89	0.49	0.00	0.01	0.00	0.00	0.00	0.06	0.00	0.61	0.00	0.00	3.08
	100	0.02	-	0.00	1.92	0.47	0.00	0.01	0.00	0.00	0.00	0.05	0.00	0.57	0.00	0.00	3.04
	101	0.01	-	0.00	1.91	0.42	0.00	0.01	0.00	0.00	0.00	0.06	0.00	0.61	0.00	0.00	3.04
	102	0.01	-	0.00	1.91	0.49	0.00	0.01	0.00	0.00	0.00	0.06	0.00	0.57	0.00	0.00	3.06
	103	0.02	-	0.00	1.91	0.57	0.00	0.01	0.00	0.00	0.00	0.05	0.00	0.49	0.00	0.00	3.06
	104	0.01	-	0.00	1.91	0.50	0.00	0.01	0.00	0.00	0.00	0.06	0.00	0.56	0.00	0.00	3.06
	105	0.01	-	0.00	1.92	0.57	0.00	0.01	0.00	0.00	0.00	0.04	0.00	0.50	0.00	0.00	3.06
	106	0.03	-	0.00	1.91	0.42	0.00	0.01	0.00	0.00	0.00	0.08	0.00	0.57	0.00	0.00	3.03
	107	0.01	-	0.00	1.91	0.64	0.00	0.01	0.00	0.00	0.00	0.03	0.00	0.45	0.00	0.00	3.07
	108	0.01	-	0.00	1.91	0.51	0.00	0.01	0.00	0.00	0.00	0.05	0.00	0.56	0.00	0.00	3.06
	109	0.01	-	0.00	1.92	0.40	0.00	0.01	0.00	0.00	0.00	0.06	0.00	0.63	0.00	0.00	3.04
	110	0.01	-	0.00	1.91	0.64	0.00	0.01	0.00	0.00	0.00	0.03	0.00	0.45	0.00	0.00	3.07
183-24.9	111	0.00	-	0.00	1.85	0.96	0.00	0.02	0.00	0.00	0.00	0.13	0.00	0.09	0.00	0.00	3.06

Appendix 2.4: Zircon Microprobe Results

Name	#	Y_2O_3	F	CaO	Nb_2O	FeO	HfO_2	SiO_2	ThO_2	ZrO_2	Ta_2O	Al_2O	Ce_2O	Eu_2O	La_2O	Er_2O_3	Nd_2O	Pr_2O	Dy_2O	Sm_2O	Gd_2O_3	Yb_2O_3	Total
131-135.8	1	0.85	0.91	0.07	2.07	0.46	0.94	29.08	0.05	59.79	0.00	0.10	0.18	0.14	0.07	0.07	0.99	0.06	0.29	0.96	1.23	0.00	97.93
	2	1.52	1.07	0.15	1.37	0.38	1.04	28.52	0.08	60.25	0.14	0.13	0.27	0.00	0.00	0.02	0.99	0.08	0.25	0.44	0.58	0.01	96.83
	3	0.25	0.60	0.14	1.52	0.87	1.20	29.65	0.00	60.07	0.07	0.29	0.21	0.18	0.01	0.03	0.96	0.07	0.15	0.59	0.76	0.00	97.38
	4	1.09	0.86	0.07	1.84	0.20	1.08	29.20	0.05	59.92	0.05	0.08	0.13	0.04	0.04	0.14	0.83	0.05	0.45	0.97	1.43	0.00	98.13
	5	1.73	0.71	0.10	1.53	0.22	1.09	28.65	0.08	60.04	0.01	0.06	0.18	0.04	0.00	0.25	0.93	0.10	0.31	0.61	0.84	0.00	97.18
	6	0.26	0.72	0.10	1.94	0.56	1.10	29.23	0.01	60.69	0.27	0.07	0.21	0.21	0.05	0.00	1.25	0.07	0.10	0.79	0.78	0.00	98.13
	7	0.22	0.60	0.12	1.79	0.31	1.05	29.27	0.02	60.98	0.19	0.09	0.23	0.23	0.02	0.06	1.21	0.11	0.13	0.79	0.81	0.00	97.94
	8	1.18	0.83	0.11	1.55	0.36	1.22	28.78	0.06	60.51	0.06	0.08	0.25	0.09	0.08	0.10	1.09	0.08	0.21	0.61	0.68	0.00	97.59
117-85.5	9	0.46	0.85	0.15	1.88	0.27	1.05	28.54	0.08	60.87	0.03	0.09	0.35	0.09	0.00	0.10	1.46	0.14	0.10	0.66	0.55	0.00	97.36
	10	0.35	1.10	0.16	1.39	0.25	1.15	28.30	0.03	60.93	0.00	0.07	0.34	0.07	0.07	0.00	1.41	0.11	0.10	0.76	0.57	0.00	96.68
	11	0.77	0.85	0.12	2.23	0.43	1.15	28.47	0.07	60.04	0.14	0.09	0.26	0.10	0.00	0.10	1.27	0.16	0.07	0.60	0.45	0.00	97.02
	12	0.51	0.80	0.08	1.30	0.16	0.86	29.00	0.06	60.06	0.07	0.07	0.29	0.16	0.09	0.13	1.34	0.05	0.21	1.15	1.13	0.00	97.17
	13	0.44	0.77	0.17	1.53	0.19	1.46	28.67	0.09	61.81	0.04	0.08	0.35	0.10	0.02	0.09	1.41	0.15	0.11	0.66	0.45	0.00	98.23
	14	0.51	0.95	0.14	1.97	0.52	1.03	28.70	0.02	59.74	0.00	0.10	0.26	0.16	0.04	0.02	1.34	0.12	0.13	0.80	0.67	0.00	96.80
	15	0.36	1.01	0.17	1.60	0.31	1.31	28.28	0.02	60.95	0.00	0.10	0.36	0.12	0.02	0.00	1.48	0.10	0.06	0.65	0.51	0.02	97.01
	16	0.62	0.80	0.07	1.85	0.47	0.91	29.03	0.03	60.28	0.03	0.09	0.20	0.07	0.00	0.06	1.15	0.08	0.21	1.06	1.00	0.00	97.64
	17	0.47	1.18	0.09	1.36	0.16	0.93	29.06	0.06	60.03	0.00	0.09	0.33	0.04	0.01	0.16	1.31	0.11	0.22	1.16	1.01	0.00	97.28
117-53.6	18	0.24	0.74	0.18	1.83	0.30	1.00	28.25	0.03	60.50	0.00	0.17	0.68	0.06	0.02	0.02	1.56	0.25	0.07	0.40	0.27	0.00	96.28
	19	0.31	0.76	0.19	1.93	0.39	1.00	28.01	0.00	60.63	0.15	0.24	0.56	0.00	0.02	0.04	1.42	0.21	0.04	0.36	0.29	0.00	96.22
	20	0.68	0.86	0.12	1.58	0.18	1.08	28.23	0.07	60.43	0.01	0.07	0.22	0.03	0.08	0.00	1.21	0.07	0.23	0.93	0.81	0.00	96.52
	21	0.67	0.91	0.10	1.48	0.13	1.41	28.07	0.05	60.07	0.00	0.06	0.21	0.06	0.02	0.00	1.13	0.07	0.25	0.84	0.87	0.00	96.03
	22	0.56	1.08	0.18	1.35	0.19	0.96	28.00	0.05	60.59	0.00	0.17	0.31	0.02	0.00	0.04	1.40	0.11	0.16	0.73	0.64	0.00	96.07
	23	0.66	0.95	0.14	1.26	0.17	0.88	28.13	0.04	60.43	0.11	0.06	0.26	0.02	0.02	0.00	1.25	0.11	0.20	0.84	0.77	0.00	95.87
	24	0.48	1.06	0.16	1.63	0.42	0.97	28.36	0.01	59.95	0.02	0.18	0.43	0.12	0.00	0.11	1.59	0.22	0.11	0.69	0.60	0.00	96.66
	25	0.55	0.79	0.16	1.91	0.38	1.05	28.28	0.04	59.48	0.10	0.21	0.39	0.10	0.04	0.00	1.48	0.13	0.13	0.66	0.62	0.02	96.20
	26	0.46	0.70	0.15	1.92	0.34	0.97	28.34	0.03	60.29	0.10	0.20	0.60	0.06	0.02	0.05	1.63	0.22	0.18	0.64	0.50	0.00	97.08
131-158.8	27	1.62	0.86	0.15	2.79	0.41	0.94	29.02	0.07	58.45	0.09	0.11	0.13	0.10	0.00	0.16	0.62	0.08	0.31	0.59	0.94	0.03	97.10
	28	0.39	0.53	0.23	3.79	0.37	0.90	29.41	0.04	59.69	0.18	0.08	0.17	0.03	0.05	0.10	1.06	0.06	0.07	0.58	0.42	0.00	97.92
	29	1.97	0.63	0.14	2.83	0.27	1.02	29.04	0.08	58.70	0.11	0.08	0.12	0.14	0.04	0.12	0.52	0.01	0.45	0.64	1.12	0.05	97.80
	30	0.29	0.70	0.16	3.73	0.45	0.70	29.56	0.01	59.81	0.24	0.04	0.18	0.10	0.02	0.00	0.95	0.07	0.07	0.47	0.31	0.00	97.54
	31	2.04	0.89	0.06	2.09	0.33	0.93	29.21	0.08	59.44	0.09	0.05	0.10	0.08	0.03	0.19	0.45	0.03	0.48	0.64	1.21	0.07	98.07
	32	4.75	0.77	0.03	1.90	0.43	1.13	28.97	0.08	56.63	0.15	0.04	0.00	0.00	0.05	0.29	0.09	0.00	0.99	0.06	1.23	0.31	97.59
	33	0.10	0.56	0.16	3.13	0.45	1.02	29.78	0.02	60.79	0.16	0.05	0.30	0.00	0.02	0.00	1.29	0.08	0.03	0.38	0.26	0.00	98.36
	34	0.10	0.62	0.15	3.96	0.34	0.93	29.40	0.01	59.93	0.19	0.06	0.21	0.02	0.00	0.02	1.09	0.12	0.01	0.44	0.23	0.00	97.57
	35	1.35	0.77	0.17	2.98	0.17	0.96	28.26	0.02	58.53	0.15	0.09	0.19	0.14	0.05	0.08	0.72	0.02	0.39	0.82	1.15	0.13	96.80

	36	0.68	0.64	0.22	3.56	0.20	1.26	29.08	0.03	59.73	0.19	0.05	0.17	0.00	0.04	0.04	1.05	0.07	0.16	0.66	0.60	0.01	98.19
131-201.3	37	0.50	0.50	0.10	1.87	0.16	1.20	29.09	0.03	60.03	0.00	0.06	0.20	0.13	0.09	0.14	0.91	0.03	0.34	1.07	1.42	0.03	97.69
	38	0.66	1.01	0.07	1.93	0.28	1.31	29.23	0.01	60.06	0.01	0.10	0.15	0.06	0.05	0.07	0.88	0.02	0.40	1.04	1.49	0.05	98.42
	39	0.29	0.91	0.27	2.70	0.24	1.20	29.02	0.02	60.13	0.13	0.09	0.27	0.03	0.00	0.00	1.39	0.13	0.14	0.72	0.60	0.02	97.91
	40	0.55	1.00	0.17	2.05	0.22	1.10	28.70	0.04	59.73	0.02	0.12	0.16	0.07	0.00	0.16	0.80	0.05	0.40	1.07	1.73	0.02	97.74
	41	0.58	0.99	0.12	1.82	0.32	0.97	28.80	0.05	59.57	0.00	0.11	0.17	0.14	0.03	0.23	0.92	0.02	0.43	1.06	1.66	0.02	97.56
	42	0.37	0.71	0.23	2.31	0.26	1.15	28.96	0.00	60.23	0.00	0.12	0.22	0.19	0.00	0.00	1.18	0.11	0.17	0.90	0.89	0.00	97.71
	43	0.67	1.16	0.26	2.54	0.27	1.07	28.45	0.05	58.16	0.18	0.13	0.11	0.25	0.00	0.04	0.72	0.06	0.50	0.99	1.89	0.06	97.05
	44	0.48	0.81	0.21	2.18	0.17	1.08	28.87	0.01	59.53	0.02	0.08	0.19	0.19	0.02	0.02	1.02	0.03	0.34	1.05	1.35	0.01	97.29
	45	0.49	0.97	0.20	2.48	0.25	0.97	29.03	0.00	59.45	0.20	0.09	0.19	0.02	0.01	0.01	0.99	0.09	0.25	1.02	1.22	0.02	97.52
	46	0.32	0.76	0.15	1.87	0.22	1.34	29.16	0.04	60.47	0.08	0.10	0.26	0.03	0.06	0.01	1.41	0.09	0.21	0.87	0.82	0.00	97.91
	47	0.90	0.91	0.11	1.78	0.22	1.03	28.77	0.05	58.44	0.03	0.07	0.07	0.08	0.01	0.00	0.41	0.03	0.87	0.78	2.66	0.08	96.92
117-112.7	48	2.73	0.66	0.07	2.23	0.37	1.28	29.30	0.15	55.17	0.03	0.22	0.08	0.04	0.03	0.22	0.26	0.02	0.52	0.41	1.08	0.88	95.46
	49	6.16	0.82	0.01	1.63	0.07	0.87	28.33	0.30	54.65	0.00	0.00	0.02	0.00	0.00	0.36	0.01	0.00	1.13	0.00	0.91	0.29	95.24
	50	6.37	0.90	0.05	1.48	0.50	0.97	28.37	0.29	53.97	0.04	0.01	0.04	0.13	0.00	0.54	0.01	0.00	1.19	0.00	0.99	0.28	95.74
	51	6.10	0.75	0.04	1.47	0.10	1.09	28.50	0.36	54.95	0.00	0.00	0.03	0.00	0.00	0.58	0.02	0.00	1.19	0.00	0.91	0.29	96.03
	52	6.48	0.76	0.07	1.38	0.26	0.80	27.93	0.27	53.90	0.00	0.03	0.05	0.05	0.05	0.50	0.00	0.00	1.16	0.00	0.94	0.28	94.58
	53	6.14	0.78	0.04	1.67	0.18	0.97	28.19	0.28	54.90	0.00	0.02	0.04	0.10	0.00	0.38	0.04	0.02	1.14	0.00	0.94	0.25	95.74
92-198.6	54	2.02	0.34	0.12	2.72	0.66	1.15	28.94	0.09	56.32	0.28	0.18	0.14	0.07	0.05	0.07	0.50	0.02	0.51	0.39	1.27	0.17	95.87
	55	1.51	0.34	0.08	3.00	0.31	1.17	29.32	0.11	57.74	0.26	0.08	0.27	0.00	0.00	0.08	0.77	0.09	0.38	0.68	1.04	0.08	97.13
	56	1.91	0.59	0.13	2.83	0.51	1.06	29.53	0.08	57.31	0.09	0.14	0.16	0.06	0.04	0.11	0.50	0.04	0.43	0.48	1.22	0.12	97.09
	57	1.15	0.65	0.07	2.88	0.36	1.21	29.61	0.14	58.65	0.19	0.08	0.21	0.14	0.07	0.06	0.81	0.02	0.31	0.87	1.35	0.05	98.59
	58	0.23	0.36	0.30	0.38	0.53	1.13	30.21	0.47	62.99	0.00	0.00	0.04	0.00	0.04	0.04	0.03	0.00	0.03	0.03	0.04	0.00	96.69
131-236.0	59	0.63	0.95	0.18	1.07	0.36	1.30	28.89	0.05	58.78	0.00	0.60	0.22	0.00	0.00	0.10	0.99	0.13	0.25	0.84	1.09	0.10	96.13
	60	0.94	1.01	0.11	1.27	0.26	1.20	28.38	0.00	59.61	0.02	0.39	0.19	0.00	0.00	0.25	0.82	0.10	0.70	1.00	1.70	0.12	97.63
	61	0.86	0.96	0.14	1.46	0.43	1.02	28.65	0.03	58.97	0.13	0.40	0.20	0.00	0.05	0.09	0.86	0.06	0.50	0.88	1.53	0.17	96.95
	62	0.56	0.85	0.13	1.47	0.32	1.22	28.51	0.01	60.17	0.14	0.35	0.29	0.09	0.02	0.06	1.14	0.10	0.27	0.82	1.06	0.09	97.32
	63	0.45	0.76	0.15	1.50	0.33	1.23	28.75	0.03	60.03	0.09	0.36	0.31	0.08	0.04	0.07	1.26	0.09	0.24	0.88	0.90	0.10	97.32
	64	0.41	0.82	0.13	1.29	0.28	1.09	28.84	0.07	60.54	0.00	0.35	0.43	0.07	0.09	0.02	1.40	0.12	0.17	0.70	0.75	0.06	97.27
	65	0.51	1.08	0.22	1.85	0.34	1.11	28.46	0.04	59.09	0.09	0.37	0.31	0.05	0.03	0.00	1.19	0.09	0.25	0.83	0.93	0.13	96.50
	66	0.53	0.74	0.15	1.90	0.34	1.43	29.08	0.05	59.45	0.16	0.40	0.33	0.03	0.05	0.22	1.15	0.07	0.19	0.66	0.66	0.11	97.39
	67	0.46	0.81	0.12	1.54	0.42	1.31	29.08	0.06	59.20	0.02	0.39	0.27	0.11	0.04	0.06	1.32	0.11	0.14	0.75	0.74	0.10	96.69
	68	0.39	0.76	0.20	1.59	0.32	1.29	28.89	0.04	59.98	0.03	0.34	0.32	0.16	0.02	0.09	1.36	0.13	0.17	0.76	0.79	0.13	97.44

Detection limits (wt. %): Y 0.04; Nb 0.09; Ta 0.18; F 0.18; Ca 0.03; Fe 0.03; Si 0.04; Th 0.03; Al 0.05; Ce 0.04; Eu 0.20; La 0.08; Hf 0.26; Er 0.26; Nd 0.08; Pr 0.08; Dy 0.10; Sm 0.08: Gd 0.09; Yb 0.12; Zr 0.09

Appendix 2.5: Fergusonite-(Y) Microprobe Results

Name	#	Y2O	F	CaO	Nb_2O_5	FeO	HfO2	SiO2	ThO2	ZrO2	Ta_2O	Al_2O_3	Ce_2O	Eu_2O	La_2O	Er_2O_3	Nd_2O_3	Pr_2O_3	Dy_2O	Sm_2O_3	Gd_2O_3	Yb_2O	Total
131-135.8	1	15.86	0.85	0.54	45.96	0.03	0.03	0.01	2.21	0.08	1.11	0.00	0.40	0.78	0.03	1.01	4.15	0.23	4.67	4.78	12.67	0.59	95.63
	2	16.06	1.05	0.30	44.27	1.59	0.12	0.00	0.36	0.01	2.02	0.00	0.56	0.92	0.06	0.81	3.68	0.25	5.24	3.31	13.74	0.60	94.49
	3	16.15	1.25	0.49	44.26	1.54	0.00	0.05	0.37	0.05	2.29	0.00	0.63	0.87	0.07	1.11	3.89	0.24	4.93	3.75	13.02	0.49	94.94
	4	15.30	1.31	0.56	43.64	1.55	0.07	0.00	0.31	0.00	2.25	0.00	0.85	0.92	0.06	0.67	4.65	0.40	4.63	4.13	12.67	0.58	93.98
131-158.8	5	23.85	0.03	0.23	47.47	0.05	0.41	0.07	0.08	0.13	2.71	0.00	1.38	0.11	0.12	2.11	4.19	0.55	6.94	0.67	6.01	1.42	98.50
	6	24.26	0.00	0.17	48.44	0.01	0.25	0.00	0.04	0.18	2.01	0.00	0.93	0.28	0.01	2.70	3.52	0.44	6.89	0.89	5.98	2.17	99.16
	7	23.78	0.10	0.18	48.93	0.00	0.35	0.00	0.03	0.23	2.06	0.00	1.05	0.17	0.11	2.85	3.72	0.38	6.70	0.91	5.92	2.28	99.70
	8	23.82	0.00	0.18	48.28	0.06	0.37	0.01	0.04	0.19	1.93	0.00	1.20	0.30	0.10	2.73	4.02	0.46	6.67	1.08	5.92	2.23	99.56
92-198.6	9	22.74	0.83	0.42	43.43	0.46	0.40	0.13	1.49	0.06	5.73	0.00	0.81	0.08	0.07	2.13	3.31	0.34	5.59	1.39	6.07	1.08	96.20
	10	21.81	0.55	0.33	46.81	1.48	0.37	0.21	0.53	0.06	3.29	0.00	0.95	0.13	0.08	2.22	3.40	0.30	5.92	1.31	6.43	1.30	97.21

Detection limits (wt. %): Y 0.04; Nb 0.09; Ta 0.19; F 0.21; Ca 0.03; Fe 0.04; Si 0.03; Th 0.03; Al 0.05; Ce 0.05; Eu 0.25; La 0.10; Hf 0.32; Er 0.32; Nd 0.09; Pr 0.10; Dy 0.12; Sm 0.12: Gd 0.11; Yb 0.14; Zr 0.09

Appendix 2.6: Pyrochlore Microprobe Results

Name	#	Y2O	F	CaO	Nb_2O	FeO	SiO2	ThO2	ZrO2	Ta_2O	Ce_2O	La_2O	Nd_2O	Pr_2O_3	UO2	K2O	Na2O	PbO	TiO2	MnO	Total
194-325.6	1	0.04	5.31	10.42	59.09	0.18	0.93	0.00	1.72	4.81	4.34	1.66	1.21	0.46	0.01	0.02	8.82	0.00	1.55	0.02	98.33
	2	0.00	5.23	9.83	58.83	0.04	0.96	0.00	1.77	5.78	4.72	1.82	1.31	0.49	0.00	0.03	9.08	0.00	1.62	0.00	99.32
	3	0.03	5.42	10.69	59.57	0.12	0.09	0.00	0.70	6.24	4.33	1.63	1.23	0.48	0.00	0.01	8.70	0.00	2.14	0.00	99.10
	4	0.03	5.06	7.78	56.46	0.10	0.33	0.03	2.52	5.18	7.03	2.67	2.22	0.75	0.12	0.01	7.64	0.00	2.51	0.01	98.30
	5	0.08	5.41	8.33	58.36	0.09	0.09	0.01	2.06	3.05	6.55	2.52	2.16	0.67	0.05	0.01	8.84	0.00	3.04	0.00	99.03
	6	0.05	5.40	7.43	57.25	0.13	0.48	0.05	2.04	2.87	7.25	2.75	2.35	0.76	0.06	0.02	8.89	0.00	3.34	0.00	98.84
	7	0.03	4.73	8.86	58.72	0.32	0.14	0.04	1.93	4.56	6.14	2.26	2.02	0.62	0.17	0.01	7.39	0.00	2.53	0.00	98.47
	8	0.03	5.08	8.09	56.24	0.15	0.57	0.04	2.39	4.25	6.59	2.45	2.19	0.78	0.08	0.02	8.41	0.00	2.72	0.00	97.93
	9	0.00	5.06	7.87	55.96	0.32	0.77	0.05	2.42	4.80	6.57	2.55	2.11	0.70	0.01	0.02	8.72	0.00	2.65	0.00	98.44
	10	0.06	5.29	7.89	57.15	0.11	0.37	0.02	2.55	4.66	6.55	2.62	2.27	0.64	0.24	0.00	7.35	0.00	2.08	0.00	97.62

Detection limits (wt. %): Y 0.10; Nb 0.09; Ta 0.34; F 0.20; Ca 0.03; Fe 0.10; Si 0.03; Th 0.04; Ce 0.05; La 0.09; Nd 0.09; Pr 0.10; U 0.06; K 0.02; Na 0.04; Pb 0.12; Ti 0.04; Mn 0.03; Zr 0.10

Appendix 2.7: Uranpyrochlore Microprobe Results

Name	#	Y2O	F	CaO	Nb_2O	FeO	SiO2	ThO2	ZrO2	Ta_2O	Ce_2O	La_2O	Nd_2O	Pr_2O_3	UO2	K2O	Na2O	PbO	TiO2	MnO	Total
83-56.1	11	0.40	0.00	5.64	44.21	6.86	1.93	0.06	0.00	0.23	1.65	0.47	1.14	0.17	27.94	0.04	0.06	0.81	2.62	0.14	94.37
117-166.5	12	3.25	0.13	5.05	41.90	4.55	2.59	0.16	0.00	1.13	0.90	0.20	0.75	0.14	23.26	0.06	0.18	0.55	3.59	0.13	88.46
	13	0.65	0.19	3.70	44.35	3.51	2.77	0.04	0.01	0.69	0.58	0.06	0.76	0.12	29.32	0.17	0.57	0.78	1.81	0.17	90.18

Detection limits (wt. %): Y 0.10; Nb 0.12; Ta 0.34; F 0.21; Ca 0.03; Fe 0.10; Si 0.03; Th 0.04; Ce 0.10; La 0.10; Nd 0.10; Pr 0.11; U 0.07; K 0.02; Na 0.05; Pb 0.13; Ti 0.04; Mn 0.03; Zr 0.10

Appendix 2.8: Samarskite-(Y) Microprobe Results

Name	#	Y2O	F	CaO	Nb_2O_5	FeO	HfO2	SiO2	ThO2	ZrO2	Ta_2O	Al_2O_3	Ce_2O	Eu_2O	La_2O	Er_2O_3	Nd_2O_3	Pr_2O_3	Dy_2O	Sm_2O_3	Gd_2O_3	Yb_2O	Total
117-112.7	1	10.21	0.36	3.33	52.66	7.06	0.00	1.39	1.50	0.08	2.29	0.03	0.35	0.46	0.09	0.98	1.28	0.10	4.24	1.15	5.44	0.83	93.67
	2	12.15	0.48	2.01	52.86	5.00	0.05	2.22	0.84	0.14	2.70	0.00	0.42	0.15	0.13	1.18	1.07	0.04	4.81	0.73	5.26	0.93	92.96
	3	11.04	0.35	2.49	51.17	6.58	0.09	2.03	1.63	0.05	1.99	0.05	0.59	0.32	0.04	1.20	1.36	0.16	4.90	0.92	5.22	0.73	92.77
	4	11.97	0.49	3.06	46.28	4.31	0.20	4.23	2.13	0.63	3.71	0.00	0.74	0.29	0.15	1.11	1.56	0.15	4.46	0.80	4.86	0.82	91.74

Detection limits (wt. %): Y 0.04; Nb 0.09; Ta 0.17; F 0.21; Ca 0.03; Fe 0.03; Si 0.03; Th 0.03; Al 0.05; Ce 0.05; Eu 0.24; La 0.09; Hf 0.30; Er 0.30; Nd 0.09; Pr 0.09; Dy 0.11; Sm 0.12: Gd 0.10; Yb 0.14; Zr 0.09

Preface to Chapter 3

In the preceding chapter, we presented field-based evidence for the local remobilization of niobium. As the study in Chapter 2 was largely qualitative in nature, further experimental evidence was necessary to ascertain the exact species responsible for niobium transport. More concrete statements regarding the conditions favoring niobium mobility, in addition to detailed geochemical modelling, were made possible with the acquisition of these speciation data.

In Chapter 3, we report results of autoclave solubility experiments with Nb_2O_5 (solid), at 150-250 °C and saturated water vapor pressure. The acidic (pH ~ 2) fluids in our experiments contained fluoride, the most likely ligand to form complexes with niobium, on the basis of their equally elevated charge to radius ratios. We interpret the results of these experiments to determine the dominant species in our solutions and calculate equilibrium constants for the relevant niobium oxide dissolution reactions. We then use these thermodynamic data to model the transport and deposition of niobium, and discuss the fluid composition best suited to its mobilization.

Chapter 3

An experimental study of the solubility and speciation of niobium in fluoride-bearing aqueous solutions at elevated temperature

TIMOFEEV, A.[1], ART.A. MIGDISOV[2] AND A.E. WILLIAMS-JONES

Department of Earth & Planetary Sciences, McGill University, 3450 University Street, Montreal, QC, Canada, H3A 0E8.

[1]alexander.timofeev@mail.mcgill.ca

[2]Earth and Environmental Division, Los Alamos National Laboratory, P.O. Box 1663, M.S. J535, Los Alamos, NM 87545, U.S.A.

Published in Geochimica et Cosmochimica Acta, June 2015

DOI: https://doi.org/10.1016/j.gca.2015.02.015

Abstract

The solubility of Nb_2O_5 and the speciation of niobium in HF-bearing aqueous solutions have been determined at temperatures of 150, 200, and 250 °C and saturated water pressure. At a pH of ~2 and at low HF concentration, niobium is transported primarily as the species $Nb(OH)_4^+$ and at high HF concentration, as the species $NbF_2(OH)_3^\circ$. Equilibrium constants for the formation of $Nb(OH)_4^+$ range from -11.23 ± 0.26 to -10.86 ± 0.24 and for the formation of $NbF_2(OH)_3^\circ$ from -3.84 ± 0.20 to -5.08 ± 0.42, at 150 and 250 °C.

The results of this study show that the solubility of Nb_2O_5 (solid) in aqueous fluids increases with increasing HF concentration, but is not strongly affected by temperature. The influence of pH is variable; at low pH and HF concentration, a decrease in pH increases the solubility of Nb_2O_5 (solid). At higher pH the reverse may be true. Modeling of the transport and deposition of niobium suggests that simple mixing with a brine is not an effective method for removing niobium from solution. By contrast, interaction of an acidic fluid with carbonate rock results in a rapid reduction of capacity of the fluid to mobilize niobium.

3.1 Introduction

In most geological environments, niobium is highly immobile and, for this reason, is often used as a normalizing element in evaluations of mass-changes accompanying hydrothermal alteration (e.g., Maclean and Kranidiotis, 1987; Christidis, 1998). However, in some settings, notably in hydrothermally altered alkaline igneous intrusions, the replacement of niobium-bearing minerals, such as pyrochlore and zircon, by secondary niobium minerals, e.g., columbite and fergusonite-(Y), provides convincing evidence of niobium mobility, at least on a local scale (e.g., Sheard et al., 2012). In some cases, e.g., at Bayan Obo, China, the Nb mineralisation (aeschynite-(Ce)) may be entirely hydrothermal. Significantly, the Nb mineralization there constitutes an economic resource of 1 million metric tons Nb hosted by dolomitic marbles (Smith and Henderson, 2000).

In principle, niobium as Nb^{5+}, is a hard acid and should form strong complexes with hard bases (Pearson, 1963). As fluorine is commonly present in elevated concentrations in alkaline igneous complexes and as F^- is a hard base, complexes involving fluoride could potentially explain the mobility of niobium in this environment. With this in mind, Zaraisky et al. (2010), measured the solubility of columbite-tantalite in fluoride-bearing aqueous solutions at temperatures up to 550 °C and pressures up to 100 Mpa. They showed that the solubility of this phase does, indeed, increase sharply with increasing fluoride ion activity, and that the efficacy of fluoride in facilitating the transport of niobium is an order of magnitude greater than that of other ligands. However, they did not evaluate the aqueous niobium or tantalum speciation and thus did not determine stability constants that could be used to quantitatively evaluate niobium transport in hydrothermal fluids. The only experimental study that has quantitatively evaluated the stability of niobium species at elevated temperature is that of Peiffert et al. (2010), but this study was limited to an investigation of niobium hydroxide complexes at temperatures from 10 ° to 70 °C. Estimates of the stability constants of niobium hydroxide species at elevated temperature are also available from extrapolations of stability constants determined experimentally for these species at ambient temperature (Shock et al., 1997). These estimates should be treated with caution, however, as it is not uncommon for them to differ by many orders of magnitude from the stability constants determined experimentally at elevated temperature (e.g., Migdisov and Williams-Jones, 2007). According to Peiffert et al. (2010), pH is the main factor controlling niobium hydroxide species solubility in fluoride-free solutions, although it needs to be noted that this conclusion is strictly valid only for temperatures below 70 °C.

In this paper, we report results of a series of experiments designed to determine the solubility of Nb_2O_5 (solid) in aqueous solutions as a function of fluoride activity and pH at temperatures of 150, 200, and 250 °C, and vapor-saturated water pressure. The results of these experiments, which are reported below, are used to evaluate the speciation of niobium at the conditions of interest, and determine formation constants for the dominant species. Based on the latter, we assess the capacity of a circulating, fluoride-bearing, hydrothermal fluid to mobilize niobium.

3.2 Methods

3.2.1 Experimental technique

Our experiments involved measuring the solubility of synthetic Nb_2O_5 (solid) (99.99%, Alfa Aesar) in aqueous solutions of variable pH and HF concentration at temperatures of 150, 200, and 250 °C, and vapor-saturated water pressure. The pH at the temperatures of interest ranged from 1.6 to 3.1, with most experiments being carried out at a pH between 2 and 2.4, and

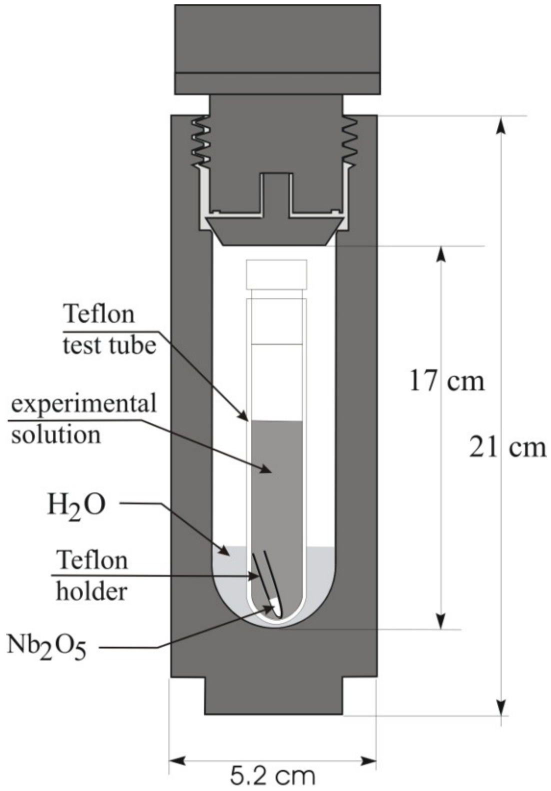

Fig. 3.1 A schematic drawing illustrating the experimental set-up.

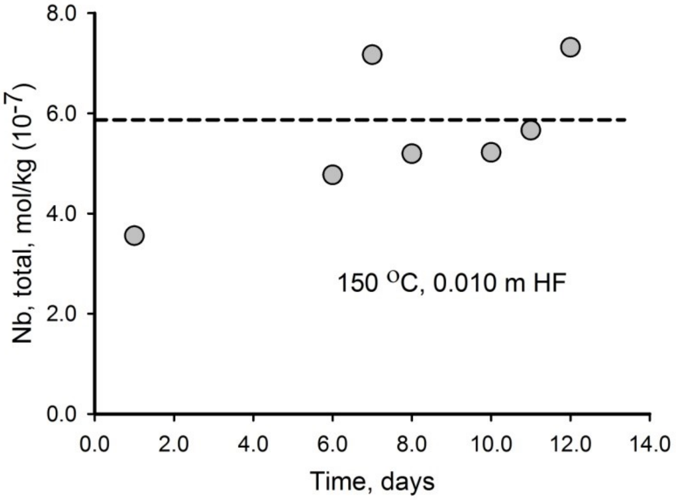

Fig. 3.2 Results from a series of experiments illustrating the solubility of Nb_2O_5 (solid) as a function of time in an aqueous solution at 150 °C containing 0.010 mol/kg HF. The data suggest that equilibrium (dashed line) was attained after 6 days.

the HF concentration ranged from 10^{-5} to 10^{-2} mol/kg. The experiments were performed in Teflon test tubes contained within titanium autoclaves (Fig. 3.1). The overall methodology employed in the experiments is similar to that of Migdisov and Williams-Jones (2007). The reader is therefore directed to this paper for information not covered in the text that follows.

The concentration of fluoride in the experimental solutions was controlled by dissolving known amounts of NaF in nano-pure water. The pH of each solution was then lowered to the level of interest by adding an appropriate amount of TM grade $HClO_4$. At the beginning of each experimental run, small Teflon holders containing Nb_2O_5 powder were placed in a Teflon test tube, to which between 17 and 20 ml of experimental solution was added depending on the size of the test tube used in the experiment. The Teflon test tubes were then placed in titanium autoclaves containing nano-pure water in order to balance pressures developed inside and outside the test tube, and heated in a Fisher Isotemp forced draft oven where they were left to equilibrate at the temperature of interest. The time required to reach equilibrium was determined from a series of experiments of variable duration performed at 150 °C. The duration of the experiments ranged from 1 to 12 days, with a steady state concentration, assumed to represent equilibrium, being reached after 6 days (Fig. 3.2). The reproducibility of the experiments with durations > 6 days was ~ ± 10%. On the basis of the results from these kinetic experiments, all subsequent experiments were conducted for durations greater than six days. Heating, quenching and sampling of the autoclaves were carried out in less than an hour to minimize Nb_2O_5 (solid) dissolution and precipitation before or after an experiment, respectively.

Following completion of an experiment, the autoclave was quenched in cold water and the Nb_2O_5-bearing Teflon holder within the larger Teflon test tube was removed. The Nb_2O_5 (solid) within the Teflon holder was analyzed by X-ray diffraction after conclusion of the experiments.

No additional solids were detected. A small aliquot (3 ml) was extracted from the Teflon test tube in order to measure the pH and fluoride concentration of the experimental solution. The pH(25 °C) of the experimental solution was determined from this aliquot potentiometrically using a glass pH electrode. The acidity of the aliquot was subsequently neutralized by the addition of 3 ml of TISAB II (Deionized water >84%, Sodium Acetate 8%, Sodium Chloride 6%, Acetic Acid 1%, CDTA <1%, Supplier: Thermo Fisher Scientific) solution and the fluoride concentration was measured using a Thermo Scientific Orion fluoride ion selective electrode. After removal of the above aliquot, one milliliter of TM grade HF was added to the Teflon test tube in order to dissolve any niobium that may have precipitated on its walls during quenching. The concentration of niobium from the resulting solutions was measured using ICP-MS (UQAM, Montreal).

Of potential concern for the interpretation of the results of the experiments is the decomposition of perchlorate at the elevated temperatures of the experiments. It is, however, unlikely that the effect of perchlorate decomposition was more than the experimental error of our experiments for the following reasons. 1) If perchlorate decomposition had significantly affected the results of our experiments, there would have been a steady deviation with time in the niobium concentration determined in our kinetic runs from the equilibrium concentration. This was not the case. 2) Similar experiments performed in perchlorate-based solutions at the same temperatures to investigate the speciation of rare-earth elements and zirconium were not affected by the decomposition of perchlorate (Migdisov and Williams-Jones, 2007; Migdisov and Williams-Jones, 2009; Migdisov et al., 2011).

3.3 Results

3.3.1 Identification of dissolved Niobium species

The results of the experiments performed at 150, 200, and 250 °C, which are reported in Table 3.1, were used to identify the dissolved niobium species. These results form two distinct populations of niobium concentration at 150 °C (Fig. 3.3). At higher temperature, the two populations are less apparent, but inferred to be present, as the value of log m_{HF} corresponding to the transition between the two species (~3) does not appear to change significantly with increasing temperature. The logarithm of niobium molality at high HF concentration has a slope of approximately two with respect to the logarithm of HF molality. Moreover, at such HF concentration, the niobium concentration, adjusted for the varying fluoride concentrations of different runs using the stoichiometry of reaction (1), appears to be independent of pH for constant HF concentration (Fig. 3.4). This suggests that the corresponding niobium species formed via a reaction that did not involve hydrogen ions. Assuming this to be the case, it follows that niobium dissolved as a neutral species. Considering that in this species niobium is bound to two atoms of F (which follows from the observed slope of ~2), the only possible neutral species is $NbF_2(OH)_3°$, which must have formed via the reaction:

$$Nb_2O_5^{cryst} + 4HF^0 + H_2O = 2NbF_2(OH)_3° \qquad \log K_1 = 2 \log a\text{NbF}_2\text{(OH)}_3° - 4 \log a_{\text{HF}} \qquad (1)$$

In contrast to the population of niobium concentrations at high HF concentration, the population at lower HF concentration shows a much weaker dependence on HF concentration, with the slope of the logarithm of niobium molality with respect to the logarithm of HF molality being significantly less than one (Fig. 3.3). As it is not possible to formulate a hydroxyl-fluoride species, which would yield a slope of less than one (a species with one fluorine atom would give rise to a slope of one in these coordinates), we conclude that the concentration of the dominant

Table 3.1 Compositions of the experimental solutions (mol/kg).

T(C)	$HClO_4$, 10^{-2}	HF, 10^{-4}	Nb, 10^{-8}	T(C)	$HClO_4$, 10^{-2}	HF, 10^{-4}	Nb, 10^{-8}
150	2.10	97.4	81.2	200	0.25	14.5	6.32
150	1.70	55.7	40.3	200	0.41	6.82	8.68
150	1.02	12.9	4.96	200	1.22	1.71	3.23
150	1.00	4.87	5.87	200	0.10	1.18	2.37
150	0.92	1.09	2.35	200	0.27	0.30	1.05
150	0.97	0.36	2.61	200	1.29	0.25	2.17
150	0.95	0.12	1.78	200	1.03	1.20	1.98
150	2.62	109	107	200	1.03	1.10	2.68
150	1.61	56.6	40.0	200	0.92	1.13	2.02
150	0.99	13.9	6.33	200	1.04	2.38	2.51
150	0.95	4.86	2.59	200	1.34	127	64.9
150	0.90	1.19	1.96	200	0.89	74.9	65.0
150	0.89	0.34	1.81	200	0.31	4.27	4.48
150	0.87	0.11	1.31	200	0.26	1.98	3.77
150	1.99	99.4	169	250	8.23	89.7	30.0
150	1.25	52.6	34.1	250	0.10	94.1	25.6
150	0.62	12.9	5.03	250	6.15	35.7	15.1
150	0.51	5.04	1.46	250	0.71	46.1	12.3
150	0.46	1.09	1.09	250	0.41	8.66	5.08
150	0.44	0.21	0.90	250	1.12	12.8	3.49
200	1.47	76.1	58.0	250	1.37	101	49.4
200	1.05	45.7	28.8	250	0.54	1.69	1.68
200	0.38	2.17	5.80	250	1.84	87.0	16.8
200	0.30	0.96	3.10	250	0.52	2.01	2.15
200	1.70	80.0	50.9	250	2.36	69.9	12.9
200	1.19	51.6	23.2	250	1.81	50.3	10.4
200	0.59	11.9	7.58	250	0.96	14.5	6.00
200	0.52	5.45	3.21	250	1.21	3.81	5.24
200	0.45	1.74	1.82	250	1.02	2.72	2.91
200	2.32	86.1	59.5	250	2.23	60.1	35.4
200	1.60	53.8	20.3	250	1.05	15.7	14.9
200	0.98	12.6	7.12	250	0.88	2.22	3.28
200	0.87	1.32	2.82	250	0.95	2.34	4.04
200	0.96	0.91	3.20	250	0.93	2.92	2.95
200	0.95	0.48	3.02				

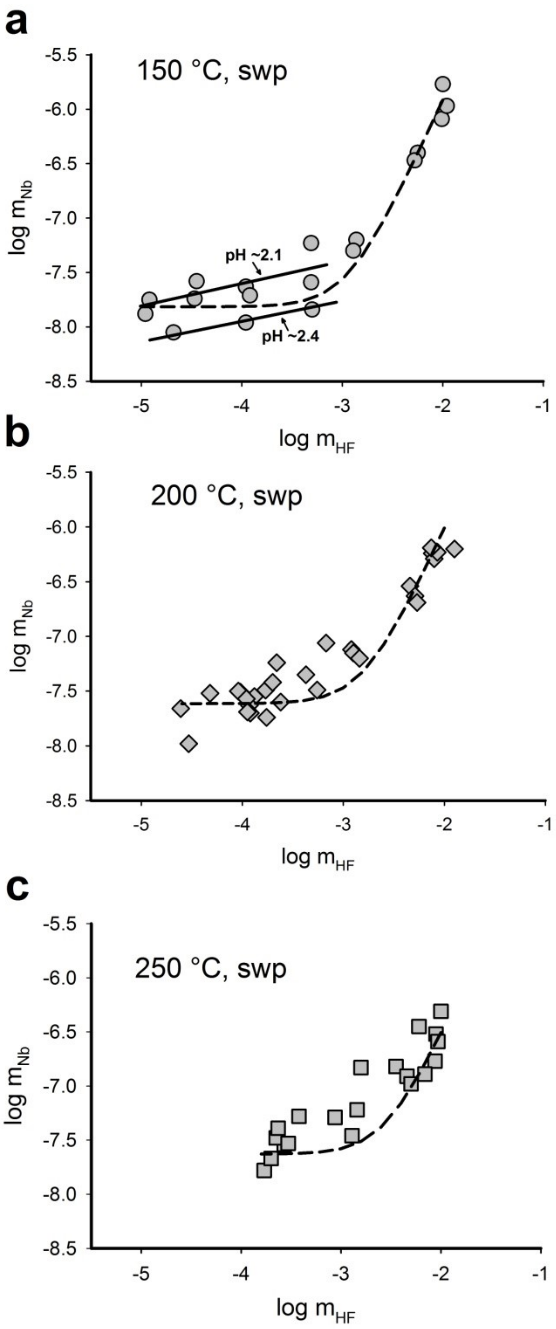

Fig. 3.3 The solubility of Nb_2O_5 (solid) as a function of the concentration of HF at (a) 150 °C (b), 200 °C and (c), 250 °C. The dashed lines indicate the solubility of Nb_2O_5 (solid) calculated from the values of log K for reactions (1) and (2) for a pH of 2.2.

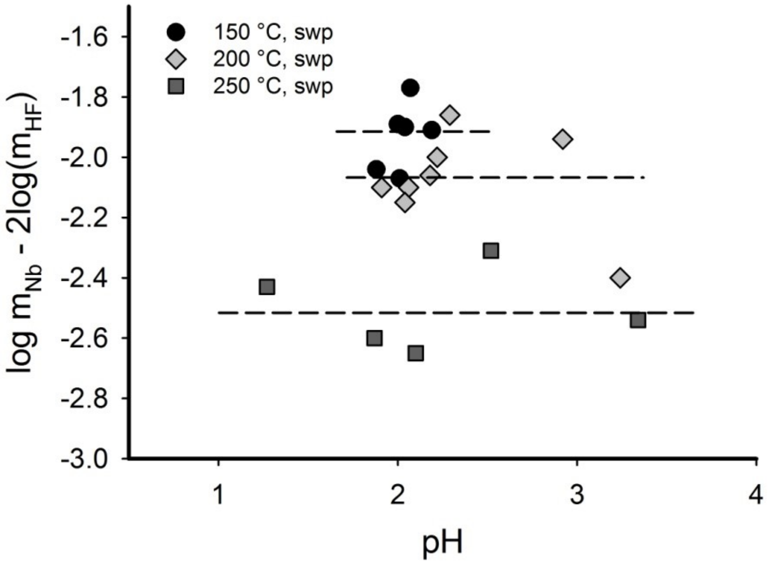

Fig. 3.4 The solubility of Nb_2O_5 (solid) as a function of pH at the temperature of interest.

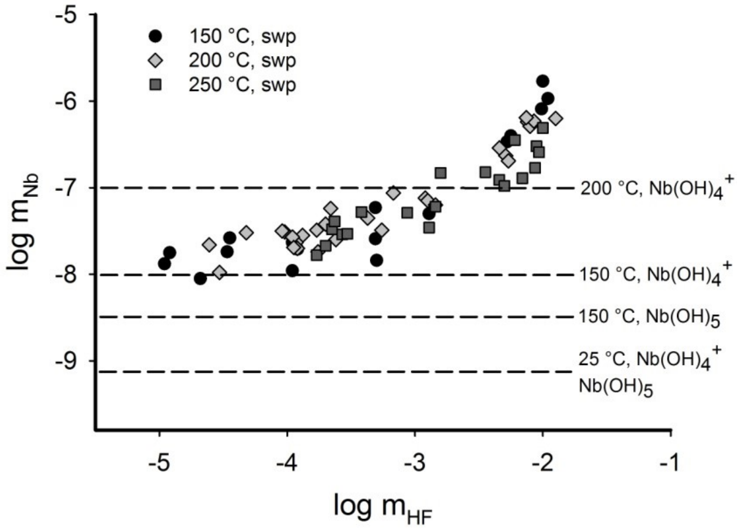

Fig. 3.5 The concentration of $Nb(OH)_4^+$ and $Nb(OH)_5^o$ predicted for various temperatures at a pH of 2 from extrapolations of the experimental data of Peiffert et al. 2010 (dashed lines). Also shown for comparison are the concentrations of Nb in experimental solutions from the current study at 150, 200 and 250 °C.

niobium species in this HF concentration range is independent of the HF concentration. The small apparent dependence on the HF concentration is interpreted to reflect mixing of this new species with a small proportion of $NbF_2(OH)_3^{\circ}$. Significantly, whereas at high HF concentration, the niobium concentration is independent of pH, the data for 150 °C show clearly that at low HF concentration, the niobium concentration increases with decreasing pH (Fig. 3.3). The above observations indicate that the dominant species at low HF is fluorine-free and charged. The latter is also suggested by the data of Peiffert et al. (2010). Extrapolations of their data to higher temperature predict, albeit with a high degree of uncertainty, that the most abundant hydroxide species for temperatures ≥150 °C is $Nb(OH)_4^+$ (Fig. 3.5). These observations suggest that at low HF concentration, the solubility of the niobium solid was controlled mainly by the reaction:

$$Nb_2O_5^{cryst} + 2H^+ + 3H_2O = 2Nb(OH)_4^+ \qquad \log K_2 = 2 \log a\mathrm{Nb(OH)_4^+} + 2\ \mathrm{pH} \qquad (2)$$

In order to calculate equilibrium constants for reactions (1) and (2), it was necessary to use an activity model. The model used to calculate the activities of the dissolved species is presented in the next section and is the same as that used to determine the pH for each experiment.

3.3.2 Methods used in calculating ion activity

The properties of water for the experimental conditions were calculated using the Haar-Gallagher-Kell (Kestin et al., 1984) and Marshall and Franck (1981) models, which allow for determination of the thermodynamic properties and dissociation constant of H_2O. To calculate the activity of the ions, we used the extended Debye-Hückel equation (Helgeson et al., 1981):

$$\log \gamma_n = \frac{\mathrm{A} \cdot [\mathrm{z_n}]^2 \cdot \sqrt{I}}{1 + \mathrm{B} \cdot \mathrm{å} \cdot \sqrt{I}} + b_\gamma \cdot I \qquad (3)$$

with A and B being the parameters of the Debye-Hückel equation, b_y the extended parameter, which depends on the nature of the background electrolyte, *å* the distance of closest approach specific to the ion of interest, *z* the charge of the ion, and *I* the true ionic strength when all dissolved components are considered. The values of b_γ, the extended parameter, were taken from Migdisov and Williams-Jones (2007), who used the same background electrolyte and studied a chemically similar system. The distances of closest approach (*å*), were set at 9 Å for H^+ (Kielland, 1937; Garrels and Christ, 1965), 3.5 Å for F^- and OH^- (Garrels and Christ 1965), 4 Å for Na^+ (Garrels and Christ, 1965) and at 4.5 Å for ClO_4^- and the charged niobium species ($Nb(OH)_4^+$). In order to calculate pH at the conditions of interest, it was assumed that $HClO_4$ dissociates completely. The pH and activity of the dissolved species were refined iteratively for each experiment considering the following species: H^+/OH^-, Na^+, $NaOH^0$, NaF^0, F^-, HF^0, ClO_4^- Niobium species were not considered in the calculation of ionic strength because of their exceptionally low concentrations in the experiments. The thermodynamic data for the other species were obtained from Ryzhenko (1965), Ryzhenko et al. (1991), Johnson et al. (1992), Sverjensky et al. (1997), and Shock et al. (1997). With this activity model in hand, it was possible to calculate the equilibrium constants of reactions (1) and (2).

3.3.3 Derivation of stability constants

The results of the experiments given in Table 3.1 were used to calculate equilibrium constants for the reactions presented in Equations (1) and (2) by iteratively minimizing the error function U, which is given by the expression:

$$U = \sum_i \left|\log C_{\mathrm{Nb}}^{\mathrm{Theo}} - \log C_{\mathrm{Nb}}^{\mathrm{Exp}}\right| \tag{4}$$

where i is the ith experimental point in the dataset, $C_{\mathrm{Nb}}^{\mathrm{Exp}}$ is the concentration of Nb determined experimentally, and $C_{\mathrm{Nb}}^{\mathrm{Theo}}$ is the concentration of Nb calculated theoretically using the starting compositions, the activity model, and the values of the formation constants, which were adjustable parameters in these iterations. The modeled system involved the same species as those considered in the calculation of ion activity. The error function, U, was minimized iteratively using the Nelder-Mead simplex search algorithm (Nelder and Mead, 1965; Dennis and Woods, 1987) for isothermal sets of solutions with the activity coefficients of the species and ionic strength recalculated after each iteration. Additional details on the methods of minimization can be found in Migdisov and Williams-Jones (2007) and Migdisov et al. (2009), which used the same data treatment method. The resulting equilibrium constants are reported in Table 3.2. Uncertainties in the values of the equilibrium constants were calculated on the basis of the standard deviations associated with the trend of each species, and are also reported in Table 3.2.

3.4 Discussion

3.4.1 Comparison to previous studies

The experiments conducted in this study are the first to be performed in the HF range of 10^{-2} to 10^{-5} mol/kg. At the lower end of this HF concentration range, niobium hydroxide species are dominant and therefore our results are directly comparable to those of Peiffert et al. (2010) and the theoretical estimates of Shock et al. (1997). At the higher end of this HF concentration range our results may be compared qualitatively to those of Zaraisky et al. (2010).

If the thermodynamic data for the species $HNbO_3$, equivalent to the species $Nb(OH)_5$, of Shock et al. (1997), are used to estimate the amount of $HNbO_3$ that might be present in a solution in equilibrium with Nb_2O_5 (solid) (the thermodynamic properties for Nb_2O_5 (solid) were taken

Table 3.2 Equilibrium constants and their associated uncertainty for the Nb_2O_5 dissolution reactions, (1) and (2).

T(°C)	150	200	250
$Nb_2O_5^{cryst} + 2H^+ + 3H_2O = 2Nb(OH)_4^+$	-11.23 ± 0.26	-10.83 ± 0.37	-10.86 ± 0.24
$Nb_2O_5^{cryst} + 4HF^0 + H_2O = 2NbF_2(OH)_3^\circ$	-3.84 ± 0.20	-4.04 ± 0.22	-5.08 ± 0.42

from Jacob et al., 2010) at a temperature of 150 °C and a pH of ~2 (controlled by the addition of $HClO_4$), the amount of $HNbO_3$ predicted to be present is on the order of ~10^{-2} mol/kg. This amount is more than four orders of magnitude higher than the amounts of niobium hydroxide species observed in this study and in the study of Peiffert et al. (2010), and shows that the data of Shock et al. (1997) cannot be used to evaluate the mobility of niobium. By contrast, extrapolations of the concentrations of niobium hydroxide species predicted from the data of Peiffert et al. (2010) are in good agreement with the results of this study. Of the four niobium hydroxide species considered by Peiffert et al. (2010), the species predicted to be predominant at both 150 and 200 °C is $Nb(OH)_4^+$, which is also the species that best fits the observations of this study (Fig. 3.5). Moreover, the concentration of $Nb(OH)_4^+$ predicted from the data of Peiffert et al. (2010) for 150 °C closely matches the concentration of niobium in the experiments of our study at which HF concentration was at its lowest. At higher HF concentration, the concentration of niobium at which hydroxyl-fluoride species predominate coincides with the concentration of $Nb(OH)_4^+$ predicted for 200 °C from the data of Peiffert et al. (2010). This bracketing of our data by extrapolations based on the data of Peiffert et al. (2010) helps confirm the conclusions of our study with respect to the importance of $Nb(OH)_4^+$ at high temperature in HF-poor solutions, and also helps validate the conclusions of their study. It should be noted, however, that the results of our study and the extrapolations of the data of Peiffert et al. (2010) are associated with large uncertainties and their accuracy is probably not better than an order of magnitude.

As mentioned earlier, Zaraisky et al. (2010) measured the concentrations of niobium and tantalum in equilibrium with columbite-(Mn) in HF-bearing solutions. The HF concentrations were much higher than those of our study (> 10^{-2} versus between 10^{-2} and 10^{-5} in our study) and the temperature and pressure were also much higher. Moreover the redox conditions were varied.

The solid in these experiments, columbite-(Mn) [$(Mn,Fe^{2+})(Nb,Ta)_2O_6$], is very different from that in our study, Nb_2O_5, although the mole fraction of niobium in columbite-(Mn) is appreciable. Thus, whereas the absolute niobium solubility should be quite different in the two studies, the dissolved species might be the same and the change in niobium concentration with HF concentration might therefore be quite similar. Indeed, the slope of the logarithm of niobium molality with the logarithm of HF molality for results of the experiments of Zaraisky et al. (2010) at 400 °C, 100 Mpa, and Co-CoO as an oxygen buffer is not only similar to that for our experiments with high HF concentration (controlled by the species $NbF_2(OH)_3^\circ$), but extends the trend of our data (Fig. 3.6). Although we cannot definitively conclude that niobium-hydroxyl fluoride species were responsible for the dissolution of niobium at the higher HF concentrations of their experiments, the similar behavior of Nb in some of the experiments of Zaraisky et al. (2010) to that of Nb at high HF concentration in our study suggests strongly that niobium hydroxyl-fluoride species may continue to play an important role at higher HF concentrations than considered by us.

3.4.2 Optimal conditions for niobium transport

The results of this study taken in conjunction with the data of Peiffert et al. (2010) and Zaraisky et al. (2010), make it possible to place some constraints on the conditions under which niobium mobility is greatest. At very low HF activity, niobium solubility is controlled by the species $Nb(OH)_4^+$ and is very low. With addition of HF, however, there is a switch in predominance to the species $NbF_2(OH)_3^\circ$ and a sharp increase in niobium concentration (in the logarithmic molal proportion of 1 Nb: 2HF; Fig. 3.3). At first glance, temperature appears to play a minor role in controlling the solubility of niobium, as the equilibrium constants obtained in the

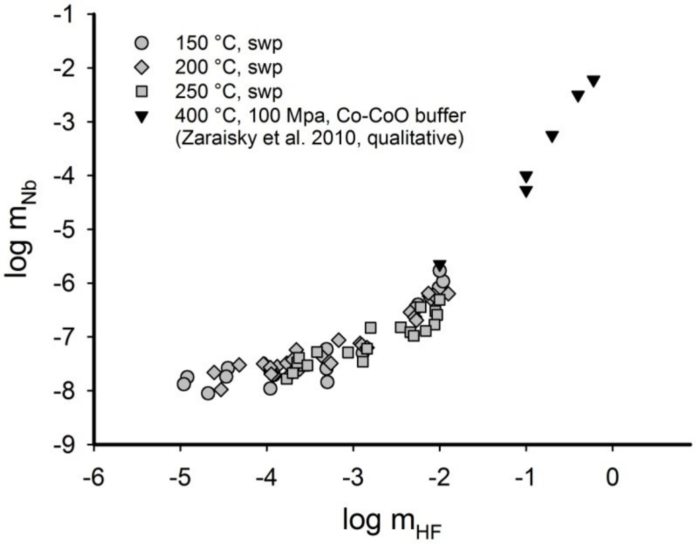

Fig. 3.6 A plot showing the concentration of Nb as a function of HF concentration determined by Zaraisky et al. (2010) in experiments at 400 °C and 100 Mpa that measured the solubility of columbite-(Mn) at conditions of the Co-CoO oxygen buffer. Also shown for comparison are the results from the experiments conducted in the current study.

temperature range of our study are quite similar within the experimental error. However, at the highest HF concentrations of this study, niobium concentration was highest in solutions at 150 °C and lowest at 250 °C, suggesting that the solubility of Nb_2O_5 (solid) as niobium hydroxyl-fluoride species may be retrograde (Fig. 3.5). This conclusion is different to that suggested by the extrapolations of the data of Peiffert et al. (2010), which predict a steady increase in niobium mobility with increasing temperature for all but one of the four niobium hydroxide species considered by them.

The influence of pH at low concentrations of HF on the solubility of niobium oxide is potentially significant. From this study, it is clear that at a pH of ~2, the solubility of niobium hydroxyl-fluoride species is not affected by pH change, whereas the concentration of the niobium hydroxide species $Nb(OH)_4^+$ increases slightly with decreasing pH. However, the pH range considered in this study is somewhat limited, ~1.6 to 3.1, with most experiments having been conducted for pH values between 2 and 2.4. Peiffert et al. (2010) employed a much larger pH range (~1 to 9) in their experiments and showed that with increasing pH, the concentration of niobium in solution reaches a minimum in the predominance field of $Nb(OH)_5$ and then increases steadily as the species $Nb(OH)_6^-$ and $Nb(OH)_7^{2-}$ become more important. Therefore, it is possible that at sufficiently basic conditions the concentration of niobium hydroxide species such as $Nb(OH)_7^{2-}$ may be even greater than that of niobium hydroxyl-fluoride species at moderate HF concentration. Although acidic to near neutral conditions are more prevalent in most ore-forming hydrothermal systems than basic conditions it is clear that the mobility of niobium may be influenced by both the pH and activity of HF in the fluid.

3.4.3 Applications to natural systems

In order to assess possible controls of hydrothermal deposition of niobium in nature, we used our data to model two scenarios. In the first scenario, one liter of an acidic (~pH 2.1) fluid with 500 ppm HF, 1.5m NaCl, 0.5m KCl, and 0.01m HCl, which was niobium saturated with respect to Nb_2O_5, was mixed iteratively with 1mL aliquots of a brine containing 0.75m NaCl, 0.25m KCl, and 1m $CaCl_2$ until a 1:1 fluid ratio was reached; both fluids were at 150 °C and saturated water pressure (Fig. 3.7a). The starting concentration of HF corresponds to that measured in fluid inclusions in the Capitan Pluton (Banks et al., 1994). In the second scenario, an acidic fluid identical to that used in the first model was reacted iteratively with 50mg aliquots of calcite, representing a limestone or marble, until one liter of acidic solution had reacted with 5 grams of calcite (Fig. 3.7b). As in the first scenario, the temperature was 150 °C. In the absence of any thermodynamic data for niobium minerals, the solid phase considered in the modeling was Nb_2O_5, the behaviour of which was modeled using the thermodynamic data of Jacob et al. (2010). Thermodynamic data for other minerals precipitated in the reaction were obtained from Holland and Powell (1998) and Robie and Hemingway (1995), and thermodynamic data for the aqueous species not considered in this study were obtained from Johnson et al. (1992), Shock et al. (1997), and Sverjensky et al. (1997).

The results of the two models clearly demonstrate the conditions under which niobium deposition is favored. In the fluid mixing model, small amounts of fluorite and Nb_2O_5 precipitate soon after mixing begins. However, the concentration of $NbF_2(OH)_3$, the dominant niobium species in solution, remains significant and greater than the amount of the precipitated Nb_2O_5(solid), which reaches a maximum of $6x10^{-4}$ moles after reaction with 1 liter of brine, corresponding to deposition of less than half of the niobium initially in solution. By contrast,

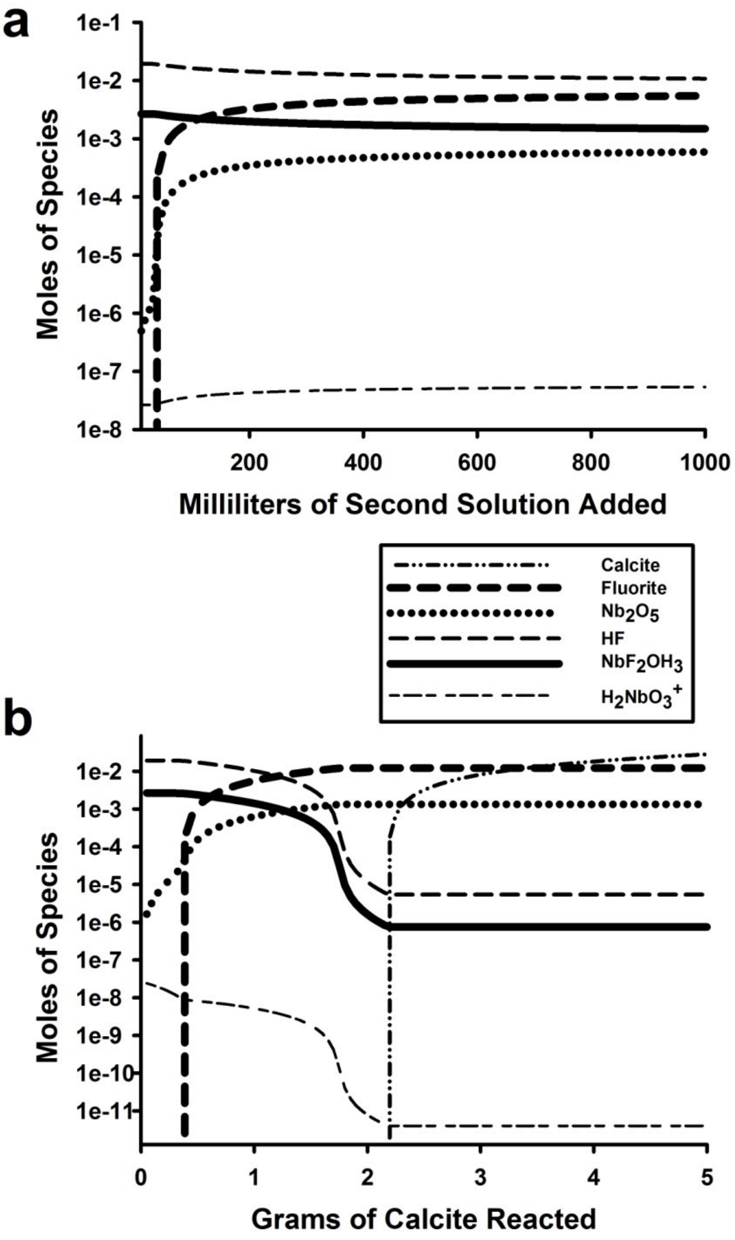

Fig. 3.7 Cumulative concentrations of aqueous species and solids precipitated at 150 °C from a fluid containing 500 ppm HF, 1.5m NaCl, 0.5m KCl, and 0.01m HCl and saturated with respect to niobium (a) during progressive mixing with a brine containing 0.75m NaCl, 0.25m KCl, and 1m $CaCl_2$, (b) and during progressive interaction with calcite (representing limestone or marble).

reaction of the acidic fluid with calcite leads to deposition of appreciable quantities of both Nb_2O_5 and fluorite. As a result, the concentrations of HF and the niobium species in solution decrease sharply; the concentration of $NbF_2(OH)_3$ decreases by more than two orders of magnitude after interacting with just 2 grams of calcite, whereas the amount of precipitated Nb_2O_5(solid) is greater than $1x10^{-3}$ moles. Niobium removal from the initial acidic fluid is largely controlled by the efficiency of each model in neutralizing the fluid. During mixing with the brine, the acidity of the starting fluid remains unchanged, most of the fluoride in the fluid remains as HF, and fluorite precipitation, together with fluoride removal from the fluid, is quite low. As a result, Nb_2O_5(solid) deposition is modest. However, in the second model, the acidity of the starting fluid is neutralized by the addition of calcite, which leads to a large increase in fluoride activity, deposition of fluorite, and the precipitation of Nb_2O_5(solid). The reaction of an acidic fluid with limestone or marble is therefore considerably more effective at removing niobium from the fluid than mixing with a calcium-bearing brine. The effectiveness of this mechanism for removing niobium from an aqueous fluid underscores the potential importance of fluid-rock interaction in hydrothermally concentrating niobium in nature. In the case of the Bayan Obo Fe-REE-Nb deposit, China, referred to in the introduction to this paper, it has been proposed that an increase in pH caused by the interaction of acidic fluids with the carbonate host rocks was the main control on REE and Fe ore mineral deposition (Smith and Henderson, 2000; Williams-Jones et al., 2012). As the results of this paper demonstrate, niobium could have been precipitated in the ores by the same mechanism.

3.5 Conclusions

The experimental data presented in this study show that significant concentrations of niobium can be dissolved at acidic conditions as the niobium hydroxide species, $Nb(OH)_4^+$, at low HF concentration and temperatures as low as 150 °C, but that much higher concentrations can be dissolved at HF concentrations > 10^{-3} mol/kg as the hydroxyl-fluoride species, $NbF_2(OH)_3^\circ$. Calculations of niobium transport and deposition based on the formation constants for the species $Nb(OH)_4^+$ and $NbF_2(OH)_3^\circ$ determined in this study show that interaction of a fluid with a sink for HF best facilitates the deposition of niobium minerals. The reaction of a niobium-bearing fluid with carbonate rocks is highly effective in this respect, because of the resulting precipitation of fluorite, whereas mixing of this fluid with a calcium-bearing brine of neutral pH leads to very modest niobium mineral deposition.

3.6 Acknowledgements

This study was supported financially by NSERC CGM and FQRNT scholarships to A.T. and NSERC Discovery and NSERC CRD grants to A.E.W.-J. The latter was matched by a grant to A.E.W.-J by Avalon Rare Metals Inc. Constructive reviews by three anonymous GCA referees helped improve the manuscript significantly.

3.7 References

Banks D., Yardley B., Campbell A. and Jarvis K. (1994) REE composition of an aqueous magmatic fluid: a fluid inclusion study from the Capitan Pluton, New Mexico, USA. *Chem. Geol.* **113**(3–4), 259–272.

Christidis G. E. (1998) Comparative study of the mobility of major and trace elements during alteration of an andesite and a rhyolite to bentonite, in the islands of Milos and Kimolos, Aegean, Greece. *Clays and Clay Minerals* **46**(4), 379-399.

Dennis, Jr., J. E. and Woods D. J. (1987) Microcomputers in large-scale computing. In *New Computing Environments* (ed. A. Wouk). SIAM, pp. 116-122.

Garrels R. M. and Christ C. L. (1965) *Solutions. Minerals. And Equilibria.* Harper & Row, New York.

Helgeson H. C., Kirkham D. H. and Flowers G. C. (1981) Theoretical prediction of the thermodynamic behavior of aqueous electrolytes at high pressures and temperatures: IV. Calculation of activity coefficients, osmotic coefficients, and apparent molal and standard and relative partial molal properties to 600°. *Am. J. Sci.* **281**, 1249-1516.

Holland T. and Powell R. (1998) An internally consistent thermodynamic data set for phases of petrological interest. *J. Metamorph. Geol.* **16**(3), 309-343.

Jacob K. T., Shekhar C. and Vinay M. (2010) Thermodynamic properties of Niobium Oxides. *J. Chem. Eng. Data* **55**(11), 4854-4863.

Johnson J. W., Oelkers E. H. and Helgeson H. C. (1992) SUPCRT92: a software package for calculating the standard molal thermodynamic properties of minerals, gases, aqueous species, and reactions from 1 to 5000 bar and 0 to 1000 °C. *Comput. Geosci.* **18**(7), 899-947.

Kestin J., Sengers J. and Kampgar-Parsi B. (1984) Thermo-physical properties of fluid H_2O. *J. Phys. Chem. Ref.* **13**(1), 175-183.

Kielland J. (1937) Individual activity coefficients of ions in aqueous solutions. *J. Am. Chem. Soc.* **59**(9), 1675-1678.

Linnen R., Trueman D. L. and Burt R. (2014) Tantalum and niobium. In *Critical Metals Handbook* (ed G. Gunn), John Wiley & Sons, Oxford.

Maclean W. H. and Kranidotis P. (1987) Immobile Elements as Monitors of Mass Transfer in Hydrothermal Alteration: Phelps Dodge Massive Sulfide Deposit, Matagami, Quebec. *Econ. Geol.* **82**, 951-962.

Marshall W. L. and Franck E. U. (1981) Ion product of water substance, 0-1000 °C, 1-10,000 bars. New international formulation and its background. *J. Phys. Chem. Ref. Data* **10**(2), 295-304.

Migdisov A. A. and Williams-Jones A. E. (2007) An experimental study of the solubility and speciation of neodymium (III) fluoride in F-bearing aqueous solutions. *Geochim. Cosmochim. Acta* **71**(12), 3056-3069.

Migdisov A. A., Williams-Jones A. E. and Wagner T. (2009) An experimental study of the solubility and speciation of the Rare Earth Elements (III) in fluoride- and chloride-bearing aqueous solutions at temperatures up to 300 °C. *Geochim. Cosmochim. Acta* **73**(23), 7087-7109.

Migdisov A. A., Williams-Jones A. E., van Hinsberg V. and Salvi S. (2011) An experimental study of the solubility of baddeleyite (ZrO_2) in fluoride-bearing solutions at elevated temperature. *Geochim. Cosmochim. Acta* **75**(1), 7426-7434.

Nelder J. A. and Mead R. (1965) A simplex method for function minimization. *Comput. J.* **7**, 308-313.

Pearson R. G. (1963) Hard and Soft Acids and Bases. *J. Am. Chem. Soc.* **85**, 3533-3539.

Peiffert C., Nguyen-Trung C., Palmer D. A., Laval J. P. and Giffaut E. (2010) Solubility of B-Nb2O5 and the Hydrolysis of Niobium(V) in Aqueous Solution as a Function of Temperature and Ionic Strength. *J. Solution. Chem.* **39**, 197-218.

Robie R.A. and Hemingway, B.S. (1995) Thermodynamic properties of minerals and related substances at 298.15 K and 1 Bar (105 Pascals) pressure and at higher temperatures. *U.S. Geological Survey Bulletin* 2131, 461pp.

Ryzhenko B. N. (1965) Determination of dissociation constant of hydrofluoric acid and conditions of replacement of calcite by fluorite. *Geokhimiya* **3**, 273-276.

Ryzhenko B. N., Kovalenko N. I. And Mironenko M. V. (1991) Ionization-constant of hydrofluoric acid at 500 °C, 1kbar. *Dokl. Akad. Nauk SSSR* **317**, 203-206.

Sheard E. R., Williams-Jones A. E., Heiligmann M., Pederson C. and Trueman D.L. (2012) Controls on the Concentration of Zirconium, Niobium, and the Rare Earth Elements in the Thor Lake Rare Metal Deposit, Northwest Territories, Canada. *Econ. Geol.* **107**, p. 81-104.

Shock E. L., Sassani D. C., Willis M. and Sverjensky D. A. (1997) Inorganic species in geologic fluids: correlations among standard molal thermodynamic properties of aqueous ions and hydroxide complexes. *Geochim. Cosmochim. Acta* **61**(5), 907-950.

Smith M. P. and Henderson, P. (2000) Preliminary Fluid Inclusion Constraints on Fluid Evolution in the Bayan Obo Fe-REE-Nb Deposit, Inner Mongolia, China. *Econ. Geol.* **95**, p. 1371-1388.

Sverjensky D., Shock E. L. and Helgeson H. C. (1997) Prediction of the thermodynamic properties of aqueous metal complexes to 1000 °C and 5kb. *Geochim. Cosmochim. Acta* **61**(7), 1359-1412.

Williams-Jones A.E., Migdisov A.A. and Samson I.M. (2012) Hydrothermal mobilisation of the rare earth elements – a tale of "Ceria" and "Yttria". *Elements* **8**(5) 355-360.

Wise M. A., Francis C. A. and Černý P. (2012) Compositional and structural variations in columbite-group minerals from granitic pegmatites of the Brunswick and Oxford fields, Maine: Differential trends in F-poor and F-rich environments. *Can. Mineral.* **50**, 1515-1530.

Zaraisky G. P., Korzhinskaya V. and Kotova N. (2010) Experimental studies of Ta_2O_5 and columbite-tantalite solubility in fluoride solutions from 300 to 550°C and 50 to 100 MPa. *Miner. Petrol.* **99**, 287-300.

Preface to Chapter 4

Experimental data presented in Chapter 3 dealt solely with the speciation of niobium and did not considered it's geochemical "twin", tantalum. In order to accurately model the behaviour of these two metals, and to consider the effect of hydrothermal alteration on Nb/Ta ratios within ore fluids or minerals, additional experimental work was performed to determine the aqueous speciation of tantalum.

In Chapter 4, we improve upon the experimental method developed in Chapter 3 and investigate the solubility of Ta_2O_5 (solid), at 100-250 °C and saturated water vapor pressure. As in Chapter 3, we considered acidic (pH ~ 2) fluids with variable HF concentrations. To identify all possible Ta-F species, we conducted experiments with HF concentrations considerably higher than those in Chapter 3, up to ~1 molal HF concentration. Following the identification of the Ta-F species in the experiments and the derivation of the thermodynamic properties of these species, we used geochemical modelling to compare the behaviour of Nb and Ta in natural hydrothermal systems.

Chapter 4

An experimental study of the solubility and speciation of tantalum in fluoride-bearing aqueous solutions at elevated temperature

TIMOFEEV, A.[1], ART.A. MIGDISOV[2] AND A.E. WILLIAMS-JONES

Department of Earth & Planetary Sciences, McGill University, 3450 University Street, Montreal, QC, Canada, H3A 0E8.

[1]alexander.timofeev@mail.mcgill.ca

[2]Earth and Environmental Division, Los Alamos National Laboratory, P.O. Box 1663, M.S. J535, Los Alamos, NM 87545, U.S.A.

Published in Geochimica et Cosmochimica Acta, January 2017

DOI: https://doi.org/10.1016/j.gca.2016.10.027

Abstract

The solubility of Ta_2O_5 (solid) and the speciation of tantalum in HF-bearing aqueous solutions have been determined at temperatures of 100-250 °C and vapour-saturated water pressure. Tantalum is transported as the species $Ta(OH)_5^0$ at low HF concentration and pH ~1-3. At higher HF concentration, tantalum mobility is controlled by the species $TaF_3(OH)_3^-$ and TaF_5; the presence of TaF_5^0 is only evident at ≤150 °C. Equilibrium constants range from -17.4 ± 0.45 to -16.4 ± 0.12 for the formation of $Ta(OH)_5$ from crystalline Ta_2O_5 and from -8.24 ± 0.64 to -8.55 ± 0.68 for the formation of $TaF_3(OH)_3^-$ at 100 and 250 °C, respectively. For TaF_5^0, they were determined to be 0.13 at 100 °C and -0.35 at 150 °C.

In many respects, the behaviour of tantalum in acidic fluoride-bearing solutions is similar to that of niobium. The solubility of Ta_2O_5 (solid) is not dependent on HF concentration in fluoride-poor fluids, but rises rapidly at higher HF concentration. However, at the conditions of our experiments, namely a pH of ~2, temperature up to 250 °C, and a wide range of HF concentrations, Ta_2O_5 (solid) solubility is almost invariably lower than that of Nb_2O_5 (solid). Modelling of Nb and Ta leaching confirmed the preferential mobility of niobium under most conditions expected in natural fluoride-rich hydrothermal systems. This modelling also demonstrated that both niobium and tantalum are rapidly deposited upon removal of fluoride from an acidic brine. As a result of hydrothermal alteration, the Nb/Ta ratios of secondary minerals may increase relative to those of the primary mineral, or remain largely unaffected, depending on the pH of the fluid.

4.1 Introduction

Niobium and tantalum are considered geochemical twins, the aqueous behaviour of which is governed by their high charge (5+) and small radius (Pearson, 1963). Although they are immobile in most hydrothermal systems, reports of parts per million concentrations of niobium in fluid inclusions indicates that under some conditions at least, niobium may be mobilized hydrothermally (Rickers et al., 2006). Further evidence of such mobility is provided by the Nechalacho alkaline igneous intrusion, in which the niobium and tantalum mineralization, with rare exception, has a hydrothermal origin (Timofeev and Williams-Jones, 2015). Alkaline igneous systems of this kind, which contain appreciable concentrations of niobium and tantalum, are typically associated with fluoride alteration (e.g., Sheard et al., 2012). Insights into the conditions under which niobium is mobile were provided recently by the experimental study of Timofeev et al. (2015). This study investigated the solubility of Nb_2O_5 (solid) in fluoride-bearing solutions and showed that the stability of niobium species increases exponentially with increasing HF concentration in the fluid. The study also emphasized the importance of acidity in promoting the mobility of niobium.

Because of the similarity of tantalum to niobium, the solubility and speciation of tantalum is predicted to be similar to that of niobium. Like Nb^{5+}, Ta^{5+} is a hard acid and should form strong complexes with the hard base, F^- (Pearson, 1963; Williams-Jones and Migdisov 2014). The first indication that tantalum might behave differently from niobium in hydrothermal solutions was provided by Zaraisky et al. (2010) who found that dissolution of columbite-(Mn) in a HF-bearing hydrothermal fluid at 400 °C and 100 Mpa yielded a concentration of tantalum that was an order of magnitude less than that of niobium. However, the results of these experiments are difficult to interpret because of the chemically complex nature of the solid and the lack of constraints placed on their experimental solution; the pH of the experimental solution and the stability constants of aqueous niobium and tantalum species were not evaluated. Nonetheless, their results indicate that the behaviour of tantalum in hydrothermal fluids may not mirror that of niobium, which is contrary to the conclusion of some studies of natural systems that the mobility of niobium and tantalum is roughly equal (e.g., Lumpkin and Ewing, 1992; Novák and Černý, 1998). They are also consistent with evidence from polyoxometalate studies that niobate and tantalate behaviour differs for some species, notably the hexaniobate and hexatantalate ions (Fullmer et al., 2014).

In this paper, we report the results of experiments conducted at 100, 150, 200, and 250 °C, and vapor-saturated water pressure designed to determine the solubility of Ta_2O_5 (solid). The experiments were conducted at pH values of ~1 to 3 and HF concentrations from 10^{-5} to 10^{0} mol/kg. Results of these experiments are used to evaluate the speciation of tantalum at the conditions of interest, and determine formation constants for the dominant species. In conjunction with the results of Timofeev et al. (2015) on niobium solubility and speciation, we evaluate the potential of an ore-forming fluid to transport tantalum and niobium under hydrothermal conditions. We then evaluate the likelihood that differences in tantalum and niobium speciation will control the Nb/Ta ratios of secondary minerals.

4.2 Methods

4.2.1 Experimental technique

The experiments involved measuring the solubility of synthetic Ta_2O_5 (solid) (99.99%, Alfa Aesar) in aqueous solutions of variable pH and HF concentration at temperatures of 100, 150, 200, and 250 °C, and vapor-saturated water pressure. The pH at the temperatures of interest ranged from 0.8 to 3.2, with most experiments being carried out at a pH of ~2.0; the HF concentration ranged from 10^{-5} to 10^{0} mol/kg. Experiments were performed in Teflon test tubes contained within titanium autoclaves (Fig. 4.1). Overall, the methodology employed in the experiments is similar to that of Migdisov and Williams-Jones (2007). The reader is therefore directed to this paper for information not covered in the text that follows.

Fluoride concentration was controlled by dissolving known amounts of NaF in nano-pure water. The pH of each solution was then reduced to the level of interest by adding an appropriate amount of trace metal grade $HClO_4$. In order to maintain the predominance of ClO_4^-, a non-complexing ligand, over HF as the background electrolyte, an amount of $NaClO_4$ approximately equal to that of NaF was added to each experimental solution containing more than 10^{-2} m NaF. Experiments were initiated by placing small sealed Teflon holders containing Ta_2O_5 powder in Teflon test tubes, to which 20 ml of experimental solution was added. The Teflon test tubes were then placed in titanium autoclaves containing water (or solutions identical in composition to that used in the experiment) in order to balance pressures developed inside and outside the test tube, and heated in a Fisher Isotemp forced draft oven to the temperature of interest.

The time required to reach equilibrium was determined from a series of experiments of variable duration performed at 100 °C and 0.075 mol/kg HF. The duration of the experiments ranged from 1 to 9 days, with a steady state concentration, assumed to represent equilibrium, being reached after 6 days (Fig. 4.2). On the basis of the results from these kinetic experiments, all subsequent experiments were conducted for durations greater than six days. Heating, quenching and sampling of the autoclaves were carried out in less than an hour to minimize Ta_2O_5 (solid) dissolution and precipitation before or after an experiment, respectively.

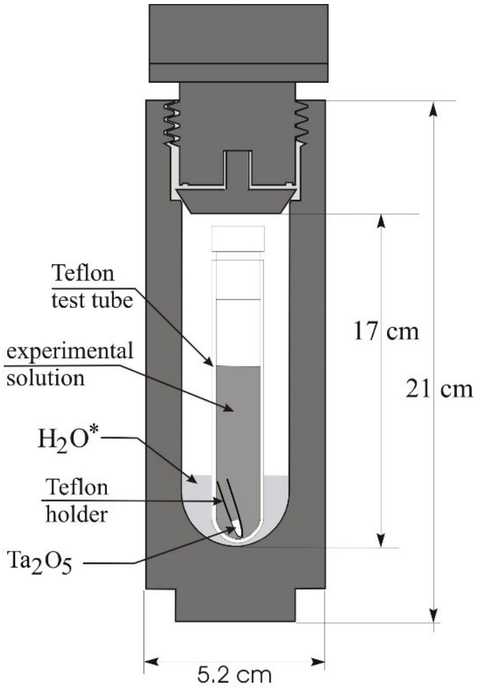

Fig. 4.1 A schematic drawing illustrating the experimental set-up. *H_2O surrounding the Teflon test tube was replaced by the experimental solution in a small number of experiments.

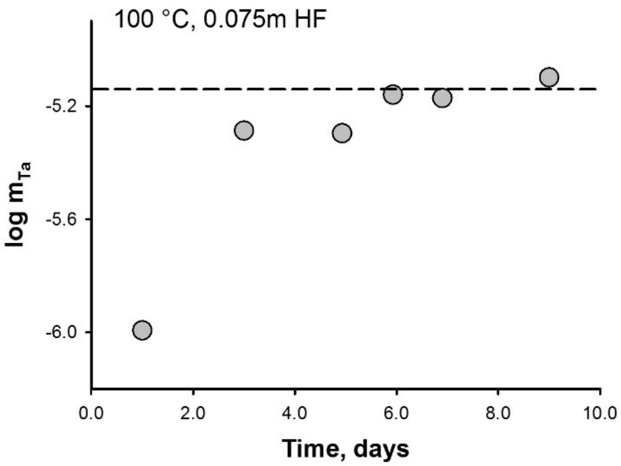

Fig. 4.2 Results from a series of experiments illustrating the solubility of Ta_2O_5 (solid) as a function of time in an aqueous solution at 100 °C containing 0.075 mol/kg HF. The data suggest that equilibrium (dashed line) was attained after 6 days.

Following completion of an experiment, the autoclave was quenched in cold water and the Ta_2O_5-bearing Teflon holder within the larger Teflon test tube was removed. The Ta_2O_5 (solid) within the Teflon holder was analyzed by X-ray diffraction after completion of the experiments. No additional solids were detected, though we cannot entirely exclude the possibility of trace amounts of a solid tantalum fluoride phase being present in the experiments. A small aliquot of liquid (2 ml) was extracted from the Teflon test tube in order to measure the pH and fluoride concentration of the experimental solution. The pH (25 °C) of the latter was determined potentiometrically using a glass pH electrode. The acidity of the aliquot of experimental solution was then neutralized by adding 2 ml of TISAB II (Deionized water >84%, Sodium Acetate 8%, Sodium Chloride 6%, Acetic Acid 1%, CDTA <1%, Supplier: Thermo Fisher Scientific) solution and the fluoride concentration was measured using a Thermo Scientific Orion fluoride ion selective electrode. After removal of the above aliquot of liquid, one milliliter of TM grade HF was added to the Teflon test tube in order to dissolve any tantalum that may have precipitated on its walls during quenching. The concentration of tantalum from the resulting solutions was measured using ICP-MS (UQAM, Montreal).

Of potential concern for the interpretation of the results of the experiments is the decomposition of perchlorate at the elevated temperature of the experiments. It is unlikely, however, that the effect of perchlorate decomposition was more than the experimental error of our experiments for the following reasons. 1) If perchlorate decomposition had significantly affected the results of our experiments, there would have been a steady deviation with time in the tantalum concentration determined in our kinetic runs from the equilibrium concentration. This was not the case. 2) Similar experiments performed in perchlorate-based solutions at the same temperatures to investigate the speciation of rare-earth elements and zirconium were not affected by the decomposition of perchlorate (Migdisov and Williams-Jones, 2007; Migdisov et al., 2009, 2011).

4.3 Results

4.3.1 Identification of dissolved tantalum species

The results of the experiments performed at 100 to 250 °C, which are reported in Table 4.1, were used to identify the dissolved tantalum species. Two distinct trends are present in the data for all temperatures investigated (Fig. 4.3). At high HF activity, the logarithm of tantalum activity has a slope of ~3 with respect to the logarithm of HF activity. In addition, experiments performed at different pH conditions indicate that at 200 and 250 °C the logarithm of tantalum activity increases with increasing pH in the proportion 1:1 (Fig. 4.4c-d). The only tantalum species which can satisfy both of these relationships via its formation reaction is $TaF_3(OH)_3^-$, which forms as follows:

$$Ta_2O_5^{cryst} + 6HF^0 + H_2O = 2TaF_3(OH)_3^- + 2H^+ \qquad (1)$$

$\log K_1 = 2 \log a\mathrm{TaF_3(OH)_3^-} + 2 \log a_\mathrm{H} - 6 \log a_\mathrm{HF}$

At lower temperature, 100 and 150 °C, the dependence of the increase in the logarithm of tantalum activity with increasing pH decreases and approaches the proportion of ~1/2 at 100 °C (Fig. 4.4a-b). Moreover, the slope in the logarithm of Ta activity versus HF activity at these temperatures exceeds 3 (Fig. 4.3a-b). By analogy with the Zr-bearing fluoride system within which species such as $Zr(OH)_3F^0$ and $Zr(OH)_2F_2^0$ predominate at >150 °C, but ZrF_5^- and ZrF_6^{2-} become increasingly abundant at <150 °C (Aja et al., 1995; Migdisov et al., 2011), we propose that this reflects the presence of a simple tantalum fluoride species, namely TaF_5^0, at lower temperature and pH:

$Ta_2O_5^{cryst} + 10HF^0 = 2TaF_5^0 + 5H_2O$ $\log K_2 = 2 \log a\mathrm{TaF}_5^0 - 10 \log a_{\mathrm{HF}}$ (2)

The stability of this species is not pH dependent. As such, the slope of ~1/2 in Ta-pH space represents the transition with decreasing pH from the predominance of $TaF_3(OH)_3^-$, having a Ta-pH slope of 1, to the predominance of TaF_5^0, having a Ta-pH slope of 0. The predicted tantalum activity calculated using the formation constants for reactions (1), (2), (3) that are derived later show this gradual transition, and are in good agreement with our experimental data (Fig. 4.4). In addition, the expected slope relating changes in TaF_5 activity to increasing HF activity is 5 ($10HF^0$:$2TaF_5^0$ -> 5:1). This explains the increase in slope that we observe in the logarithm of tantalum activity with respect to HF activity at 100 and 150 °C; TaF_5^0 becomes increasingly more abundant at higher HF activity at these temperatures (Fig. 4.3).

The trends in the data are strikingly different at lower HF concentration. The activity of tantalum is unaffected by HF activity at all temperatures, nor is it affected by the pH of the solution (Fig. 4.3, Fig. 4.5). These observations, coupled with the identification of niobium hydroxide species by Timofeev et al. (2015) at similar conditions, lead us to conclude that the predominant tantalum species at these lower HF concentrations is $Ta(OH)_5^0$:

$Ta_2O_5^{cryst} + 5H_2O = 2Ta(OH)_5^0$ $\log K_3 = 2 \log a\mathrm{Ta(OH)}_5^0$ (3)

In order to calculate equilibrium constants for reactions (1), (2), and (3), it was necessary to use an activity model. The model used to calculate the activity of the dissolved species is presented in the next section and is the same as that used to determine the pH for each experiment.

Table 4.1 Compositions of the experimental solutions (mol/kg).

T(°C)	$\sum ClO_4$	Na^+/HF^0, 10^{-2}	Ta, 10^{-8}	pH (25 °C)
100	0.036	1.20	1.81	1.67
	0.024	0.572	0.47	1.78
	0.0153	0.108	0.199	1.89
	0.0149	0.0549	0.177	1.89
	0.0127	0.0103	0.138	1.94
	0.0127	0.00523	0.385	1.94
	0.0107	0.00158	0.144	2.01
	1.685	88.4	256000	2.7
	1.28	75.5	209000	2.69
	0.92	45.8	54500	2.66
	0.37	19.8	8240	2.64
	0.151	8.22	418	2.55
	0.099	5.22	177	2.44
	0.0412	1.89	32.3	2.25
	0.342	7.32	260	1.69
	0.266	7.47	382	1.96
	0.218	7.69	449	2.2
	0.19	7.56	591	2.4
	0.208	7.53	726	2.51
	0.165	7.56	1060	2.6
	0.207	7.44	693	2.51
↓	0.207	7.47	674	2.51
100	0.208	7.56	798	2.51
150	0.029	1.04	2.02	1.77
	0.0203	0.525	0.504	1.86
	0.013	0.0991	0.438	1.96
	0.0125	0.0524	0.381	1.96
	0.0105	0.00979	0.211	2.02
	0.0102	0.00516	0.311	2.03
	0.0102	0.00107	0.204	2.03
	0.0325	1.15	1.65	1.72
	0.0234	0.584	0.528	1.8
	0.015	0.112	0.414	1.9
	0.0132	0.0572	0.391	1.94
	0.0116	0.0105	0.270	1.98
	0.0124	0.00577	0.307	1.95
	0.0115	0.00107	0.244	1.98
	0.873	42.4	208000	2.71
	0.358	18.0	18100	2.65
	0.122	6.07	784	2.71
	0.039	1.81	25.9	2.3
	1.60	74.6	558000	2.69
	1.16	59.3	448000	2.7
	0.87	37.9	207000	2.65
	0.35	16.8	20900	2.65
	0.14	7.03	759	2.55
	0.09	4.31	209	2.46
	0.04	1.70	24.0	2.29
	0.00112	0.0481	0.186	3.08
	0.0024	0.0483	0.202	2.71
	0.0048	0.046	0.219	2.38
	0.0104	0.0483	0.221	2.04
	0.028	0.0463	0.179	1.61
	0.059	0.0437	0.432	1.29
	0.14	0.0414	0.183	0.92
	0.338	7.3	188	1.7
	0.27	7.65	314	1.95
	0.218	7.62	553	2.2
↓	0.191	7.71	938	2.4
150	0.207	7.56	1070	2.52
200	0.0303	0.915	1.10	1.72
	0.0212	0.492	1.00	1.83
	0.0149	0.0981	1.40	1.9
	0.0141	0.0613	1.13	1.91
	0.0108	0.0115	0.411	2.01
	0.011	0.00753	0.665	2
	0.0107	0.00223	0.473	2.01
	1.35	54.4	449000	2.83
	1.02	48.3	399000	2.8
	0.828	36.7	133000	2.72
	0.362	19.1	22600	2.67
	0.145	7.67	538	2.57
	0.0898	4.56	119	2.43
	0.0423	1.87	14.6	2.22
	0.00116	0.0549	0.495	3.08
	0.00226	0.0494	0.425	2.74
	0.00515	0.0432	0.547	2.35
	0.0104	0.052	0.856	2.04
	0.03	0.0419	0.617	1.64
	0.06	0.0369	0.639	1.29
	0.13	0.0355	0.434	0.94
	0.20	8.16	348	2.38
	0.21	7.94	929	2.52
↓	0.17	8.36	2150	2.59
200	0.17	8.03	3770	2.64
250	0.0332	1.05	0.546	1.69
	0.0252	0.60	1.08	1.76
	0.0173	0.132	0.618	1.84
	0.0167	0.0708	0.757	1.84
	0.0128	0.0154	0.548	1.94
	0.0119	0.0122	0.701	1.97
	0.0126	0.00506	0.680	1.94
	0.648	28.9	113000	2.68
	0.541	24.2	64400	2.61
	0.226	10.7	469	2.38
	0.179	8.46	334	2.47
	0.132	5.79	84.8	2.48
	0.0526	2.35	8.86	2.17
	0.295	8.92	54.2	1.9
	0.241	9.21	153	2.14
	0.208	8.71	240	2.33
↓	0.218	8.46	311	2.49
250	0.174	8.43	3060	2.61

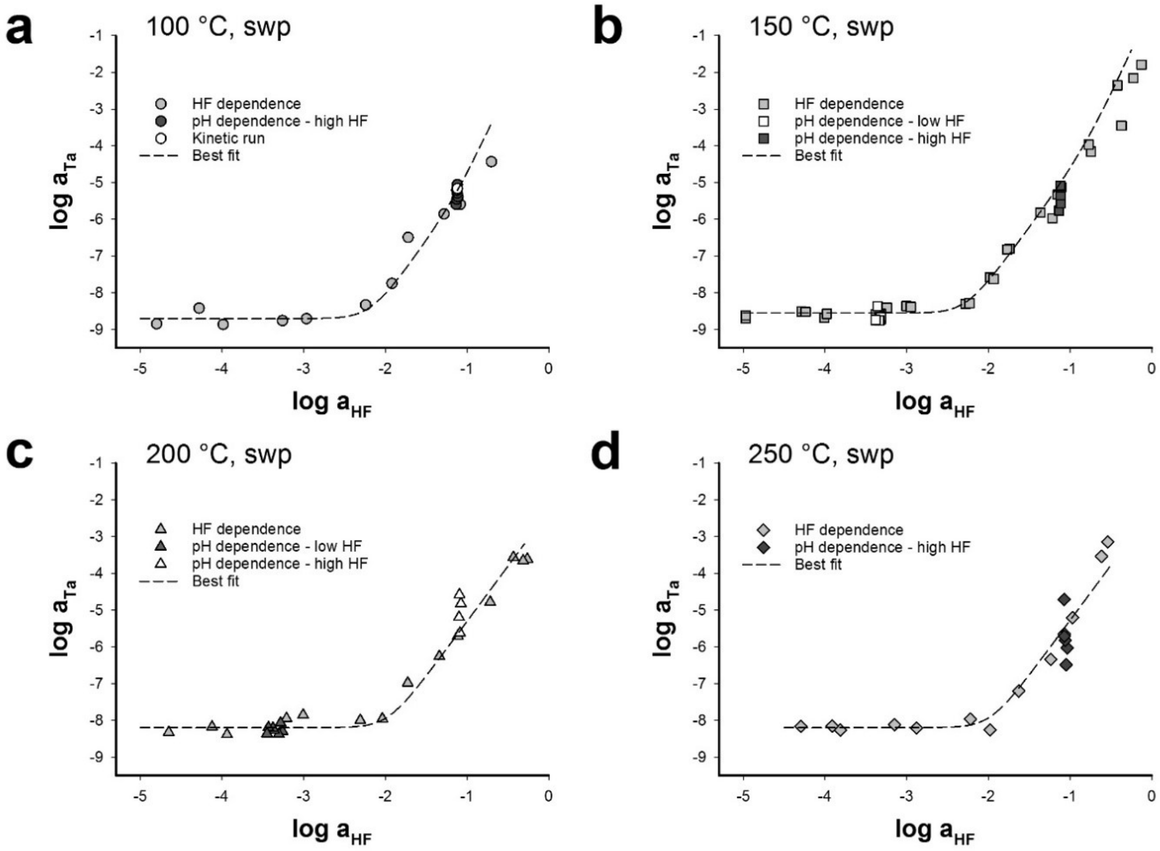

Fig. 4.3 The solubility of Ta_2O_5 (solid), normalized to a pH of 2.0 on the basis of reactions (1), (2), and (3), as a function of the concentration of HF at (a) 100 °C (b), 150 °C, (c), 200 °C, and (d) 250 °C. The dashed lines indicate the solubility of Ta_2O_5 (solid) calculated from the values of log K for reactions (1), (2), and (3) at each respective temperature. Results from the pH dependence experiments illustrated in Figure 4.4 are also shown, but have not been normalized to a pH of 2. The results of kinetic run experiments of duration of 6 days or more are included in the data set for 100 °C.

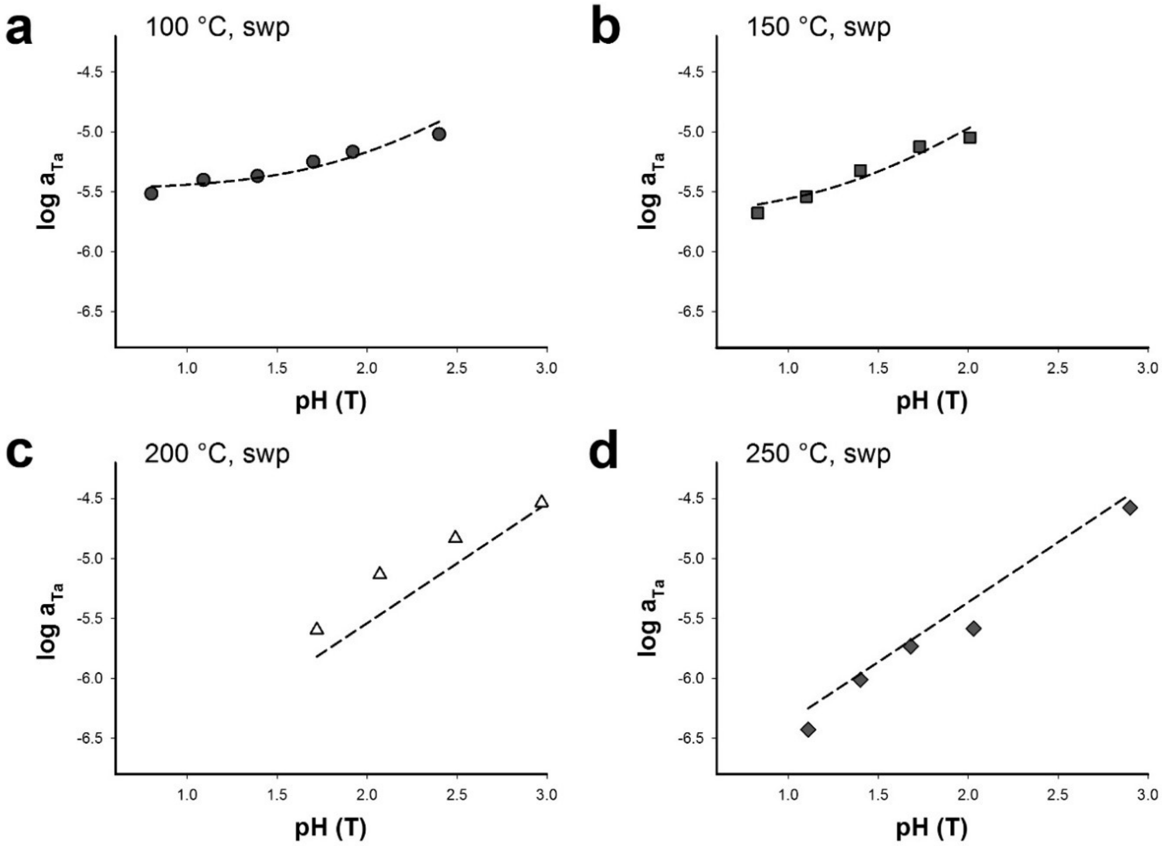

Fig. 4.4 The solubility of Ta_2O_5 (solid) as a function of pH at 100 °C (a), 150 °C (b), 200 °C (c), and 250 °C (d) for solutions containing > 0.075 mol/kg HF. The dashed lines indicate the solubility of Ta_2O_5 (solid) calculated from the values of log K for reactions (1), (2), and (3) at each respective temperature.

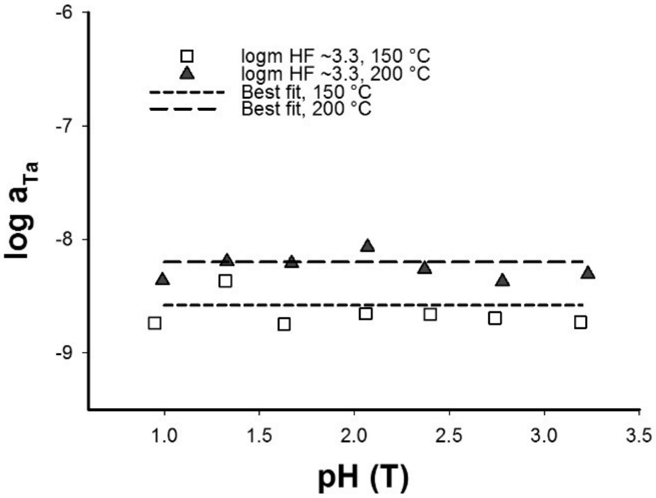

Fig. 4.5 The solubility of Ta_2O_5 (solid) as a function of pH at 150 and 200 °C in solutions containing ~5×10^{-4} mol/kg HF. The dashed lines represent best fits to the data calculated from the log K value of reaction (1).

4.3.2 Methods used in calculating ion activity

To calculate the activity of the ions, we used the extended Debye-Hückel equation (Helgeson et al., 1981):

$$\log \gamma_n = -\frac{\mathrm{A} \cdot [\mathrm{z_n}]^2 \cdot \sqrt{I}}{1 + \mathrm{B} \cdot \mathring{\mathrm{a}} \cdot \sqrt{I}} + b_\gamma \cdot I \qquad (4)$$

with A and B being the parameters of the Debye-Hückel equation, b_γ the extended parameter, which depends on the nature of the background electrolyte, *å* the distance of closest approach, which is specific to the ion of interest, *z* the charge of the ion, and *I* the true ionic strength when all dissolved components are considered. The values of b_γ, the extended parameter, were taken from Migdisov and Williams-Jones (2007), who determined the best fit b_γ values for ClO_4^- in a chemically similar system. The distances of closest approach (*å*), were set at 9 Å for H^+ (Kielland, 1937; Garrels and Christ, 1965), 3.5 Å for F^- and OH^- (Garrels and Christ 1965), 4 Å for Na^+ (Garrels and Christ, 1965) and at 4.5 Å for ClO_4^- and $TaF_3(OH)_3^-$. In order to calculate pH at the conditions of interest, it was assumed that $HClO_4$ dissociates completely. The pH and activity of the dissolved species were refined iteratively for each experiment considering the following species: H^+/OH^-, Na^+, HF^0, ClO_4^-, $Ta(OH)_5^0$, TaF_5^0, $TaF_3(OH)_3^-$. The Haar-Gallagher-Kell (Kestin et al., 1984) and Marshall and Franck (1981) models were used to determine the thermodynamic properties and dissociation constant of H_2O under our experimental conditions. Thermodynamic data for the aqueous species were obtained from Ryzhenko (1965), Ryzhenko et al. (1991), Johnson et al. (1992), Sverjensky et al. (1997), and Shock et al. (1997). With this activity model in hand, it was possible to calculate the equilibrium constants of reactions (1), (2) and (3).

4.3.3 Derivation of stability constants

The results of the experiments given in Table 4.1 were used to calculate equilibrium constants for the reactions presented in Equations (1), (2), and (3) by iteratively minimizing the error function U, which is given by the expression:

$$U = \sum_i \left(\frac{\log C_{\mathrm{Ta}}^{\mathrm{Theo}} - \log C_{\mathrm{Ta}}^{\mathrm{Exp}}}{\log C_{\mathrm{Ta}}^{\mathrm{Exp}}} \right)^2 \qquad (5)$$

where i is the ith experimental point in the dataset, $C_{\mathrm{Ta}}^{\mathrm{Exp}}$ is the concentration of Ta determined experimentally, and $C_{\mathrm{Ta}}^{\mathrm{Theo}}$ is the concentration of Ta calculated theoretically using the starting compositions, the activity model, and the values of the formation constants, which were adjustable parameters in these iterations. The modeled system involved the same species as those considered in the calculation of ion activity. The error function, U, was minimized iteratively using the Nelder-Mead simplex search algorithm (Nelder and Mead, 1965; Dennis and Woods, 1987) for isothermal sets of solutions with the activity coefficients of the species and ionic strength recalculated after each iteration. Additional details on the methods of minimization can be found in Migdisov and Williams-Jones (2007) and Migdisov et al. (2009), which used the same data treatment method. The resulting equilibrium constants are reported in Table 4.2. Equilibrium constant uncertainties were calculated by propagating the error (1σ) associated with tantalum species activity, normalized to the same HF concentration, using reactions (1), (2), and (3), and are also reported in Table 4.2. Uncertainties for the equilibrium constants associated with the species, TaF_5 (Reaction 2), are not provided as the data were only sufficient to permit approximate values for these equilibrium constants to be determined.

Table 4.2 Equilibrium constants and their associated uncertainty for the Ta_2O_5 dissolution reactions, (1), (2), and (3).

T(°C)	100	150	200	250
$Ta_2O_5^{cryst} + 5H_2O = 2Ta(OH)_5^\circ$	-17.4 ± 0.45	-17.1 ± 0.32	-16.4 ± 0.36	-16.4 ± 0.12
$Ta_2O_5^{cryst} + 6HF^0 + H_2O = 2TaF_3(OH)_3^- + 2H^+$	-8.24 ± 0.64	-7.45 ± 0.65	-8.60 ± 0.64	-8.55 ± 0.68
$Ta_2O_5^{cryst} + 10HF^0 = 2TaF_5^\circ + 5H_2O$	~ 0.13	~ -0.35	-	-

4.4 Discussion

4.4.1 Comparison to previous studies

Results of previous studies that are directly comparable to the data presented in this paper are limited to those reported in the study of Zaraisky et al. (2010). In their experiments Zaraisky et al. (2010) employed two starting solids; Ta_2O_5 of greater than 99.99% purity, and a single crystal of columbite-tantalite from a quartz-amazonite-mica pegmatite. Whereas the solubility of Ta_2O_5 (solid) determined by Zaraisky et al. (2010) can be compared easily to that reported in this study, the activity of tantalum oxide within the columbite-(Mn) sample is uncertain and cannot be evaluated. Fortunately, electron microprobe analyses of this crystal suggest that it is relatively homogeneous. Thus, although the absolute solubility of the columbite-(Mn) may be difficult to interpret, relationships such as the change in solubility of the columbite-(Mn) with an increase in HF activity should be consistent with this study, at similar experimental conditions.

Two experiments were conducted by Zaraisky et al. (2010) at HF concentrations ranging from 0.01 to ~1 molal HF. The first at 400 °C used columbite-(Mn) as the solid, and the second at 550 °C employed Ta_2O_5 (solid). A pressure of 100 Mpa and a Co-CoO oxygen buffer were employed in both experiments. It was assumed that the solution descriptions of Zaraisky et al. (2010) were complete despite their lack of detail. A 0.1 molal HF solution was therefore considered to have been prepared by the addition of an appropriate amount of trace metal grade hydrofluoric acid to nanopure water. Using these compositions, we calculated the pH and HF activity of each solution at the respective temperatures of the two experiments. We then assumed that the tantalum species, $TaF_3(OH)_3^-$, identified at higher HF concentrations in this study is also stable at the higher temperature and pH (~4) conditions of the experiments conducted by

Zaraisky et al. (2010). The concentrations of tantalum in solution determined by Zaraisky et al. (2010) were accordingly adjusted to a pH of 2.0 using the stoichiometry of reaction (1). The results of these calculations are shown in Figure 4.6. A strong dependence of tantalum solubility with increasing HF concentration is observed at both 400 and 550 °C. The slope of ~3 of this dependence is identical to that observed by us at 100-250 °C, and would be the predicted slope, if our previous assumption about $TaF_3(OH)_3^-$ being the dominant tantalum species at higher temperature is correct. In addition, the lower solubility of a tantalum solid at high temperature is consistent with the trends in the stability of $TaF_3(OH)_3^-$ determined in this study. The concentration of $TaF_3(OH)_3^-$ reaches a maximum at ~150 °C, i.e., the concentration of this species is lower at higher and lower temperature (Table 4.2, Fig. 4.7). Therefore, consistent with this trend, the concentration of dissolved tantalum in equilibrium with columbite-(Mn) at 400 °C should be less than that predicted by the best fit to our data for 250 °C, which is what we observe (Fig. 4.6). If we extrapolate the results of this study to 400 °C, the curve of best fit for this temperature lies just above and parallel to the data of Zaraisky et al. (2010). This constitutes a remarkably high level of agreement, particularly considering that our study and that of Zaraisky et al. (2010) employed different solids for this temperature.

At the lowest HF concentration considered by Zaraisky et al. (2010), 0.01 m HF, at 550 °C, the solubility of Ta_2O_5 (solid) is higher than would be expected solely from the presence of $TaF_3(OH)_3^-$. This could be due to the transition to the predominance field of $Ta(OH)_5^0$, which we predict to be increasingly stable at elevated temperature.

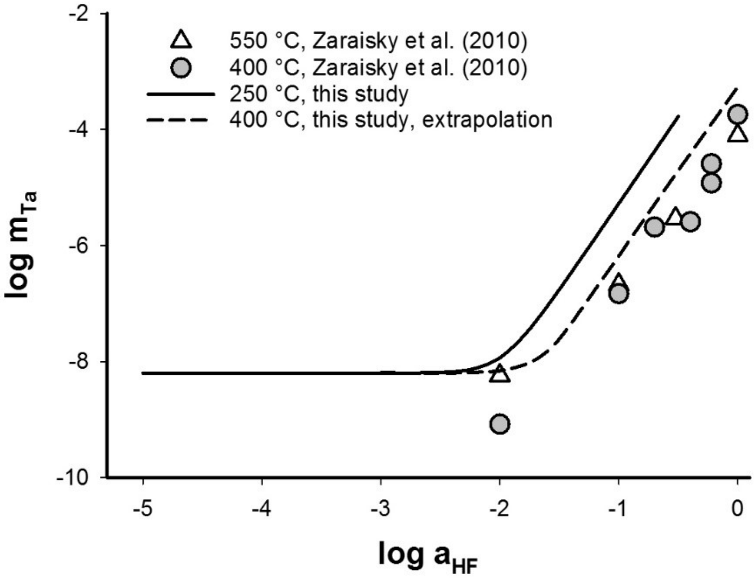

Fig. 4.6 Tantalum concentrations in equilibrium with columbite-(Mn) at 400 °C and Ta_2O_5 at 550 °C calculated using data obtained by Zaraisky et al. (2010). The best fit of the solubility data obtained at 250 °C in this study and extrapolated to 400 °C are shown for reference.

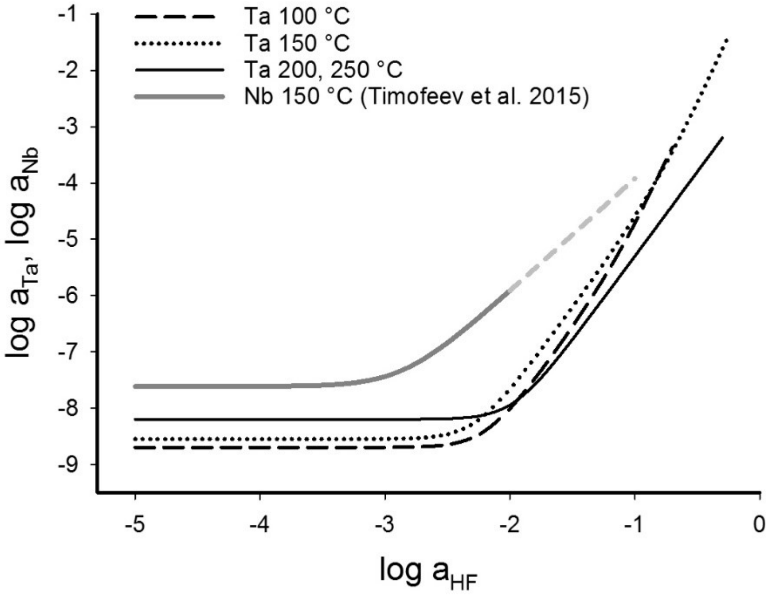

Fig. 4.7 The activity of Ta in equilibrium with Ta_2O_5 (solid) determined in this study at 100-250 °C compared to the activity of Nb in equilibrium with Nb_2O_5 (solid) as determined by Timofeev et al. (2015) at 150 °C.

4.4.2 Differences in the behaviour of tantalum and niobium

Tantalum-bearing minerals, such as the columbite and pyrochlore group minerals, commonly contain appreciable quantities of niobium. Therefore, a scenario favourable for the transport of tantalum, such as the interaction of an acidic fluoride-bearing solution at elevated temperature with a tantalum-bearing rock, might also be favorable for the transport of niobium. After this interaction, however, the relative proportions of niobium and tantalum in the rock might have changed significantly. The results of this study and those for niobium in similarly acidic, fluoride-bearing solutions reported by Timofeev et al. (2015) allow us to assess the relative behaviour of these two metals during fluid-rock interaction.

At low HF activity ($< \sim 10^{-3}$) and a pH of 2, the solubility Nb_2O_5 (solid) is independent of HF activity but at higher HF activity the logarithm of the solubility of Nb_2O_5 (solid) increases at a rate of approximately twice that of the logarithm of HF activity (Timofeev et al., 2015). By contrast, the solubility of Ta_2O_5 (solid) is lower and begins rising at a much higher HF activity (10^{-2}). The rate of increase in the solubility of Ta_2O_5 (solid) with increasing HF activity, however, is higher, i.e., the logarithm of aTa/aHF is ~3 (Fig. 4.7). If the data for niobium are extended to higher HF activity, it can be seen that, despite the greater rate of increase in the solubility of Ta_2O_5 (solid) with increasing HF activity, Ta_2O_5 (solid) solubility does not exceed that for Nb_2O_5 (solid) until a HF activity of ~0.25 or concentration of ~5,000 ppm is reached. Although such a high fluoride concentration has been reported for a natural system (Banks et al., 1994, reported HF concentrations for hypersaline fluids in the Capitan Pluton, New Mexico, USA, ranging between ~500-5000 ppm), HF concentrations in most naturally occurring fluids are likely to be significantly lower; they are buffered to low values by the precipitation of very weakly soluble minerals, such as fluorite and topaz.

In order to evaluate the effect of an acidic, fluoride-bearing solution on a niobium- and tantalum- bearing host rock, we modelled the progressive flushing of 50 grams of host rock containing 25 grams each of Nb_2O_5 and Ta_2O_5 with a brine containing 50, 500, or 5000 ppm HF in addition to 1.5m NaCl, 0.5m KCl, and 0.01m HCl, at 150 °C. The niobium and tantalum oxides were chosen due to the absence of thermodynamic data for niobium and tantalum minerals. Their thermodynamic data were obtained from Jacob et al. (2010) and Jacob et al. (2009), respectively. It should be noted that separate minerals may control the relative solubility of niobium and tantalum in natural systems, thereby making the use of niobium and tantalum oxides in the model a necessary, but potentially important simplification. Thermodynamic data for the other minerals were obtained from Holland and Powell (1998) and Robie and Hemingway (1995). Thermodynamic data for the aqueous species not considered in this study were obtained from Johnson et al. (1992), Shock et al. (1997), Sverjensky et al. (1997), and Timofeev et al. (2015). Extended parameters for NaCl in the Debye-Hückel equation were taken from Oelkers and Helgeson (1991).

The results of this model are shown in Figure 4.8. The quantity of brine (containing 50 ppm HF) needed to leach significant niobium from the original host rock exceeds a million liters. After interaction of this amount of fluid with the rock, the content of tantalum was effectively unchanged. Increasing the HF concentration to 500 ppm resulted in a two orders of magnitude reduction in the amount of brine necessary to remove significant niobium. However, tantalum is difficult to mobilize, and approximately one and a half order of magnitude more solution was required to leach tantalum in a proportion similar to that of niobium. In our most HF-rich example, a brine containing 5,000 ppm HF is able to efficiently leach both niobium and tantalum

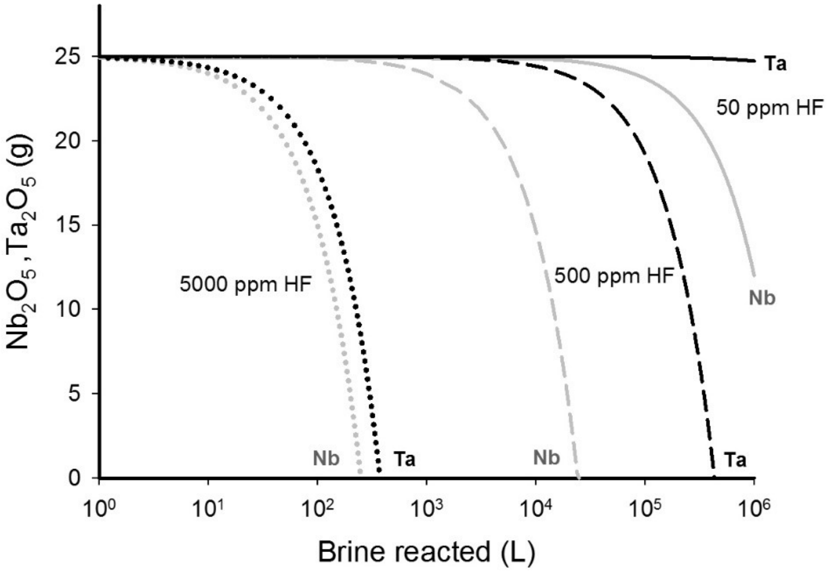

Fig. 4.8 Amounts of Nb_2O_5 and Ta_2O_5 remaining from a sample initially containing 25 grams of each oxide following progressive flushing of the sample with brine containing 50, 500, or 5000 ppm HF in addition to 1.5m NaCl, 0.5m KCl, and 0.01m HCl, at 150 °C.

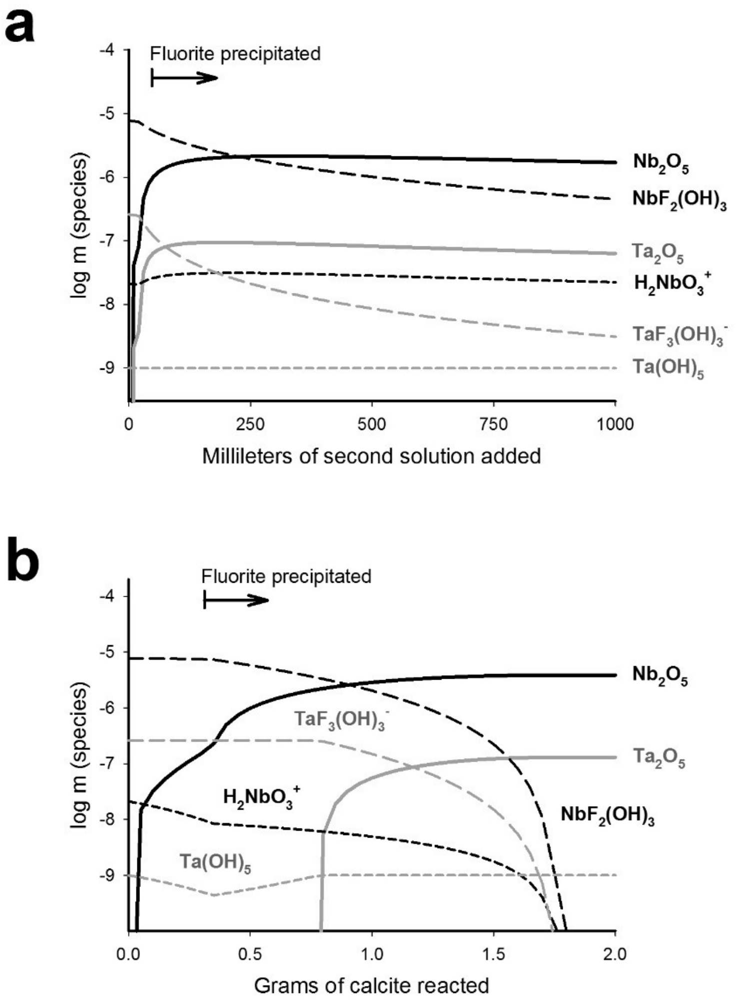

Fig. 4.9 The instantaneous concentrations of aqueous species and cumulative concentrations of precipitated solids at 150 °C in a niobium- and tantalum-saturated fluid containing 500 ppm HF, 1.5m NaCl, 0.5m KCl, and 0.01m HCl (a) during progressive mixing with a brine containing 0.75m NaCl, 0.25m KCl, and 1m $CaCl_2$, and (b) during progressive interaction with calcite (representing limestone or marble).

after interacting with less than a thousand liters of brine. Nevertheless, more niobium is mobilized than tantalum in this fluoride-rich solution, albeit by a small margin.

It should be noted that the data for tantalum collected in this study was to a higher HF activity (log a HF ~-0.4) than that for niobium (log aHF ~-2) collected by Timofeev et al. (2015). Thus, it is plausible that at higher HF activity than considered by Timofeev et al. (2015), the dependence of niobium solubility on HF activity increases from a logarithmic slope of 2 to a slope of 3. Such an increase is suggested by the observation that concentrations of niobium and tantalum in equilibrium with columbite-(Mn) at 400 °C have similar dependencies on HF activity (Zaraisky et al., 2010). If the logarithm of the slope of Nb solubility over HF activity were to approach that for tantalum at high HF activity, transport of niobium would predominate relative to that of tantalum under almost any fluoride activity at acidic conditions. However, Zaraisky et al. (2010) recognised a logarithmic molal Nb/HF slope of 2 for their columbite-(Mn) solubility data, which is consistent with the neutral $NbF_2(OH)_3^0$ species identified by Timofeev et al. (2015). In order to achieve a logarithmic slope of 3, a pH dependence similar to that suggested for the species $TaF_3(OH)_3^-$ in this study would have to be present for a negatively charged niobium hydroxyl-fluoride species.

If previously collected niobium speciation data are accurate to higher fluoride activity, pH could play an important role in niobium-tantalum fractionation. The species, $TaF_3(OH)_3^-$, is more stable at a higher pH, whereas the stability of $NbF_2(OH)_3^0$ is pH-independent (Timofeev et al., 2015). Therefore, the HF activity at which tantalum species are more abundant than their niobium counterparts would decrease considerably at elevated pH (e.g., 3-4 versus the value of ~2 employed in this study). During fluid-rock interaction, however, although interaction of an acidic fluid with a calcium-bearing rock will lead to an increase in its pH, the associated precipitation of fluorite and decrease in HF activity will result in the deposition of Ta_2O_5 (solid) (Fig. 4.9). Thus, despite a delay in the deposition of Ta_2O_5 relative to Nb_2O_5 because of the increase in pH, niobium species will remain more abundant in solution until the concentration of all niobium and tantalum species fall below that of $Ta(OH)_5^0$, the stability of which is independent of pH and HF activity.

4.4.3 Applications to natural systems

Niobium-tantalum fractionation can occur not only during hydrothermal alteration of a host rock, but also during subsequent events that result in the precipitation of niobium-tantalum bearing minerals. To assess this latter possibility, we modelled two scenarios identical to those used by Timofeev et al. (2015) to evaluate the hydrothermal deposition of niobium in natural systems. Both scenarios were evaluated at 150 °C and saturated water pressure. In the first scenario, one liter of an acidic (~pH 2.1) fluid with 500 ppm HF, 1.5m NaCl, 0.5m KCl, and 0.01m HCl, which was saturated with respect to Nb_2O_5 (solid) and Ta_2O_5 (solid), was mixed iteratively with 1mL aliquots of a brine containing 0.75m NaCl, 0.25m KCl, and 1m $CaCl_2$ until a 1:1 fluid ratio was reached (Fig. 4.9a). The starting concentration of HF corresponds to that measured in fluid inclusions in the Capitan Pluton (Banks et al., 1994). In the second scenario, an acidic fluid identical to that used in the first model was reacted iteratively with 10 mg aliquots of calcite, representing a limestone or marble, until one liter of acidic solution had reacted with 2 grams of calcite (Fig. 4.9b). Thermodynamic data for the minerals and aqueous species involved in this model are identical to those employed for the previous model addressing Nb_2O_5 and Ta_2O_5 dissolution.

By incorporating the data of this study, these models demonstrate the behaviour of tantalum relative to niobium. Increases in pH in the first fluid mixing scenario are relatively minor and as such, although concentrations of $NbF_2(OH)_3^0$ and $TaF_3(OH)_3^-$ decrease with progressive mixing and fluorite deposition, both niobium and tantalum remain in solution. This decrease would be progressively minimized with fluid mixing models incorporating lesser amount of calcium; fluorite would not precipitate and most of the niobium and tantalum would remain in the fluid. By contrast, interaction of the acidic brine with calcite (model 2) results in a large increase in pH, deposition of considerable amounts of fluorite, and a rapid decrease in the concentration of the aqueous species of both niobium and tantalum. From this perspective, the behaviour of niobium and tantalum appears to be quite similar and the conclusions of Timofeev et al. (2015) validated; the neutralization of an acidic brine by limestone or marble is a far more effective method for limiting the mobility of niobium and tantalum than mixing with another brine. There is one notable difference in behaviour of the two metals in the second model. As $TaF_3(OH)_3^-$ is a pH-dependent species, the initially rapid rise in pH offsets the decrease in HF activity caused by fluorite precipitation and results in an initial suppression of Ta_2O_5 (solid) precipitation relative to that of Nb_2O_5 (solid). This interpretation is predicated on the assumption that the niobium hydroxyl-fluoride species is neutrally charged. A negatively charged niobium hydroxyl-fluoride species would eliminate this small depositional gap. However, this small difference is potentially significant in interactions involving large amounts of fluid with wall rocks containing relatively minor volumetric proportions of a Ca-bearing mineral (e.g., calcite). A hydrothermal fluid interacting with small amounts of calcite would precipitate niobium-bearing minerals and in the process become progressively enriched in tantalum relative to niobium. Further along the fluid pathway and following additional neutralization, tantalum would be deposited. As a result, domains distinctly enriched in niobium and tantalum may form upstream and downstream in the fluid conduit, respectively. Such domains would be difficult to identify in natural environments, however, as the proportion of calcite required for such a scenario has a very restricted range.

The results of the above models suggest that niobium and tantalum do not behave in an identical fashion in hydrothermal fluids. If these two metals are leached from a host rock, a much lower fluid/rock ratio is required to mobilize niobium than is the case for tantalum. Once the chemistry of the fluid is altered such that the pH increases or HF activity decreases both niobium and tantalum precipitate. In rare cases deposition of tantalum may be temporarily suppressed.

Niobium- and tantalum-bearing pegmatites that have experienced hydrothermal alteration commonly demonstrate evidence of niobium and tantalum mobilization. For example, fine-grained secondary muscovite containing ~50 ppm Ta and ~25 ppm Nb in the Tanco pegmatite is interpreted to have crystallized from Ta-bearing aqueous fluids during a late hydrothermal event (Van Lichtervelde et al. 2008). In another example, Rickers et al. (2006) reported the occurrence of early fluid inclusions in the Variscan Ehrenfriedersdorf complex that contain up to 29 ppm Nb; Ta was not analyzed.

Pegmatites that have been hydrothermally altered may retain their primary Nb/Ta ratios or have quite different ratios of these metals. In the Moose II LCT (Li-Cs-Ta) pegmatite in the Northwest Territories, Canada, the secondary muscovite is enriched in niobium and depleted in tantalum relative to the primary muscovite (Anderson et al., 2013). Furthermore, overgrowths of columbite-(Fe) on primary columbite-(Fe) crystals in the Moose II pegmatite are commonly Nb-rich. Based on these observations, Anderson et al. (2013) concluded that the pegmatite had been enriched in Nb by a F- and Nb-rich fluid. Indeed, the behaviour of Nb and Ta in this pegmatite is entirely consistent with the results of this study. In other settings Nb/Ta ratios may remain largely unaffected by hydrothermal alteration. For example, secondary tantalum oxide phases in the Moldanubicum granitic pegmatites, Czech Republic, have similar Nb/Ta ratios to their primary counterparts (Novák and Černý, 1998). In the Tanco pegmatite, the Nb/Ta ratios of the primary and secondary muscovite grains also do not differ greatly (Van Lichtervelde et al., 2008). Two factors may be responsible for Nb/Ta ratios remaining unaffected. The first is the pH of the hydrothermal fluid. As mentioned previously, the solubility of tantalum in HF-rich systems increases with increasing pH. Therefore, the Nb/Ta ratios of the secondary minerals could reflect the pH of the altering hydrothermal fluid. Hydrothermal alteration of the Moose II pegmatite may have occurred at a lower pH than the Tanco pegmatite, but this is not known as the pH of the altering fluid in these systems was not constrained. Alternatively, the kinetics of Nb-Ta bearing mineral dissolution may be such that the hydrothermal fluid does not achieve Nb-Ta saturation and the results of this study are not applicable. However, kinetic runs performed in this study and by Timofeev et al. (2015) suggest that Nb_2O_5 (solid) dissolution is faster than that of Ta_2O_5 (solid). As a result, we propose that pH, in addition to HF activity, may play a role in determining the Nb/Ta ratios of secondary minerals.

4.5 Conclusions

The results of this study show that transport of tantalum in fluoride-bearing hydrothermal fluids is controlled by $Ta(OH)_5^0$ at low fluoride concentration, and $TaF_3(OH)_3^-$ and TaF_5^0, at high fluoride concentration. Dissolved tantalum concentration rises rapidly at $>10^{-2}$ HF mol/kg. Niobium is more soluble than tantalum in acidic hydrothermal fluids, except for those containing extremely high concentrations of fluoride, explaining why niobium is commonly mobilized preferentially from niobium-tantalum-bearing rocks. At higher pH, tantalum concentrations may approach those of niobium in hydrothermal fluids, which could explain why Nb/Ta ratios of secondary minerals remain unchanged from those of the primary minerals in some hydrothermally altered rocks.

4.6 Acknowledgements

This study was supported financially by NSERC CGM and FQRNT scholarships to A.T. and NSERC Discovery and NSERC CRD grants to A.E.W.-J. The manuscript was improved significantly by comments from three anonymous reviewers.

4.7 References

Aja S.U., Wood S.A. and Williams-Jones A.E. (1995) The aqueous geochemistry of Zr and the solubility of some Zr-bearing minerals. *Appl. Geochem.* **10**, 603-620.

Anderson M.O., Lentz D.R., McFarlane C.R.M. and Falck H. (2013) A geological, geochemical and textural study of a LCT pegmatite: implications for the magmatic versus metasomatic origin of Nb-Ta mineralization in the Moose II pegmatite, Northwest Territories, Canada. *J. Geosci.* **58**, 299-320.

Banks D., Yardley B., Campbell A. and Jarvis K. (1994) REE composition of an aqueous magmatic fluid: a fluid inclusion study from the Capitan Pluton, New Mexico, USA. *Chem. Geol.* **113**, 259–272.

Dennis Jr. J. E. and Woods D. J. (1987) Microcomputers in large-scale computing. In *New Computing Environments* (ed. A. Wouk). SIAM, pp. 116-122.

Fullmer L.B., Molina P.I., Antonio M.R. and Nyman, M. (2014) Contrasting ion-association behaviour of Ta and Nb polyoxometalates. *Dalton Trans.* **43**, 15295-15299.

Garrels R.M. and Christ C. L. (1965) *Solutions. Minerals. And Equilibria.* Harper & Row, New York.

Helgeson H. C., Kirkham D. H. and Flowers G. C. (1981) Theoretical prediction of the thermodynamic behavior of aqueous electrolytes at high pressures and temperatures: IV. Calculation of activity coefficients, osmotic coefficients, and apparent molal and standard and relative partial molal properties to 600°. *Am. J. Sci.* **281**, 1249-1516.

Holland T. and Powell R. (1998) An internally consistent thermodynamic data set for phases of petrological interest. *J. Metamorph. Geol.* **16**, 309-343.

Jacob K.T., Shekhar C. and Waseda Y. (2009) An update on the thermodynamics of Ta_2O_5. *J. Chem. Thermodyn.* **41**, 748-753.

Jacob K. T., Shekhar C. and Vinay M. (2010) Thermodynamic properties of Niobium Oxides. *J. Chem. Eng. Data* **55**, 4854-4863.

Johnson J. W., Oelkers E. H. and Helgeson H. C. (1992) SUPCRT92: a software package for calculating the standard molal thermodynamic properties of minerals, gases, aqueous species, and reactions from 1 to 5000 bar and 0 to 1000 °C. *Comput. Geosci.* **18**, 899-947.

Kestin J., Sengers J. and Kampgar-Parsi B. (1984) Thermo-physical properties of fluid H_2O. *J. Phys. Chem. Ref.* **13**, 175-183.

Kielland J. (1937) Individual activity coefficients of ions in aqueous solutions. *J. Am. Chem. Soc.* **59**, 1675-1678.

Lumpkin G.R., and Ewing, R.C. (1992) Geochemical alteration of pyrochlore group minerals: Microlite subgroup. *Am. Mineral.* **77**, 179-188.

Marshall W. L. and Franck E. U. (1981) Ion product of water substance, 0-1000 °C, 1-10,000 bars. New international formulation and its background. *J. Phys. Chem. Ref. Data* **10**(2), 295-304.

Migdisov A. A. and Williams-Jones A. E. (2007) An experimental study of the solubility and speciation of neodymium (III) fluoride in F-bearing aqueous solutions. *Geochim. Cosmochim. Acta* **71**(12), 3056-3069.

Migdisov A. A., Williams-Jones A. E. and Wagner T. (2009) An experimental study of the solubility and speciation of the Rare Earth Elements (III) in fluoride- and chloride-bearing aqueous solutions at temperatures up to 300 °C. *Geochim. Cosmochim. Acta* **73**, 7087-7109.

Migdisov A. A., Williams-Jones A. E., van Hinsberg V. and Salvi S. (2011) An experimental study of the solubility of baddeleyite (ZrO_2) in fluoride-bearing solutions at elevated temperature. *Geochim. Cosmochim. Acta* **75**(1), 7426-7434.

Nelder J. A. and Mead R. (1965) A simplex method for function minimization. *Comput. J.* **7**, 308-313.

Novák M. and Černý P. (1998) Niobium-tantalum oxide minerals from complex granitic pegmatites in the Moldanubicum, Czech Republic: primary versus secondary compositional trends. *Can. Mineral.* **36**, 659-672.

Oelkers E. and Helgeson H. C. (1991) Calculation of activity coefficients and degrees of formation of neutral ion pairs in supercritical electrolyte solutions. *Geochim. Cosmochim. Acta* **55**, 1235–1251.

Rickers K., Thomas R. and Heinrich W. (2006) The behaviour of trace elements during the chemical evolution of the H2O-, B-, and F-rich granite-pegmatite-hydrothermal system at Enhrenfriedersdorf, Germany: a SXRF study of melt and fluid inclusions. *Miner. Deposita.* **41**, 229-245.

Robie R.A. and Hemingway B.S. (1995) Thermodynamic properties of minerals and related substances at 298.15 K and 1 Bar (105 Pascals) pressure and at higher temperatures. *U.S. Geological Survey Bulletin* 2131, 461pp.

Ryzhenko B. N. (1965) Determination of dissociation constant of hydrofluoric acid and conditions of replacement of calcite by fluorite. *Geokhimiya* **3**, 273-276.

Ryzhenko B. N., Kovalenko N. I. And Mironenko M. V. (1991) Ionization-constant of hydrofluoric acid at 500 °C, 1kbar. *Dokl. Akad. Nauk SSSR* **317**, 203-206.

Sheard E. R., Williams-Jones A. E., Heiligmann M., Pederson C. and Trueman D.L. (2012) Controls on the Concentration of Zirconium, Niobium, and the Rare Earth Elements in the Thor Lake Rare Metal Deposit, Northwest Territories, Canada. *Econ. Geol.* **107**, p. 81-104.

Sverjensky D., Shock E. L. and Helgeson H. C. (1997) Prediction of the thermodynamic properties of aqueous metal complexes to 1000 °C and 5kb. *Geochim. Cosmochim. Acta* **61**, 1359-1412.

Timofeev A., Migdisov A.A. and Williams-Jones A.E. (2015) An experimental study of the solubility and speciation of niobium in fluoride-bearing aqueous solutions at elevated temperature. *Geochim. Cosmochim. Acta* **158**, 103-111.

Timofeev A. and Williams-Jones A.E. (2015) The origin of niobium and tantalum mineralization in the Nechalacho REE Deposit, NWT, Canada. *Econ. Geol.* **110**, 1719-1735.

Van Lichtervelde M., Grégoire M., Linnen R.L., Béziat D. and Salvi S. (2008) Trace element geochemistry by laser ablation ICP-MS of micas associated with Ta mineralization in the Tanco pegmatite, Manitoba, Canada. *Contrib. Mineral. Petrol.* **155**, 791-806.

Williams-Jones A.E. and Migdisov A.A. (2014) Experimental constraints on the transport and deposition of metals in ore-forming hydrothermal systems. *Society of Economic Geologist, Special Publication* 18, 77-95.

Wise M. A., Francis C. A. and Černý P. (2012) Compositional and structural variations in columbite-group minerals from granitic pegmatites of the Brunswick and Oxford fields, Maine: Differential trends in F-poor and F-rich environments. *Can. Mineral.* **50**, 1515-1530.

Zaraisky G. P., Korzhinskaya V. and Kotova N. (2010) Experimental studies of Ta_2O_5 and columbite-tantalite solubility in fluoride solutions from 300 to 550°C and 50 to 100 MPa. *Miner. Petrol.* **99**, 287-300.

Preface to Chapter 5

Niobium and tantalum do not stand alone as metals considered to be immobile in hydrothermal solutions. Uranium, the mobility of which is central to the formation of ore deposits, the safety of nuclear waste repositories, and its containment during catastrophic nuclear accidents, has had its predicted behaviour at reducing conditions dictated by dogma. Unlike the case for niobium and tantalum, for which the concentration of the dominant ligand in the hydrothermal solution is central to determining their solubility and speciation, the behavior of uranium is governed not only by ligand availability, but also by the oxidation state of the fluid. Oxygen-rich fluids are considered to be favorable for the dissolution and transport of uranium as U^{6+}, whereas reducing, oxygen-poor fluids are considered to significantly inhibit U^{4+} mobility.

As in Chapters 3 and 4, we tackle this assumption in Chapter 5 by conducting autoclave solubility experiments, at 250-350 °C and saturated water vapor pressure, to determine the solubility and speciation of uranium under oxidizing (MoO_2-MoO_3 buffer) and reducing (Ni-NiO, Co-CoO buffer) conditions. We then use the identified uranium species to examine the behaviour of uranium under a variety of conditions, including those encountered in reduced settings, such as in iron-oxide copper gold (IOCG) deposits. In doing so, we challenge the assumption that uranium is immobile under reducing conditions.

Chapter 5

Uranium transport in acidic brines under reducing conditions

Alexander Timofeev[1]*, Artaches A. Migdisov[2], Anthony E. Williams-Jones[1], Robert Roback[2], Andrew Nelson[3], Hongwu Xu[2]

[1] Department of Earth & Planetary Sciences, McGill University, 3450 University Street, Montreal, QC, Canada, H3A 0E8.

[2] Earth and Environmental Division, Los Alamos National Laboratory, P.O. Box 1663, M.S. J535, Los Alamos, NM 87545, U.S.A.

[3] Materials Science and Technology Division, Los Alamos National Laboratory, P.O. Box 1663, M.S. E549, Los Alamos, NM 87545, U.S.A.

Published in Nature Communications, April 2018

DOI: https://doi.org/10.1038/s41467-018-03564-7

Abstract:

The behavior of uranium in environments ranging from natural systems responsible for the formation of uranium deposits to nuclear reactors providing 11% of the world's electricity, is governed by processes involving high temperature aqueous solutions. It has been well documented that uranium is mobile in aqueous solutions in its oxidized, U^{6+} state, whereas in its reduced, U^{4+} state, uranium has been assumed to be immobile. Here we present experimental evidence from high temperature (>100 °C) acidic brines that disproves this assumption. Our experiments have identified a new uranium chloride species (UCl_4^0) that is more stable under reducing than oxidized conditions. These results indicate that uranium is mobile under reducing conditions and necessitate a re-evaluation of the mobility of uranium, particularly in ore deposit models involving this metal. Regardless of the scenario considered, reducing conditions can no longer be considered a guarantee of uranium immobility.

5.1 Introduction:

From source to sink, the nuclear applications and associated chemistry of uranium have been extensively investigated. As most processes of enrichment and uses of uranium involve its contact, either direct or indirect, with aqueous solutions, many studies have focused on its interactions with high temperature (100 to ≥400 °C) aqueous fluids. However, our understanding of the behavior of uranium has been governed by the belief that uranium in its U^{4+} state, cannot be present in significant concentrations (>ppt) in aqueous fluids[1]. In other words, uranium is immobile under reducing conditions. Thus, hydrothermal models for the formation of uranium deposits call for the mobilization of the metal as U^{6+} and its precipitation as a U^{4+} mineral, e.g., uraninite, due to a reduction in oxygen fugacity (fO_2) (refs. 2,3).

The accepted model for the formation of unconformity-type uranium deposits involves the interaction of an oxidized basinal brine, which transports the uranium as U^{6+}, with a reducing, graphite-bearing pelite that leads to the precipitation of uraninite or the U^{4+} bearing phase, pitchblende[2,3]. However, evidence collected from magnetite group iron oxide copper-gold (IOCG) deposits, which are another important source of uranium, suggests that, whereas this paradigm satisfies observations made at low to moderate temperatures, e.g., for unconformity-type uranium deposits, it likely fails at temperatures greater than 250 °C (ref. 4). In order to explain the formation of the high temperature IOCG-type deposits, a means of transporting uranium under reducing conditions is necessary.

In nuclear waste management, there is an underlying assumption that reducing conditions will prevent uranium migration[5-7]. This extends also to catastrophic accidents, such as that at the Fukushima power plant, for which it is believed that reducing conditions will inhibit uranium migration. A lack of thermodynamic data for uranium species at elevated temperatures is a key factor preventing accurate predictions of uranium behavior during such an event[8,9]. These and other conclusions about the behavior of uranium in the presence of aqueous fluids, whether it be for nuclear industry applications or models of uranium ore-formation, routinely draw upon the dogma that "uranium is immobile in the reduced state".

Despite the importance of understanding the behavior of uranium in high temperature (>100 °C) fluids, there have been very few studies of uranium mineral solubility at elevated temperature, particularly under reducing conditions. Laboratory and field-based observations indicate that oxidizing, oxygen rich, fluids are capable of transporting considerable (ppm) concentrations of this metal as an aqueous species[10-12]. By contrast, studies of uranium behavior in reduced fluids have either not defined the exact oxygen fugacity of the fluid (i.e., the accurate redox state of the solution) or neglected to consider the impact of common ligands in the fluid such as chloride, fluoride, sulfate and carbonate[13-15]. Such ligands may enhance the solubility of metals due to the formation of metal complexes (e.g., $UO_2CO_3^0$)[16]. At high temperatures their impact on uranium mobility is uncertain. However, both oxygen fugacity and ligand concentration must be considered in order to accurately evaluate uranium mobility.

The most abundant ligand in seawater[17], most ore-forming fluids[18], and many waters surrounding underground waste repositories[19] is chloride (Cl^-), which can attain weight percent concentrations in these fluids. Because of the ubiquitous presence of chloride in natural systems, results of measurements of the solubility of hydrated $UO_3.nH_2O$ in NaCl-H_2O solutions[12] and spectroscopic data suggesting that U-Cl complex formation may be important at elevated temperature[20,21], we have made U-Cl speciation the focus of this paper. We also do so because of observations of uranium- and chloride-rich fluid inclusions suggesting that the impact of chloride may be underestimated in current models of uranium ore formation[12]. In this study, we identify a high temperature U-Cl species that explains these observations and extract thermodynamic data for this species from experiments conducted at variable chloride and fO_2 conditions. As the thermodynamic properties of uranium minerals such as uraninite are known, we use this information in conjunction with the data for the U-Cl species to predict uranium behavior in hydrothermal fluids for a range of reducing conditions in which uranium mobility has previously been discounted.

5.2 Results

5.2.1 The U-Cl species

To determine the stability of U-Cl complexes, we conducted solubility experiments in titanium autoclaves (Supplementary Figures 5.1 and 5.2, Supplementary Table 5.1). Acidic solutions ($pH_{25°C}$ ~2) having variable NaCl concentrations (0.1−1m) were equilibrated with a synthetic uranium oxide powder (Supplementary Figure 5.3) at temperatures ranging from 250 to 350 °C and saturated water vapor pressure. A MoO_2-MoO_3, and a Ni-NiO or Co-CoO buffer, all having no contact with the experimental solution were employed to maintain either oxidizing or reducing conditions, respectively (Supplementary Table 5.2). Changes in the dissolved uranium concentrations with increases in chloride activity were used to identify corresponding U-Cl species. Initial experiments with the Ni-NiO buffer (reducing conditions) employed the uranium oxide UO_2^{cryst}. These experiments yielded a dependence of the log activity of uranium on the log activity of chloride with a slope of four (Fig. 5.1a), which is consistent with the dissolution reaction:

$$UO_2^{cryst} + 4Cl^- + 4H^+ = UCl_4^\circ + 2H_2O \quad (1)$$

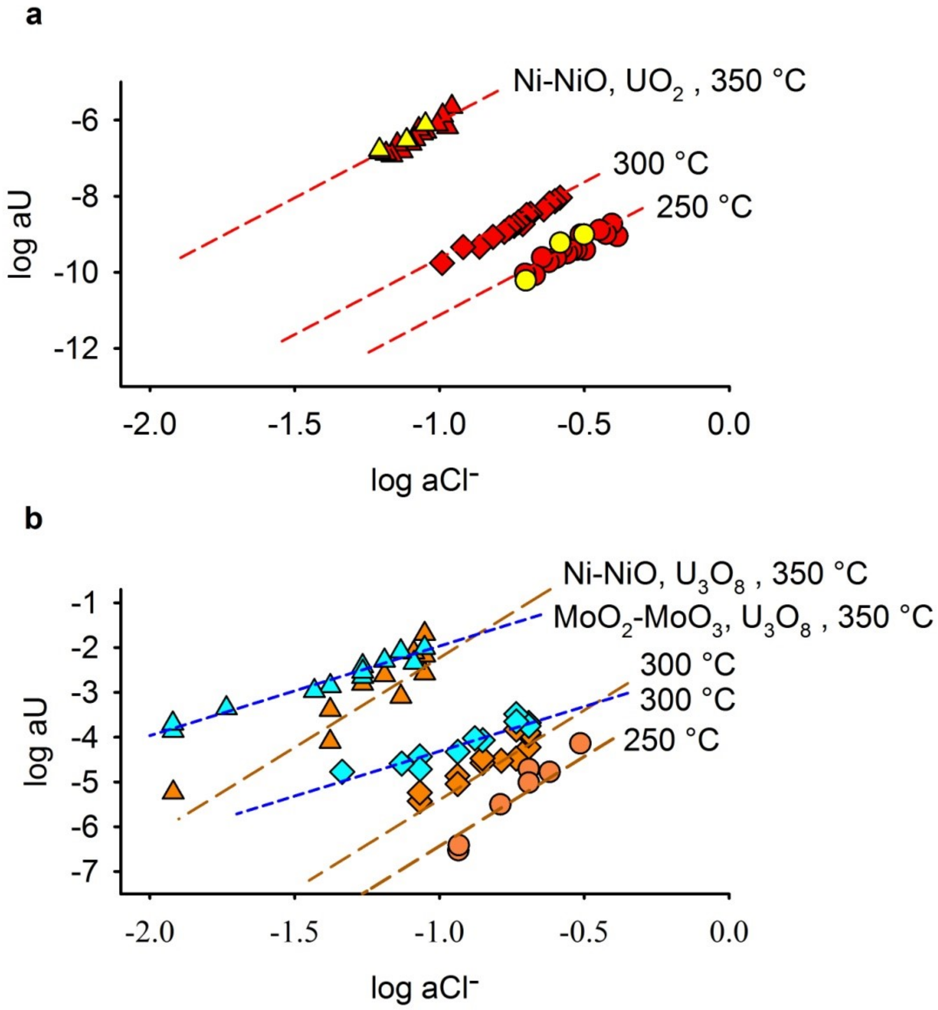
a
Ni-NiO, UO$_2$, 350 °C
300 °C
250 °C
log aU
-6
-8
-10
-12
-2.0
-1.5
-1.0
-0.5
0.0
log aCl$^-$
b
Ni-NiO, U$_3$O$_8$, 350 °C
MoO$_2$-MoO$_3$, U$_3$O$_8$, 350 °C
300 °C
300 °C
250 °C
log aU
-1
-2
-3
-4
-5
-6
-7
-2.0
-1.5
-1.0
-0.5
0.0
log aCl$^-$

Figure 5.1: **The activity of uranium determined experimentally to be in equilibrium with uranium oxide solids.** **a**, Uranium activity as a function of chloride activity for experiments conducted using UO_2^{cryst} under reducing conditions. Red circles, diamonds, and triangles indicate results obtained at 250, 300, and 350 C, respectively. The slope of all trendlines is 4. The yellow circle and triangle symbols indicate use of the Co-CoO buffer at 300 and 350 °C, respectively. The results of these experiments are indistinguishable from those utilizing the Ni-NiO buffer. All data are normalized to a pH of 2.5 using the stoichiometry of Reactions (1), (2), and (3). The trend lines represent the best fits to the data, and were calculated using the equilibrium constants for the speciation reaction (Table 5.2). **b,** Uranium activity determined from solubility experiments employing $U_3O_8^{cryst}$ plotted for specified temperature (circles-250 °C, diamonds-300 °C, triangles-350 °C) and oxygen fugacity (oxidizing-blue; reducing-brown) as a function of chloride activity. The slope of the fit under oxidizing conditions is 2, and under reducing conditions it is 4. Trend lines for data representing oxidizing conditions were calculated using equilibrium constants of 39.6 and 50.9 at 300 and 350 °C, respectively. They were fitted independently of those described in ref. 21.

The dissolved uranium species at reducing conditions was not known a priori to contain either uranium in the reduced, U^{4+} form, or in its oxidizing, U^{6+} state, although we assume the former in the fO_2 independent Reaction (1). If the uranium was in the 6+ state, the uranium dissolution reaction would be fO_2 dependent. To determine if this was the case, we conducted additional experiments with a Co-CoO buffer and a UO_2^{cryst} solid. The results of these experiments were well within the experimental uncertainty of data obtained using the Ni-NiO buffer, thereby supporting our interpretation of the species at reducing conditions as being UCl_4^0, and validating Reaction (1) (Fig. 5.1a). The rapid increase in stability with increasing temperature of this newly discovered species leads to concentrations of uranium that reach ppm levels (e.g. ~4 ppm at 400 ºC with $aCl^- = 0.10$ and a pH of 2.5) (Fig. 5.1a).

In addition, we conducted experiments under reducing conditions with $U_3O_8^{cryst}$ so as to assess the impact of U^{6+} in the solid, for example as $U_3O_8^{cryst}$ inclusions in pitchblende, on uranium mobility in a reducing environment (Fig. 5.1b). The reaction inferred from these results is similar to Reaction (1):

$$U_3O_8^{cryst} + 12Cl^- + 12H^+ = 3UCl_4^\circ + 6H_2O + O_2 \tag{2}$$

The data from these experiments also allowed us to compare the thermodynamic data and formation constants obtained for UCl_4° from Reaction (1) with those obtained from Reaction (2). The two sets of data were found to be in good agreement (Table 1). Under oxidizing conditions, the logarithm of uranium activity has a slope of two with respect to log chloride activity at both 300 and 350 °C (Fig. 5.1b). The dissolution reaction for the species that best fits this trend is as follows:

$$2U_3O_8^{cryst} + 12Cl^- + 12H^+ + O_2 = 6UO_2Cl_2^\circ + 6H_2O \tag{3}$$

On the basis of these results we conclude that uranium speciation in chloride-bearing solutions at elevated temperature is dominated by $UO_2Cl_2^0$ and UCl_4^0 under oxidizing and reducing conditions, respectively.

5.2.2 Formation constants

In order to make our data accessible for thermodynamic modelling, we calculated formation constants (logß), which are independent of the experimental uranium oxide solid, for $UO_2Cl_2^0$ and UCl_4^0. The formation constant reaction for $UO_2Cl_2^0$ is written as follows:

$$UO_2^{2+} + 2Cl^- = UO_2Cl_2^\circ \qquad \log\beta_1 = \log a_{UO_2Cl_2^0} - \log a_{UO_2^{2+}} - 2\log a_{Cl^-} \qquad (4)$$

We calculated the formation constants for Reaction (4) to be 4.29 ± 0.08 at 300 °C and 7.21 ± 0.07 at 350 °C. These values are in good agreement with those obtained independently using ultraviolet-visible spectroscopy (UV-VIS) measurements at temperatures ≤ 250 °C (Fig. 5.2) (ref. 21). The corresponding reaction for UCl_4^0 is:

$$U^{4+} + 4Cl^- = UCl_4^\circ \qquad \log\beta_2 = \log a_{UCl_4^0} - \log a_{U^{4+}} - 4\log a_{Cl^-} \qquad (5)$$

We had two data sets to choose from for our calculation of $\log\beta_2$. Formation constants calculated using data from Reaction (1) ($\log\beta_1$) are 13.4 ± 0.05, 15.6 ± 0.06, and 19.8 ± 0.06 for 250, 300, and 350 °C respectively. The values of $\log\beta_2$ calculated using $U_3O_8^{cryst}$ were 13.5 ± 0.08 at 250 °C, 16.0 ± 0.08 at 300 °C and 20.0 ± 0.14 at 350 °C (Fig. 5.2), which are very close to those obtained using Reaction (1) (see above). This confirms the dominance of UCl_4^0 in the solutions. The presence of a neutral species is consistent with the observation that, with increasing temperature, the dipole moment of water decreases and its hydrogen bonding network weakens considerably, thereby favoring aqueous species of low or no charge[22].

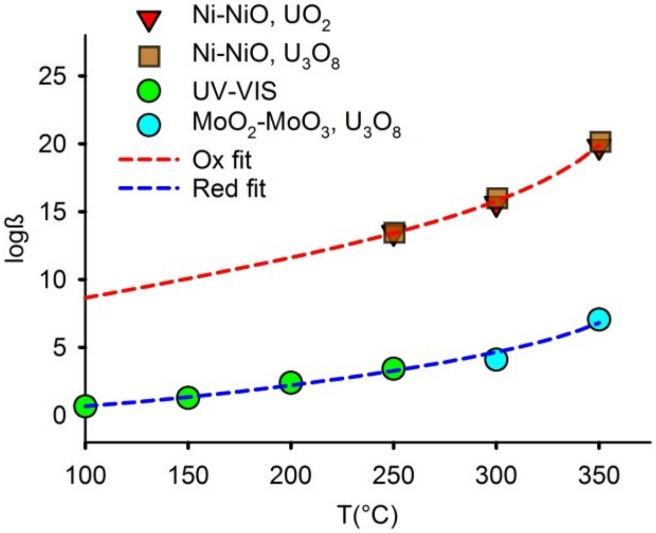

Figure 5.2: Comparison of formation constants determined in this study to those previously reported. Formation constants for UCl_4^0 at reducing condition (Ni-NiO oxygen fugacity buffer) conditions were fitted to the Bryzgalin-Ryzhenko model (red dashed line). Regardless of whether the experiments used UO_2^{cryst} or $U_3O_8^{cryst}$, the resulting formation constants are indistinguishable. Uncertainties for the formation constants are smaller than the symbols. A similar fit for $UO_2Cl_2^0$ at oxidizing conditions (blue dashed line) demonstrates that data obtained in this study (blue circles) are consistent with those of ref. 21 (green circles).

5.3 Discussion

It is clear from the results of our experiments that considerable uranium transport can take place under reducing conditions. If the chemical composition of a chloride-bearing reducing fluid is fixed, an increase in temperature from 250 to 350 °C will result in a five orders of magnitude rise in uranium solubility. Raising the chloride activity of the fluid by one logarithmic unit or decreasing the pH by one unit will increase uranium solubility by four orders of magnitude (Fig. 5.1a). Comparable, but less pronounced effects are evident for oxidizing conditions; the aforementioned changes in chloride activity and pH result in increases of uranium solubility by two rather than four orders of magnitude (Fig. 5.1b). In short, the ideal fluid for moving uranium is hot, chloride-rich, and highly acidic. The opposite is true for uranium removal from a fluid. This could be accomplished by cooling (fluids at ≤150 °C are U^{4+} poor[23]), a reduction in chloride concentration or increasing the pH of the fluid. Any one or more of these changes are common to both man-made and natural uranium-bearing systems. An important example of the latter is provided by the hot, saline brine responsible for the formation of magnetite- and uranium-bearing iron oxide copper-gold (IOCG) deposits within which, at depth, a predominance of magnetite in observed alteration assemblages demonstrates reducing conditions[4]. We chose this setting to illustrate the importance of these newly identified U-Cl species.

We constructed a model to evaluate uranium transport by a magmatic fluid under reducing conditions in an IOCG setting. Firstly, with formation constants for the aqueous species in hand, we fitted our reducing (Fig. 5.2) and oxidizing data to the Bryzgalin-Ryzhenko equation of state[24]. We then saturated the fluid (a 2*m* NaCl acidic brine) with respect to uraninite at 400 °C, 500 bar and reducing conditions ($\log fO_2 = -35$, ~QFM-4) and determined that this fluid is capable of dissolving ~0.27 ppm of the UCl_4^0 species. This sizable amount of uranium must be

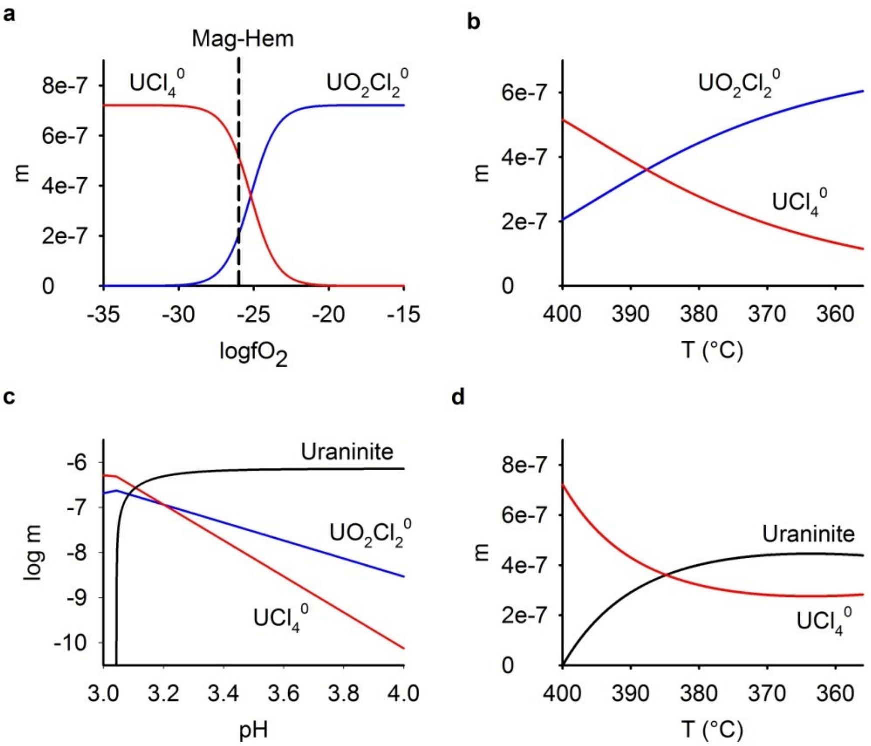

Figure 5.3: A model of uranium behavior in a magnetite-bearing IOCG system. a, b, Raising the oxygen fugacity of a 2*m* NaCl acidic brine at 400 °C and 500 bar does not induce uraninite precipitation, nor does cooling under oxidizing conditions (**b**). **c, d,** However, increasing the pH at oxidizing conditions (**c**) or decreasing the temperature of a reduced solution (**d**) triggers uraninite deposition.

precipitated as uraninite (UO_2^{cryst}) in order to form an ore deposit. Mixing of the reduced fluid with an oxidizing ($\log fO_2 = -26$), but otherwise identical fluid does not lead to uraninite precipitation, but rather a change in speciation (Fig. 5.3a). Indeed, at the magnetite-hematite fO_2 buffer ($\log fO_2 = -26$), corresponding to shallower, more oxidizing parts of IOCG systems, UCl_4^0 remains the predominant aqueous species in solution. Cooling of an oxidizing fluid results in a similar and gradual change in speciation, but no uraninite precipitation (Fig. 5.3b). By contrast, increasing the pH of the oxidizing solution through interaction with the wall rocks or mixing with meteoric waters rapidly removes the dissolved uranium (Fig. 5.3c). At reducing ($\log fO_2 = -35$) conditions, a decrease in temperature promotes uraninite deposition (Fig 5.3d). In summary, the model outlined above clearly identifies mechanisms by which uranium transport and deposition can both occur under reducing conditions in natural systems.

Reducing conditions in uranium-bearing systems are not limited to IOCG deposits and some models explaining the formation of unconformity-type uranium deposits involve reduced basement rocks containing uranium oxides[25]. Moreover, our data suggest that seawater used to cool fuel assemblies after the Fukushima nuclear accident, which likely remained at temperatures near or above boiling for months following the event[8,9] would have the potential to dissolve and mobilize uranium at ppm concentrations. These and other natural and anthropogenic scenarios involving uranium transport under reducing conditions, for which our study represents a starting point, require further investigation. It is also important to note that ligands other than chloride may play an important role in reduced uranium transport. Hard-soft-acid-base principles suggest that uranium, a hard (high charge to radius ratio) cation, should form strong complexes with fluoride and carbonate ions, which are both hard anions[26]. Indeed, both ions have been proposed as ligands likely to form complexes with uranium in IOCG systems[27]. The presence of these additional ligands in hydrothermal brines will further promote the dissolution of uranium under reducing conditions. This study represents a first attempt to identify and determine thermodynamic constants for U-Cl species under reducing conditions at elevated temperature, and to evaluate the potential for uranium mobility under such conditions. The new species identified in this study may be just the first of many.

5.4 Methods:

5.4.1 Experimental setup and procedure

The experiments involved measuring the solubility of synthetic U_3O_8 and UO_2 (solid) in aqueous solutions of variable NaCl concentration at temperatures of 250, 300, and 350 °C, and vapor-saturated water pressure. All the experiments with U_3O_8 (solid), and those with UO_2 (solid) at 300 and 350 °C, were performed in titanium autoclaves (Supplementary Figure 5.1). Experiments with UO_2 (solid) at 250 °C were conducted in titanium autoclaves containing a Teflon liner that limited contact of the experimental solution with the autoclave body (Supplementary Figure 5.2). The consistency of the results of the Teflon-lined experiments with those of the Teflon-free runs demonstrated that the extent of reaction between the titanium autoclaves and the experimental solution was negligible and did not affect the outcome of the experiments (Fig. 5.2 and Supplementary Table 5.1). Experiments with Teflon could not be conducted at 300 and 350 °C as perfluoroalkoxy (PFA) Teflon has a maximum operating temperature of ~260 °C (ref. 28).

Chloride concentrations were controlled by dissolving known amounts of NaCl in nano-pure water. The pH of each solution was then reduced to the level of interest by adding an appropriate amount of trace metal grade HCl. The pH (25 °C) of the solutions used for the $U_3O_8^{cryst}$ experiments ranged from 2.2 to 2.6 prior to the start of the experiments. Solutions containing higher chloride concentrations experienced a more rapid increase in pH with increasing temperature than those of lower salinity. Therefore, high salinity solutions were created with a lower pH so as to have similar acidity at the temperatures of interest. The pH (25 °C) for the experiments with UO_2^{cryst} was kept constant at ~1.5.

Experiments were initiated by placing small quartz holders containing uranium oxide powder in the titanium autoclaves, to which 15−18 ml of experimental solution was added. Experimental solution volumes were calculated to prevent solution contact with the inside of the oxygen fugacity buffer holder during volume increases associated with heating (~20% at 350 °C and saturated water vapor pressure). The quartz holders contained fine quartz wool above the uranium oxide solid to prevent any back-reaction during cooling of the experiment. A quartz holder just shorter than the height of the autoclave containing oxygen fugacity buffers was then added to the autoclave. Oxidizing experiments employed MoO_2 and MoO_3 powders placed one atop the other and covered by fine quartz wool (Supplementary Figure 5.1), whereas reducing experiments used three strands of nickel metal wire (Supplementary Figure 5.2). The nickel wires were replaced for every experiment and during the course of the experimental run reacted with oxygen to form nickel oxide, thereby producing the Ni-NiO buffer. A small number of additional experiments with UO_2^{cryst} were conducted with a reducing Co-CoO buffer at 250 °C. The $\log fO_2$ values for the buffer equilibria at 250 °C-350 °C are shown in Supplementary Table 5.2. Prior to closure of the autoclave, high purity argon was flushed through the experimental solution for 30 minutes to significantly reduce the oxygen contained therein. After sealing the autoclave with a flexible carbon ring, the autoclave was heated in a Fisher Isotemp forced draft oven to the temperature of interest. An aluminum box lined the oven to reduce temperature gradients. The duration of each experiment was 7 days, which allowed the experiments to reach equilibrium.

Following completion of an experiment, the autoclave was air-cooled with a fan for 20 minutes and then unsealed. After removing the buffer and uranium oxide holders, an aliquot of the experimental solution was removed for measurement of the solution pH. For experiments with UO_2^{cryst}, the pH of the experimental solution was measured directly in the autoclave. To dissolve any potential precipitates formed during cooling, 5 ml of trace metal grade nitric acid was added to the autoclave and allowed to remain there for a minimum of 30 minutes.

The pH of the aliquots and the solutions of UO_2^{cryst}-based experiments was measured potentiometrically using a calibrated glass electrode. The concentrations of dissolved uranium were analyzed by inductively coupled plasma mass spectrometry (ICP-MS). The activity of chloride and the pH of each experimental solution were then recalculated at the temperature of the experiment using the initial composition of the solution and the measured pH, respectively. Following completion of the experiments, samples of uranium oxide powder from oxidizing (MoO_2-MoO_3) and reducing (Ni-NiO) experiments were analyzed using X-ray diffraction (XRD) to verify the continued presence of $U_3O_8^{cryst}$ in experiments using this uranium oxide solid. The resulting XRD spectra confirmed the presence of $U_3O_8^{cryst}$ (Supplementary Figure 5.3).

5.4.2 Data optimization

The uranium species responsible for the observed uranium concentrations were recognized on the basis of trends observed in the data, specifically the slope of the logarithm of uranium activity with respect to the logarithm of chloride activity. As stated in the main text, the two species identified in this study are $UO_2Cl_2^0$ and UCl_4^0.

The excel optimization code titled “OptimA” included as part of the Hch software package of ref. 29 was used to calculate standard Gibbs free energies of the two uranium species. Inputs to the code included the NaCl and HCl molality of every experiment, in addition to the molality of uranium analyzed in each experiment using ICP-MS. The molality of HCl of each experiment was calculated on the basis of the starting NaCl concentration and the pH measured after each experiment. Excess amounts of the relevant uranium oxide solid (UO_2^{cryst} or $U_3O_8^{cryst}$) were included in the optimization, as well as the relevant oxygen fugacity buffers (MoO_2, MoO_3 or Ni, NiO). Aqueous species considered during the optimization were H^+, OH^-, Na^+, NaOH, NaCl, Cl^-, and HCl. The activity of the ions was calculated using the extended Debye-Hückel equation[30]:

$$\log \gamma_n = -\frac{\mathrm{A} \cdot [\mathrm{z_n}]^2 \cdot \sqrt{I}}{1 + \mathrm{B} \cdot \mathrm{å} \cdot \sqrt{I}} + b_\gamma \cdot I \qquad (4)$$

with A and B being the parameters of the Debye-Hückel equation, b_γ the extended parameter, which depends on the nature of the background electrolyte, *å* the distance of closest approach, which is specific to the ion of interest, *z* the charge of the ion, and *I* the true ionic strength when all dissolved components are considered. The Haar-Gallagher-Kell[31] and Marshall and Franck[32] models were used to determine the thermodynamic properties and dissociation constant of H_2O under our experimental conditions. Thermodynamic data for the aqueous species were obtained from refs 33,34,35,36, and 37. Extended parameters for NaCl in the Debye-Hückel equation were taken from ref. 38. Thermodynamic data for the uranium oxides was taken from refs 16 and 39. The thermodynamic data for MoO_2, MoO_3, Ni, and NiO was taken from refs 39,40, and 41.

Optimizations were conducted separately for UCl_4^0 data collected using UO_2^{cryst} and $U_3O_8^{cryst}$. These optimizations also calculated the chloride activity in each experiment, which was used to construct Figure 5.1. As the two aqueous uranium species are uncharged, the activity of uranium shown in Figure 5.1 is equivalent to the molality of uranium. The Gibbs free energy changes for the reactions responsible for the formation of $UO_2Cl_2^0$ and UCl_4^0 were calculated using the standard Gibbs free energy of the other species involved in the reactions, namely UO_2^{2+}, Y^{4+}, and Cl^-. The Gibbs free energy change was then converted to a formation constant (logß) using the relationship $\Delta G^0 = -RT\ln K$. These formation constants are shown in Table 5.1. The uncertainty reported is that calculated using the OptimA program.

All calculated formation constants were fitted separately for $UO_2Cl_2^0$ and UCl_4^0 to the Bryzgalin-Ryzhenko equation of state[24]. Formation constants from ref. 21 for 100−250 °C were included in the optimization for $UO_2Cl_2^0$. The fit was then used to calculate equilibrium constants (logK) for the uranium oxide dissolution reactions. These are shown in Table 5.2. Uncertainties in the equilibrium constants were obtained by adjusting the measured uranium activity to the same pH and chloride activity using the stoichiometry of Reactions (1), (2), or (3), taking their standard deviation, and propagating this standard deviation to the equilibrium constant. The trend lines to the experimental data shown in Figure 5.1 were calculated on the basis of these equilibrium constants with the exception of oxidizing data the trend lines of which were calculated using equilibrium constants of 39.6 and 50.9 at 300 and 350 °C, respectively. These were fitted independently of the equilibrium constants reported in ref. 21.

5.4.3 IOCG modelling

The model depicting scenarios that could be encountered by a reduced uranium-bearing fluid in a magnetite-bearing IOCG deposit was made using the Hch software package[29]. The ore-forming temperature for magnetite-bearing IOCG deposits can exceed 500 °C (refs. 27,42,43). However, a temperature of 400 °C was selected for our calculations so as to not significantly exceed the 250-350 °C temperature range of our experiments. The conclusions of this model would be the same for 500 °C except that the absolute concentration of dissolved uranium would be orders of magnitude higher. A pressure of 500 bars was used to maintain supercritical fluid conditions and to simulate conditions for an aqueous fluid at depth. Thermodynamic data sources for the dissolved aqueous species and solids used in the model are identical to those given in the preceding data optimization section of the supplementary information.

In the first model, which depicts a reduced fluid becoming progressively more oxidized, a fluid with 2*m* NaCl, 0.055*m* HCl, at 400 °C, 500 bar, and at a pH of 3.0 was saturated with respect to uraninite at a log fO_2 of -35 and had its log fO_2 progressively raised until a log fO_2 of -15 was achieved (Fig. 5.3a). Uraninite did not precipitate and the dominant aqueous uranium species in solution shifted from UCl_4^0 to $UO_2Cl_2^0$. Therefore, in the absence of an increase in pH, interactions with an oxidizing fluid, or wall rocks that may oxidize the fluid will not result in uranium deposition.

The initial fluid in the second model was more oxidizing with a log fO_2 of -26, equivalent to that of the magnetite-hematite redox buffer, but otherwise identical to that used in the first model. Progressive cooling of this fluid resulted in a change in speciation due to the more rapid decrease in stability of the UCl_4^0 species with decreasing temperature relative to the $UO_2Cl_2^0$ species, but no uraninite precipitation (Fig. 5.3b). The oxidizing and cooler conditions encountered at shallower depths in an IOCG system are therefore insufficient for uranium deposition in the absence of a pH increase.

The pH increase was considered in the third model. The same initial fluid as in the second model is titrated with NaOH to produce a pH increase. Uraninite deposition rapidly follows (Fig. 5.3c). Whereas this fluid is initially capable of dissolving considerable amounts of uranium, this metal cannot be transported at less acidic conditions.

The last model explores the impact of a temperature decrease on the preceding fluid, at reducing conditions (log fO_2 = -35). As the stability of UCl_4^0 is considerably more temperature dependent than that of $UO_2Cl_2^0$ (Fig. 5.2), uraninite deposition occurs rapidly, despite the pH decrease accompanying NaCl dissociation (Fig. 5.3d). Therefore, these models demonstrate that in a magnetite-bearing IOCG system temperature decreases at reducing conditions, or pH increases are necessary to remove the considerable amounts of uranium that could be present under reducing conditions.

5.5 Data availability:

The data supporting the findings of this work are available within the article and its Supplementary Information files. All other relevant data supporting the findings of this study are available from the corresponding author upon reasonable request.

5.6 Acknowledgments:

Funding for A.T.'s visit to the Los Alamos National Laboratory (LANL) was provided by a Seaborg Institute Summer Research Fellowship and is gratefully acknowledged. Additional support for A.T.'s stay at LANL was supplied by Natural Sciences and Engineering Research Council of Canada Alexander Graham Bell and Michael Smith Foreign Study Supplement Canada Graduate Scholarships. Research presented in this article was supported by the Laboratory Directed Research and Development program of Los Alamos National Laboratory under project number 20180007DR.

5.7 Author contributions:

A.A.M. conceived the research. A.T. developed the experimental method and conducted experiments with U_3O_8. A.A.M. performed experiments with UO_2. A.T. wrote the manuscript in collaboration with A.A.M. and A.E.W-J. Additional comments were provided by R.R., A.N, and H.X.

5.8 Competing interests:

The authors declare no conflict of interests.

5.9 References:

1. Romberger, S. B. Transport and deposition of uranium in hydrothermal systems at temperatures up to 300°C: geological implications. In: De Vivo, B., Ippolito, F., Capaldi, G. & Simpson P.R. (eds) Uranium geochemistry, mineralogy, geology, exploration and resources. (Springer, Dordrecht, 1984).
2. Jefferson, C. W. et al. Unconformity-associated uranium deposits of the Athabasca Basin, Saskatchewan and Alberta. *Bulletin-Geol. Surv. Canada* **588**, 273-305 (2007).
3. Hoeve, J. & Sibbald, T. I. I. On the genesis of Rabbit Lake and other unconformity-type uranium deposits in northern Saskatchewan, Canada. *Econ. Geo.* **73**, 1450-1473 (1978).
4. Montreuil, J.-F., Corriveau, L. & Potter, E. G. Formation of albitite-hosted uranium within IOCG systems: the Southern Breccia, Great Bear magmatic zone, Northwest Territories, Canada. *Miner. Deposita* **50**, 293-325 (2015).
5. Grambow, B. Geological disposal of radioactive waste in clay. *Elements* **12**, 239-245 (2016).
6. Hedin, A. & Olsson, O. Crystalline rock as a repository for Swedish spent nuclear fuel. *Elements* **12**, 247-252 (2016)

7. Swift, P. N. & Bonano, E. J. Geological disposal of nuclear waste in tuff: Yucca Mountain (USA). *Elements* **12**, 263-268 (2016).
8. Grambow, B. & Poinssot, C. Interactions between nuclear fuel and water at the Fukushima Daiichi reactors. *Elements* **8**, 213-219 (2012).
9. Burns, P. C., Ewing, R. C. & Navrotsky, A. Nuclear Fuel in a Reactor Accident. *Science* **335**, 1184-1188 (2012).
10. Langmuir, D. Uranium solution-mineral equilibria at low temperatures with applications to sedimentary ore deposits. *Geochim. Cosmochim. Acta* **42**, 547-569 (1978).
11. Lemire, R. J. & Tremaine, P. R. Uranium and plutonium equilibria in aqueous solutions to 200 °C. *J. Chem. Eng. Data* **25**, 361-370 (1980).
12. Richard, A. et al. Giant uranium deposits formed from exceptionally uranium-rich acidic brines. *Nature Geosci.* **5**, 142-146 (2012).
13. Parks, G. A. & Pohl, D. C. Hydrothermal solubility of uraninite. *Geochim. Cosmochim. Acta* **52**, 863-875 (1988).
14. Casas, I. et al. The role of pe, pH, and carbonate on the solubility of UO_2 and uraninite under nominally reducing conditions. *Geochim. Cosmochim. Acta* **62**, 2223-2231 (1998).
15. Rai, D., Felmy, A. R. & Ryan, J. L. Uranium(IV) hydrolysis constants and the solubility product of $UO_2 \cdot xH_2O$(am). *Inorg. Chem.* **29**, 260-264 (1990).
16. Guillaumont, R. et al. *Chemical Thermodynamics Volume 5: Update on the Chemical Thermodynamics of Uranium, Neptunium, Plutonium, Americium and Technetium* (Elsevier, 2003).

17. Millero, F. J., Feistel, R., Wright, D. G. & McDougall, T. J. The composition of Standard Seawater and the definition of the Reference-Composition Salinity Scale. *Deep-Sea Research I* **55**, 50-72 (2008).

18. Seward, T. M., Williams-Jones, A. E. & Migdisov, A. A. "[The chemistry of metal transport and deposition by ore-forming hydrothermal fluids]" in *Treatise on Geochemistry 2nd Edition*, H. Holland, K. Turekian, Ed. (Oxford: Elsevier, 2014), pp. 29-57.

19. Berlepsch, T. & Haverkamp, B. Salt as a host rock for the geological repository for nuclear waste. *Elements* **12**, 257-262 (2016).

20. Dargent, M. et al. Experimental study of uranyl(VI) chloride complex formation in acidic LiCl aqueous solutions under hydrothermal conditions (T = 21 °C-350 °C, Psat) using Raman spectroscopy. *Eur. J. Mineral.* **25**, 765-775 (2013).

21. Migdisov, A. A. et al. A spectroscopic study of uranyl speciation in chloride-bearing solutions at temperatures up to 250 °C. *Geochim. Cosmochim. Acta* **222**, 130-145 (2018).

22. Fernández, D. P., Goodwin, A. R H, Lemmon, E. W., Levelt Sengers, J. M H & Williams, R. C. A formulation for the static permittivity of water and steam at temperatures from 238 K to 873 K at pressures up to 1200 MPa, including derivatives and Debye-Hückel coefficients. *J. Phys. Chem. Ref. Data* **26**, 1125-1166 (1997).

23. Richard, A. et al. Synchrotron XRF and XANES investigation of uranium speciation and element distribution in fluid inclusions from unconformity-related uranium deposits. *Geofluids* **13**, 101-111 (2013).

24. Ryzhenko, B. N., Bryzgalin, O. V., Artamkina, I. Y., Spasennykh, M. Y. & Shapkin, A. I. An electrostatic model for the electrolytic dissociation of inorganic substances dissolved in water. *Geochem. Int.* **22**, 138-144 (1985).

25. Mercadier, J., Annesley, I. R., McKechnie, C. L., Bogdan, T. S. & Creighton, S. Magmatic and metamorphic uraninite mineralization in the western margin of the Trans-Hudson orogen (Saskatchewan, Canada): A uranium source for unconformity-related deposits?. *Econ. Geo.* **108**, 1037-1065 (2013).

26. Pearson, R. G. Hard and Soft Acids and Bases. *J. Am. Chem. Soc.* **85**, 3533-3539 (1963).

27. Montreuil, J.-F., Potter, E. G., Corriveau, L. & Davis, W. J. Element mobility patterns in magnetite-group IOCG systems: The Fab IOCG system, Northwest Territories, Canada. *Ore Geol. Rev.* **72**, 562-584 (2016).

28. Rowan, H. I. Thermoplastic fluoropolymers of engineering plastics, in: Engineered Materials Handbook, vol. 2, ASM International, Metals Park, OH, 115–119 (1988).

29. Shvarov, Y. V. Algorithmization of the numeric equilibrium modeling of dynamic geochemical processes. *Geochem. Int.* **37**, 571-576 (1999).

30. Helgeson, H. C., Kirkham, D. H. & Flowers, G. C. Theoretical prediction of the thermodynamic behavior of aqueous electrolytes at high pressures and temperatures: IV. Calculation of activity coefficients, osmotic coefficients, and apparent molal and standard and relative partial molal properties to 600°. *Am. J. Sci.* **281**, 1249-1516 (1981).

31. Kestin, J., Sengers, J. & Kampgar-Parsi B. Thermo-physical properties of fluid H_2O. *J. Phys. Chem. Ref.* **13**, 175-183 (1984).

32. Marshall, W. & Franck E. U. Ion product of water substance, 0-1000 °C, 1-10,000 bars. New international formulation and its background. *J. Phys. Chem. Ref. Data* **10**, 295-304 (1981).

33. Ryzhenko, B. N. Determination of dissociation constant of hydrofluoric acid and conditions of replacement of calcite by fluorite. *Geokhimiya* **3**, 273-276 (1965).

34. Ryzhenko, B. N., Kovalenko, N. I. & Mironenko, M. V. Ionization-constant of hydrofluoric acid at 500 °C, 1kbar. *Dokl. Akad. Nauk SSSR* **317**, 203-206 (1991).

35. Johnson, J. W., Oelkers, E. H. & Helgeson, H. C. SUPCRT92: a software package for calculating the standard molal thermodynamic properties of minerals, gases, aqueous species, and reactions from 1 to 5000 bar and 0 to 1000 °C. *Comput. Geosci.* **18**, 899-947 (1992).

36. Sverjensky, D., Shock, E. L. & Helgeson, H. C. Prediction of the thermodynamic properties of aqueous metal complexes to 1000 °C and 5kb. *Geochim. Cosmochim. Acta* **61**, 1359-1412 (1997).

37. Shock, E. L., Sassani, D. C., Willis, M. & Sverjensky, D. A. Inorganic species in geologic fluids: correlations among standard molal thermodynamic properties of aqueous ions and hydroxide complexes. *Geochim. Cosmochim. Acta* **61**, 907-950.

38. Oelkers, E. & Helgeson, H. C. Calculation of activity coefficients and degrees of formation of neutral ion pairs in supercritical electrolyte solutions. *Geochim. Cosmochim. Acta* **55**, 1235–1251 (1991).

39. Robie, R. A. & Hemingway, B. S. Thermodynamic properties of minerals and related substances at 298.15 K and 1 Bar (105 Pascals) pressure and at higher temperatures. *U.S. Geological Survey Bulletin* 2131, 461pp (1995).

40. Holland, T. & Powell, R. An internally consistent thermodynamic data set for phases of petrological interest. *J. Metamorph. Geol.* **16**, 309-343 (1998).

41. Pankratz, L. B. & Mrazek, R. V. *Thermodynamic properties of elements and oxides* (U.S. Bureau of Mines Bulletin 672, 1982)

42. Williams, P. J. et al. Iron oxide copper–gold deposits: geology, space–time distribution, and possible modes of origin. *Econ. Geol. Bull. Soc. Econ. Geol. 100th Anniversary*, 371–405 (2005).

43. Perring, C. S., Pollard, P. J., Dong, G., Nunn, A. J. & Blake, K. L. The Lightning Creek sill complex, Cloncurry District, northwest Queensland: a source of fluids for Fe oxide Cu–Au mineralisation and sodic–calcic alteration. *Econ. Geo.* **95**, 1067 – 1089 (2000).

Table 5.1 Calculated logß formation constants for the uranium species identified in this study

T(°C)	250	300	350
$UO_2^{2+} + 2Cl^- = UO_2Cl_2^\circ$ ($U_3O_8^{cryst}$)	-	4.29 ± 0.08	7.21 ± 0.07
$U^{4+} + 4Cl^- = UCl_4^\circ$ ($U_3O_8^{cryst}$)	13.5 ± 0.08	16.0 ± 0.08	20.0 ± 0.14
$U^{4+} + 4Cl^- = UCl_4^\circ$ (UO_2^{cryst})	13.4 ± 0.05	15.6 ± 0.06	19.8 ± 0.06

The formation constants are separated according to experiments conducted with different uranium oxide solids, which are shown in brackets. Dashes indicate temperatures not covered in this paper.

Table 5.2 LogK equilibrium constants and their associated 1σ uncertainty for uranium oxide dissolution reactions

T(°C)	250	300	350
Oxidizing (MoO_2-MoO_3 buffer)			
$2U_3O_8^{cryst} + 12Cl^- + 12H^+ + O_2 = 6UO_2Cl_2^\circ + 6H_2O$	-	42.3 ± 0.96	49.6 ± 0.72
Reducing (Ni-NiO buffer)			
$U_3O_8^{cryst} + 12Cl^- + 12H^+ = 3UCl_4^\circ + 6H_2O + O_2$	-18.0 ± 0.72	-10.5 ± 0.60	3.01 ± 1.02
$UO_2^{cryst} + 4Cl^- + 4H^+ = UCl_4^\circ + 2H_2O$	2.88 ± 0.17	4.37 ± 0.07	7.96 ± 0.14

The equilibrium constants are grouped according to whether they were from oxidizing (MoO_2-MoO_3) or reducing (Ni-NiO) oxygen fugacity buffer experiments. Data from ref. 21 for 100−250 °C were included during the optimization of $UO_2Cl_2^0$. Dashes indicate temperatures for which data were not collected in this study.

Supplementary Materials for

Uranium transport in acidic brines under reducing conditions

Timofeev et al.

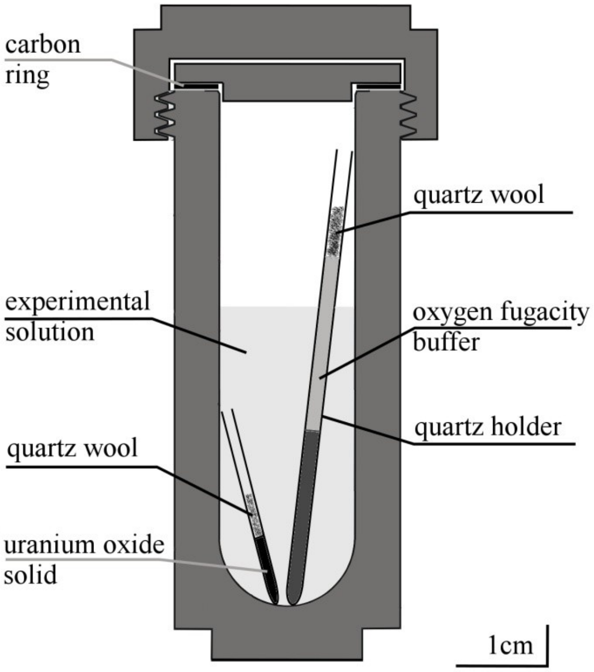

Supplementary Figure 5.1: A schematic diagram illustrating the experimental setup for $U_3O_8^{cryst}$ experiments and UO_2^{cryst} experiments at 300 and 350 °C. Malleable carbon rings provided an airtight seal upon closure of the autoclave. For experiments involving the Ni-NiO buffer, three new strands of nickel wire were placed into the extended quartz holder prior to the start of each experiment. Quartz wool was not added above nickel wires.

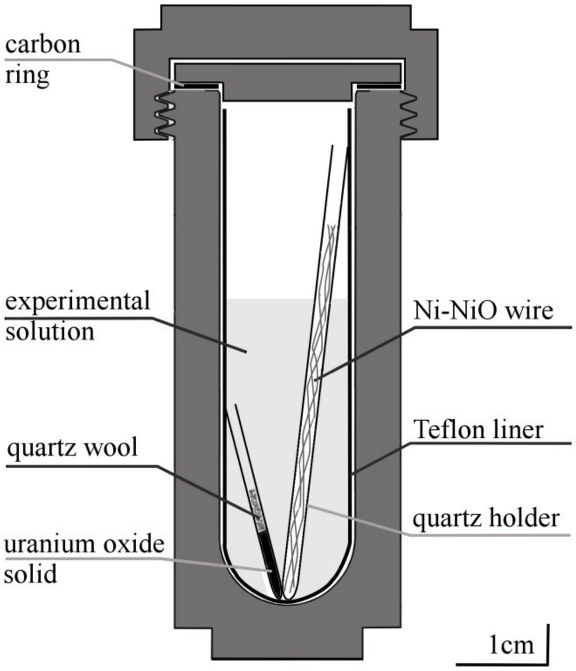

Supplementary Figure 5.2: A schematic diagram illustrating the experimental setup for UO_2^{cryst} experiments at 250 °C. The Ni-NiO wires described in the caption of Supplementary Figure 5.1 are shown in this diagram.

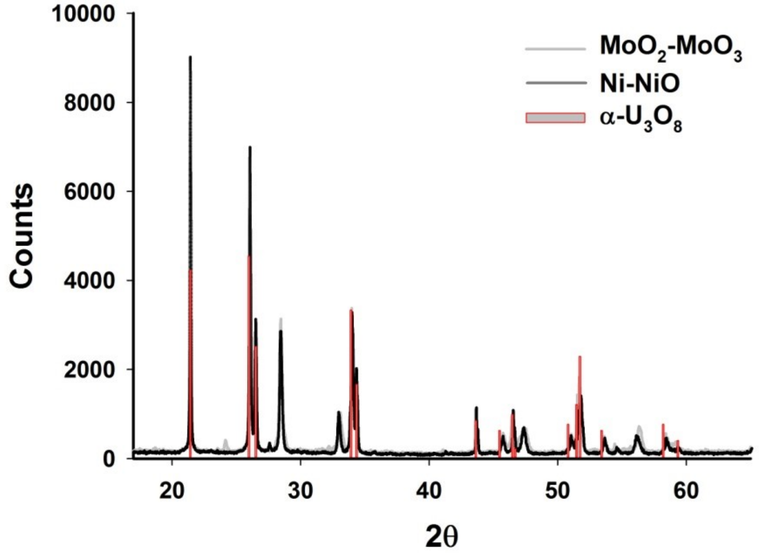

Supplementary Figure 5.3: X-ray diffraction (XRD) analyses of uranium oxide solids following completion of the experiments. Uranium oxide powders were chosen for analysis by XRD from initially $U_3O_8^{cryst}$ bearing oxidizing (MoO_2-MoO_3) and reducing (Ni-NiO) experiments. The close match between predicted XRD diffraction peaks for α-$U_3O_8^{cryst}$ and those observed in the experimental powders demonstrates that the powder remained largely unchanged.

Supplementary Table 5.1. Compositions of the experimental solutions. Concentrations are given for solutions at 25 °C. The data are organized in sections according to the oxygen fugacity buffer and uranium oxide solid employed in the experiments.

MoO_2-MoO_3, $U_3O_8^{cryst}$

T(°C)	NaCl(m)	HCl(m), 10^{-3}	U(m), 10^{-7}	pH (25 °C)
300	1.00	13.7	1000	2.08
↓	1.00	13.4	822	2.09
↓	0.85	10.5	1030	2.19
↓	0.85	10.5	706	2.19
↓	0.55	8	236	2.29
↓	0.50	5.5	130	2.45
↓	0.40	8.1	172	2.27
↓	0.25	6.3	118	2.36
↓	0.25	6.3	61.5	2.36
↓	0.20	6.7	107	2.32
300	0.10	3.8	38.5	2.54
350	1.00	7.3	1040	2.35
↓	0.85	12.4	1510	2.12
↓	0.70	8.2	1510	2.29
↓	0.55	7.4	1020	2.32
↓	0.40	6.0	672	2.40
↓	0.40	5.7	352	2.42
↓	0.40	6.9	668	2.34
↓	0.25	6.9	503	2.32
↓	0.20	5.1	270	2.44
↓	0.060	3.4	153	2.57
↓	0.030	2.7	60.6	2.64
350	0.030	2.5	73.5	2.68

Ni-NiO, $U_3O_8^{cryst}$

T(°C)	NaCl(m)	HCl(m), 10^{-3}	U(m), 10^{-7}	pH (25 °C)
250	1.00	10.6	808	2.19
↓	0.70	8.4	111	2.28
↓	0.55	8.9	219	2.24
↓	0.55	8.9	111	2.24
↓	0.40	6.6	17.0	2.36
↓	0.25	6.7	3.76	2.33
250	0.25	7.9	7.90	2.26
300	1.00	12.8	121	2.11
↓	1.00	11.7	147	2.15
↓	1.00	11.7	165	2.30
↓	0.85	10.0	37.5	2.41
↓	0.85	10.0	133	2.21
↓	0.70	8.6	25.5	2.27
↓	0.55	7.4	18.6	2.32
↓	0.55	7.4	22.3	2.45
↓	0.40	5.9	7.51	2.41
↓	0.40	7.5	13.2	2.30
↓	0.25	6.0	5.20	2.38
300	0.25	6.0	6.91	2.43
350	1.00	11.1	29.8	2.17
↓	1.00	11.6	62.5	2.15
↓	1.00	11.1	131	2.17
↓	0.85	8.7	29.8	2.27
↓	0.70	8.2	10.2	2.29
↓	0.55	6.2	8.42	2.40
↓	0.40	4.7	1.71	2.51
↓	0.25	5.7	0.500	2.40
↓	0.25	6.1	3.40	2.37
350	0.030	2.8	0.121	2.63

Ni-NiO, UO_2^{cryst}

T(°C)	NaCl(m)	HCl,(m) 10^{-3}	U(m), 10^{-7}	pH (25 °C)
250	1.50	68	14.1	1.40
	1.40	68	20.4	1.40
	1.30	66	11.2	1.41
	1.20	67	17.0	1.40
	1.00	66	5.62	1.41
	0.95	64	14.1	1.41
	0.90	65	6.17	1.40
	0.85	63	6.03	1.41
	0.80	65	6.03	1.40
	0.75	63	7.59	1.41
	0.70	61	4.17	1.42
	0.65	49	1.41	1.51
	0.60	49	2.04	1.51
↓	0.55	47	0.708	1.52
250	0.50	36	0.275	1.64
300	1.50	45.5	1.21	1.57
	1.40	43.2	0.892	1.59
	1.30	44.8	1.022	1.58
	1.20	43.2	0.711	1.59
	1.00	42.9	0.715	1.59
	0.95	42.1	0.671	1.59
	0.90	42.4	0.421	1.59
	0.85	42.2	0.526	1.59
	0.80	42.1	0.458	1.59
	0.75	42.3	0.489	1.58
	0.70	42	0.420	1.58
	0.60	41.8	0.370	1.58
	0.50	41.5	0.270	1.57
↓	0.40	41.1	0.349	1.57
300	0.30	41.4	0.213	1.55
350	1.50	34	0.467	1.70
	1.40	38	0.237	1.65
	1.30	34	0.362	1.70
	1.20	36	0.306	1.67
	1.00	38	0.378	1.64
	0.95	37	0.308	1.65
	0.90	39	0.585	1.62
	0.85	35	0.240	1.67
	0.80	37	0.239	1.64
	0.75	39	0.429	1.62
	0.70	35	0.166	1.66
	0.65	35	0.279	1.66
	0.60	33	0.130	1.68
↓	0.55	31	0.143	1.70
350	0.50	35	0.299	1.65

Co-CoO, UO_2^{cryst}

T(°C)	NaCl(m)	HCl(m), 10^{-3}	U(m), 10^{-7}	pH (25 °C)
250	0.50	40	0.509	1.53
250	0.75	49	7.20	1.45
250	1.00	54	14.2	1.41
350	0.50	27	0.218	1.70
350	0.75	34	0.470	1.60
350	1.00	34	0.705	1.61

Supplementary Table 5.2. The logarithm of the oxygen fugacity of the buffers employed in the experiments at 250-350 °C. The Co-CoO buffer was used at 250 °C and 350 °C, the MoO_2-MoO_3 buffer at 300 and 350 °C, and the Ni-NiO buffer at all three temperatures.

T(°C)	250	300	350
MoO_2-MoO_3	-26.5	-23.5	-20.7
Ni-NiO	-40.7	-36.3	-32.3
Co-CoO	-42.0	-37.5	-33.6

Chapter 6

General Conclusions

6.1 General Conclusions

Experimental and field-based results presented in this thesis invalidate previously held ideas regarding the mobility of niobium, tantalum, and reduced uranium during hydrothermal fluid-rock interaction. Niobium and tantalum form hydroxide and hydroxyl-fluoride species in acidic, fluoride-rich solutions, whereas uranium forms U-Cl species in acidic, chloride-rich brines, not only at oxidizing conditions, as previously demonstrated, but also at reducing conditions. Therefore, at conditions relevant to natural hydrothermal systems, all three of these metals are mobile in hydrothermal solutions.

Autoclave solubility experiments conducted with Nb_2O_5 (solid) and Ta_2O_5 (solid) identified the hydroxide ($Nb(OH)_4^+$, $Ta(OH)_5^\circ$), hydroxyl-fluoride ($NbF_2(OH)_3^\circ$, $TaF_3(OH)_3^-$) and TaF_5° species responsible for the transport of these metals, at temperatures $\geq$100 °C. A change in predominance with increasing HF concentration, from hydroxide to hydroxyl-fluoride species, at a $\sim 10^{-3}$ molal HF concentration for Nb and a $\sim 10^{-2}$ molal HF concentration for Ta, results in an increase in the solubility of Nb and Ta by several orders of magnitude. By contrast, at 100-250 °C, differences in temperature do not affect niobium or tantalum mobility appreciably. Changes in the acidity of an HF bearing fluid affect the dissolution of niobium and tantalum through two competing processes. At acidic conditions (pH ~2), the identified dissolution reactions predict that an increase in pH will lead to higher concentrations of the corresponding aqueous species. However, this statement is only valid in HF-rich solutions. With increasing pH, HF will dissociate and concentrations of HF in the fluid will fall precipitously, thereby decreasing the solubility of niobium and tantalum. Over a wide pH range, this effect overrides the former. Of particular importance is the observation that, in our experiments, niobium is more soluble than tantalum. Owing to the presence of different niobium and tantalum hydroxyl-fluoride species and differences in how their solubility varies with changing pH, the solubility of tantalum may approach that of niobium with increasing pH. Nevertheless, given the high temperature niobium solubility data summarized by Lukyanova et al. (2017), we expect the niobium hydroxyl-fluoride species to have the same stoichiometry at elevated HF concentration as the tantalum species $TaF_3(OH)_3^-$, and so the range of fluoride activity over which the solubility of tantalum could approach that of niobium is expected to be limited.

Geochemical modeling of HF rich, acidic brines demonstrated that deposition of niobium and tantalum from a brine saturated in these metals is most easily accomplished by an increase in the pH of the solution. The interaction of such a brine with carbonate lithological units will neutralize the solution and rapidly precipitate niobium and tantalum, whereas mixing with a brine of different composition will result in low to moderate levels of deposition.

These observations and geochemical modeling are consistent with the observed occurrence of niobium and tantalum mineralization at the Nechalacho deposit, which contains one of the world's largest known resources of these metals. The relative impact of magmatic and hydrothermal processes on niobium-tantalum mineralization was evaluated and niobium was found to occur predominantly as primary columbite-(Fe) aggregates in the Upper Zone, and fergusonite-(Y) aggregates in the Basal Zone crystallizing directly from the melt and subsequently being altered. These primary minerals, in addition to pyrochlore outside the ore zones and abundant secondary zircon, served as precursors to secondary niobium-tantalum minerals. Depending upon the amount of niobium mobilized from the zircon, the contribution of zircon to the observed abundances of columbite-(Fe) and fergusonite-(Y) may range from ~25% to more than half of what is observed, based on mass balance calculations. This is an entirely different genetic sequence for niobium mineralization than that within the more commonly studied niobium-yttrium-fluoride (NYF) pegmatites within which crystal fractionation results in the formation of columbite-(Fe,Mn) with steadily changing composition.

Whereas alteration was sufficiently intense as to leave only a single example of primary columbite-(Fe) behind, a strong bulk drill core niobium versus zirconium correlation, along with textural observations of columbite-(Fe) and fergusonite-(Y) forming within zircon, suggest that niobium was mobilized at less than the meter scale. By contrast, the presence of fluorite in the Nechalacho deposit and the results of the above experiments suggest the potential for considerable niobium-tantalum transport. However, the pH of the hydrothermal fluid at the Nechalacho deposit has been constrained to be ~3.7-5.7 on the basis of observed mineral assemblages (Möller and Williams-Jones 2017). At these elevated pH values, the solubility of niobium and tantalum would have been suppressed, thereby accounting for our observations.

The solubility and speciation of uranium in acidic, chloride-bearing brines was also considered using the autoclave solubility method. Two aqueous species, $UO_2Cl_2^0$ and UCl_4^0, were recognized and their equilibrium and formation constants were calculated. The solubility of both species is highly dependent on temperature, pH, and chloride activity. Increases in temperature and chloride activity result in rapid increases in uranium concentration, particularly for UCl_4^0 the abundance of which increases by four logarithm units for every logarithm unit increase in chloride activity. In addition, for every unit decrease in pH, the logarithm of $UO_2Cl_2^0$ activity increases by two orders of magnitude, and UCl_4^0 activity increase by four order of magnitude. These observations demonstrate that reducing fluids can surpass oxidizing fluids in their ability to transport uranium. Furthermore, the reducing, high temperature (≥ 400 °C), acidic fluids encountered in iron oxide-copper gold (IOCG) deposits have the capability of accounting for the uranium enrichments encountered in this class of deposits.

More broadly, the successful application of autoclave solubility experiments in challenging long held beliefs regarding the mobility of high field strength elements underscores the importance of testing observations made in the field, and within ore deposits, with empirical observations made in a controlled, laboratory environment.

6.2 Contributions to knowledge

The results of this study provide one of the first overviews of niobium and tantalum mineralization in a world class rare earth element deposit, within which most of the niobium mineralization is secondary in origin. Textural relationships along with mineral composition were shown to be effective tools in the reconstruction of the alteration sequence of niobium assemblages in the deposit. As a result, we demonstrated that niobium was remobilized at the scale of microns to perhaps centimeters, but not over a much wider area, despite the presence of hydrothermal alteration that was sufficiently intense as to eliminate most primary minerals.

This thesis is the first to result in the publication of thermodynamic data for niobium and tantalum species present in acidic HF-bearing aqueous solutions at elevated temperature. The only previous studies investigating niobium in aqueous solutions in the presence of HF were either qualitative in nature (Zaraisky et al. 2010) or did not publish their experimental data in accessible international journals (Korzhinskaya and Kotova 2012, Kotova 2012, Kotova 2014). Furthermore, by conducting experiments at low HF activity, niobium hydroxide species were recognized, which enabled evaluation of the accuracy of the extrapolations of Peiffert et al. (2010). The effects of temperature and pH on the stability of niobium and tantalum hydroxide and hydroxyl-fluoride species were also evaluated. These results will allow for the incorporation of these species in future geochemical models and the evaluation of niobium and tantalum mobility in a variety of hydrothermal, metamorphic and magmatic fluid settings. Of particular significance is the generation of thermodynamic data for both niobium and tantalum hydroxyl-fluoride species. Both of these metals are commonly analyzed and the variability in Nb/Ta ratios found within whole rock or aqueous geochemical data is frequently discussed. In the absence of experimental constraints, discussions of the significance of Nb/Ta ratios until now, has been speculative. However, our demonstration of the greater mobility of niobium relative to tantalum in fluoride rich systems, will allow the controls underlying variations in Nb/Ta values to be discussed in a more informed manner.

6.3 Recommendations for future studies

The thermodynamic data for niobium species need to be extended to higher fluoride activity, similar to those considered in the tantalum experiments discussed in Chapter 4 (up to ~1m aHF) in order to better compare the behaviour of these two metals. The recent study of Lukyanova et al. (2017), which fit our data for niobium speciation to niobium solubility data previously obtained at temperatures up to 550 °C, suggests that, whereas our data obtained at 150 °C, is accurate, our experiments at 250 °C may have underestimated niobium solubility at higher HF activity. These higher temperature data were not considered in this thesis as they are reported in Russian publications, which were not accessible (Korzhinskaya and Kotova 2012, Kotova 2012, 2014). In fact, the study of Lukyanova et al. (2017) indicates that niobium speciation at high HF activity may be similar to that of tantalum with a dependence of the logarithm of niobium solubility on the logarithm of HF activity having a slope of 3 rather than 2. We point out this possibility in the discussion section of Chapter 4 but experiments are needed to test this hypothesis. In addition, a wide range of temperature, pressure, and pH conditions remain to be tested for their impact on niobium and tantalum solubility and speciation. Studies to obtain this data could be performed using methods similar to that described in this thesis and would allow for further modelling under the varying conditions that would be expected in a hydrothermal fluid. Furthermore, no thermodynamic data are available for Nb^{5+} or for niobium- and tantalum-bearing phases such as the columbite group minerals. The accumulation of these thermodynamic data would facilitate more accurate geochemical modelling, which would help better explain the formation of ore deposits such as the Nechalacho Layered Suite.

Additional fieldwork would provide better constraints on the behaviour of niobium and tantalum. The behaviour of tantalum in the Nechalacho Layered Suite was not explored to the same extent as niobium, due in part due to the much lower concentration of tantalum, which is typically an order of magnitude lower than that of niobium. Analytical techniques, such as LA-ICP-MS, could be used to examine minerals such as biotite, which is both abundant and mainly hydrothermal in origin in the Nechalacho Layered Suite, but contains concentrations of niobium and tantalum below the detection limits of an electron microprobe. In addition, the zonation of niobium from the core to rim of primary crystals of minerals such as zircon and magnetite, combined with the determination of mineral-melt partition coefficients of niobium for such minerals, would allow investigation of how niobium concentration changes with progressive crystal fractionation.

Experimental studies addressing the aqueous behaviour of uranium at elevated temperature are currently lacking and are necessary to model the geochemical behaviour of this metal. In particular, it would be instructive to conduct uranium solubility experiments in the presence of the fluoride ligand, as both elements are "hard" (high charge to radius ratio) ions, according to Pearson's rules (Pearson, 1963), and are therefore likely to form stable aqueous complexes with one another. Other ligands such as sulphate should also be considered. These experiments could be conducted with the autoclave solubility method, with modifications made corresponding to each ligand; experiments with fluoride would have to be performed in Teflon test tubes or within Teflon liners so as to limit the contact of fluoride with the titanium autoclave walls, which are corrodible by the former.

Whereas the experiments described in Chapter 5 demonstrate that uranium can be transported in reducing systems in acidic, chloride-rich brines, field-based evidence regarding the nature of fluids mobilizing uranium in settings containing reduced rock units, such as unconformity-type deposits, is not unambiguous. A field-based study of an unconformity-type deposit where, with increasing depth, the temperature, acidity, and oxygen fugacity of the ore forming fluid were constrained, would be highly complementary to the results of Chapter 5. Combining these constraints with knowledge of the distribution of uranium concentrations in an ore deposit would allow for the relative impact of oxidizing and reducing fluids on uranium transport to be recognized. It should be noted that a similar field-based approach to a uranium bearing IOCG deposit would be of much use. In short, the experimental observations of Chapter 5 need to be tested using natural samples.

6.4 References

Korzhinskaya V.S. and Kotova N.P. (2012) Experimental modeling of possibility of hydrothermal niobium transport by fluid solutions. *Vestn. Otd. Nauk Zemle Ross. Akad. Nauk* **4**, NZ9001.

Kotova, N.P. (2012) Experimental study of concentration dependence of solubility of niobium oxide in fluoride solutions at T = 550°C, P = 1000 bar and low oxygen fugacity (buffer Co–CoO). *Vestn. Otd. Nauk Zemle Ross. Akad. Nauk* **4**, NZ9001.

Kotova, N.P. (2014) Experimental study of Nb_2O_5 solubility in fluoride solutions at T = 550°C and P = 500 bar. *Eksp. Geokhim.* **2**, 319–321.

Lukyanova E. V., Akinfiev N. N., Zotov A. V., Rass I. T., Kotova N. P. and Korzhinskaya V. S. (2017) Niobium in hydrothermal systems related to alkali granites: Thermodynamic description of hydroxo and hydroxofluoride complexes. *Geol. Ore Deposits* **59**, 305-314.

Möller V. and Williams-Jones A.E. (2017) Magmatic and Hydrothermal Controls on the Mineralogy of the Basal Zone, Nechalacho REE-Nb-Zr Deposit, Canada. *Econ. Geo.* **112**, 1823-1856.

Pearson R. G. (1963) Hard and Soft Acids and Bases. *J. Am. Chem. Soc.* **85**, 3533-3539.

Peiffert C., Nguyen-Trung C., Palmer D. A., Laval J. P. and Giffaut E. (2010) Solubility of B-Nb2O5 and the Hydrolysis of Niobium(V) in Aqueous Solution as a Function of Temperature and Ionic Strength. *J. Solution. Chem.* **39**, 197-218.

Zaraisky G. P., Korzhinskaya V. and Kotova N. (2010) Experimental studies of Ta_2O_5 and columbite-tantalite solubility in fluoride solutions from 300 to 550°C and 50 to 100 MPa. *Miner. Petrol.* **99**, 287-300.